Stratosphere-troposphere Processes
And their Role in Climate

SPARC

Core Project of the WMO/ICSU/IOC
World Climate Research Programme

Lifetimes of Stratospheric Ozone-Depleting Substances, Their Replacements, and Related Species

Edited by M. K. W. Ko, P. A. Newman, S. Reimann, S. E. Strahan

SPARC Report No. 6, WCRP-15/2013
December 2013

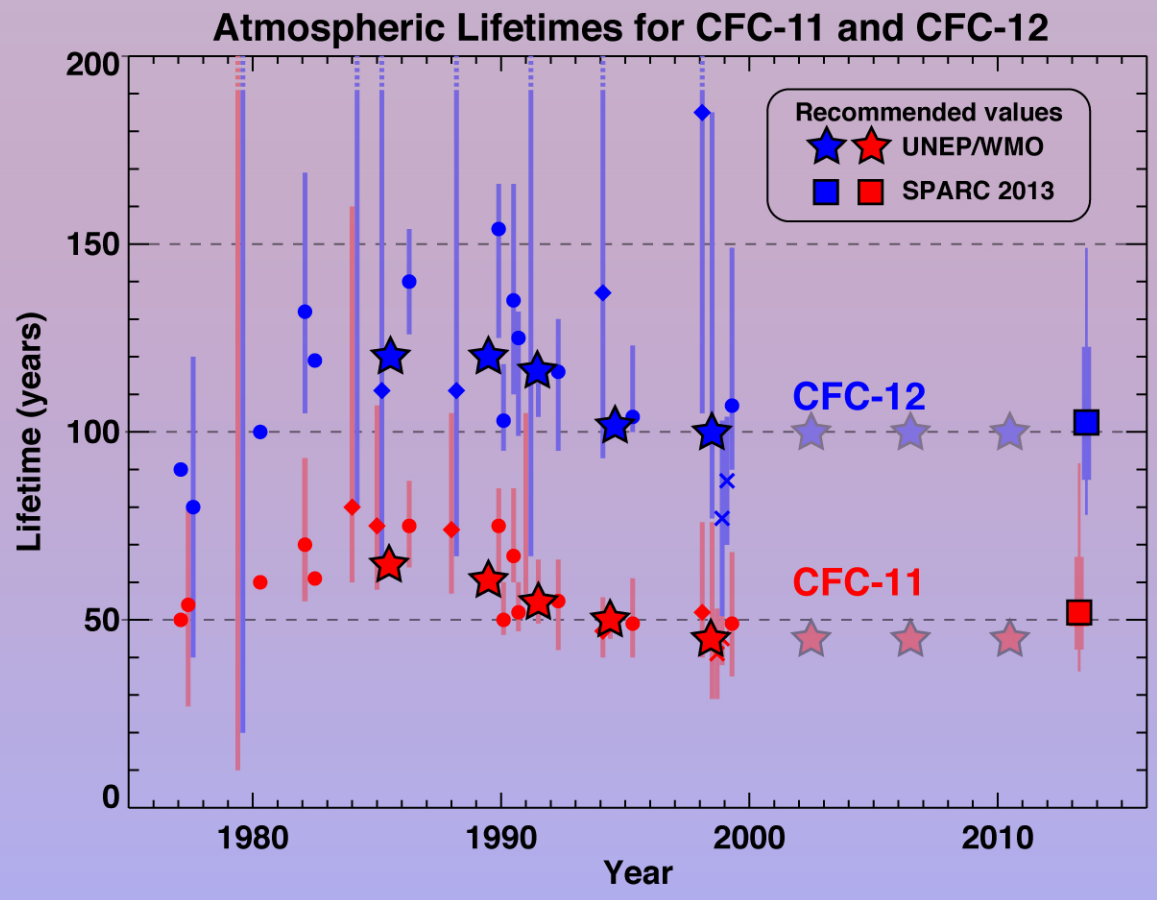

WMO UNESCO IOC ICSU International Council for Science

STRATOSPHERE-TROPOSPHERE PROCESSES
AND THEIR ROLE IN CLIMATE

SPARC

A project of the WMO/ICSU/IOC World Climate Research Programme

---

SPARC Report on the Lifetimes of Stratospheric Ozone-Depleting Substances, Their Replacements, and Related Species

December 2013

Prepared under auspices of the SPARC Scientific Steering Group

Edited by M. K. W. Ko, P. A. Newman, S. Reimann, and S. E. Strahan

WCRP – 15/2013
SPARC Report No. 6

Editing, Design, and Layout: Kathy A. Thompson and Rose M. Kendall

Citation, SPARC (2013):
SPARC Report on the Lifetimes of Stratospheric Ozone-Depleting Substances, Their Replacements, and Related Species, M. Ko, P. Newman, S. Reimann, S. Strahan (Eds.), SPARC Report No. 6, WCRP-15/2013.

Available at http://www.sparc-climate.org/publications/sparc-reports/sparc-report-no6/

The editors sincerely thank Kathy Thompson and Rose Kendall for their tireless and dedicated effort in the production of this report.

LIST OF INTERNATIONAL AUTHORS, CONTRIBUTORS, AND REVIEWERS

SCIENTIFIC STEERING COMMITTEE

Malcolm K. W. Ko	NASA Langley Research Center	USA
Paul A. Newman	NASA Goddard Space Flight Center	USA
Stefan Reimann	Empa	Switzerland
Susan E. Strahan	Universities Space Research Association	USA

AUTHORS AND CONTRIBUTORS

Chapter 1
Introduction

Chapter Lead Authors

Stefan Reimann	Empa	Switzerland
Malcolm K. W. Ko	NASA Langley Research Center	USA
Paul A. Newman	NASA Goddard Space Flight Center	USA
Susan E. Strahan	Universities Space Research Association	USA

Chapter 2
The Theory of Estimating Lifetimes Using Models and Observations

Chapter Lead Authors

R. Alan Plumb	Massachusetts Institute of Technology	USA
Richard S. Stolarski	Johns Hopkins University	USA

Co-Authors

Michaela I. Hegglin	University of Reading	UK
Michael J. Prather	University of California, Irvine	USA
C. Michael Volk	Universität Frankfurt	Germany

Chapter 3
Evaluation of Atmospheric Loss Processes

Chapter Lead Authors

James B. Burkholder	NOAA Chemical Sciences Division	USA
Wahid Mellouki	Institut de Combustion, Aérothermique, Réactivité, et Environnement, ICARE – CNRS/OSUC, Orléans	France

Co-Authors

Eric L. Fleming	Science Systems and Applications, Inc.	USA
Christian George	CNRS/Université Claude Bernard Lyon 1	France
Dwayne E. Heard	University of Leeds	UK
Charles H. Jackman	NASA Goddard Space Flight Center	USA
Michael J. Kurylo	Universities Space Research Association	USA
Vladimir L. Orkin	National Institute of Standards and Technology	USA
William H. Swartz	The Johns Hopkins University Applied Physics Laboratory	USA
Timothy J. Wallington	Ford Motor Company	USA

Chapter 4
Inferred Lifetimes from Observed Trace-Gas Distributions

Chapter Lead Authors

Andreas Engel	Universität Frankfurt	Germany
Elliot L. Atlas	University of Miami	USA

Co-Authors

Peter F. Bernath	University of York	UK
Harald Bönisch	J. W. Goethe Universität Frankfurt	Germany
Alex Brown	University of York	UK
Johannes Laube	University of East Anglia	UK
Kenneth R. Minschwaner	New Mexico Institute of Mining and Technology	USA
Stephen A. Montzka	NOAA ESRL Global Monitoring Division	USA
Simon O'Doherty	University of Bristol	UK
Ronald G. Prinn	Massachusetts Institute of Technology	USA
Matthew Rigby	University of Bristol	UK
Susan M. Schauffler	National Center for Atmospheric Research	USA
C. Michael Volk	Universität Frankfurt	Germany
Shari A. Yvon-Lewis	Texas A&M University	USA

Chapter 5
Inferred Lifetimes from Observed Trace-Gas Distributions

Chapter Lead Authors

Martyn Chipperfield	University of Leeds	UK
Qing Liang	Universities Space Research Association	USA

Co-Authors

Luke Abraham	University of Cambridge	UK
Slimane Bekki	Laboratoire Atmosphères, Milieux, Observations Spatiales / Institut Pierre-Simon Laplace	France
Peter Braesicke	University of Cambridge	UK
Sandip Dhomse	University of Leeds	UK
Glauco Di Genova	Università degli Studi di Salerno	Italy
Eric L. Fleming	Science Systems and Applications, Inc.	USA
Steven Hardiman	UK Met Office	UK
Daniela Iachetti	Università degli Studi L'Aquila	Italy
Charles H. Jackman	NASA Goddard Space Flight Center	USA
Douglas E. Kinnison	National Center for Atmospheric Research	USA
Marion Marchand	Laboratoire Atmosphères, Milieux, Observations Spatiales / Institut Pierre-Simon Laplace	France
Giovanni Pitari	Università degli Studi L'Aquila	Italy
Eugene Rozanov	Physical and Meteorological Observatory / World Radiation Center	Switzerland
Andrea Stenke	Eidgenössiche Technische Hochschule Zürich	Switzerland
Fiona Tummon	Eidgenössiche Technische Hochschule Zürich	Switzerland

Contributors

Jérémie Burgalat	Laboratoire Atmosphères, Milieux, Observations Spatiales / Institut Pierre-Simon Laplace	France
David Cugnet	Laboratoire Atmosphères, Milieux, Observations Spatiales / Institut Pierre-Simon Laplace	France
Stacey M. Frith	Science Systems and Applications, Inc.	USA
Charlotte Pascoe	British Atmospheric Data Centre / STFC Rutherford Appleton Laboratory	UK
Matthew Rigby	University of Bristol	UK

Chapter 6
Recommended Values for Steady-State Lifetimes

Chapter Lead Authors

Malcolm K. W. Ko	NASA Langley Research Center	USA
Paul A. Newman	NASA Goddard Space Flight Center	USA
Stefan Reimann	Empa	Switzerland
Susan E. Strahan	Universities Space Research Association	USA

Co-Authors

Elliot L. Atlas	University of Miami	USA
James B. Burkholder	NOAA ESRL Chemical Sciences Division	USA
Martyn Chipperfield	University of Leeds	UK
Andreas Engel	Universität Frankfurt	Germany
Qing Liang	Universities Space Research Association	USA
Wahid Mellouki	Institut de Combustion, Aérothermique, Réactivité, et Environnement, ICARE – CNRS/OSUC, Orléans	France
R. Alan Plumb	Massachusetts Institute of Technology	USA
Richard S. Stolarski	Johns Hopkins University	USA
C. Michael Volk	Universität Frankfurt	Germany

REVIEWERS

Super Reviewers – Overall Report

Marvin A. Geller	State University of New York, Stony Brook	USA
Neil R. P. Harris	University of Cambridge	UK
Rolf Müller	Forschungszentrum Jülich	Germany

Principal Reviewers – Individual Chapters

Chapter 2

John S. Daniel	NOAA ESRL Chemical Sciences Division	USA

Chapter 3

Paul H. Wine	Georgia Institute of Technology	USA

Chapter 4

William T. Sturges	University of East Anglia	UK

Chapter 5

Olaf Morgenstern	National Institute of Water and Atmospheric Research	New Zealand

Mail and Meeting Reviewers

Elliot L. Atlas	University of Miami	USA
Slimane Bekki	Laboratoire Atmosphères, Milieux, Observations Spatiales / Institut Pierre-Simon Laplace	France
James B. Burkholder	NOAA ESRL Chemical Sciences Division	USA
Martyn Chipperfield	University of Leeds	UK
Catherine Clerbaux	Laboratoire Atmosphères, Milieux, Observations Spatiales / Institut Pierre-Simon Laplace	France
Michael T. Coffey	NASA Headquarters	USA
John S. Daniel	NOAA ESRL Chemical Sciences Division	USA
Andreas Engel	Universität Frankfurt	Germany
David W. Fahey	NOAA ESRL Chemical Sciences Division	USA
Eric L. Fleming	Science Systems and Applications, Inc.	USA
Marvin A. Geller	State University of New York, Stony Brook	USA
Neil R. P. Harris	University of Cambridge	UK
Peter Hoor	Johannes Gutenberg-Universität Mainz	Germany
Robert E. Huie	REH Kinetics, Inc.	USA
Elena Jimenez	Universidad de Castillo La Mancha	Spain
Ken Jucks	NASA Headquarters	USA
Malcolm K. W. Ko	NASA Langley Research Center	USA
Michael J. Kurylo	Universities Space Research Association	USA
Qing Liang	Universities Space Research Association	USA
Patricia Martinerie	Laboratoire de Glaciologie et Géophysique de l'Environnement / Université Joseph Fourier Grenoble	France
Wahid Mellouki	Institut de Combustion, Aérothermique, Réactivité, et Environnement, ICARE – CNRS/OSUC, Orléans	France
Martine Michou	GAME/CNRM, Météo-France	France
Olaf Morgenstern	National Institute of Water and Atmospheric Research	New Zealand
Rolf Müller	Forschungszentrum Jülich	Germany
Hideaki Nakane	Kochi University of Technology	Japan
Paul A. Newman	NASA Goddard Space Flight Center	USA
Johannes Orphal	Karlsruhe Institute of Technology	Germany
R. Alan Plumb	Massachusetts Institute of Technology	USA
A. R. Ravishankara	NOAA ESRL Chemical Sciences Division	USA
Stefan Reimann	Empa	Switzerland
Ross J. Salawitch	University of Maryland, College Park	USA
Kiyotaka Shibata	Japan Meteorological Agency	Japan
Johannes Stähelin	Eidgenössiche Technische Hochschule Zürich	Switzerland
Richard S. Stolarski	Johns Hopkins University	USA
Susan E. Strahan	Universities Space Research Association	USA
William T. Sturges	University of East Anglia	UK
Fiona Tummon	Eidgenössiche Technische Hochschule Zürich	Switzerland

Guus J. M. Velders	National Institute for Public Health and the Environment	Netherlands
C. Michael Volk	Universität Frankfurt	Germany
Nicola Warwick	University of Cambridge	UK
Ray Weiss	University of California, San Diego	USA
Paul H. Wine	Georgia Institute of Technology	USA
Donald J. Wuebbles	University of Illinois at Urbana-Champaign	USA

CONFERENCE SUPPORT

Rose M. Kendall	CSC	USA
Kathy A. Thompson	CSC	USA
Anke Witten	SPARC Office, Eidgenössiche Technische Hochschule Zürich	Switzerland

PUBLICATION SUPPORT

Carolin Arndt	SPARC Office, Eidgenössiche Technische Hochschule Zürich	Switzerland
Rose M. Kendall	CSC	USA
Kathy A. Thompson	CSC	USA

CONTENTS

PREFACE

The concept of using lifetimes to relate atmospheric burdens to emissions has proven useful for quantifying the effects of ozone depleting substances and their replacements on ozone and climate. While the issue was addressed in each of the WMO Ozone Assessment Reports, there has not been a focused effort since the last report was published in 1994 (Kaye and Penkett, 1994). In the interim, we learned that the lifetime of a species in the atmosphere is not only defined by the chemical reactivity of the species but also by the physical and chemical state of the surrounding atmosphere and the emission history.

This reevaluation is the first attempt in nearly two decades to estimate atmospheric lifetimes of these substances using state-of-the art analysis techniques. It was motivated by findings that the lifetimes of some of the ODSs (i.e., CFC-11 and CCl_4) could be longer than previously accepted and because some of the replacement compounds were not yet in use at the time of the last evaluation in the 1990s. In addition, a new evaluation is warranted because of tremendous advancements in the abilities of models used to derive atmospheric lifetimes and the availability of a wealth of additional measurement data not only from ground-based stations but also from high-altitude sampling and satellite observations.

At the 2011 SPARC Scientific Steering Group meeting (Pune, India), the WCRP launched the activity "Lifetime of halogen source gases" as one of the SPARC core projects. This report was prepared by an international team of scientists comprising of 4 coordinating lead authors, 10 lead authors, and approximately 40 co-authors and contributors. In addition, 10 principal reviewers worked with the lead authors to respond to mail review comments provided by over 30 reviewers. The final draft of the report was discussed at the Review Meeting in Zürich (Switzerland) in January 2013. The financial, personnel, and in-kind support provided by SPARC, WCRP, and the U. S. National Aeronautics and Space Administration (NASA) was crucial to the success of this report.

The estimated lifetimes and their uncertainties presented in this report were obtained using the best available data and methods at the time of the final preparation of the report. Nevertheless, this report is only a snapshot of our current understanding. As mentioned above, atmospheric lifetimes are not fixed constants and depending on new findings and atmospheric changes, will change in the future.

CHAPTER 1

Introduction

Lead Authors:
Stefan Reimann
Malcolm K. W. Ko
Paul A. Newman
Susan E. Strahan

Summary

- The lifetimes of chemical species are used to predict their future abundances, to perform emission estimates, and to calculate the ozone-depletion potentials (ODPs) and global warming potentials (GWPs). It is therefore very important to have the best possible estimates of lifetimes of ozone depleting substances (ODSs), replacement compounds, and climate forcing gases to guide policy making of these substances.

- Twenty-seven chemical species are evaluated in this report. These substances were chosen because they are either ODSs, are being used as replacements for ODSs, or are major climate-forcing gases. No comprehensive evaluation of lifetimes of these substances has been performed since the mid-1990s. Important progress in modeling and observations along with unresolved science challenges necessitate revisions to current lifetime estimates.

Chapter 1: An Introduction to the Lifetimes of Stratospheric Ozone-Depleting Substances, Their Replacements, and Related Species

For a long-lived halocarbon source gas (atmospheric lifetime > 0.5 years), knowing the time evolution of surface concentrations is the first step in obtaining estimates for its contribution to both ozone depletion and radiative forcing. This behavior can be approximated by a simple integral (see Equation 1.4) if an appropriate constant lifetime is specified. Unfortunately, the lifetime of a chemical species in the atmosphere is not an observable quantity. Slightly different values for the lifetime are derived using different methods that, to varying degrees, make use of the following information:

- Physical and chemical properties of the species
- Chemical and radiative environment of the atmosphere
- Spatial and temporal distribution of the species in the atmosphere
- Spatial and temporal information of the species' emissions
- Transport pathways in the atmosphere

Different values for the lifetime of an ozone depleting substance (ODS) are being used to predict its future abundances from given emissions, to derive estimates for emissions based on observed abundance, and to calculate the ozone-depletion potentials (ODPs) and global warming potentials (GWPs). Thus, changes in the recommended value have implications for estimates of the timing for ozone recovery as the concentrations of the controlled ODSs fall below the threshold for ozone depletion. This will also have an indirect effect on the radiative forcing. It is therefore very important to have the best possible estimates of ODS lifetimes to guide policy making on these substances.

Comprehensive atmospheric chemistry/transport models provide a self-consistent framework for calculating lifetimes, but the accuracy of lifetimes calculated with models depends on their ability to represent the atmosphere. While models have significantly improved since the last lifetime evaluation (Kaye *et al.,* 1994), estimates of CFC and other species' lifetimes still include significant uncertainties resulting from model representations of chemistry, radiation, and transport. Accurate determination of lifetimes using observations (i.e., concentration measurements) requires knowledge of the atmospheric burden, its rate of change, and quantification of past emissions. There is insufficient information to determine lifetimes (particularly steady-state lifetimes, see Chapter 2) solely from observations.

Theoretical concepts as well as numerical results derived from modeling studies are needed to bridge the gap. The quality of information on the burdens, the emissions, and the loss rate is limited and so all have associated uncertainties which limit the accuracy of the derived lifetime estimates. Therefore, evaluating the various sources of uncertainty is a central part of this report.

In the past several years it has become evident that recommended lifetimes of some ODSs do not agree with lifetimes deduced from sophisticated models or lead to inferred emissions (from observed atmospheric burden) that do not agree with independent bottom-up emission estimates. For example, in the 2010 Ozone Assessment Report (Montzka and Reimann, 2011) an inconsistency was noted in the global budget of carbon tetrachloride (CCl_4). Resolving the inconsistency will require a combination of identifying missing sources and/or assuming a longer lifetime for CCl_4. The other example has to do with the lifetime of CFC-11. Modeling studies (e.g., Douglass *et al.* 2008) indicated that the global CFC-11 lifetime was possibly longer than the value of 45 years, which has been used since the 1998 Ozone Assessment Report (WMO, 1999). This is of particular importance since CFC-11 is the reference species in defining ODPs, and its lifetime is used as a reference to obtain lifetimes of other ODSs (see Chapter 4).

This report is the first comprehensive attempt in over a decade to assess the impact of new developments in existing methods and models for the evaluation of atmospheric lifetimes. This lifetime evaluation report aims not only to provide new estimates of lifetimes but also to deliver an in-depth analysis of their uncertainties.

This report is limited to analyzing and estimating atmospheric lifetimes and their uncertainties for substances with atmospheric lifetimes greater than 6 months. Very short-lived substances (VSLSs) are not included in this report since the concept of a single atmospheric lifetime cannot be used to relate VSLS emissions to observed concentrations (see e.g., Montzka and Reimann, 2011 and references therein). This report also does not include estimates of either ODPs or GWPs. Although a substance's ODP and GWP are approximately proportional to its lifetime, there are a number of theoretical considerations that cause empirical estimates to differ from model-estimated values. This report also does not include analysis of emissions or how uncertainty in the emissions affects the budget uncertainties. All of these limitations are mainly a result of the desire to constrain the scope of the report. Finally, carbon dioxide (CO_2) is not considered in this report because its atmospheric lifetime is ultimately defined by the exchange with the ocean and land surfaces.

Table 1.1 lists the 27 species evaluated in this report. Also given are the previously recommended lifetimes, the 2008 atmospheric mixing ratios, and the basis for their inclusion in this report. The species marked in bold indicate the high priority for model simulations performed for this report. The reasons for a special focus on these species are:

- CFC-11 and CFC-12 are major ODSs with long data records for surface concentrations and historical emission rates.
- There is a need to reconcile the lifetime of carbon tetrachloride (CCl_4), which is in conflict with the observed trends of surface mixing ratios and reported emissions (Montzka and Reimann, 2011).
- The model calculated methyl chloroform (CH_3CCl_3) lifetime has served as a proxy for model calculated tropospheric OH abundance (Prinn *et al.,* 1987). Subsequently, this OH value is used to estimate the lifetimes of substances that are primarily removed in the

troposphere (Table 1.1) from their reaction rate constants with OH. Observations of methyl chloroform surface concentration in the next decade should provide further validation of its lifetime since banking is not an issue for its applications.

- HCFC-22 is the ODS replacement with the highest current emissions.
- Methane (CH_4) and nitrous oxide (N_2O) are not only greenhouse gases but they are also critical for stratospheric ozone chemistry because of their roles as sources gases of odd hydrogen and odd nitrogen radicals. Their lifetimes and distributions are important diagnostics of model performance. Furthermore, the CH_4 chemistry is needed for proper simulations of tropospheric OH radicals.
- HCFCs and HFCs are included because they are replacement compounds for many ODS uses and have relatively high GWP values.
- Halons are evaluated because of their contribution to stratospheric ozone depletion.

Lifetime and Atmospheric Burden

A full description of the different definitions of lifetime, and the relationship among lifetime, emission and burden are provided in Chapter 2 of this report. Specifically, the formalism explains how a given lifetime value can be used to predict burdens from emissions, and how the observed burden and emission history can be used to derive a value for the lifetime. The atmospheric lifetime of a molecule can be simply thought of as the time it remains in the atmosphere. As noted above, its magnitude depends on the properties of the molecule, the properties of the atmosphere, and where and when the molecule is emitted. This means that a molecule does not have a unique lifetime and that the lifetime is time-dependent. Calculation of the lifetimes relies on the basic equation that relates the time evolution of the atmospheric burden $B(t)$ of an atmospheric constituent to its sources $S(t)$ (emissions or *in situ* production) and its removal processes $R(t)$:

$$\frac{\partial B(t)}{\partial t} = S(t) - R(t) \tag{1.1}$$

The 2nd term on the right (R) represents the removal rate of the molecule and is related to the local concentration $n(x,y,z,t)$ of the species and the local removal frequency $L(x,y,z,t)$ (with $R(t)=\int Ln\, dV$, where the volume integral $dV=dxdydz$ is over the whole atmosphere).

Equation (1.1) is not very useful in practice because we often do not have sufficient information to solve for $n(x,y,z,t)$ and $L(x,y,z,t)$ explicitly. It is desirable to have alternative methods to calculate burdens from emissions. If we define the global atmospheric lifetime $\tau(t)$ as

$$\tau(t) = \frac{B(t)}{R(t)} \tag{1.2}$$

Equation (1.1) becomes:

$$\frac{\partial B}{\partial t} = S(t) - \frac{B(t)}{\tau(t)} \tag{1.3}$$

Table 1.1. The list of 27 species evaluated in this report, with previous lifetimes and 2008 mixing ratios (WMO, 2011). Bold fonts represent high priority species.

Name	Formula	Lifetimes from WMO (2011) [a]	Mixing Ratio in 2008 [b]	Remarks [c]
Primarily stratospheric removal				
CFC-11	CCl_3F	45 yr	244.1 ppt	Long-lived ODS, reference for ODP, chlorine source gas
CFC-12	CCl_2F_2	100 yr	536.5 ppt	Long-lived ODS, chlorine source gas
CFC-113	CCl_2FCClF_2	85 yr	76.9 ppt	Long-lived ODS, chlorine source gas
CFC-114	$CClF_2CClF_2$	190 yr	16.4 ppt	Long-lived ODS, chlorine source gas
CFC-115	$CClF_2CF_3$	1020 yr	8.4 ppt	Long-lived ODS, chlorine source gas
CCl_4	CCl_4	35 yr [d]	89.8 ppt	Long-lived ODS, chlorine source gas
Nitrous oxide	N_2O	114 yr [e]	321.6 ppb	Natural and anthropogenic sources Greenhouse gas, odd-nitrogen source gas
Halon-1211	$CBrClF_2$	16 yr [f]	4.2 ppt	Long-lived ODS, bromine source gas
Halon-1301	$CBrF_3$	65 yr	3.2 ppt	Long-lived ODS, bromine source gas
Halon-2402	$CBrF_2CBrF_2$	20 yr [f]	0.5 ppt	Long-lived ODS, bromine source gas
Nitrogen trifluoride	NF_3	500 yr	0.45 ppt [g]	Greenhouse gas
Primarily tropospheric removal				
Methane	CH_4	8.7yr/12.0 yr [e,h]	1781.3 ppb	Natural and anthropogenic sources Greenhouse gas, odd-hydrogen source in the atmosphere
Methyl chloroform	CH_3CCl_3	5 yr	10.9 ppt	Long-lived ODS, chlorine source gas
Methyl chloride	CH_3Cl	1.5 yr [i]	546.0 ppt	Mainly natural sources, chlorine source gas
Methyl bromide	CH_3Br	1.9 yr [i]	7.4 ppt	Natural and anthropogenic sources, bromine source gas
HCFC-22	$CHClF_2$	11.9 yr	191.5 ppt	CFC replacement, chlorine source gas
HCFC-141b	CH_3CCl_2F	9.2 yr	19.4 ppt	CFC replacement, chlorine source gas
HCFC-142b	CH_3CClF_2	17.2 yr	18.7 ppt	CFC replacement, chlorine source gas
HFC-23	CHF_3	222 yr	21.8 ppt	Mainly a by-product in HCFC-22 production
HFC-32	CH_2F_2	5.2 yr	2.7 ppt	ODS replacement
HFC-125	CHF_2CF_3	28.2 yr	6.1 ppt	ODS replacement
HFC-134a	CH_2FCF_3	13.4 yr	47.9 ppt	ODS replacement
HFC-143a	CH_3CF_3	47.1 yr	8.5 ppt	ODS replacement
HFC-152a	CH_3CHF_2	1.5 yr	5.9 ppt	ODS replacement
HFC-227ea	CF_3CHFCF_3	38.9 yr	0.45 ppt [j]	ODS replacement
HFC-245fa	$CHF_2CH_2CF_3$	7.7 yr	1.0 ppt	ODS replacement
Halon-1202	CF_2Br_2	2.9 yr [k]	0.03 ppt [l]	Long-lived ODS, bromine source gas

[a] Previous atmospheric lifetimes are from WMO (2011), unless indicated otherwise.
[b] Mixing ratios in 2008 are an average of NOAA and AGAGE measurements from Table 1-1 of WMO (2011), if not indicated otherwise.
[c] Unless indicated otherwise, sources of the substances in this table are exclusively anthropogenic. Chlorine/bromine/odd-nitrogen source gas signifies inorganic chlorine/bromine/odd-nitrogen source gas to the stratosphere. All long-lived ODSs and replacements (i.e., HCFCs, HFCs) are greenhouse gases.
[d] This lifetime does only include the stratospheric sink and not sinks in the ocean, and the soil.
[e] Lifetime from IPCC (2007).
[f] The stratospheric and tropospheric removal rates (both by photolysis) are comparable for the species.
[g] Global mean mixing ratio in 2008 from Weiss *et al.* (2008).
[h] Total lifetime/pulse decay lifetime from IPCC (2007).

[i] This lifetime only includes tropospheric sinks. In addition, there is a small stratospheric sink (WMO, 2003)
[j] Global mean mixing ratio in 2008 from Vollmer *et al.* (2011).
[k] This lifetime is due primarily to tropospheric photolysis, with a smaller contribution associated with the stratospheric photolysis (WMO, 2011).
[l] University of East Anglia flask measurements

If we further assume that $\tau(t)$ is constant in time (a major assumption) and roughly independent of emission patterns, Equation (1.3) can be expressed in integral form as:

$$B(t) = B(0)e^{-t/\tau} + e^{-t/\tau}\int_0^t S(t')e^{t'/\tau}dt' \qquad (1.4)$$

Equation (1.4) provides an efficient way to compute burdens for different emission scenarios.

There are several options for computing τ. Chapter 2 defines and discusses different methods for calculating lifetimes. The steady-state global atmospheric lifetime can be calculated for a specific emission pattern as calculated by an atmospheric model (Chapter 5) using the available kinetic data for the reaction rate constants (Chapter 3). Alternatively, observations can be combined with a model to derive an instantaneous lifetime (see Chapter 4).

Historical Perspective

Historically the first estimates of CFC lifetimes were based solely upon atmospheric observations and a simple global 1-box model. Lovelock *et al.* (1973) measured the surface concentration of CFC-11 in 1971-72, showing that it had accumulated, consistent with the time-integrated global production and very slow loss processes. They estimated that the lifetime was greater than 10 years. However, this estimate was poorly constrained because emissions were not well known, and there was no knowledge of the mechanism for possible sinks.

Molina and Rowland (1974) sparked great interest in the atmospheric lifetimes of CFC-11 and CFC-12 by suggesting that the chlorine released from these molecules could deplete the stratospheric ozone layer. Specifically, they used the measured absorption spectra of CFC-11 and CFC-12 to calculate the photochemical loss from a one-dimensional (1-D) diffusion model of the atmosphere and estimated that the atmospheric lifetimes of CFC-11 and CFC-12 fell in the range of 40-150 years. Rowland and Molina (1975) followed by looking at a series of 1-D models to estimate lifetimes of 29-85 years for CFC-11 and 53-205 years for CFC-12. NAS (1976) provided a detailed discussion of the lifetime, and, based upon the photolysis rates, estimated the lifetimes of CFC-11 and 12 to be 54 and 80 years, respectively. Further evolutions of the ground-based observation network and models are summarized in Boxes 1.1 and 1.2. Discussions of how measured concentrations of the species in the stratosphere are used to derive lifetime values are found in Chapter 4.

Figure 1.1 shows how estimates for the atmospheric lifetimes of CFC-11 and CFC-12 have changed over the past four decades. The results illustrate how knowledge from laboratory measurements, atmospheric observations, and models evolved and provided improved information. The two dozen lifetimes estimates for CFC-11 and CFC-12 shown in Figure 1.1 were calculated using various methods yet have consistent results: the means and one standard deviation are 58±10 and 116±24 years, respectively.

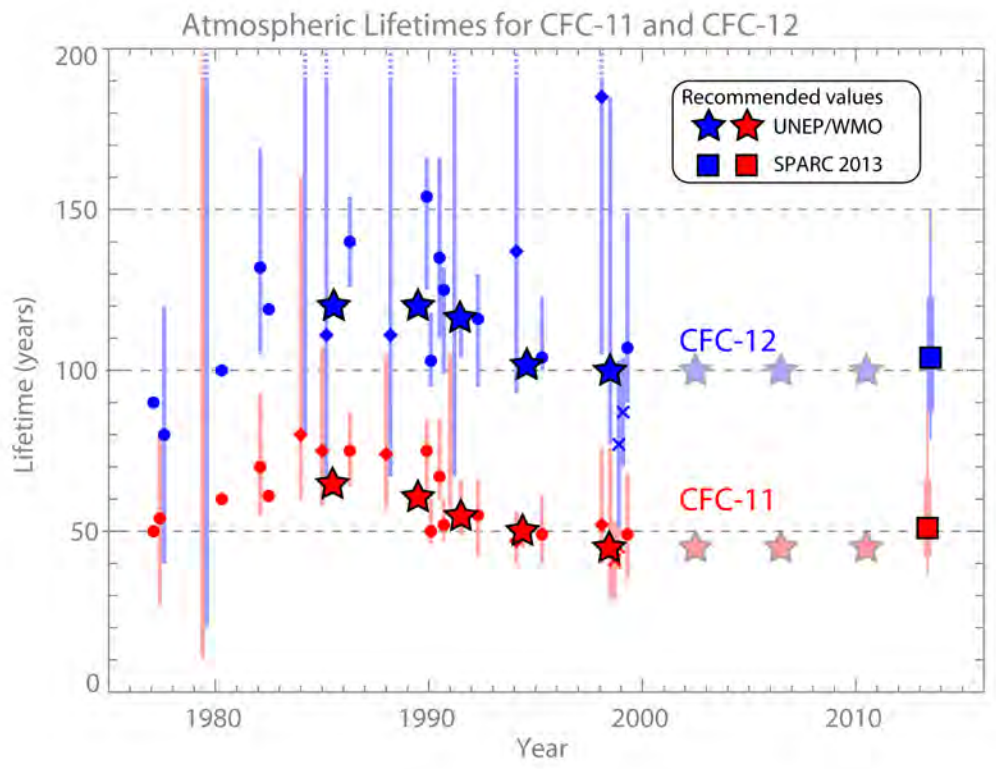

- ● Model-calculated values and model range (primarily 1-D models prior to 1988, and 2-D models from 1988 to 1998).
- ♦ Values derived from NOAA and AGAGE observed surface concentrations and uncertainties.
- ✖ Values from the Volk *et al.* (1997) method using aircraft observations as cited in WMO (1999).
- ★ Values reported in assessment reports - lighter colors in 2002, 2006, and 2010 reflect that these values have not been adjusted since WMO (1999).

Figure 1.1. Lifetime estimates from various reports between 1976 and 2010 for CFC-11 (red) and CFC-12 (blue). Uncertainty estimates (or ranges) are shown as vertical bars (lifetimes without vertical bars did not include uncertainty estimates; Watson *et al.* (1984) included only a range of lifetimes for CFC-12). Some reports included multiple estimates for lifetimes using different methods. 2010 (WMO, 2011); 2006 (WMO, 2007); 2002 (WMO, 2003); 1998 (WMO, 1999; Volk *et al.,* 1997); 1994a (WMO, 1995); 1994b (Kaye *et al.,* 1994); 1991 (WMO, 1992); 1989 (WMO, 1989); 1988 (WMO, 1988); 1985a (WMO, 1985); 1985b (WMO, 1985); 1984 (Watson *et al.*, 1984); 1981 (WMO, 1981); 1979 (Hudson and Reed, 1979); 1976 (NAS, 1976).

Box 1.1. Development of Ground-Based Observation Networks

During the period 1974-1978 sporadic ground-based measurements of CFCs around the globe were accumulating from various researchers. Cunnold *et al.* (1978) identified the problems associated with estimating lifetimes based upon atmospheric observations: uncertainties in emissions, uncertainties in measurements of mixing ratios, and atmospheric variability. They provided the theoretical basis to establish a set of measurement stations that became the Atmospheric Lifetime Experiment (ALE), which was founded in 1978. The major goal of ALE was to measure the trends of the surface concentrations of long-lived atmospheric species with common calibrations to define their atmospheric lifetimes. Cunnold *et al.* (1983) used the observations from ALE to estimate the lifetime of CFC-11 as 83 years. Since then, ALE has evolved to the Advanced Global Atmospheric Gases Experiment (AGAGE, see Prinn *et al.,* 2000). In parallel to AGAGE, the Global Monitoring Division of the National Oceanic and Atmospheric Administration (NOAA, USA) established and maintains a network that provides measurements of halocarbons and other trace gases at a variety of stations worldwide. It has been operating since 1977 (http://www.esrl.noaa.gov/gmd/hats/). These two networks are regularly inter-calibrated and provide mixing ratios from globally representative ground-based stations as input into models (e.g., for deriving lifetimes of long-lived atmospheric species). See additional details in Chapter 4.

Several Ozone Assessment Reports attempted to provide reference lifetimes or best values for the steady-state lifetimes. These are denoted by the stars (★) in Figure 1.1. However, it should be noted that not every report placed the same emphasis on the evaluation of the uncertainties in the quantities used for the lifetime estimates. The most comprehensive lifetime assessment was made in the 1994 NASA 'Report on Concentrations, Lifetimes, and Trends of CFCs, Halons, and Related Species' (Kaye *et al.,* 1994). In that report, lifetimes for numerous ODSs were estimated based on both observations and available models. The report concluded that significant differences in model photolysis rates and transport led to a considerable range in lifetime estimates, and that the available observations were not sufficient to constrain the uncertainty in the model estimates. The calculated 2-D model lifetimes for CFC-11, for example, ranged from 40 to 61 years. The reported estimate inferred from atmospheric observations and a 2-D model with parameterized transport was 42 years (+7, -5, with 68% confidence). Later, Chapter 1 of the 1998 WMO Ozone Assessment (Prinn and Zander, 1999) refined the values with best estimates of 45 years and 100 years for the lifetimes of CFC-11 and CFC-12, respectively. WMO (1999) used these results to present a more integrated approach compared to some previous WMO reports. There has been no attempt to assess lifetimes since, and the same reference values (shown as faded stars) were adopted in subsequent reports (WMO, 2003; 2007; 2011).

Report Outline

This report has an introduction (this chapter) and a summary section (Chapter 6). The body of the report is composed of four chapters. This report recognizes that it is not possible to use observations exclusively to define values for the lifetimes. A theoretical framework is always needed to provide missing information and to derive estimates for the steady-state lifetime (Chapter 2). Figure 1.2 presents a schematic overview of the procedure used in this report to estimate atmospheric lifetimes. A more detailed explanation is provided in Chapter 6. Input variables needed for the different models and methods are discussed in Chapters 3

and 4. These include photochemical constants (e.g., photolytic and kinetic rates), observations (e.g., atmospheric distribution of ODSs, climatological data), and emission data. The best lifetimes estimates and related uncertainties from Chapter 4 and Chapter 5 are aggregated using a statistical method to produce a recommended atmospheric lifetime and its uncertainty. In Chapter 5, results from extensively evaluated three-dimensional (3-D) coupled chemistry climate models (CCMs) are presented that were not available for previous assessments. Brief descriptions of the chapters are given below.

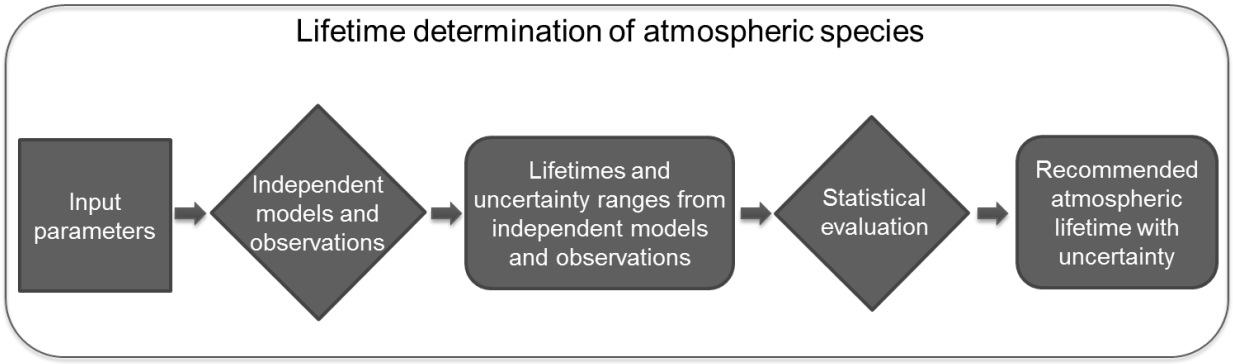

Figure 1.2. Schematic procedure for deriving recommended lifetimes of atmospheric species. Input and output parameters are shown in rectangles and processes in diamonds.

Chapter 2: The Theory of Estimating Lifetimes Using Models and Observations

While Equations 1.3 and 1.4 give a simple description of a lifetime, the theoretical basis of lifetimes is much more complex. For example, in Equation 1.3 we assume that the loss can be represented as a linear process that is proportional to the global burden of the trace gas. In reality, the removal is only linear in the local concentration, and $R(t)$ depends on location and time. In Chapter 2 of this document, the theoretical basis of lifetimes is extensively explored and updated. It is pointed out that, while the reactivity of the molecule determines its lifetime to a large extent, the lifetime also depends on reactants in the atmosphere, atmospheric transport, and emission histories. Various techniques for estimating lifetimes are examined.

This theory chapter sets the stage for subsequent chapters by introducing concepts and approaches that have been used to estimate global lifetimes. For each approach, the observational information and the modeling capabilities required are presented, along with general concepts about the most important factors in determining lifetimes. Discussions are presented on the different definitions of lifetimes (e.g., steady-state vs. instantaneous), the general strengths and weaknesses of the various approaches used to derive the values, and how those values are used. Past and projected future deviations of lifetimes from steady-state values are addressed. Differences between the decay of a tracer pulse and the global lifetime of that tracer are differentiated.

Chapter 3: Evaluation of Atmospheric Loss Processes

This chapter provides a comprehensive evaluation and recommendations for kinetic and photochemical parameters relevant for the atmospheric loss processes of the molecules listed in Table 1.1. Kinetic and photochemical data evaluations include Lyman-α and UV absorption cross sections and OH radical, $O(^1D)$, and Cl reaction rate coefficients. A critical evaluation of the uncertainties in the kinetic and photochemical parameters, and the resulting range in calculated atmospheric lifetimes is also evaluated using a 2-D model.

Box 1.2. Evolution of Modeling Approaches in Lifetime Estimates

Prior to 1988, the results in Figure 1.1 are indicative of the range and means from 1-D models. After 1988, the ranges and means are from two-dimensional (2-D) models. As each model class matured in its ability to simulate the physical processes, and as more observations became available to evaluate the performance of the models, the model ranges for lifetimes have generally become smaller. The Kaye *et al.* (1994) lifetimes assessment used six 2-D and one 3-D model to calculate ODS lifetimes based on global atmospheric burdens and loss rates ($\tau = B/R$). The range of model-calculated CFC-11 lifetimes was 40-61 years, which was attributed to model differences in both photochemistry and transport. This assessment revealed that models used different CFC photolysis rates, and a comparison of simulated N_2O and CFC-11 profiles with mid-latitude data from balloons illustrated large differences in transport representation. The 1994 lifetime assessment noted that sparse global stratospheric data with large uncertainties in the middle stratosphere was a limiting factor in evaluating model transport and reducing the effect of transport uncertainty on the lifetime calculation.

Since the Kaye *et al.* (1994) assessment, an abundance of stratospheric trace gas observations from satellites (e.g., NASA's UARS and Aura, CSA's SCISAT, and ESA's Envisat) and high-flying aircraft campaigns has dramatically improved the understanding of stratospheric chemistry and transport. This in turn has allowed major improvements in the performance of 2-D and 3-D models. The concept of stratospheric mean age permits evaluation of model transport independent of chemistry. Hall *et al.* (1999) evaluated stratospheric transport in nearly two dozen 2-D and 3-D models using mean age derived from aircraft observations of CO_2 and SF_6 and the distribution of water vapor in the tropical lower stratosphere using satellite observations (Mote *et al.*, 1996). This study showed that most models had mean age younger than observed (i.e., had circulations that were too fast) along with too much horizontal mixing (i.e., not enough isolation of the stratospheric tropical upwelling region). They also demonstrated that distributions of long-lived trace gases such as N_2O and the CFCs were highly correlated with mean age, concluding that most models had significant transport inaccuracies.

The recent availability of multi-year global stratospheric constituent data sets has provided additional information necessary for model improvements. The advent of faster computers and inexpensive data storage has made it practical for 3-D models to be run at higher resolution and with more complete chemistry, allowing a more physical representation of atmospheric processes. In 2010, a comprehensive chemistry climate model evaluation project, the SPARC CCM Validation (CCMVal) (SPARC 2010), used observationally derived diagnostics to evaluate the representation of radiation, dynamics, chemistry, and transport in 18 CCMs. This project produced an unprecedented look 'under the hood' of the sophisticated 3-D models used in WMO (2011). Using diagnostics developed during CCMVal, chemical and transport processes essential for realistic representation of stratospheric composition and hence lifetimes are evaluated for the models used in this report.

Evaluating the uncertainties in a molecule's lifetime involves modeling its distribution in the atmosphere. Current 3-D coupled chemistry-climate models are time-consuming and expensive to run. Hence, a 2-D model is used in this chapter to estimate lifetimes and

uncertainties due solely to the uncertainties in the kinetic and photochemical parameters recommended in this chapter and compared with values obtained using the JPL10-6 recommended parameters (Sander *et al.,* 2011). The 2-D model produces an excellent simulation of stratospheric transport (e.g., age of air), and is an efficient tool for performing multiple simulations for the evaluation of lifetime uncertainties. The 2-D model is also used as an effective transfer standard between the more complex 3-D models in Chapter 5 and the complex photochemical and kinetic information of Chapter 3.

Chapter 4: Inferred Lifetimes from Observed Trace Gas Distributions

The aim of this chapter is to update atmospheric lifetimes (and uncertainties) using recent measurements from all observation platforms (surface *in-situ*, high-altitude (aircraft, balloon), and satellite retrievals) and appropriate models that utilize these observations.

Several approaches have been applied in the past to calculate atmospheric lifetimes of gases listed in Table 1.1 either by using atmospheric observations on their own or in combination with emission inventories. These methods are re-evaluated in Chapter 4 using both new measurement data and updated observation inversion models. Some methods derive instantaneous lifetimes, which then can be converted to steady-state lifetimes. In addition to the methods using *in-situ* and aircraft/balloon data this chapter gives a comprehensive overview of satellite observations and their ability to contribute new independent estimates of atmospheric lifetimes for ODSs and greenhouse gases.

Chapter 5: Model Estimates of Lifetimes

Analogous to the goals of Chapter 4, Chapter 5 uses CCMs (six 3-D models and one 2-D model) to estimate lifetimes of the gases listed in Table 1.1. In contrast to the methods used in Chapter 4, CCMs only use the atmospheric observations as boundary conditions so the lifetime estimates are purely model-based. Since the Kaye *et al.* (1994) lifetimes assessment, 3-D chemical-dynamical models have advanced significantly and are now more appropriate tools for lifetime estimates. The CCMs use an agreed-upon set of photochemical data (Sander *et al.,* 2011) and many have a realistic description of the transport, as judged by their ability to reproduce stratospheric distributions of a variety of long-lived trace gases and mean age-of-air (SPARC 2010). Chapter 5 applies key transport and photochemical diagnostics to the participating models, which were developed during the CCMVal-2 effort (SPARC, 2010). Model lifetime estimates for present-day conditions are interpreted in light of each model's ability to realistically represent essential stratospheric processes. Model simulations are also used to predict how lifetimes may change for a year 2100 atmosphere.

Chapter 6: Recommended Steady-State Lifetimes and Their Uncertainties

Key results relevant to the determination of steady-state lifetimes from Chapters 2 through 5 are presented. The lifetime estimates and other results from these chapters are merged to produce a recommended set of lifetimes along with their uncertainties (Tables 6-1 to 6-3). The methodology for merging the lifetime estimates and calculating uncertainties is given in the Appendix. In order to improve future lifetime estimates, research recommendations are made for closing scientific gaps in our understanding that limit the determination of lifetimes.

References

Cunnold, D., F. Alyea, and R. Prinn, A methodology for determining the atmospheric lifetime of fluorocarbons, *J. Geophys. Res., 83*, 5493-5500, 1978.

Cunnold, D. M., R. G. Prinn, R. A. Rasmussen , P. G. Simmonds, F. N. Alyea, C. A. Cardelino, A. J. Crawford, P. J. Fraser, and R. D. Rosen, The Atmospheric Lifetime Experiment. 3. Lifetime methodology and application to three years of CFCI3 data, *J. Geophys. Res., 88*, 8379-8400, 1983.

Douglass, A. R., R. S. Stolarski, M. R. Schoeberl, C. H. Jackman, M. L. Gupta, P. A. Newman, J. E. Nielsen, and E. L. Fleming, Relationship of loss, mean age of air and the distribution of CFCs to stratospheric circulation and implications for atmospheric lifetimes*, J. Geophys. Res., 113*, D14309, doi: 10.1029/2007JD009575, 2008.

Hall, T. M., D. W. Waugh,, K. A. Boering, and R. A. Plumb, Evaluation of transport in stratospheric models*, J. Geophys. Res., 104*, 18815-18839, 1999.

Hudson, R. D., and E. I. Reed, eds., *The Stratosphere: Present and Future,* NASA Reference Publication 1049, National Aeronautics and Space Administration, Goddard Space Flight Center, 1979.

IPCC (Intergovernmental Panel on Climate Change), *Climate Change 2007: The Physical Science Basis*, *Contribution of Working Group I to the Fourth Assessment Report of the Intergovernmental Panel on Climate Change*, edited by S. Solomon, D. Qin, M. Manning, Z. Chen, M. Marquis, K. B. Averyt, M. Tignor, and H. L. Miller, 996 pp., Cambridge University Press, Cambridge, U.K., and New York, NY, U.S.A., 2007.

Kaye, J. A., S. A. Penkett, and F. M. Ormond (eds.), *Report on Concentrations, Lifetimes, and Trends of CFCs, Halons, and Related Species*, NASA Reference Publication 1339, Washington, D.C., 1994.

Lovelock, J. E., R. J. Maggs, and R. J. Wade, Halogenated hydrocarbons in and over the Atlantic, *Nature, 241*, 194-196, 1973.

Molina, M. J., and F. S. Rowland, Stratospheric sink for chlorofluoromethanes: Chlorine atom-catalysed destruction of ozone, *Nature, 249*, 810-812, 1974.

Montzka, S. A., and S. Reimann (Coordinating Lead Authors), A. Engel, K. Krüger, S. O'Doherty, and W. T. Sturges (Lead Authors), Ozone-Depleting Substances (ODSs) and Related Chemicals, Chapter 1 in *Scientific Assessment of Ozone Depletion: 2010, Global Ozone Research and Monitoring Project–Report No. 52*, 516 pp., World Meteorological Organization, Geneva, Switzerland, 2011.

Mote, P. W., K. H. Rosenlof, M. E. McIntyre, E. S. Carr J. C. Gille, J. R. Holton, J. S. Kinnersley, H. C. Pumphrey, J. M. Russell,, and J. W. Waters, An atmospheric tape recorder: The imprint of tropical tropopause temperatures on stratospheric water vapor*, J. Geophys. Res., 101*, 3989-4006, 1996.

NAS, *Halocarbons: Effects on Stratospheric Ozone*, National Academy of Science, Washington, D.C., 1976.

Prinn, R. G., D. Cunnold, R. Rasmussen, P. Simmonds, F. Alyea, A. Crawford, P. Fraser, and R. Rosen, Atmospheric trends in methylchloroform and the global average for the hydroxyl radical, *Science, 238*, 945-950, 1987.

Prinn, R. G., and R. Zander (Lead Authors), D. M. Cunnold, J. W. Elkins, A. Engel, P. J. Fraser, M. R. Gunson, M. K. W. Ko, E. Mahieu, P. M. Midgley, J. M. Russell III,

C. M. Volk, and R. F. Weiss, Long-lived ozone-related compounds, Chapter 1 in *Scientific Assessment of Ozone Depletion: 1998, Global Ozone Research and Monitoring Project–Report No. 44*, World Meteorological Organization, Geneva, Switzerland, 1999.

Prinn, R. G., R. F. Weiss, P. J. Fraser, P. G. Simmonds, D. M. Cunnold, F. N. Alyea, S. O'Doherty, P. Salameh, B. R. Miller, J. Huang, R. H. J. Huang, D. E. Hartley, C. Harth, L. P. Steele, G. Sturrock, P. M. Midgley, and A. M. McCulloch, A history of chemically and radiatively important gases in air deduced from ALE/GAGE/AGAGE, *J. Geophys. Res.*, *105*, 17751-17792, doi: 10.1029/2000JD900141, 2000.

Rowland, F. S., and M. Molina, Chlorofluoromethanes in the environment, *Rev. Geophys., 13*, 1-35, 1975.

Sander, S. P., J. Abbatt, J. R. Barker, J. B. Burkholder, R. R. Friedl, D. M. Golden, R. E. Huie, C. E. Kolb, M. J. Kurylo, G. K. Moortgat, V. L. Orkin, and P. H. Wine, *Chemical Kinetics and Photochemical Data for Use in Atmospheric Studies, Evaluation Number 17, JPL Publication 10-6,* Jet Propulsion Laboratory, California Institute of Technology 2011.

SPARC CCMVal (Stratospheric Processes And their Role in Climate), *SPARC CCMVal Report on the Evaluation of Chemistry-Climate Models*, edited by V. Eyring, T. G. Shepherd, and D. W. Waugh, SPARC Report No. 5, WCRP-132, WMO/TD-No. 1526, http://www.atmosp.physics.utoronto.ca/SPARC/ccmval_final/index.php, 2010.

Volk, C. M., J. W. Elkins, D. W. Fahey, G. S. Dutton, J. M. Gilligan, M. Loewenstein, J. R. Podolske, K. R. Chan, and M. R. Gunson, Evaluation of source gas lifetimes from stratospheric observations, *J. Geophys. Res., 102*, 25543-25564, 1997.

Vollmer, M. K., B. R. Miller, M. Rigby, S. Reimann, J. Mühle, P. B. Krummel, S. O'Doherty, J. Kim, T. S. Rhee, R. F. Weiss, P. J. Fraser, P. G. Simmonds, P. K. Salameh, C. M. Harth, R. H. J. Wang, L. P. Steele, D. Young, C. R. Lunder, O. Hermansen, D. Ivy, T. Arnold, N. Schmidbauer, K.-R. Kim, B. R. Greally, M. Hill, M. Leist, A. Wenger, and R. G. Prinn, Atmospheric histories and global emissions of the anthropogenic hydrofluorocarbons (HFCs) HFC-365mfc, HFC-245fa, HFC-227ea, and HFC-236fa, *J. Geophys. Res*., *116* (D8), D08304, 2011.

Watson, R. T., M. A. Geller, and R. S. Stolarski, *Present State Of Knowledge of The Upper Atmosphere*, NASA Technical Memorandum 87-559, Washington, D.C., 1984.

Weiss, R. F., J. Mühle, P. K. Salameh, and C. M. Harth, Nitrogen trifluoride in the global atmosphere, *Geophys. Res. Lett., 35*, L20821, 2008.

WMO (World Meteorological Organization), *The Stratosphere 1981: Theory and Measurements, Global Ozone Research and Monitoring Project–Report No. 11*, Geneva, Switzerland, 1981.

WMO (World Meteorological Organization), *Atmospheric Ozone 1985, Global Ozone Research and Monitoring Project–Report No. 16*, Geneva, Switzerland, 1985.

WMO (World Meteorological Organization), *Report of the International Ozone Trends Panel 1988, Global Ozone Research and Monitoring Project–Report No. 18*, Geneva, Switzerland, 1988.

WMO (World Meteorological Organization), *Scientific Assessment of Stratospheric Ozone: 1989, Global Ozone Research and Monitoring Project–Report No. 20*, Geneva, Switzerland, 1989.

WMO (World Meteorological Organization), *Scientific Assessment of Ozone Depletion: 1991, Global Ozone Research and Monitoring Project–Report No. 25*, Geneva, Switzerland, 1992.

WMO (World Meteorological Organization), *Scientific Assessment of Ozone Depletion: 1994, Global Ozone Research and Monitoring Project–Report No. 37*, Geneva, Switzerland, 1995.

WMO (World Meteorological Organization), *Scientific Assessment of Ozone Depletion: 1998, Global Ozone Research and Monitoring Project–Report No. 44*, Geneva, Switzerland, 1999.

WMO (World Meteorological Organization), *Scientific Assessment of Ozone Depletion: 2002, Global Ozone Research and Monitoring Project–Report No. 47*, Geneva, Switzerland, 2003.

WMO (World Meteorological Organization), *Scientific Assessment of Ozone Depletion: 2006, Global Ozone Research and Monitoring Project–Report No. 50*, Geneva, Switzerland, 2007.

WMO (World Meteorological Organization), *Scientific Assessment of Ozone Depletion: 2010, Global Ozone Research and Monitoring Project–Report No. 52*, Geneva, Switzerland, 2011.

CHAPTER 2

The Theory of Estimating Lifetimes Using Models and Observations

Lead Authors:
R. Alan Plumb
Richard S. Stolarski

Co-Authors:
Michaela I. Hegglin
Michael J. Prather
C. Michael Volk

CHAPTER 2

The Theory of Estimating Lifetimes Using Models and Observations

Contents

This chapter sets the stage for subsequent chapters by defining lifetime and other metrics with units of time such as inverse loss frequency and mode time scales that apply to atmospheric constituents. It describes the approaches that have been used to estimate global lifetimes, and recognizes that definitions and interpretations in the literature (e.g., Junge, 1974; O'Neill *et al.,* 1994) have not always been consistent. For example, the lifetime of an atmospheric trace gas is often reported in assessments as a single constant, and here we show that the state of the atmosphere and the history of emissions can change the lifetime.

The chapter covers the underlying theory and methods, and not specific methods of implementation. The chapter begins with the definitions of loss frequency, time scales, and the various usages of lifetime. The lifetime of an emitted species is defined in terms of budgets, and as such it depends in general on the history and location of emissions, as well as on loss rates and the atmospheric circulation. When emissions balance losses, the budget is steady in time, and the steady-state lifetime of a gas is derived as the ratio of its global burden to net emissions (or sinks). For gases of interest in this assessment, we examine how the lifetime manifests itself in some simple instances such as constant source strength or source-free decay, and assess the general applicability of the steady-state lifetime. The application becomes more complex when the chemical loss of the gas is non-linear or is coupled with other gases. The second section of the chapter introduces the primary loss terms by region, considering stratosphere-mesosphere, troposphere, and the land surface/soils or ocean mixed layer as a third trace-gas reservoir. The third section of the chapter deals with the application of basic theory to the practical derivation of lifetimes with major subsections addressing lifetimes derived solely from model simulations (see Chapter 5) and lifetimes derived from a combination of measurements and models (see Chapter 4). A summary and recommendations conclude this chapter.

2.1 Time Scales and Lifetimes

2.1.1 Local Loss Rates and Global Lifetime

The concentration n of an atmospheric chemical constituent is governed by the continuity equation:

$$\frac{\partial n}{\partial t} + \nabla \cdot F = s - l \tag{2.1}$$

where n is the concentration (molecules per unit volume), F is the transport flux, and s and l represent local sources and sinks in molecules per unit volume per unit time. An important concept is the local loss rate, the rate at which a gas at a specific locality is destroyed due to chemical reaction at that location. Thus, assuming a first order, linear, loss ($l = \alpha n$ with α constant) and local chemical production to be independent of the constituent ($ds/dn = 0$), we can rewrite Equation (2.1) as:

$$\frac{\partial n}{\partial t} + \nabla \cdot F = s - \alpha n \tag{2.2}$$

where α is the local loss frequency. The local loss rate for dichlorodifluoromethane (CF_2Cl_2), for example, is essentially zero in the troposphere, as it has no local sinks. In the upper stratosphere, by contrast, its local loss rate is very fast ($\alpha^{-1} << 1$ year), as is evident in Figure 2.1. In fact, most of the loss of CF_2Cl_2 (or of N_2O or similar gases with stratospheric loss)

occurs in a fairly narrow region, indicated by the shaded area in Figure 2.1, where the inverse of the local loss rate starts to become comparable with or less than transport time scales.

The spatial distribution of such gases, with surface sources and stratospheric loss, is controlled by a balance between emissions, transport, and chemical destruction. For long-lived gases, the tropospheric time scales for vertical mixing (weeks) and global latitudinal mixing (months) tend to produce a nearly well-mixed troposphere with almost uniform mixing ratio (or mole fraction). For example in the 1980s when chlorofluorocarbons (CFCs) were increasing globally at 5-10% per year from northern sources, the largest gradients in the troposphere were 5-10% across the equatorial region.

As illustrated schematically in Figure 2.2, the stratospheric circulation picks up trace gases at the tropical tropopause and is characterized by tropical upwelling and extratropical downwelling. There appear to be two branches of the circulation (e.g., Birner and Boenisch, 2011; Volk *et al.,* 1996), the shallower branch extending into both hemispheres, while the deeper branch is concentrated in the winter hemisphere. This circulation is not the only factor affecting transport of trace gases; there is also quasi-horizontal (in fact, almost isentropic) mixing that acts more rapidly than the mean advection. Accordingly, tropospheric source gases are advected upward in the tropical stratosphere, and mixed outward into extratropical latitudes where the air subsides.

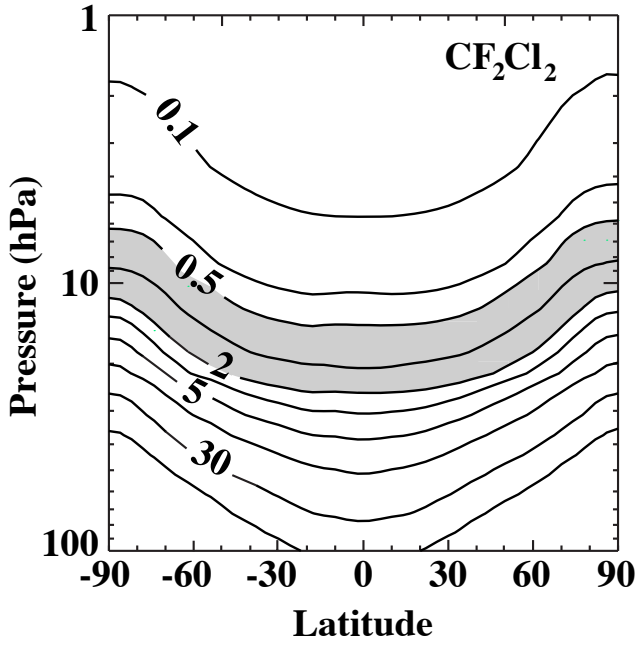

Figure 2.1. The inverse loss frequency (α^{-1}; yr) of CF_2Cl_2 as a function of latitude and altitude from Douglass *et al.* (2008). Within the shaded region, the inverse loss rate is between 0.5 – 2 yr and comparable with typical time scales for vertical transport in this part of the stratosphere.

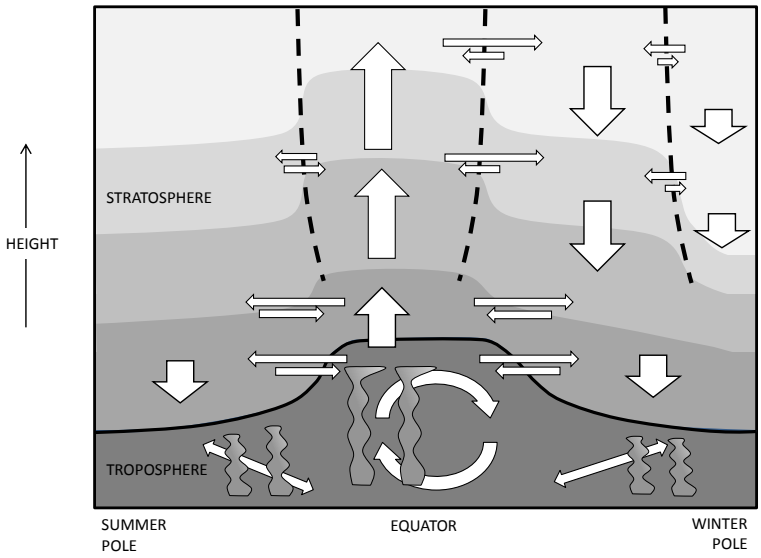

Figure 2.2. Schematic representation of stratospheric transport. The large upward/downward arrows depict vertical (diabatic) advection by the mean circulation: air ascends in the tropical stratosphere and descends within the horizontally well-mixed "surf zone" of the midlatitude winter hemisphere and within the winter polar vortex. The heavy dashed lines mark the partial transport barriers at the edges of the tropics, and the edge of the polar vortex; the heavy continuous curve marks the tropopause. Air is exchanged asymmetrically across the transport barriers, as depicted by the smaller horizontal arrows. These transport characteristics lead to characteristic poleward/downward slopes of the isopleths on long-lived tracers, which are depicted schematically by the background grey-scale shading, with slopes being greatest at the transport barriers.

The characteristic shape of the mixing ratio isopleths, bulging upward in the tropics and downward at high latitude, is determined primarily by transport, while the general decrease of mixing ratio with altitude is a consequence of chemical loss.

Integration of the local continuity equation over the entire globe gives the equation for the time evolution of the global atmospheric burden of a species:

$$\frac{\partial B}{\partial t} = S(t) - L(t) \tag{2.3}$$

where $B = \int n \cdot dV$ is the global burden (e.g., total number of molecules), $S = \int s \cdot dV$ is the globally integrated source (molecules/yr), and $L = \int l \cdot dV = \int \alpha n \cdot dV$ is the globally integrated loss (molecules/yr). Defining the global lifetime to be:

$$\tau = B/L \tag{2.4}$$

Equation (2.3) becomes:

$$\frac{\partial B}{\partial t} = S(t) - \frac{B}{\tau} \tag{2.5}$$

The global lifetime τ satisfies:

$$\tau^{-1} = \frac{\int \alpha n \cdot dV}{\int n \cdot dV} \tag{2.6}$$

so that the inverse of the global lifetime is a tracer-mass-weighted mean of the local loss frequencies (α).

In steady state, when emissions are exactly balanced by losses, the steady lifetime satisfies:

$$\tau_{ss} = \frac{B}{L} = \frac{B}{S} \tag{2.7}$$

As Equation (2.6) makes clear, the lifetime of any trace gas depends not only on the magnitude and distribution of chemical loss frequencies, but also on the spatial distribution of the trace gas itself. This in turn depends on loss rates, on transport, and on the history and location of emissions, and will therefore evolve with time as any or all of these factors change. There is, therefore, no unique lifetime for a given gas. After sources are removed, for example, decay of concentrations occurs at rates dictated by the modes of the unforced problem (i.e., of Equation (2.2) with s=0), so that, eventually, decay becomes dominated by the slowest decaying mode (Prather, 1994, 2007; Farrell and Ioannou, 2000). The time scale of this decay can be quite distinct from the steady lifetime τ_{ss} given by Equation (2.7) (Prather 1994; 1997; 1998). Accordingly, in principle one cannot rely on determinations of lifetime in near-steady state to predict rates of decay following removal of sources.

In practice, however, the distinction between steady lifetime and the time scale of decay may be very small, especially for long-lived gases with stratospheric sinks. Figure 2.3 illustrates this point with results from a one-dimensional model calculation for a gas with a surface source and a constant loss rate (i.e., constant α) confined to altitudes above 22 km. The source is introduced at t=0, and held constant until 50,000 days (137 years) of integration, at which time it is suddenly turned off. The figure shows the global burden *B* and the lifetime τ, as given by Equation (2.6), through the integration. During the period in which the source is present, the burden asymptotes toward steady state, and the lifetime rapidly adjusts to the steady value of 35.2 years. Following removal of the source, the burden exhibits near-perfect exponential decay; correspondingly, the lifetime, following a brief period of adjustment, arrives at the constant value 34.5 years, the time scale of the slowest eigenmode. The transition from steady state to decay, too rapid to be visible in Figure 2.3, is more complex as seen in Figure 2.4. The lifetime is slightly longer when forced to steady state by surface sources because there is more burden in the lower troposphere driving the flux into the stratosphere; and when left to decay, the troposphere becomes more uniformly mixed. The application of eigenvalues and eigenmodes in atmospheric chemistry is discussed in Prather (1994, 2007); Daniel and Solomon (1998); Manning (1999); Farrell and Ioannou (2000); Waugh and Hall (2002); and Ehhalt *et al.* (2004).

Such close correspondence between steady lifetime and decay times is in fact typical of long-lived gases with constant stratospheric sinks. A wide range of calculations with the same model, but sinks at different stratospheric altitudes, reveals that these two time scales differ by no more than 2% for gases with lifetimes greater than 10 years. (Note that this statement is not valid if the loss rate changes with time, as it can in coupled systems, even when the lifetime is long; such systems are addressed in Section 2.1.2, below.)

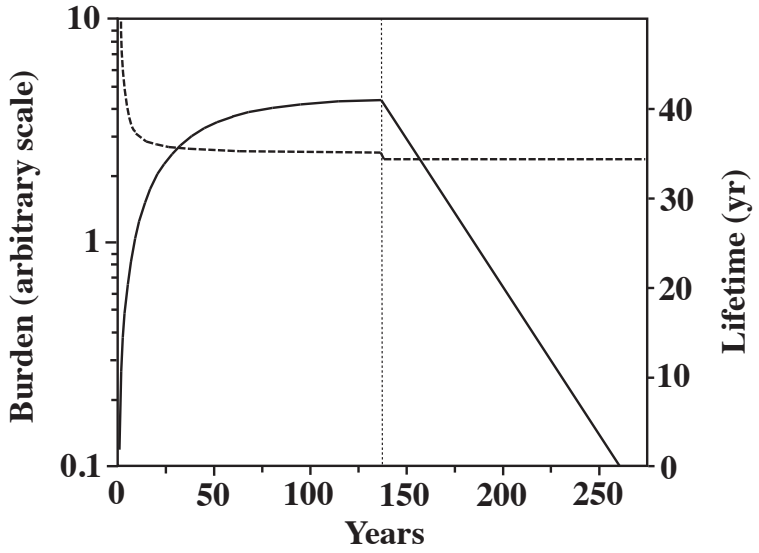

Figure 2.3. Results from a calculation from a one-dimensional model for a species with a surface source and stratospheric sink (in this case, above 22 km). The source is held constant for t<137 years, at which point it is suddenly removed. The solid curve shows the global burden, the dashed curve shows the lifetime defined by Equation (2.4).

For shorter-lived gases with tropospheric sinks, however, the differences become more substantial. An example is shown in Figure 2.4, for methyl bromide (Prather, 1997). The figure shows the evolution of the global burden and lifetime during decay of an initially steady solution following removal of sources. The decay of the burden is not quite exponential, the lifetime increasing from the steady value of 1.75 years to almost 2.1 years after 14 years. (Note this example does not include the oceanic reservoir and sink, which reduces the lifetime to about 0.8 year) In free decay, the abundance decreases fastest in the vicinity of the sinks, thereby reducing the total loss relative to the global burden and, thus, increasing the lifetime.

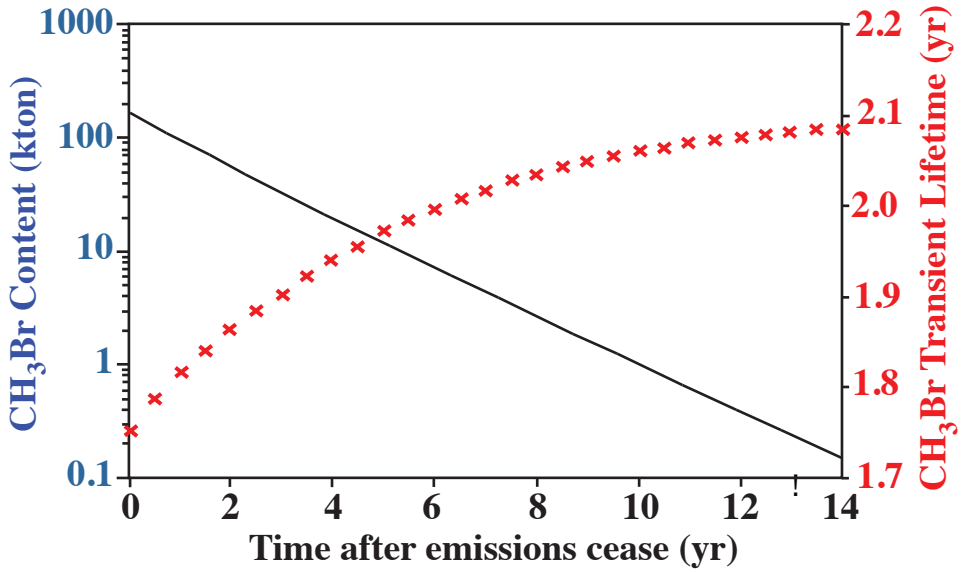

Figure 2.4. Evolution of methyl bromide (CH_3Br) following removal of sources. (After Prather, 1997) This case is atmosphere only; the inclusion of oceanic sinks and reservoirs drops the lifetime to 0.8 yr (see Hu *et al.,* 2012).

Accordingly, lifetimes determined from calculations of burden/loss in the presence of sources can be used with a good degree of accuracy to predict the source-free decay of long-lived gases with constant stratospheric sinks. Not so, however, for those shorter-lived gases with sinks in the troposphere, nor for coupled systems. The procedure for determining τ, using Equation (2.6), given good estimates for emissions and the global burden, will be addressed in Section 2.3.

2.1.2 Coupled Lifetimes

The recognition that atmospheric chemistry was coupled, that abundances of one gas could perturb those of another, was recognized early by Isaksen and Hov (1987). Prather (1994) developed this concept further by demonstrating theoretically that this coupling could change the inherent times scales of the system. He showed with eigenvalue decomposition that the methane (CH_4), carbon monoxide (CO), hydroxyl radical (OH) chemical system had a time scale for a CH_4 perturbation that was 1.4 times longer than the lifetime of CH_4 in the system. The basic idea is that an increase in CH_4 will increase CO and that both of these will decrease OH. The decrease in OH will slow the loss of CH_4 thus giving it an extended lifetime as seen in Figure 2.5. In fact, since a small change in OH affects the entire burden of CH_4 and not just the perturbation, the effect can be quite large. Thus the response time of methane to a perturbation will be longer than would be predicted from the steady-state lifetime.

A similar example for CO was shown by Daniel and Solomon (1998). They considered the characteristics of the CH_4, CO, OH chemical system in response to a CO pulse and showed that the CO steady-state lifetime was 52 days while the pulse-decay time averaged over the first 10 days of the model experiment was 58 days. These results follow directly from a simple linearization of the system and demonstrate that the longer time scale is nearly independent of the magnitude of the perturbation. As a result of these considerations, the greenhouse warming potentials (GWPs) for direct CH_4 emissions were revised upward by 40% in the Intergovernmental Panel on Climate Change (IPCC) Second Assessment Report (1996). An important corollary was that perturbations were coupled across species and hence emissions of the relatively short-lived species CO and nitrogen oxides (NO_x), for example, would produce a perturbation to atmospheric CH_4 that lasts more than a decade (Prather, 1996; Daniel and Solomon, 1998; Wild *et al.,* 2001; Derwent *et al.,* 2001). This resulted in indirect GWPs being assessed for direct emissions of NO_x, CO, and volatile organic compound (VOC).

The analysis of time scales was extended to more complex coupled systems like that of stratospheric nitrous oxide (N_2O), total reactive nitrogen (NO_y), and ozone (O_3) (Prather, 1998) where the coupling through transport (nearest neighbors) and radiation (non-local, overhead column O_3) was now included. An increase in N_2O increases NO_x, which reduces O_3 locally, allowing more ultraviolet (UV) penetration to layers below and increases N_2O loss by photolysis, thus decreasing its lifetime. N_2O in the coupled N_2O-NO_y-O_3 system thus responds to an increase with a time constant that is shorter than the steady-state N_2O lifetime. This 8% reduction in the effective GWP of N_2O was adopted in the IPCC Third Assessment Report (2001) based on 2-D model corroboration by AER, Goddard, and Oslo. Prather and Hsu (2010) completed similar century-long N_2O perturbation studies in a 3-D model with both stratospheric and tropospheric chemistry. Results confirmed the 8% offset between N_2O lifetime and time scale, and further identified the coupling of N_2O perturbations with tropospheric OH, whereby +10 molecules of N_2O induce –3.6 molecules of CH_4. This coupled CH_4 perturbation decays with the long-term N_2O primary time scale of a century,

rather than the decade time scale for CH_4. Similar assessment of CFC ozone depleters, focusing on the upper stratosphere where ClO+O reactions are important, has not yet been made.

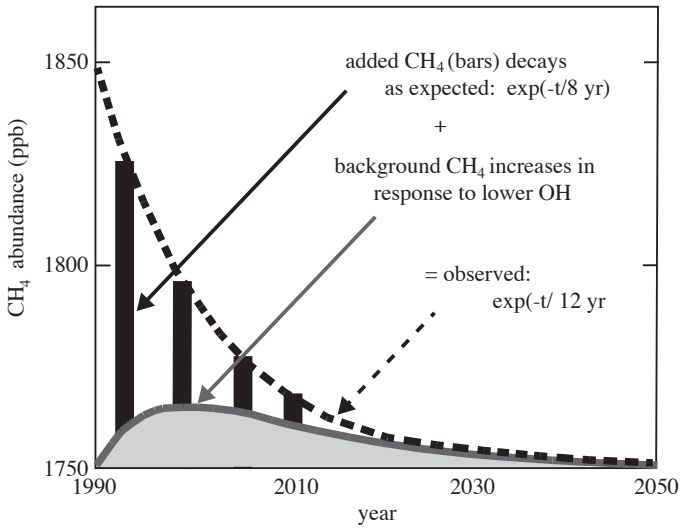

Figure 2.5. From Prather (2007), showing the decay response of pulses of CH_4 and the response of the background to the lower OH concentration caused by the CH_4 perturbation.

Why are chlorofluorocarbon (CFC) lifetimes so long?

- Time lag for transport from surface to stratosphere for chlorine release is 3-5 years.
- Stratospheric age of air ranges up to ~5 years.
- Loss rates in mid-stratosphere-to-mesosphere loss region are short (can be less than 1 year).
- So how do we get a 50- or 100-year lifetime?
- The loss region itself is a small fraction of the atmosphere.

Lifetime is governed by the rate of delivery of air containing the CFC to the loss region. Some of that air can be delivered rather quickly (3-5 years) in tropical upward motion. But no more than about 1% of air can be delivered from the troposphere (say, 200-1000hPa) to the atmosphere above 10 hPa in one cycle of the circulation, since the latter region contains 1/80 of the air mass of the former. The rest of the air will be detrained from the upward motion and re-circulated into the lower stratosphere or troposphere with no loss of CFC. The air will eventually be re-injected into the upward flow whence another fraction of the CFCs will be destroyed in the loss region. Thus the overall lifetime is extended by recirculation. The higher in the atmosphere that a species must go to experience the loss process, the longer will be the lifetime.

2.2 Loss Processes

Long-lived tracers (τ several decades or longer) have loss processes dominated by stratospheric photolysis with additional contributions in some cases from reaction with OH and $O(^1D)$. In general compounds with shorter lifetimes will be less effective at making it to the stratosphere. These molecules tend to be those with significant reactions with tropospheric OH. Finally, many species have both sources and sinks at the surface. A prime example is the methyl bromide (CH_3Br).

2.2.1 Stratospheric Loss

Stratospheric loss for many of the long-lived species, such as N_2O, trichlorofluoromethane ($CFCl_3$) and CF_2Cl_2, is dominated by photolysis, particularly in the spectral interval from 190 to 215 nm (Minschwaner *et al.,* 1993). The cross sections for absorption by long-lived species in this wavelength region vary slowly with wavelength compared to the extreme variation of the Schumann-Runge bands of molecular oxygen (O_2) that determine the amount of UV flux that penetrates into the stratosphere.

Figure 2.6 from Minschwaner *et al.* (1993) illustrates the altitude and wavelength dependence of the loss rate for $CFCl_3$ calculated using measured profiles of $CFCl_3$ and ozone for tropical noontime, equinox conditions.

At 40 km the loss rate has significant contributions between 190 and 220 nm. By 20 km the loss rate is constrained to wavelengths between 195 and 210 nm because both the shorter and longer wavelengths have been absorbed by O_2 and O_3. Note that the contours in Figure 2.4 represent changes of orders of magnitude. This was emphasized in Douglass *et al.* (2008) as shown previously in Figure 2.1, where it was pointed out that the effective photolysis occurs over a narrow range of altitudes.

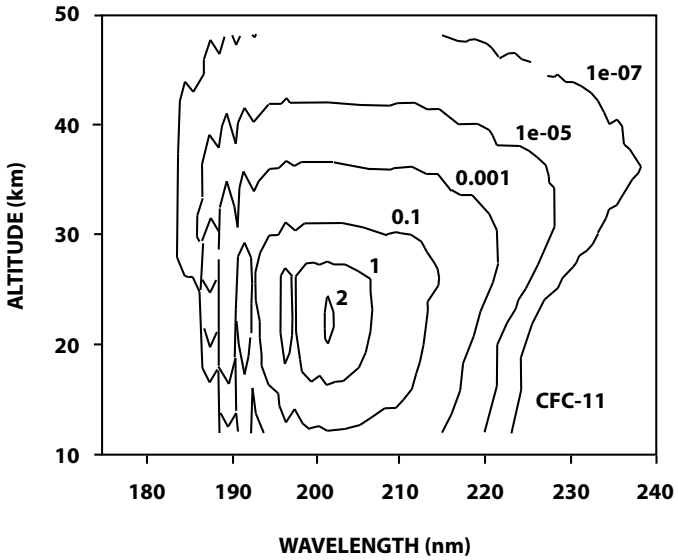

Figure 2.6. $CFCl_3$ loss rate (molecules $cm^{-3}sec^{-1}$ per nm) as a function of wavelength (nm) calculated with a photochemical model using measured concentrations of ozone and $CFCl_3$ (Minschwaner *et al.,* 1993). Calculations are for the tropics at local noon for equinox conditions. This calculation effectively combines the loss frequencies (shown for CF_2Cl_2 but not $CFCl_3$ in Figure 2.1) and the profile of the CFC.

The calculations of Minschwaner *et al.* (1993) illustrated that we can calculate loss rates from a photochemical model based on data in locations where we have measurements. Model output can be used to examine the spatial and temporal distribution of calculated loss rates in more detail. Figure 2.7 shows the loss rates for CCl_4, $CFCl_3$, CF_2Cl_2 and N_2O as a function of altitude and latitude. The results come from one of the models in Chapter 5 (GEOSCCM) and have been averaged over 6 years (2000-2005) of a time-dependent simulation. They thus represent annually averaged loss rates.

A problem with combining observations with a model for the photochemical loss frequency is that they may not be consistent with each other, and error in the photochemical model may induce biases in the integrated loss used to calculate the lifetime. One advantage of using a complete chemistry-transport model is self-consistency in that transport limits the fluxes of the trace gas to the regions of rapid loss. In all, the best solution is finding a self-consistent model that matches the measured abundances and thus should give the best value for integrated loss.

We can see from Figure 2.7 that the loss rates maximize at the lower altitude (higher pressure) for $CFCl_3$, and significantly higher altitude for CF_2Cl_2 and N_2O. The order of the altitude of maximum loss is in the same order as the increase in the lifetime of the species. Thus one of the major determinants of lifetime is the altitude at which loss occurs. This results from the fact that the lifetime for species that have only stratospheric losses, such as those in Figure 2.7, is dependent on the rate at which those species can be transported to the loss region. Once air containing these species reaches the loss region, loss occurs rapidly.

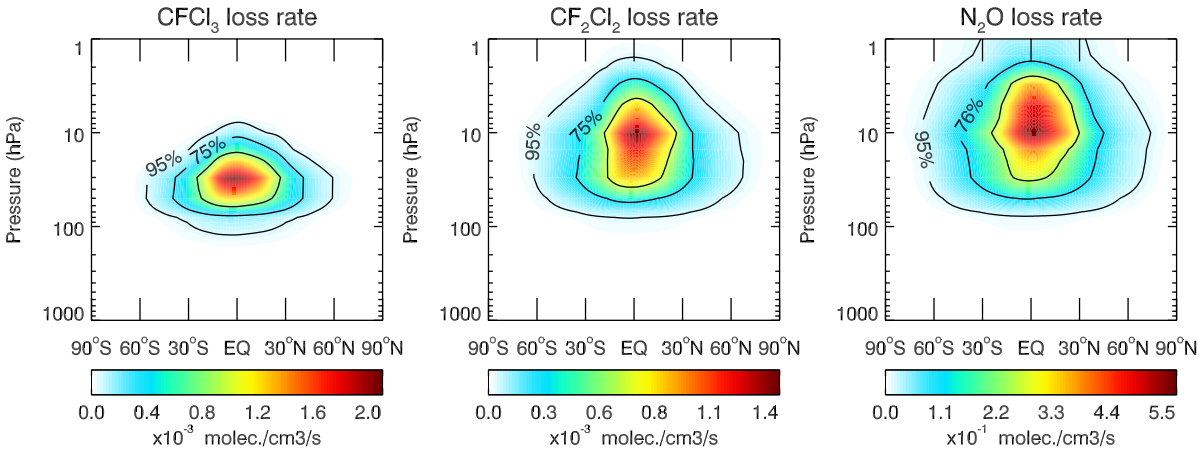

Figure 2.7. An example of latitude-pressure cross section of zonally integrated annual loss rates (molecules cm^{-3} $s^{-1)}$o) of $CFCl_3$, CF_2Cl_2, N_2O between 2000 and 2005 from the WACCM REF-C1 simulation (see Chapter 5) with warm colors indicating faster loss rates. The solid contours outline the regions within which 95%, 75% and 50% of the loss occurs. Loss rates values are given by the colors as indicated in the color bars below each panel.

2.2.2 Tropospheric Loss by Reaction with OH

Hydrochlorofluorocarbons (HCFCs) and hydrofluorocarbons (HFCs), along with methane, methyl chloride, and other hydrogen-containing compounds have losses dominated by reaction with tropospheric OH. Given the short time scale for odd hydrogen (HO_x) chemistry and large variations in OH concentration, there is no way to measure directly the global abundance of tropospheric OH. Most evaluations of lifetimes of these compounds depend on estimates of tropospheric OH from models that inform us on how to scale the integrated loss from one gas to another (Prather and Spivakovsky, 1990; Spivakovsky *et al.,* 2000; Lawrence *et al.,* 2001). When calculating a "mean OH concentration" it is important to carefully define the weighting kernel and recognize that even tropospheric mean OH varies almost a factor of 2 for different weightings (Prather and Spivakovsky, 1990; Lawrence *et al.,* 2001). The modeled mean OH is weighted by mass and the loss rate that is dependent on temperature (for methyl chloroform (CH_3CCl_3) the temperature dependence is $e^{-1520/T}$). The resulting OH concentrations have been tested by comparisons to estimates derived from methyl chloroform and its time trend (e.g., Prinn *et al.,* 1995; Montzka *et al.,* 2011). Going from the observed decay of methyl chloroform to an estimate of its lifetime against OH-loss and then deriving the similar lifetime for CH_4 requires careful attention to the loss by other processes (e.g., ocean exchange (Wennberg *et al.,* 2004) and stratospheric photolysis) and the correct atmospheric burden, see Prather *et al.* (2012). These scaling approaches do not work for short-lived halocarbons, some of which are important to lower stratospheric ozone, for which the lifetime depends on where and when emissions occur. Investigation of very short-lived halocarbons (Ko *et al.,* 1997) was spurred by the U.S. EPA workshop in 1999 (Bridgeman *et al.,* 2000; Wuebbles *et al.,* 2001; Olsen *et al.,* 2000). A theoretical framework for handling the geographic dependence of such short-lived species is discussed in Pisso *et al.* (2010) and Brioude *et al.* (2010).

If the emissions of CH_3CCl_3 are well known, then an average OH concentration can be derived from knowledge of the reaction rate coefficient for OH + CH_3CCl_3.

The average obtained for tropospheric loss of methyl chloroform or of methane will be heavily weighted towards the tropical lower troposphere as illustrated in Figure 2.8. The reactions of these molecules with OH are strongly temperature dependent (exp(-1775/T) for methane and exp(-1520/T) for methyl chloroform (from the JPL-2010 kinetics evaluation (Sander *et al.,* 2011)). Although each of these molecules will have its loss weighted towards the tropical lower troposphere, the differences in temperature dependence of their reaction rates with OH will lead to a difference in the effective average OH concentration (Prather and Spivakovsky, 1990; Lawrence *et al.,* 2001).

While both methane and methyl chloroform have their predominant losses in the troposphere, they also have stratospheric losses. It is sometimes beneficial to separate these losses and calculate individual losses and lifetimes for the troposphere and stratosphere. Thus we can rewrite Equation (2.4) as:

$$\frac{1}{\tau} = \frac{L_{strat} + L_{trop}}{B} = \frac{1}{\tau_{strat}} + \frac{1}{\tau_{trop}} \tag{2.8}$$

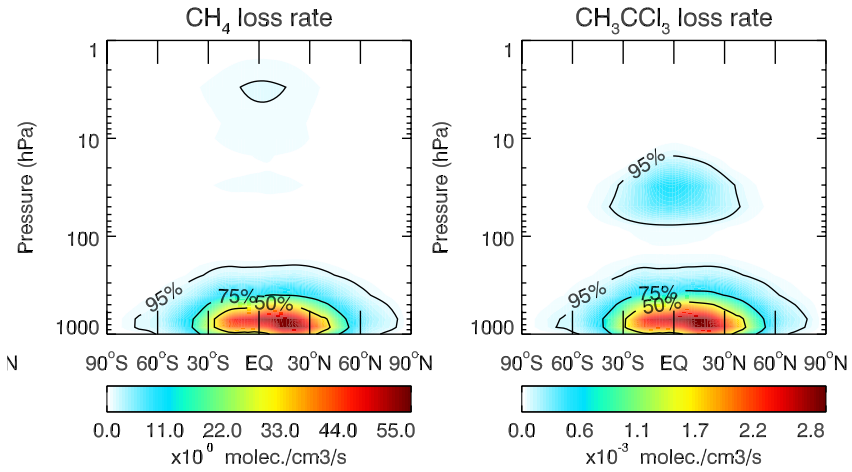

Figure 2.8. Same as Figure 2.7, but for CH_4 and CH_3CCl_3. These species are destroyed primarily through reaction with OH, except in the stratosphere where CH_3CCl_3 is destroyed primarily through photolysis.

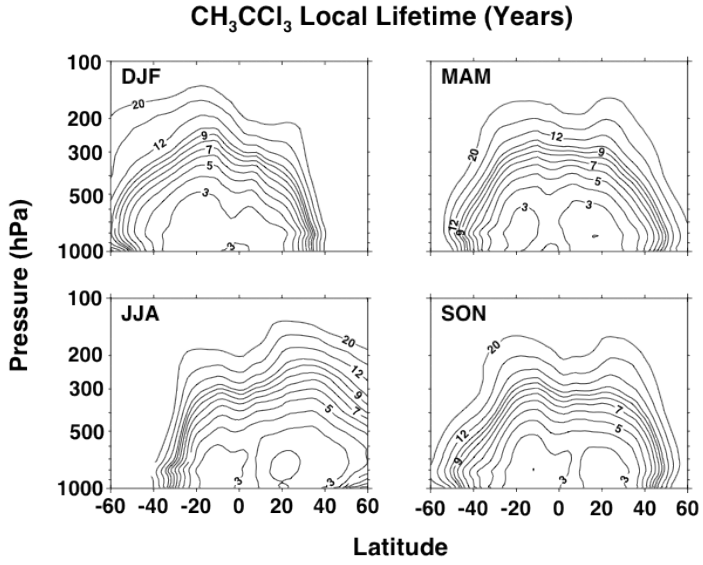

Figure 2.9. Inverse loss frequencies (yr) for methyl chloroform (CH_3CCl_3) as a function of latitude and pressure, averaged zonally and over a season. Computation is for 2005 conditions in GEOSCCM.

Local lifetimes for loss by reaction with OH calculated from the inverse of the loss frequency are shortest in the tropical lower troposphere. Figure 2.9 illustrates the seasonal variation of the local lifetime for methyl chloroform reaction with OH. The local lifetimes are somewhat less than 3 years in the tropical lower troposphere and the minimum shifts toward the summer hemisphere as a function of time of year.

When a molecule has a tropospheric lifetime of less than a year (e.g., bromoform, $CHBr_3$), the average loss frequency over all seasons would not correctly represent the lifetime. The actual lifetime would depend both on the time of year of the release and on the location of the release relative to the primary region for loss. Even with uniform emissions the abundance

and losses are less in the summer season. Brioude (2010) and Pisso *et al.* (2010) considered the impact of emission location on the calculated ozone depletion potential for several short-lived species. If a short-lived species is emitted at mid or high latitudes, much of it will be lost before it reaches the tropics where it can be injected into the stratosphere to have a potential impact on ozone. Conversely, emissions in the tropics near the region of injection into the stratosphere can make a larger contribution to potential ozone depletion. The same principle affects the lifetime of a short-lived species, but in the other direction. Emissions far from the tropical lower troposphere will result in longer lifetimes while emissions in the tropical lower troposphere will have shorter lifetimes.

2.2.3 Loss at the Surface and Additional Reservoirs

For species such as methyl bromide (CH_3Br) the ocean mixed layer is an additional reservoir, having both internal production and loss, and being able to serve as either source or sink for the atmosphere (Butler, 1994; Prather, 1997; Yvon-Lewis and Butler, 1997). The impact of changed emissions of methyl bromide must take into account this additional reservoir, both in terms of integrating losses and in terms of integrating the total burden of CH_3Br that is used in the lifetime definition. The lifetime will be determined by a combination of the lifetimes for loss in the troposphere and stratosphere as before but with inclusion of the ocean layer and soil uptake (Rhew *et al.,* 2003):

$$\frac{1}{\tau} = \frac{1}{\tau_{ocean}} + \frac{1}{\tau_{soil}} + \frac{1}{\tau_{trop}} + \frac{1}{\tau_{strat}}$$

Hu *et al.* (2012) have recently shown that the measured oceanic saturation anomalies for CH_3Br are significantly smaller than those measured previously. They attribute this to the decrease in the atmospheric concentrations of CH_3Br under the provisions of the Montreal Protocol. They point out that a further decrease in the atmospheric concentration could result in the ocean becoming a net source for CH_3Br. These results indicate a limitation in the conceptual model of considering the ocean (or possibly even the land) as a boundary condition with known fluxes. A more complete conceptual model would include oceanic boxes for CH_3Br that could react with changes in the atmosphere.

In the case of CH_4 (and several other gases), we need to consider also the lifetime against loss by soil uptake and by tropospheric Cl radicals:

$$\frac{1}{\tau_{CH_4}} = \frac{1}{\tau_{OH}} + \frac{1}{\tau_{Cl}} + \frac{1}{\tau_{soil}} + \frac{1}{\tau_{strat}}$$

2.3 Methods for Calculating Lifetimes and Time Scales

2.3.1 Model-Based Computations from Burden over Loss

2.3.1.1 Atmospheric Variability

The standard method for determining global lifetimes from model computations is to use the definition (2.4) of lifetime as the global atmospheric burden divided by the global atmospheric loss. This method is an extension of the method of instantaneous rates applied by Minschwaner *et al.* (1993) to a limited set of measurements. For model output or a modern global satellite data set, a full year (or even several years) is used to calculate the

annual average burden of the molecule in question and to calculate the annual average loss rate. Calculating total loss from data is not completely model free as the photolysis must be determined using a radiative transfer code and ozone concentrations obtained from either data or models. A molecule with a lifetime of many decades (such as CFCs or N_2O) will be subject to many seasonal cycles during its time in the atmosphere and the average over these seasonal cycles will give an accurate representation of its lifetime. A lifetime calculated in this manner may still be referred to as an "instantaneous" lifetime although it was actually averaged over one or more years. A similar concept is applicable to variations over the quasi-biennial oscillation and El Niño cycles.

2.3.1.2 Atmospheric Change over Time

Butchart *et al.* (2006) demonstrated that all of the climate models they diagnosed predicted an increase in the speed of the Brewer-Dobson circulation as CO_2 was added to the model's atmosphere. Douglass *et al.* (2008) showed that, in their chemistry climate model (CCM), the speed-up of the Brewer-Dobson circulation corresponded to a decrease in the atmospheric lifetime of CFC-11 by 5 to 10% by the year 2100 and almost no change in the CFC-12 lifetime. They also deduced a current lifetime for CFC-11 that was ~20% greater (56 years) than that used in recent assessments (45 years). They attributed the difference to the modern general circulation models that have a slower stratospheric circulation than those that were in use at the time the 45-year lifetime was established, but it could also be that the value of 45 years determined from the observed CFC-11 vs. age relationship (Volk *et al.,* 1997) needs revision (Section 2.3.3). The above discussion emphasizes that the lifetime of a molecule is dependent on the state of the atmosphere. For long-lived CFCs we saw above that the lifetime was controlled by the rate of transport to the region of primary loss. Changing the underlying atmospheric dynamics will change the atmospheric distribution of the gas and therefore the "instantaneous" lifetime that we deduce.

Aside from changes in the transport patterns, climate change can also affect tracer lifetimes through redistribution of ozone and resulting effects on ultra-violet radiation and ozone transport into the troposphere (Stevenson *et al.,* 2006; Hegglin and Shepherd, 2009) or through changes in climatological temperature distributions. In the stratosphere, temperatures are predicted to decrease due to increasing greenhouse gases, which leads to an increase in ozone due to a slowing down of ozone loss reactions (Li *et al.,* 2009). In the troposphere, increasing temperatures are expected to affect the lifetime of methane due to effects of rising atmospheric water vapour content on OH-abundances, the effect of rising temperature on the OH + CH_4 reaction rate, and the effects of increasing NO_x sources from lightning, fires, and soil emissions (John *et al.,* 2012) as discussed further below.

2.3.1.3 Source Variability over Time

Instantaneous lifetimes can be calculated from either observations or a model simulation by evaluating the total loss term and dividing it into the total burden as indicated by Equation (2.3). As mentioned earlier, the instantaneous lifetime is not exactly the same as the steady-state lifetime. We can estimate the difference by solving Equation (2.5) for τ without invoking the steady-state approximation:

$$\tau(t) = \frac{B(t)}{S(t) - \partial B/\partial t} \tag{2.9}$$

Thus, for example, during the 1980s when CFCs were increasing at about 5%/year, the calculated instantaneous lifetime using the steady relationship (2.7) based on net emissions, τ=B/S, would be biased about 5% high compared to the definition (2.4). In 2010 CFCs were decreasing and the instantaneous lifetime would be biased low by the current decay rate, ~2% for CFC-11 and ~1% for CFC-12. In the context of the discussion above, following Equation (2.7), these differences reflect the impact of growth and decay of the CFC abundances on their spatial distributions. In general, note that Equation (2.9) still yields the instantaneous lifetime, not the steady-state lifetime, since the spatial structure of the gas within the atmosphere will differ in the two cases (cf. Equation (2.6) and subsequent discussion).

As discussed above, the lifetime of methane can be strongly affected by changes in methane emissions itself due to the potential feedbacks on OH abundances. For different climate change scenarios John *et al.* (2012) found that the methane lifetime decreases between 5 and 13% between 1960 and 2100, except for the most extreme warming case (RCP8.5), where the lifetime increased by 4%. This increase was due to a near doubling of CH_4 emissions in this simulation. On shorter timescales, source variability is especially hard to assess in the case of methane due to relatively large natural and intermittent sources such as volcanic eruptions, wildfires, permafrost, oceans, low-latitude wetlands, and termites (Lelieveld *et al.,* 1998).

2.3.2 Inverse Methods

In forward models, of the type just discussed, the tracer continuity Equation (2.2) is used to calculate concentrations from given atmospheric transport parameters, sources and loss rates as the drivers of the system. Inverse modeling, by contrast, is an approach used to estimate these drivers based on observed concentrations as constraints to the model output. The relationship between the model variables (called state vector x) and the observed variables (called the observational vector y) is given by the forward model F

$$y = F(x, b) + \epsilon \tag{2.10}$$

where b represents the known model parameters and ε is the error vector describing the uncertainty in the observations, the known model parameters, and the forward model. The choice of which variables to include in x or b is dependent on the variable that needs to be optimized. x can then be calculated given y from the inversion of Equation (2.10).

The forward model used in inverse modeling approaches can be of different complexity, from simple single-box (e.g., Cunnold *et al.,* 1983; Montzka *et al.,* 1999, 2011) or multi-box models (Rigby *et al.,* 2012) to full chemistry transport models (e.g., Hartley and Prinn, 1993; Bergamaschi *et al.,* 2009; Lee *et al.,* 2011; Patra *et al.,* 2011). In the single- to multi-box models, the model parameters are strongly simplified, but offer the advantage that the computational costs are small and large sets of runs can be carried out easily to test the sensitivity to changes in the different model parameters. Accurate knowledge of the emissions is necessary in order to obtain meaningful lifetime estimates, which is not readily available for all species of interest (see Montzka *et al.,* 2011). Chemistry transport models (CTMs) on the other hand rely on the quality of model transport, which is known to have limitations and can lead to error growth as many studies on inverse modeling of emission sources have shown (Hartley and Prinn, 1993), also a valid concern for inverse modeling used to estimate lifetimes. An advantage is that these models can be used also for shorter-lived species that are not well mixed in the atmosphere.

Sufficiently simple forward models can sometimes be inverted, either exactly or statistically. But especially for CTMs, the forward model is too nonlinear to invert and so a linearization of the forward model is employed. The simplest case is provided by sequential estimation. Let the gridded concentrations in the CTM at time t be the state vector $x(t)$, and the observations be the observational vector $y(t)$. Given an initial condition, the CTM is used to produce a forecast or an a priori (x_a) at a subsequent time. The forward model is linearized around this *a priori* estimate yielding

$$y = F(x_a, b) + k(x - x_a) + O((x - x_a)^2) \tag{2.11}$$

where $K = \partial y / \partial x$ is the Jacobian matrix of the forward model evaluated at $x = x_a$.

If the dimension of *y(t)* equals the dimension of *x(t)*, then (assuming no error) the Jacobian is invertible, yielding the state vector

$$x = x_a + K^{-1}(y - F(x_a, b)) \tag{2.12}$$

In practice, however, the observations are usually sparse so the dimension of *y(t)* is much smaller than the dimension of *x(t)*. Then the Jacobian is not invertible, and the estimate of *x* can only be optimal, not exact, i.e., representing the most likely state given knowledge of the uncertainties in both observations and forward model parameters, taking account of any expected correlations between parameters. For a full discussion of the inverse modeling approach the reader is referred to Kalnay (2003).

Examples, and further discussion, of the application of the inverse modelling approach to the determination of lifetimes is given in Chapter 4.2.1.

2.3.3 Relative Lifetimes: Tracer-Tracer Method

Plumb and Ko (1992) showed that the compact relationships between two long-lived stratospheric species could be used to determine their relative lifetimes. (In this context, "long-lived" implies that local loss rates are slow compared to transport rates.) Under their assumption that rapid isentropic mixing is global in extent, then the ratio of net global fluxes of two species of mixing ratio χ_1, χ_2, through a surface of constant mixing ratio (such surfaces coincide where the species are locally long-lived) is

$$\frac{F_1}{F_2} = \frac{d\chi_1}{d\chi_2} \tag{2.13}$$

i.e., the slope of the tracer-tracer relationship evaluated at the mixing ratios on the surface. If this surface is chosen to lie below all sinks of the two tracers then, in equilibrium, these fluxes balance the net losses. Hence, if the atmospheric burden of each is known, the ratio of lifetimes is

$$\frac{\tau_1}{\tau_2} = \frac{B_1}{B_2} \cdot \frac{d\chi_2}{d\chi_1} \tag{2.14}$$

where B_1 and B_2 are the respective burdens.

In fact, if the tracer surface chosen is located very close to the tropopause (and the tropopause does indeed appear to coincide with isopleths of long-lived species; Prather *et al.* (2011)), then the local mixing ratios are approximately representative of tropospheric values, and the net atmospheric burden of each tracer is approximately the product of the mixing ratio and the atmospheric mass. In that case, the ratio of lifetimes is

$$\frac{\tau_1}{\tau_2} \approx \frac{\chi_2}{\chi_1}\frac{d\chi_1}{d\chi_2} \tag{2.15}$$

The greatest advantage to this approach is that it can be applied from local observations without model input, i.e., that observations in the extratropical lower stratosphere are sufficient to determine the slope of the tracer-tracer relationship and thence to obtain the lifetime ratio. The disadvantage is that Equation (2.15) delivers the ratio of two lifetimes, and not the absolute value of either. However, Volk *et al.* (1997) used "age," determined from the temporal tracer SF_6, as a reference, since its flux is known from first principles. For a linearly growing, transient, tracer the local age is just the time lag of mixing ratio $\chi(t)$ relative to that, $\chi_o(t)$, at the tropical tropopause, i.e.,

$$\Gamma = \frac{\chi_o(t) - \chi(t)}{\partial\chi/\partial t} \tag{2.16}$$

from which age (using (2.1)) can be treated itself as a tracer with a unit source,

$$\nabla \cdot F_r = 1 \tag{2.17}$$

and a boundary condition Γ_0=0 (Boering *et al.,* 1996; Waugh and Hall, 2002). In equilibrium, the global flux of age through any global surface is known from first principles to equal the mass of the atmosphere M_u above the surface (Volk *et al.,* 1997; Neu and Plumb, 1999; Plumb, 2002). Equation (2.13) can be used to derive the net flux of any species from the slope of the tracer vs. age (or tracer vs. transient tracer) relationship, thus yielding an absolute estimate of tracer lifetime, i.e.,

$$\tau = -\frac{d\Gamma}{d\chi}\cdot\frac{B}{M_u} \tag{2.18}$$

However, Plumb and Ko's result (2.13) rests on assumptions about stratospheric transport (specifically, the absence of transport barriers) that are now known to be invalid. In particular, the assumption that isentropic mixing has global reach led to the conclusion that net vertical transport of tracers (through surfaces of constant mixing ratio) is equivalent to vertical diffusion, and hence that the net vertical flux is proportional to the vertical gradient of mixing ratio. It is this equivalence on which the result (2.13) rests.

The theory of tracer-tracer relationships for the more realistic case with leaky subtropical barriers was outlined in detail in Plumb (2007; see also Volk *et al.,* 1996, 1997; Neu and Plumb, 1999). For the issues of interest here, the most important consequence of the presence of barriers is that the net vertical tracer flux is not purely diffusive, but partly advective, thus undermining (2.13). The implications for these developments for the determination of lifetimes have not been fully addressed in the literature. However, Plumb (2007) argued that the flux-gradient relation remains approximately valid for *locally*

conserved tracers in equilibrium, thus allowing determination of *relative* lifetimes of such tracers via Equation (2.14). However, since age has a source everywhere, no similar relationship has been demonstrated under such circumstances when age is one of the tracers. At present, therefore, use of tracer-age slopes to determine *absolute* tracer lifetimes is open to question.

Aside from such unresolved conceptual matters, there are also practical difficulties with the application of the absolute method. These difficulties, discussed by Volk *et al.* (1997), include the errors inherent in determining age from observations of transient tracers such as SF_6 or CO_2 (neither of which is growing perfectly linearly, although correction can be made for this) and in calculating the tracer-age slope at the tropopause, given the observed fact that the age-tracer relationship for many species of interest is curved in the lower stratosphere. (Both of these issues are evident in, e.g., Figure 6 of Volk *et al.* (1997).)

Another limitation of the applicability of both Equations (2.15) and (2.18) is the requirement of an equilibrium situation, which is rarely met in practice. Atmospheric growth of a tracer adds curvature to its correlation with another tracer (or with age) resulting in a change of the correlation slope at the tropopause on the order of $\sim 0.1\tau$ times the relative growth rate, e.g., ~10% for a lifetime of 100 years and a growth rate of 1% per year (Volk *et al.,* 1997). A formalism to correct the correlation slopes for tracer transience has been developed by Volk *et al.* (1997). Taking advantage of the fact that tracer mixing ratios are tightly correlated with age in the extratropical lowermost stratosphere, the method derives tracer-age slopes representative of a steady-state situation using the observed (transient) tracer-age slopes at the *extratropical tropopause* along with the temporal development of the tropospheric mixing ratio and information on the width of the stratospheric age spectrum. Use of these corrected (steady) slopes in Equations (2.15) and (2.18) then yields, in principle, (relative) steady-state lifetimes (within the various conceptual and practical limitations discussed above).

Finally, the theoretical basis of the tracer-tracer method has not, as yet, taken account of the seasonal variability of transport. At this stage, therefore, there is little if any theoretical guidance on how best to deal with such variability when applying the technique to observations or model output.

2.4 Summary

Lifetime is a combined property of the molecule, the background atmosphere (combined chemistry and transport), and the emission scenario. The lifetime can be defined from the global budget as the total burden in the atmosphere divided by the integrated loss over the entire atmosphere. The result depends on loss processes for the specific gas and on the distribution of the gas, which can depend on the emission scenario. The lifetime computed from the global budget is sometimes referred to as an instantaneous lifetime as it is calculated from the state of the atmosphere at a specific time or averaged over a short time interval such as a single year or a few years.

When emissions are continued long enough for the system to reach a steady state in which the average source equals the average loss, we can define a steady-state lifetime from the burden over the loss. The steady-state lifetime depends in principle on the emission pattern used to create that steady-state pattern of abundance, though for long-lived gases it is insensitive to the pattern of surface sources.

A response lifetime is defined simply from the change in burden divided by the change in loss caused by a given perturbation and will differ from the global lifetime when there are chemical feedbacks. The lifetime can be represented as a weighted mix of the time scales (e-folding times) that describe the temporal response of the atmosphere to a single pulse of a gas. It is not in general equal to any one of the time scales. These individual time scales depend on both transport times and local chemical time scales but not on the emission pattern. When the source of a gas is suddenly eliminated, the decay rate of the gas will evolve from the inverse of its instantaneous lifetime to that of a freely decaying mode (the longest time scale).

For gases that are well mixed in the troposphere, lifetime is a reasonably robust concept. The steady-state lifetime is then nearly independent of where the gas is emitted within the troposphere. Well-mixed gases have lifetimes (against surface emissions) of a couple years or more, and steady-state tropospheric variability of about ten percent or less. Thus, well-mixed gases include both long-lived CFCs and relatively short-lived gases like CH_3CCl_3 and some HFCs.

For gases that are not well mixed, the lifetime and time scales must be carefully diagnosed for emissions that vary with time, either systematically or seasonally, and location. The difference between lifetime and decay time can be substantial, making problematic the use of steady lifetimes to predict the future evolution. These not-well-mixed gases include gases like CH_3Br and $NO+NO_2$.

Comprehensive atmospheric chemistry-transport models provide the most self-consistent framework for calculating lifetimes, but the accuracy of such lifetimes can only be based on the corresponding ability of the models to simulate the observed abundances and atmospheric distributions of many trace species, thus requiring accurate transport and chemistry.

Determination of lifetimes from observation has improved greatly with the availability of global, satellite-based retrievals of important trace gases and *in situ* campaign data with simultaneous, high precision measurements of multiple species.

Direct determination of lifetimes from global burdens and loss rates via Equation (2.4) requires global information about both over a large altitude and temporal range, and the accuracy of any such determination depends on the availability of such data. Models provide this information, but the reliability of lifetimes thus calculated rests on the accuracy with which the models represent reality. Determination via (2.4) from observations has become feasible, as global satellite-based retrievals of many of the important trace gases are now available, but theoretical loss rates (to calculate L) or accurate source information (if Equation (2.7) is used) are also required.

Tracer-tracer methods appear to be theoretically justified, and useful in practice, as a route to calculating *relative* lifetimes against stratospheric loss and they are applied as such in Chapter 6. However, use of age, or of a transient conservative tracer, as a reference in order to yield *absolute* lifetimes is problematic, given current perspectives on the nature of stratospheric transport, and is likely to yield inaccurate answers. Specifically, model experiments conducted for Chapter 5 imply that lifetimes thus calculated are likely to be underestimated by about 20%. This systematic error is in addition to errors incurred as a result of the difficulty in determining accurate tracer-age slopes, both from observations (Volk *et al.,* 1997) and models (Chapter 4).

By whichever means lifetime is calculated, temporal variability – of the atmosphere, or of sources – must be borne in mind. The stratosphere, especially, exhibits a high degree of interannual variability and the impact of such variability on calculated lifetimes should not be ignored. Moreover, lifetimes can also change with time if the sources change, because of the dependence of net loss on the spatial distribution of the gas. For a source gas whose source is suddenly eliminated, its decay rate will evolve from the inverse of its steady-state lifetime to that of a freely decaying mode. For long-lived gases with stratospheric sinks, the difference between steady lifetime and decay time is very small; hence lifetimes determined for current conditions are useful as predictors of future decay if sources are removed. For shorter-lived gases with tropospheric sinks, however, the differences are substantial, making problematic the use of current lifetimes to predict future evolution.

Table 2.1 below is a short guide to connect the description of the theory of various methods for determining lifetime to the subsequent chapters that describe and apply those methods.

Table 2.1. Short guide to the use of methods in subsequent chapters of this report.

Section	Method	Chapter
2.3.1	Model-based computations from burden over loss	3, 5
2.3.1	Observation-based computations from burden over loss	4
2.3.2	Inverse methods	4
2.3.3	Tracer-tracer methods	4

In the box below we summarize the definitions of lifetime used throughout this report.

Lifetime Definitions

Global Atmospheric Lifetime (τ): Calculated from the global budget equation of a species as global atmospheric burden divided by global loss rate. This is also called an **instantaneous lifetime** and has been referred to as a **turnover time**.

Transient lifetime (τ): Another term for global atmospheric lifetime or instantaneous lifetime of a gas that is not in steady state.

Steady-state lifetime (τ_{SS}): Special case of global atmospheric lifetime calculated for a system that is at or near steady state. In steady state, the source and loss rates are equal.

Local lifetime: Inverse loss frequency at a specific point in the atmosphere.

Response lifetime: The time scale characterizing the decay of an instantaneous pulse input added to the atmosphere. This has also been referred to as an adjustment time.

Partial lifetimes:

OH (τ_{OH}): Global atmospheric burden divided by loss due to OH reaction rate
Cl (τ_{Cl}): Global atmospheric burden divided by loss due to Cl atom reaction rate
O(^{1}D) (τ_{O1D}): Global atmospheric burden divided by loss due to O(^{1}D) reactions rate
Photolysis (τ_{phot}): Global atmospheric burden divided by loss due to photolysis rate

Tropospheric (τ_{trop}): Global atmospheric burden divided by tropospheric loss rate
Stratospheric (τ_{strat}): Global atmospheric burden divided by stratospheric loss rate
Mesospheric (τ_{meso}): Global atmospheric burden divided by mesospheric loss rate

Oceanic (τ_{ocean}): Global atmospheric burden divided by loss to ocean surface rate
Soil (τ_{soil}): Global atmospheric burden divided by loss to land surface rate

In this report the global atmospheric lifetime will be referred to as just lifetime with symbol τ. Partial lifetimes and pulse-response lifetimes will be referred to with their specific subscripted symbols.

2.5 References

Bergamaschi, P., C. Frankenberg, J. F. Meirink, M. Krol, M. G. Villani, S. Houweling, F. Dentener, E. J. Dlugokencky, J. B. Miller, L. V. Gatti, A. Engel, and I. Levin, Inverse modeling of global and regional CH_4 emissions using SCIAMACHY satellite retrievals, *J. Geophys. Res., 114*, D22301, doi: 10.1029/2009JD012287, 2009.

Birner, T., and H. Boenisch, Residual circulation trajectories and transit times into the extratropical lowermost stratosphere, *Atmos. Chem. Phys.*, 11817-11827, doi: 10.5194/acp-11-817-2011, 2011.

Boering, K. A., S. C. Wofsy, B. C. Daube, H. R. Schneider, M. Loewenstein, J. R. Podolske, and T. J. Conway, Stratospheric mean ages and transport rates from observations of CO_2 and N_2O, *Science*, *274*, 1340-1343, doi: 10.1126/science.274.5291.1340, 1996.

Bridgeman, C. H., J. A. Pyle, and D. E. Shallcross, A three-dimensional model calculation of the ozone depletion potential of 1-bromopropane (1-C3H7Br), *J. Geophys. Res., 105,* 26493, 2000.

Brioude, J., R. W. Portmann, J. S. Daniel, O. R. Cooper, G. J. Frost, K. H. Rosenlof, C. Granier, A. R. Ravishankara, S. A. Montzka, and A. Stohl, Variations in ozone depletion potentials of very short-lived substances with season and emission region, *Geophys. Res. Lett., 37*, L19804, doi: 10.1029/2010GL044856, 2010.

Butchart, N., A. A. Scaife, M. Bourqui, J. de Grandpré, S. H. E. Hare, J. Kettleborough, U. Langematz, E. Manzini, F. Sassi, K. Shibata, D. Shindell, and M. Sigmond, Simulations of anthropogenic change in the strength of the Brewer–Dobson circulation, *Clim. Dyn.*, *27* (7-8), 727-741, doi: 10.1007/s00382-006-0162-4, 2006.

Butler, J. H., The potential role of the ocean in regulating atmospheric CH_3Br, *Geophys. Res. Lett., 21,* 185-189, 1994.

Cunnold, D., R. Prinn, R. Rasmussen, P. Simmonds, F. Alyea, C. Cardelino, A. Crawford, P. Fraser, and R. Rosen, The Atmospheric Lifetime Experiment 3. Lifetime Methodology and Application to Three Years of $CFCl_3$ Data, *J. Geophys. Res.*, *88* (C13), 8379-8400, 1983.

Daniel, J. S., and S. Solomon, On the climate forcing of carbon monoxide, *J. Geophys. Res., 103*, 13249-13260, 1998.

Derwent, R. G., W. J. Collins, C. E. Johnson, and D. S. Stevenson, Transient behaviour of tropospheric ozone precursors in a global 3-D CTM and their indirect greenhouse effects, *Clim. Change*, *49* (4), 463-487, 2001.

Douglass, A. R., R. S. Stolarski, M. R. Schoeberl, C. H. Jackman, M. L. Gupta, P. A. Newman, J. E. Nielsen, and E. L. Fleming, Relationship of loss, mean age of air and distribution of CFCs to stratospheric circulation and implications for atmospheric lifetimes, *J. Geophys. Res*., *113*, D14309, doi: 10.1029/2007JD009575, 2008.

Ehhalt, D. H., R. Rohrer, S. Schauffler, and M. Prather, On the decay of stratospheric pollutants: Diagnosing the longest-lived eigenmode, *J. Geophys. Res., 109*, D08102, doi: 10. 1029/2003JD004029, 2004.

Farrell, B. F., and P. J. Ioannou, Perturbation dynamics in atmospheric chemistry, *J. Geophys. Res., 105,* 9303-9320, 2000.

Hartley, D. and R. Prinn, Feasibility of determining surface emissions of trace gases using an inverse method in a three-dimensional chemical transport model, *J. Geophys. Res., 98*, 5183-5198, 1993.

Hegglin, M. I., and T. G. Shepherd, Large climate-induced changes in UV index and stratosphere-to-troposphere ozone flux, *Nature Geoscience 2*, 687-691, 2009.

Hu, L., S. Yvon-Lewis, Y. Liu, and T. S. Bianchi, The ocean in near equilibrium with atmospheric methyl bromide, *Global Biogeochem. Cycles*, *26*, GB3016, doi: 10.1029/2011GB004272, 2012.

IPCC (Intergovernmental Panel on Climate Change), *Climate Change 1995: The Science of Climate Change*, edited by J. T. Houghton, L. G. Meira Filho, B. A. Callander, N. Harris, A. Kattenberg, and K. Maskell, 572 pp., Cambridge University Press, Cambridge, U. K., 1996.

IPCC (Intergovernmental Panel on Climate Change), *Climate Change 2001: The Scientific Basis, Contribution of Working Group I to the Third Assessment Report of the Intergovernmental Panel on Climate Change*, edited by J. T. Houghton, Y. Ding, D. J. Griggs, M. Noguer, P. J. van der Linden, X. Dai, K. Maskell, and C. A. Johnson, 881 pp., Cambridge University Press, Cambridge, U. K., 2001.

Isaksen, I. S. A., and O. Hov, Calculation of trends in tropospheric O_3, OH, CH_4, and NO_x, *Tellus B, 39*, 271-285, 1987.

John, J. G., A. M. Fiore, V. Naik, L. W. Horowitz, and J. P. Dunne, Climate versus emission drivers of methane lifetime from 1860–2100, *Atmos. Chem. Phys. Discuss., 12,* 18067-18105, doi: 10.5194/acpd-12-18067-2012, 2012.

Junge, C. E., Residence time and variability of tropospheric trace gases, *Tellus, 26*, 477-488, 1974.

Kalnay, E., Atmospheric modeling, data assimilation and predictability, Cambridge University Press, 2003.

Ko, M. K. W., N. D. Sze, C. J. Scott, and D. K. Weisenstein, On the relation between stratospheric chlorine/bromine loading and short-lived tropospheric source gases. *J. Geophys. Res., 102*, 25507-25517, doi: 10.1029/97JD02431, 1997.

Lawrence, M. G., P. Jöckel, and R. von Kuhlmann, What does the global mean OH concentration tell us?, *Atmos. Chem. Phys., 1,* 37-49, doi: 10.5194/acp-1-37-2001, 2001.

Lee, C., R. V. Martin, A. van Donkelaar, H. Lee, R. R. Dickerson, J. C. Hains, N. Krotkov, A. Richter, K. Vinnikov, and J. J. Schwab, SO_2 emissions and lifetimes: Estimates from inverse modeling using *in situ* and global, space-based (SCIAMACHY and OMI) observations, *J. Geophys. Res., 116*, D06304, doi: 10.1029/2010JD014758, 2011.

Lelieveld, J., P. J. Crutzen, and F. J. Dentener, Changing concentration, lifetime and climate forcing of atmospheric methane, *Tellus, Ser., B, 50*, 128-150, 1998.

Li, F., R. S. Stolarski, and P. A. Newman, Stratospheric ozone in the post-CFC era, *Atmos. Chem. Phys.*, *9*, 2207-2213, http://www.atmos-chem-phys.net/9/2207/2009/, 2009.

Manning, M. R., Characteristic modes of isotopic variations in atmospheric chemistry. *Geophys. Res. Lett., 26,* 1263-1266, doi: 10.1029/1999GL900217, 1999.

Minschwaner, K., R. J. Salawitch, and M. B. McElroy, Absorption of solar Radiation by O_2; Implications for O_3 and Lifetimes of N_2O, $CFCl_3$, and CF_2Cl_2, *J. Geophys. Res., 98*, 10543-10561, 1993.

Montzka, S. A., J. H. Butler, J. W. Elkins, T. M. Thompson, A. D. Clarke, and L. T. Lock, Present and future trends in the atmospheric burden of ozone-depleting halogens, *Nature, 398*, 690-694, 1999.

Montzka, S. A., M. Krol, E. Dlugokencky, B. Hall, P. Jöckel, and J. Lelieveld, Small interannual variability of global atmospheric hydroxyl, *Science,* 7 January 2011, 67-69, doi: 10.1126/science.1197640, 2011.

Neu, J. L., and R. A. Plumb, Age of air in a "leaky pipe" model of stratospheric transport, *J. Geophys. Res.*, *104* (D16), 19243-19255, doi: 10.1029/1999JD900251, 1999.

Olsen, S. C., B. J. Hannegan, X. Zhu, and M. J. Prather, Evaluating ozone depletion from very short-lived halocarbons, *Geophys. Res. Lett., 27*, 1475-1478, 2000.

O'Neill, B. C., Gaffin, S. R., Tubiello, F. N. and Oppenheimer, M., Reservoir timescales for anthropogenic CO_2 in the atmosphere, *Tellus-B, 46,* 378-389, 1994.

Patra, P. K., S. Houweling, M. Krol, P. Bousquet, D. Belikov, D. Bergmann, H. Bian, P. Cameron-Smith, M. P. Chipperfield, K. Corbin, A. Fortems-Cheiney, A. Fraser, E. Gloor, P. Hess, A. Ito, S. R. Kawa, R. M. Law, Z. Loh, S. Maksyutov, L. Meng, P. I. Palmer, R. G. Prinn, M. Rigby, R. Saito, and C. Wilson, TransCom model simulations of CH_4 and related species: Linking transport, surface flux and chemical loss with CH_4 variability in the troposphere and lower stratosphere, *Atmos. Chem. Phys., 11*, 12813-12837, 2011.

Pisso, I., P. H. Haynes, and K. S. Law, Emission location dependent ozone depletion potentials for short-lived halogenated species, *Atmos. Chem. Phys., 10*, 12025-12036, 2010.

Plumb, R. A., Stratospheric Transport, *J. Meteor. Soc. Japan, 80*, 793-809, 2002.

Plumb, R. A., Tracer interrelationships in the stratosphere, *Rev. Geophys.*, *45*, RG4005, doi: 10.1029/2005RG000179, 2007.

Plumb, R. A., *et al.*, in preparation, 2013.

Plumb, R. A., and M. K. W. Ko, Interrelationships between mixing ratios of long-lived stratospheric constituents, *J. Geophys. Res*., *97*, 10140-10156, 1992.

Prather, M. J., Lifetimes and eigenstates in atmospheric chemistry, *Geophys. Res. Lett., 21*, 801-804, 1994.

Prather, M. J., Time scales in atmospheric chemistry: Theory, GWPs for CH_4 and CO, and runaway growth, *Geophys. Res. Lett*., *23,* 2597-2600, 1996.

Prather, M. J., Timescales in atmospheric chemistry: CH_3Br, the ocean, and ozone depletion potentials, *Global Biogeochem. Cycles*, *11* (3), 393-400, 1997.

Prather, M. J., Time scales in atmospheric chemistry: Coupled perturbations to N_2O, NO_y, and O_3, *Science, 279*, 1339-1341, 1998.

Prather, M. J., Lifetimes and time scales in atmospheric chemistry, *Phil. Trans. Roy. Soc. A, 365 (1856),* 1705-1726, 2007.

Prather, M. J., and J. Hsu, Coupling of nitrous oxide and methane by global atmospheric chemistry. *Science*, *330* (6006), 952-954, 2010.

Prather, M. J., and C. Spivakovsky, Tropospheric OH and the lifetimes of hydrochlorofluorocarbons, *J. Geophys. Res., 95*, 18433-18439, doi: 10.1029/JD095iD11p18723, 1990.

Prather, M. J., X. Zhu, Q. Tang, J. N. Hsu, and J. L. Neu, An atmospheric chemist in search of the tropopause, *J. Geophys. Res., 116,* D04306, doi: 10.1029/2010JD014939, 2011.

Prather, M. J., C. D. Holmes, and J. Hsu, Reactive greenhouse gas scenarios: Systematic exploration of uncertainties and the role of atmospheric chemistry, *Geophys. Res. Lett*., *39*, L09803, doi: 10.1029/2012GL051440, 2012.

Prinn, R., R. Weiss, B. Miller, J. Huang, F. Alyea, D. Cunnold, P. Fraser, D. E. Hartley, and P. G. Simmonds, Atmospheric trends and lifetime of CH_3CCl_3 and global OH concentrations, *Science*, *269* (5221), 187-192, 1995.

Rhew, R. C., M. Aydin, and E. S. Saltzman, Measuring terrestrial fluxes of methyl chloride and methyl bromide using a stable isotope tracer technique, *Geophys. Res. Lett., 30* (21), 2103, doi: 10.1029/2003GL018160, 2003.

Rigby, M., R. G. Prinn, S. O'Doherty, S. A. Montzka, A. McCulloch, C. M. Harth, J. Mühle, P. K. Salameh, R. F. Weiss, D. Young, P. G. Simmonds, B. D. Hall, G. S. Dutton, D. Nance, D. J. Mondeel, J. W. Elkins, P. B. Krummel, L. P. Steele, and P. J. Fraser, Re-evaluation of the lifetimes of the major CFCs and CH_3CCl_3 using atmospheric trends, *Atmos. Chem. Phys., 13,* 2691-2702, doi: 10.5194/acp-13-2691-2013, 2013.

Sander, S. P., J. Abbatt, J. R. Barker, J. B. Burkholder, R. R. Friedl, D. M. Golden, R. E. Huie, C. E. Kolb, M. J. Kurylo, G. K. Moortgat, V. L. Orkin and P. H. Wine, *Chemical Kinetics and Photochemical Data for Use in Atmospheric Studies, Evaluation No. 17*, JPL Publication 10-6, Jet Propulsion Laboratory, Pasadena, http://jpldataeval.jpl.nasa.gov/, 2011.

Spivakovsky, C. M., J. A. Logan, S. A. Montzka, Y. J. Balkanski, M. Foreman-Fowler, D. B. A. Jones, L. W. Horowitz, A. C. Fusco, C. A. M. Brenninkmeijer, M. J. Prather, S. C. Wofsy, and M. B. McElroy, Three-dimensional climatological distribution of tropospheric OH: Update and evaluation, *J. Geophys. Res.*, *105* (D7), 8931-8980, doi: 10.1029/1999JD901006, 2000.

Stevenson, D. S., F. J. Dentener, M G. Schultz, K. Ellingsen, T. P. C. van Noije, O. Wild, G. Zeng, M. Amann, C. S. Atherton, N. Bell, D. J. Bergmann, L. Bey, T. Butler, J. Cofala, W. J. Collins, R. G. Derwent, R. M. Doherty, J. Drevet, H. J. Eskes, A. M. Fiore, M. Gauss, D. A. Hauglustaine, L. W. Horowitz, I. S. A. Isaksen, M. C. Krol, J.-F. Lamarque, M. G. Lawrence, V. Montanaro, J.-F. Müller, G. Pitari, M. J. Prather, J. A. Pyle, S. Rast, J. M. Rodriguez, M. G. Sanderson, N. H. Savage, D. T. Shindell, S. E. Strahan, K. Sudo, and S. Szopa, Multimodel ensemble simulations of present-day and near-future tropospheric ozone, *J. Geophys. Res.*, *111*, D08301, doi: 10.1029/2005JD006338, 2006.

Volk, C. M., J. W. Elkins, D. W. Fahey, R. J. Salawitch, G. S. Dutton, J. M. Gilligan, M. H. Proffitt, M. Loewenstein, J. R. Podolske, K. Minschwaner, J. J. Margitan, and K. R. Chan, Quantifying transport between the tropical and mid-latitude lower stratosphere, *Science* , *272*, 1763-1768, 1996.

Volk, C. M., J. W. Elkins, D. W. Fahey, D. S. Dutton, J. M. Gilligan, M. Loewenstein, J. R. Podolske, K. R. Chan, and M. R. Gunson, Evaluation of source gas lifetimes from stratospheric observations, *J. Geophys. Res., 102*, 25543-25564, 1997.

Waugh, D. W., and T. M. Hall, Age of stratospheric air: Theory, observations, and models, *Rev. Geophys.*, *40* (4), 1010, doi: 10.1029/2000RG000101, 2002.

Wennberg, P. O., S. Peacock, J. T. Randerson, and R. Bleck, Recent changes in the air-sea gas exchange of methyl chloroform, *Geophys. Res. Lett.*, *31*, L16112, doi: 10.1029/2004GL020476, 2004.

Wild, O., M. J. Prather, and H. Akimoto, Indirect long-term global cooling from NO_x emissions, *Geophys. Res. Lett., 28*, 1719-1722, doi: 10.1029/2000GL012573, 2001.

Wuebbles, D. J., K. O. Patten, M. T. Johnson, and R. Kotamarthi, New methodology for ozone depletion potentials of short-lived compounds: n-propyl bromide as an example, *J. Geophys. Res., 106*, 14551-14571, 2001.

Yvon-Lewis, S. A., and J. H. Butler, The potential effect of oceanic biological degradation on the lifetime of atmospheric CH_3Br, *Geophys. Res. Lett.*, *24* (10), 1227-1230, 1997.

CHAPTER 3

Evaluation of Atmospheric Loss Processes

Lead Authors:
James B. Burkholder
Wahid Mellouki

Co-Authors:
Eric L. Fleming
Christian George
Dwayne E. Heard
Charles H. Jackman
Michael J. Kurylo
Vladimir L. Orkin
William H. Swartz
Timothy J. Wallington

CHAPTER 3

Evaluation of Atmospheric Loss Processes

Contents

3.0 Summary

- Hydroxyl radical (OH), electronically excited atomic oxygen ($O(^1D)$), and atomic chlorine (Cl) reaction rate coefficient data were evaluated and the estimated uncertainties in the recommended parameters reduced, in general, from those currently recommended in the NASA/Jet Propulsion Laboratory (JPL) and International Union of Pure and Applied Chemistry (IUPAC) kinetic and photochemical data evaluations.
- New studies of several $O(^1D)$ reaction rate coefficients, reaction yields, and their temperature dependences provided data needed to reduce uncertainties in calculated lifetimes.
- Lyman-α (121.567 nm) absorption cross-section recommendations are provided and uncertainties estimated. Lyman-α photolysis is shown to be a dominant mesospheric loss process, but makes only a minor contribution to the total global atmospheric lifetimes for the molecules included in this report.
- Ultraviolet (UV) absorption cross-section data were evaluated and new cross-section parameterizations recommended for CCl_4 (carbon tetrachloride), CF_2Br_2 (Halon-1202), CF_2ClBr (Halon-1211), CF_2BrCF_2Br (Halon-2402), and NF_3 (nitrogen trifluoride). In addition, systematic errors in the UV spectrum parameterizations for $CFCl_3$ (CFC-11), CF_2Cl_2 (CFC-12), $CFCl_2CF_2Cl$ (CFC-113), CF_2ClCF_2Cl (CFC-114), CH_3CCl_3, CH_3Cl, and CHF_2Cl (HCFC-22) given in literature and quoted in NASA/JPL (JPL10-6) from the original literature are corrected here. Uncertainties in absorption cross-sections and their temperature dependence are estimated for 5 key photolysis wavelength regions.
- Two-dimensional (2-D) atmospheric model calculations were used to quantify the fractional contribution of the OH, $O(^1D)$, and Cl reactive losses as well as photolytic loss to the global annually averaged local and overall lifetimes for each of the molecules included in this report. For hydrogen containing molecules, loss due to the OH reaction is dominant (>90%). The dominant loss process for the chlorofluorocarbons (CFCs), CCl_4, N_2O (nitrous oxide), CF_3Br (Halon-1301), and NF_3 is photolysis primarily in the stratosphere in the 190-230 nanometer (nm) wavelength region. For CF_2Br_2 (Halon-1202), CF_2BrCl (Halon-1211), and CF_2BrCF_2Br (Halon-2402) photolysis in the 190-230 and >286 nm regions contribute to their atmospheric removal. Loss due to $O(^1D)$ atom reaction, which is primarily a stratospheric loss process, is generally of secondary importance. Loss due to Cl atom reaction is minor (<1.5% for CH_4 (methane) and <0.5% for the other molecules in this study).
- 2-D atmospheric model calculations showed that existing uncertainties in kinetic and photochemical parameters contribute substantial uncertainty to calculated atmospheric lifetimes. The estimated uncertainties given in the present Stratospheric Processes and Their Role in Climate (SPARC) parameter recommendations, in general, lead to a reduction in the range of calculated lifetimes from those calculated using the NASA/JPL (JPL10-6) recommended kinetic parameters. For $CFCl_3$ (CFC-11), CF_2Cl_2 (CFC-12), CCl_4, and N_2O the range in calculated lifetimes is between 5 and 10%, while for CH_3CCl_3 (methyl chloroform) and CHF_2Cl (HCFC-22) it is ~20%.

3.1 Introduction

An evaluation of the atmospheric lifetime of a trace gas requires a thorough understanding of its chemical loss processes. In this chapter, a comprehensive evaluation of the available experimental data for the key atmospheric removal processes, including results of a thorough uncertainty analysis, is presented. This chapter includes an evaluation of the OH, $O(^1D)$, and Cl gas-phase reaction rate coefficients, *k*, and their temperature dependences, and of the vacuum ultraviolet/ultraviolet (VUV/UV) absorption spectra (photodissociation) for each of the molecules included in this report. Atmospheric lifetimes were evaluated using 2-D atmospheric model calculations, based on the recommendations given in the NASA/JPL evaluation (Sander *et al.*, 2011) and those presented here. The range in the calculated lifetimes determined from the ranges of uncertainties in the chemical loss parameters (reaction and photolysis) are also presented.

The recommendations given in this assessment benefit significantly from the activities of two long-term independent international photochemistry and kinetics data evaluation panels: the NASA/JPL Panel for Data Evaluation, "Chemical Kinetics and Photochemical Data for Use in Atmospheric Studies" (Sander *et al.*, 2011) (herein referred to as JPL10-6), and the IUPAC Subcommittee for Gas Kinetic Data Evaluation (Atkinson *et al.*, 2008) (herein referred to as IUPAC). In addition, the Max Planck Institute (MPI) for Chemistry spectral data compilation (Keller-Rudek and Moortgat) was a useful resource in the photolysis data evaluation.

Hydrochlorofluorocarbons (HCFCs) and hydrofluorocarbons (HFCs) are, in most cases, primarily removed from the atmosphere by reaction with the OH radical. There are relatively few new studies since JPL10-6 and a focus of the present evaluation of the OH kinetics was on the recommended uncertainties in the kinetic parameters. The $O(^1D)$ reaction, which is primarily a stratospheric loss process, evaluation includes studies by Feierabend *et al.* (2010), Baasandorj *et al.* (2011; 2012; 2013), and Nilsson *et al*. (2012) that provide additional rate coefficient and product yield data that were not available for the JPL10-6 evaluation. The results from these studies combined with previous works have enabled a refinement of the rate coefficients, product yields, and reaction yields as well as a reduction in the recommended uncertainties for a number of reactions. While Cl atom reaction represents a minor loss process for the molecules considered here, the present evaluation has revised several kinetic recommendations and estimated uncertainty parameters. Gas-phase reactions with other atmospheric oxidants, such as O_3 (ozone) and NO_3 (nitrogen trioxide), are expected to be negligible for the molecules included in this report and are not considered further.

Photodissociation is an important loss process for N_2O and NF_3 and for the chlorofluorocarbons (CFCs), hydrochlorofluorocarbons (HCFCs), and fluorochlorobromocarbons (Halons) included in this report. CFCs and HCFCs are photodissociated by UV radiation primarily in the stratosphere, while Halons are photodissociated in the troposphere and stratosphere. Absorption cross sections at the hydrogen Lyman-α wavelength (121.567 nm) were evaluated and photolysis at this wavelength was shown to be a minor loss process in terms of the total global atmosphere in nearly all cases; Lyman-α is the predominate source of photodissociation radiation in the VUV region. Since the JPL10-6 evaluation was released, Papanastasiou *et al.* (2013) reported cross-section data for CF_2Br_2 (Halon-1202), CF_2ClBr (Halon-1211), and CF_2BrCF_2Br (Halon-2402) at wavelengths $\geq$300 nm and Papadimitriou *et al.* (2013) reported NF_3 UV absorption cross-section data and its temperature dependence. The results from these studies have enabled a significant reduction of the uncertainties in the photolysis lifetimes of these molecules. In addition, improved UV absorption cross-section

parameterizations for $CFCl_3$ (CFC-11), CF_2Cl_2 (CFC-12), $CFCl_2CF_2Cl$ (CFC-113), CF_2ClCF_2Cl (CFC-114), CH_3CCl_3, CH_3Cl, and CHF_2Cl (HCFC-22) over those reported in the literature and quoted in JPL10-6 from the original literature are provided in the supplementary material.

Data evaluation is not an exact science and does not conform to a set of rules governing the process. However, consideration of uncertainties in the kinetic and photochemical parameters used in atmospheric models plays a key role in determining the reliability/uncertainty of the model results. Quite often the cause of differences in experimental results from various laboratories cannot be determined with confidence and making recommendations for the uncertainties is often more difficult to derive than for the parameters themselves. In many cases, the investigators only suggest possible qualitative reasons for disagreements among datasets. Thus, data evaluators necessarily consider a variety of factors in assigning a recommendation including factors such as the chemical complexity of the system, sensitivities and shortcomings of the experimental techniques employed, similarities or trends in reactivity, and the level of agreement among studies using different techniques. The rate coefficient uncertainties presented in this evaluation follow the formalism given in JPL10-6

$$f(\mathrm{T}) = f(298\ \mathrm{K}) \exp\left(\left|g\left(\frac{1}{\mathrm{T}} - \frac{1}{298}\right)\right|\right)$$

where $f(\mathrm{T})$ is an uncertainty factor for $k(\mathrm{T})$, $f(298\ \mathrm{K})$ is the 1σ estimated uncertainty factor for the room temperature rate coefficient, $k(298\ \mathrm{K})$, and g is a parameter used to describe the increase in uncertainty at temperatures other than 298 K. An upper and lower bound of the rate coefficient at any temperature can be obtained by multiplying or dividing the recommended value, $k(\mathrm{T})$, by the factor $f(\mathrm{T})$. The 2σ uncertainty is given by $f(\mathrm{T})^2$.

The uncertainty recommendations given in the past JPL10-6 and IUPAC evaluations are often rather conservative in that they were chosen, in many cases, to cover the full range of the available experimental data even including results that were not used in quantifying the recommended kinetic parameters. In the present evaluation, the most stringent uncertainty limits (at the 2σ uncertainty level) that can be justified by the available experimental data are reported. In cases where the experimental data did not extend to the lowest temperatures representative of the upper troposphere and lower stratosphere, the uncertainty recommendations were based on a comparison with similar compounds for which studies by multiple investigators or using different experimental techniques did extend to lower temperatures.

An extensive evaluation of the uncertainties in the photochemical data, absorption cross sections, and their temperature dependences, an issue that has not been comprehensively addressed in previous JPL or IUPAC data evaluations, is reported here. The cross-section uncertainties were estimated by comparing the agreement among multiple experimental datasets, whenever possible. Where experimental data do not exist for a compound, e.g., Lyman-α cross sections, cross sections were estimated based on trends observed for similar compounds and relatively conservative uncertainties were assigned. Details of the evaluation for each compound are provided in the supplementary material for this chapter.

Overall, the uncertainty in an atmospheric loss process, for even the most highly studied compounds, is typically >10% and, in many cases, the cumulative uncertainties of the most important loss processes are greater. The NASA/Goddard Space Flight Center (GSFC) two-

dimensional (2-D) coupled chemistry-radiation-dynamics model (Fleming *et al.*, 2011) was used to evaluate the impact of the kinetic and photochemical recommendations and their uncertainties on atmospheric lifetimes. Model calculations of lifetimes and uncertainties are discussed in Section 3.5.

Section 3.6 considers the sensitivity of the calculated lifetimes to the uncertainty in the O_2 and O_3 UV absorption cross sections used in the model calculations. Uncertainty in the O_2 and O_3 cross sections represent a potential uncertainty in the calculated lifetimes via their impact on: (1) the ozone concentration, and (2) the incident solar UV radiation throughout the atmosphere. An evaluation of the 2σ lifetime uncertainty for the species primarily removed in the stratosphere is presented.

Supplemental material for this chapter includes (1) a comprehensive graphical analysis of the available OH, $O(^1D)$, and Cl atom kinetic data, (2) summaries of the available photochemical data and the basis for the recommendations given here, and (3) a graphical summary of the 2-D model results obtained using kinetic and photochemical input parameters from the JPL10-6 data evaluation and the recommendations given here for each of the molecules included in this report.

3.2 Gas-Phase Reactive Loss Processes

Reaction rate coefficients, $k(T)$, for the OH radical, $O(^1D)$ atom, and Cl atom reactions were parameterized using an Arrhenius expression where $k(T) = A \exp(-E/RT)$ and the pre-exponential, A, and activation energy, E, parameters were taken as variables in the fitting of the experimental data. Figure 3.1 shows an Arrhenius plot, $\ln(k(T))$ vs. $1/T$, for the OH + CHF_2Cl (HCFC-22) reaction (Arrhenius plots are provide in the supplementary material for all the compounds and reactions). Over the temperature range most relevant for atmospheric chemistry, 200 to 300 K, the Arrhenius expression reproduces the experimental data to within the measurement precision, although over a broader temperature range non-Arrhenius behavior (curvature) is observed in some cases, e.g., the Cl and OH reactions with CH_4. The OH + CHF_2Cl reaction is an example where the available experimental data do not cover the complete temperature range applicable for atmospheric chemical processes. In these cases, the higher temperature data were used to extrapolate, using the fitted Arrhenius expression, to lower temperatures. The estimated uncertainty in the extrapolated low temperature rate coefficient values was increased, as shown in Figure 3.1, to reflect the increased uncertainties associated with such an extrapolation. The rate coefficient recommendations for the OH radical, $O(^1D)$ atom, and Cl atom reactions given here are based on a comprehensive evaluation of all available laboratory data. In cases where data do not exist, best estimates for the rate coefficient parameters are based on the recommendations for similar compounds.

3.2.1 OH Radical Chemistry

While a thorough examination of the OH kinetic data available for every molecule was conducted, particular attention was paid to those molecules for which new data have appeared since the latest data panel evaluations, new insights into chemical mechanisms now exist, or differences between the JPL10-6 and IUPAC recommendations exceed the combined recommended uncertainty limits. The present recommendations are given in Table 3.1. The recommendations do not differ appreciably from those given in JPL10-6 or IUPAC, and details of the evaluation are provided in the footnotes of Table 3.1. The uncertainty parameters given in Table 3.1 are, however, typically smaller than those reported in the JPL10-6 and IUPAC evaluations.

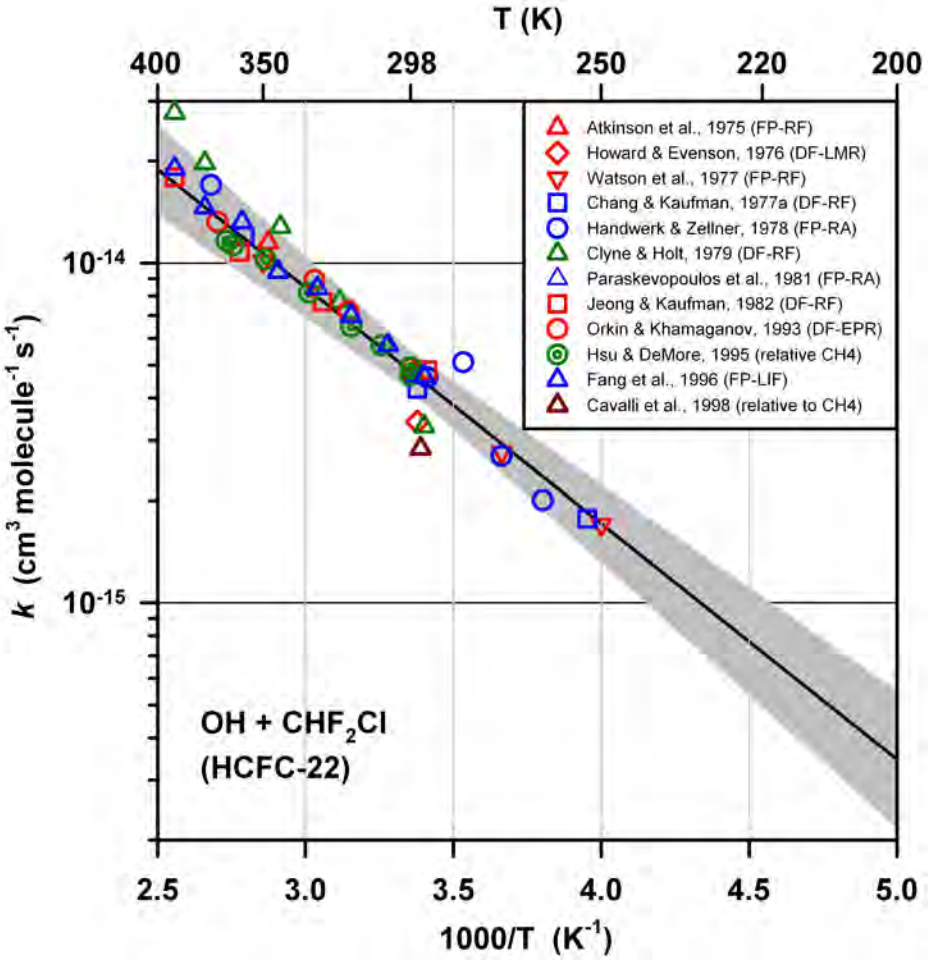

Figure 3.1. Arrhenius plot for the OH + CHF_2Cl (HCFC-22) reaction including all available experimental data (see legend) over the temperature range 200 to 400 K. The solid line is the recommended rate coefficient for use in atmospheric models (see Table 3.1). The gray shaded region represents the estimated 2-σ uncertainty range in k(T) from the present evaluation. Note that there are no experimental data currently available for this reaction below ~250 K and the estimated uncertainties in the extrapolated Arrhenius expression (g factor) are such that the uncertainty in this region is greater.

The recommended kinetic parameters for CH_3CCl_3, CH_3CFCl_2 (HCFC-141b), CH_3CF_2Cl (HCFC-142b), CHF_3 (HFC-23), CH_2F_2 (HFC-32), CHF_2CF_3 (HFC-125), CH_3CHF_2 (HFC-152a), and $CHF_2CH_2CF_3$ (HFC-245fa) are unchanged from those given in JPL10-6. However, the uncertainty recommendations have been reduced in most cases. Minor changes to the JPL10-6 recommendations were made for CH_3Cl, CHF_2Cl (HCFC-22) (see Figure 3.1), CH_2FCF_3 (HFC-134a), and CH_3CF_3 (HFC-143a), based on slight differences in the way that the multiple experimental datasets were combined for fitting. For example, care was taken to not unduly weight a particular study in which multiple data points were reported at a given temperature over those studies that averaged data prior to reporting. For CH_3Br (methyl bromide) and CF_3CHFCF_3 (HFC-227ea), the present recommendations differ more appreciably from those given in JPL10-6 and IUPAC. The difference for CH_3Br stems from the decision to base the temperature dependence on the study by Mellouki *et al.* (1992), rather than on a combined fit to the slightly more scattered data from three other studies that did not extend to as low a temperature (see footnote in Table 3.1). For HFC-227ea, an improved fit of the multiple datasets, which exhibited slight systematic differences, but similar temperature dependences, was made. More specifically, all of the datasets were

normalized to a common value of the rate coefficient at room temperature prior to fitting, thereby reducing biases in the obtained temperature dependence (see supplement). For CH_4, the recommended Arrhenius parameters were taken from the IUPAC evaluation (see supplement).

The rate coefficient upper-limit recommendations for the fully halogenated species $CFCl_3$ (CFC-11), CF_2Cl_2 (CFC-12), $CF_2ClCFCl_2$ (CFC-113), CF_2ClCF_2Cl (CFC-114), CF_3CF_2Cl (CFC-115), and CCl_4, which are considered as non-reactive towards the OH radical because the abstraction reactions are endothermic, have been reduced by more than an order of magnitude from the upper limits given in JPL10-6 and IUPAC. For CFC-11, CFC-12, and CCl_4, the reaction endothermicities have been taken as lower-limits of the reaction activation energies, *E*. The *E*/R lower-limits have been combined with an estimated upper-limit for the Arrhenius *A* factor, based on the largest *A* factor observed in any experimental study of OH + halocarbon reactions. This method of analysis provides a more representative/realistic upper-limit for these reaction rate coefficients for use in atmospheric models. The recommended upper limits are considerably lower than those resulting from actual laboratory studies that are limited by the capabilities of the experimental techniques. For CFC-113, CFC-114, and CFC-115 for which thermochemical data for the possible reaction products are not available, the rate coefficient recommendation for CCl_4 was taken as an upper-limit; the upper-limit recommended for CCl_4 is the highest among the fully halogenated compounds not containing bromine (Br) and having known thermochemistry. As shown in Section 3.5, the estimated rate coefficients for these reactions result in a negligible contribution to the molecules' atmospheric lifetimes.

3.2.2 $O(^1D)$ Atom Chemistry

$O(^1D)$ reactions are complex with several possible exothermic reaction pathways, which include (1) collisional (physical) quenching of $O(^1D)$ to ground state oxygen atoms, $O(^3P)$, (2) abstraction or addition-elimination, and (3) reactive quenching to form $O(^3P)$ and products other than the reactant, including stable and radical species. Although some laboratory kinetic studies have directly observed the temporal profile of $O(^1D)$ atoms using absorption (Heidner and Husain, 1973), laser-induced fluorescence (Blitz *et al.*, 2004), or emission spectroscopy (Davidson *et al.*, 1978), the majority of measurements have utilized indirect methods. The indirect methods used include (1) detection of $O(^3P)$ by atomic resonance absorption (Amimoto *et al.*, 1978) or fluorescence (Wine and Ravishankara, 1981), (2) a competitive reaction technique in which the detection of OH following the reaction of $O(^1D)$ with an atomic hydrogen donor molecule is used (Baasandorj *et al.*, 2011, 2012, 2013; Blitz *et al.*, 2004; Vranckx *et al.*, 2008), and (3) CH radical chemiluminescence following the reaction of $O(^1D)$ with the ethynyl radical (C_2H) (Vranckx *et al.*, 2008). Some studies have also used relative rate measurements for the determination of reactive rate coefficients (Baasandorj *et al.*, 2012, 2013; Nilsson *et al*., 2012; Force and Wiesenfeld, 1981; Green and Wayne, 1976/77), which is critically important to determining the loss of the molecular reactant in the $O(^1D)$ reaction.

Product yields at room temperature have been determined for the majority of the reactions included in this report, for example: ClO (chlorine monoxide) radical yields for the CFC reactions and other chlorine containing reactants (Baasandorj *et al.*, 2011; Feierabend *et al.*, 2010), OH radical yields for the CH_4 reaction and other hydrogen containing reactants (Vranckx *et al.*, 2008), BrO (bromine monoxide) radical yields for several bromine containing reactants including CF_3Br, CF_2ClBr, and CH_3Br (Cronkhite and Wine, 1998), and the NO (nitric oxide) yield in the N_2O reaction (Greenblatt and Ravishankara, 1990). Highly

precise measurements of the $O(^3P)$ yield for several $O(^1D)$ reactions were determined using a CH radical chemiluminescence method (Vranckx *et al.*, 2008).

Recommended overall rate coefficients (i.e., $O(^1D)$ loss), reaction yields, and estimated uncertainties for all of the molecules included in this report are given in Table 3.2, with the footnotes and supplementary material providing details for the recommendations. The recommendations for the overall rate coefficients, in most cases, do not differ appreciably from JPL10-6, although the uncertainty parameters given in Table 3.2 are typically reduced as a result of considering studies that became available after the JPL10-6 evaluation was finalized. In particular, recent studies that included measurements over a range of temperatures enabled significant reductions in the estimated rate coefficient uncertainties (*g* factor). In general, over the atmospherically relevant temperature range, there is only a weak, if any, temperature dependence for the $O(^1D)$ reaction rate coefficients as shown in Figure 3.2 for the $O(^1D) + CHF_2Cl$ (HCFC-22) reaction.

The reaction yields reported in Table 3.2 are in some cases appreciably different from JPL10-6. The uncertainties in the reaction yields are, in general, reduced from those reported in JPL10-6 owing to the results from recent studies. Consideration of results from the studies of Feierabend *et al.* (2010) and Baasandorj *et al.* (2011; 2012; 2013) for CFC-11, CFC-12, CCl_4, HCFC-22, CFC-113, CFC-115, HFC-143a, HFC-23, CFC-114, HCFC-142b, HFC-125, HFC-227ea, and NF_3 (nitrogen trifluoride), which became available after the JPL10-6 evaluation was finalized, have resulted in revisions to the recommendations from those given in JPL10-6. An average of the kinetic results from Matsumi *et al.* (1993) and Force and Wiesenfeld (1981) for CH_3Cl and the reactive rate coefficient for CH_3CCl_3 reported by Nilsson *et al.* (2012), which were not included in JPL10-6, are recommended here. The recommendations that are revised from JPL10-6 are summarized briefly below.

The kinetic results from the Baasandorj *et al.* (2013) study are consistent with the JPL10-6 recommendation for CFC-11 and HCFC-22, but enabled a reduction in the estimated rate coefficients and their temperature dependence uncertainty. For CFC-12, the recommended rate coefficient is slightly greater than the JPL10-6 recommendation and the reported small negative temperature dependence is recommended. On the basis of the Feierabend *et al.* (2010) study, the recommended ClO radical yields for the CFC-11, CFC-12, and CCl_4 reactions are ~10% lower than given in JPL10-6.

The recommended kinetic values for the CFC-113, CFC-115, HFC-143a, and HFC-23 reactions given here reflect the results from recent studies and differ from those given in JPL10-6. On the basis of the Baasandorj *et al.* (2011) study, the recommended ClO yield for CFC-113 is lower than given in JPL10-6.

The rate coefficients and ClO yield for the CFC-114 reaction are greater than given in JPL10-6. For HCFC-142b and HFC-125, the recent Baasandorj *et al.* (2013) study provided temperature dependent data, which results in a reduced estimated rate coefficient and temperature dependence uncertainty. HFC-227ea and HFC-245fa were not evaluated by JPL10-6. The kinetic parameters from Baasandorj *et al.* (2013) for the HFC-227ea reaction, which displays a weak negative temperature dependence, are recommended. For the HFC-245fa reaction, the rate coefficient and reaction yield were estimated. On the basis of the results from Zhao *et al.* (2010) and Baasandorj *et al.* (2012), a reactive yield of 0.93 was recommended for the NF_3 reaction.

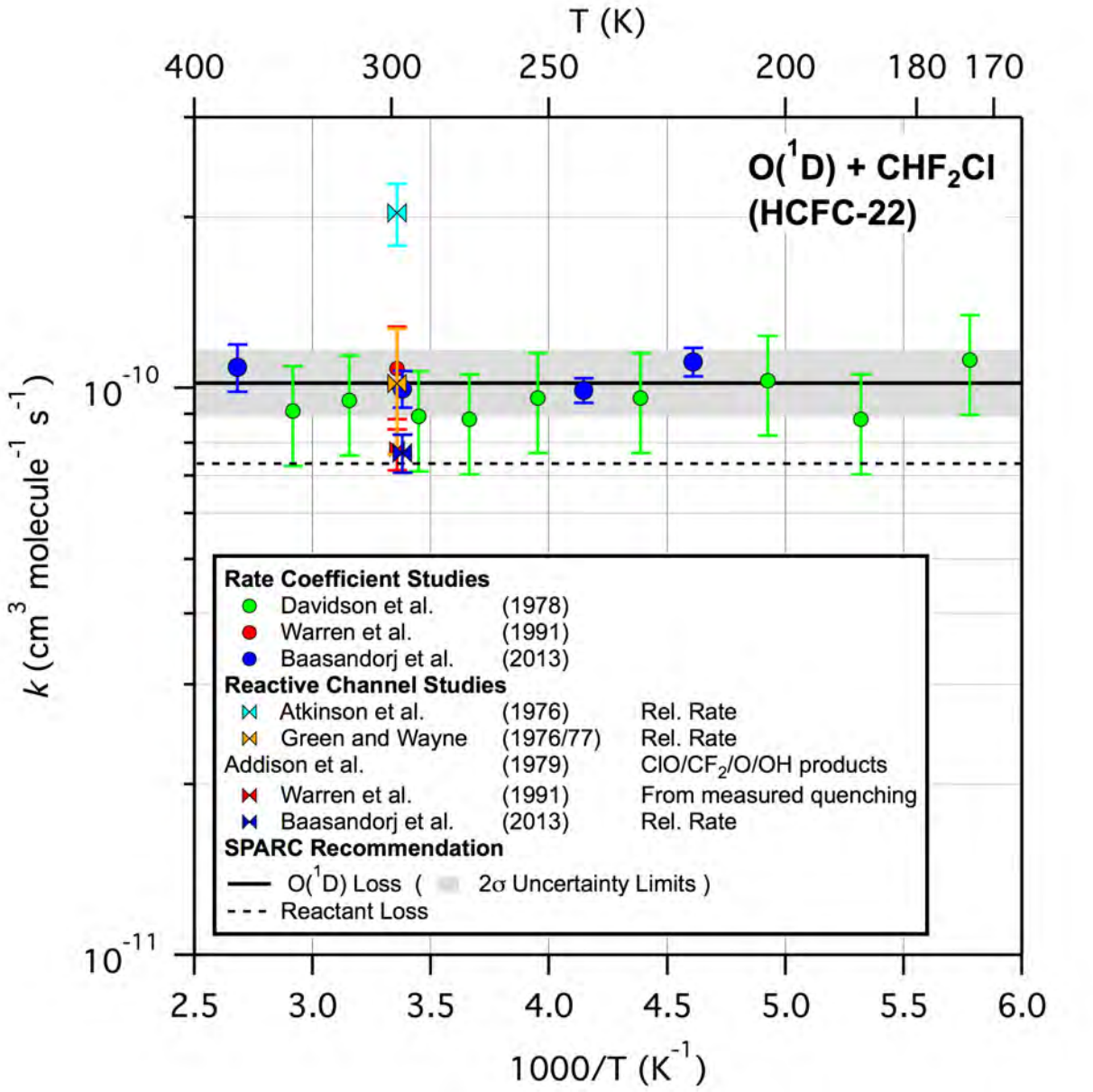

Figure 3.2. Arrhenius plot for the $O(^1D)$ + CHF_2Cl (HCFC-22) reaction including all available experimental total and reactive rate coefficient data (see legend). The product yield data from the Addison *et al*. (1979) study are not included in the figure. The solid and dashed lines are the total and reactive rate coefficient recommendations, respectively, from the present evaluation and the shaded region represents the 2σ range from estimated uncertainty in the total rate coefficient.

3.2.3 Cl Atom Chemistry

Reaction rate coefficient and estimated uncertainty recommendations for the Cl atom reactions are given in Table 3.3, with the footnotes of Table 3.3 providing the details for the recommendations. The recommended kinetic parameters, in most cases, do not differ appreciably from those given in IUPAC and JPL10-6. For compounds with rate coefficients $>10^{-14}$ cm^3 molecule^{-1} s^{-1} at 298 K, there is good agreement, typically within a few percent, between the recommendations from the IUPAC and JPL10-6 data panels. For compounds with rate coefficients $<10^{-14}$ cm^3 molecule^{-1} s^{-1} at 298 K, there are, in some cases, significant

differences between the IUPAC and JPL10-6 recommendations, e.g., ~40% for CF_3CH_3 (HFC-143a) at 220 K. The uncertainty factors given in Table 3.3 are based on the available experimental data as described in the footnotes, where in many cases the recommendation does not differ from that given in JPL10-6. Further details of the present evaluation are given below.

No experimental data are available for the 10 fully halogenated compounds. For CCl_3F, CCl_2F_2, CCl_4, $CBrClF_2$, $CBrF_3$, CBr_2F_2, and $CBrF_2CBrF_2$ the recommended kinetic parameters were estimated by setting the Arrhenius pre-exponential factor (A) to 1×10^{-10} cm^3 $molecule^{-1}$ s^{-1} and the activation energy (E) to the reaction endothermicity using available thermochemical parameters (Atkinson *et al.*, 2008; Sander *et al.*, 2011). This procedure results in upper limits for the reaction rate coefficients that are considerably less than those reported in laboratory studies that are often limited by the capabilities of the experimental techniques. For CCl_2FCClF_2 (CFC-113), $CClF_2CClF_2$ (CFC-114), and CF_3CClF_2 (CFC-115), where thermochemical data for reaction products are not available, the recommended activation energy for CCl_4 was assigned. The estimated activation energy for CCl_4 is the lowest among the fully halogenated compounds not containing Br that have known reaction product thermochemistry. The rate coefficients for the three fully halogenated chlorofluoroethanes are expected to be less than that for CCl_4 because the presence of fluorine increases the reaction endothermicity; see the trend in endothermicity for the fluorinated molecules given in Table 3.1.

The recommended pre-exponential factors and the activation energies are unchanged from the JPL10-6 recommendations for CHF_2Cl (HCFC-22), N_2O, CH_4, CHF_3 (HFC-23), CH_3Br, and CHF_2CF_3 (HFC-125). Minor changes to the JPL10-6 recommendations were made for CH_3CCl_3, CH_3CFCl_2 (HCFC-141b), CH_3CClF_2 (HCFC-142b), CH_3Cl, and CH_3CHF_2 (HFC-152a) based on slight differences in the way that the multiple data sets were combined for analysis (see Table 3.3 footnotes). For CH_2F_2 (HFC-32) the difference in the recommended parameters stems from the inclusion of a recent laboratory study that was conducted after the JPL10-6 evaluation was finalized. For CH_2FCF_3 (HFC-134a) and CF_3CH_3 (HFC-143a) the differences from the JPL10-6 recommendations are more significant. For CH_2FCF_3 (HFC-134a) the difference is due to the consideration of a recent study (Nilsson *et al.*, 2009) made after JPL10-6 was finalized and by only considering experimental data at temperatures <330 K because of slight non-Arrhenius behavior (curvature). For CF_3CH_3 (HFC-143a), the JPL10-6 recommendation is revised following the consideration of the room temperature rate coefficient reported by Nielsen *et al.* (1994) (see Table 3.3 footnote and supplement). The reactions for CF_3CHFCF_3 (HFC-227ea) and $CHF_2CH_2CF_3$ (HFC-245fa) were not included in the JPL10-6 evaluation. Only 298 K experimental data are available for these reactions and E/R was estimated by comparison with compounds having similar halogen substitution and similar reactivity at 298 K.

3.3 Photochemical Loss Processes

The evaluation of the Vacuum Ultraviolet (VUV) and Ultraviolet (UV) absorption spectra presented here was based on an examination of published experimental data. It includes recommendations for hydrogen Lyman-α (121.567 nm) absorption cross sections, σ(L-α), as well as absorption spectra and their temperature dependences for wavelengths (λ) >169 nm. As part of this evaluation, a critical assessment of the wavelength and temperature-dependent uncertainties in the recommended cross sections was made in order to better quantify uncertainties in atmospheric photolysis lifetime calculations. A brief summary of the evaluation is given below.

Currently there are no UV (λ >169 nm) absorption spectrum data available for the hydrofluorocarbons (HFCs) CH_2FCF_3 (HFC-134a), CH_3CF_3 (HFC-143a), CHF_3 (HFC-23), CH_2F_2 (HFC-32), CHF_2CF_3 (HFC-125), CH_3CHF_2 (HFC-152a), CF_3CHFCF_3 (HFC-227ea), and $CHF_2CH_2CF_3$ (HFC-245fa) or for CH_4 (methane) due primarily to their weak absorption in this wavelength region. The UV absorption cross sections for these compounds at λ >169 nm are expected to be sufficiently small that atmospheric photolysis in this wavelength region would make a negligible contribution to that molecule's atmospheric loss and, therefore, are not considered further.

Table 3.4 gives the σ(L-α) values for each of the molecules included in this report. The JPL10-6 evaluation provided a σ(L-α) recommendation for N_2O and citations to the literature for several other molecules. The recommended σ(L-α) values and uncertainty estimates given in Table 3.4 were derived from an evaluation of the available experimental data, all of which were obtained at room temperature, nominally 298 K. In cases where no experimental data are available, σ(L-α) values were estimated based on the measured cross sections for similar molecules. For the HFCs and HCFCs, σ(L-α) exhibits a trend of decreasing cross sections with increasing F atom substitution that was used to estimate cross-section values in some cases.

For the majority of the compounds included in this report for which UV (λ >169 nm) absorption spectra are available, the cross-section recommendations and their temperature dependences are as recommended in JPL10-6. The exceptions are CCl_4, CF_2Br_2 (Halon-1202), CF_2ClBr (Halon-1211), and CF_2BrCF_2Br (Halon-2402) where new laboratory measurements have become available since the JPL10-6 recommendations were finalized and CF_3Br (Halon-1301), CH_3CClF_2 (HCFC-142b), and NF_3 where specific recommendations were not provided in JPL10-6. In addition, inaccuracies in the cross-section parameterizations for $CFCl_3$ (CFC-11), CF_2Cl_2 (CFC-12), $CFCl_2CF_2Cl$ (CFC-113), CF_2ClCF_2Cl (CFC-114), CH_3CCl_3, CH_3Cl, and CHF_2Cl (HCFC-22) given in the literature and quoted in JPL10-6 from the original publications (Simon *et al.,* 1988a, b) are corrected here (see supplementary material).

Recommended uncertainties in the absorption cross sections as well as in their temperature dependences are given in Table 3.4. The estimated uncertainties are not statistical quantities, but rather are based on an evaluation of the reliability of the experimental measurements and the level of agreement among different studies where available. The uncertainties in an absorption spectrum and in its absolute cross sections are generally wavelength dependent, where the weaker absorption regions of a spectrum usually have greater uncertainty. Uncertainty parameters are provided for σ(L-α) and for the wavelength ranges 169-190, 190-230, 230-286, and >286 nm in order to provide an analysis that is sufficiently detailed to permit evaluation of the wavelength regions that are most critical to the photolytic loss of these molecules. For example, HFCs do not undergo UV photolysis and are photolyzed in the atmosphere primarily by absorption at Lyman-α, while Halons are lost by a combination of UV photolysis in the 190-230 and >286 nm regions where the relative importance of these wavelength regions is altitude dependent and quantified using an atmospheric model as shown later in this chapter.

The cross-section uncertainties given here are parameterized using a formalism similar to that used for gas-phase reaction rate coefficients where p(298 K) represents the 2σ (95% confidence) level uncertainty in the 298 K absorption cross-section data and w is a parameter used to represent the increase in the cross-section 2σ uncertainty at other temperatures

$$p(\mathrm{T}) = p(298\ \mathrm{K})\ exp\left(\left|w\left(\frac{1}{\mathrm{T}} - \frac{1}{298}\right)\right|\right)$$

The JPL10-6 evaluation provides estimated uncertainties for the product of the absorption cross sections and photolysis quantum yields for N_2O, CCl_4, $CFCl_3$, CF_2Cl_2, CF_3Br, CF_2ClBr, and CF_2BrCF_2Br. The uncertainty estimates provided in this chapter were derived for the absorption cross sections alone, but can be compared with those reported in JPL10-6 assuming a quantum yield of unity for photolytic loss of the compound.

As indicated above, there are a number of compounds for which the UV cross-section recommendations in this assessment differ from those given in JPL10-6. Details of these differences are as follows.

CCl_4 (Carbon Tetrachloride): A recent study by Rontu *et al.* (2010) reported CCl_4 absorption cross sections at 183.95, 202.206, 206.200, 213.857, and 228.8 nm, using atomic line sources, and the spectrum between 200 and 235 nm measured using diode array spectroscopy. Their results are in agreement with previously reported values that are discussed in JPL10-6, but are of higher precision and accuracy. The uncertainty factor given in Table 3.4 is reduced from that given in JPL10-6 primarily due to inclusion of these new results. For the temperature dependence of the cross sections JPL10-6 recommends the parameterization reported by Simon *et al.* (1988b) (174-250 nm; 225-295 K), which reproduces their experimental values to within ±5%. The revised CCl_4 absorption cross-section parameterization reported in Rontu *et al.* (given below) is recommended here, while the uncertainty parameters given in Table 3.4 encompass the range of the data from the Rontu *et al.* and Simon *et al.* studies.

Absorption cross-section parameterization for CCl_4 taken from Rontu *et al.* (2010)

$$\log_{10}\sigma(\lambda,\mathrm{T}) = \sum_i A_i\lambda^i + (\mathrm{T} - 273)\sum_i B_i\lambda^i$$

CCl_4 (Carbon Tetrachloride)		
i	A_i	B_i
0	1112.736208	-1.116511649
1	-22.02146808	0.02447268904
2	0.1596666745	-0.0001954842393
3	-0.0005104078676	$6.775547148 \times 10^{-7}$
4	$6.062440506 \times 10^{-7}$	$-8.621070147 \times 10^{-10}$

CF_2ClBr (Halon-1211): The recommendations provided here are based on the studies reviewed in JPL10-6 together with the recent investigation by Papanastasiou *et al.* (2013) who reported CF_2ClBr absorption cross sections between 300 and 350 nm that included corrections for Rayleigh scattering. The room temperature cross sections recommended here are a combination of the JPL10-6 recommendation for $\lambda < 260$ nm and the parameterization reported in Papanastasiou *et al.* for $\lambda \geq 260$ nm. The recommendation for the cross-section temperature dependence in the short-wavelength region is taken from Burkholder *et al.* (1991) (190-320 nm; 210-296 K). In the long-wavelength region, $\lambda \geq 260$ nm, the cross-section parameterization recommendation (given below) is taken from Papanastasiou *et al.*, which was derived from their data and the data of Gillotay and Simon (1989) (169-302 nm; 210-295 K) and Burkholder *et al.* (1991) (190-320 nm; 210-296 K). The uncertainty factors

given in Table 3.4 are significantly reduced from those reported in JPL10-6 due primarily to the consideration of the Papanastasiou *et al.* study.

CF_3Br (Halon-1301): The recommendation given here for the room temperature absorption spectrum is the same as JPL10-6. There are currently no available Halon-1301 cross-section data for wavelengths >300 nm, however, this region makes only a minor contribution to the calculated photolytic lifetime as shown in Section 3.5. No recommendation was given in JPL10-6 for the spectrum temperature dependence, although the cross-section parameterizations reported in Gillotay and Simon (1989) (178-280 nm, 210-300 K) and Burkholder *et al.* (1991) (190-285 nm, 210-296 K) were provided. The cross-section temperature dependences in the short-wavelength region from these studies are in relatively poor agreement, e.g., differences of ~20% at 205 nm and 210 K. Differences in the absolute cross-section values and their temperature dependence in the longer-wavelength region, λ >260 nm, exist between the data sets as well, e.g., the difference at 270 nm and 250 K is ~30%. The parameterization from Burkholder *et al.* (1991) is recommended here. The uncertainty factors given in Table 3.4 cover the range of the reported values in the various wavelength regions.

CH_3CF_2Cl (HCFC-142b): The recommendations given here for the CH_3CF_2Cl absorption cross sections and their temperature dependence are from the parameterization given by Nayak *et al.* (1996). JPL10-6 does not make a recommendation for the cross-section temperature dependence, but does report the parameterizations from Gillotay and Simon (1991), Orlando *et al.* (1991), and Nayak *et al.* The results from Nayak *et al.* and Gillotay and Simon differ significantly at shorter wavelengths, but are in reasonable agreement in the critical wavelength region for atmospheric photolysis, 205-220 nm, while the data from Orlando *et al.* and Hubrich and Stuhl (1980) are systematically different. The uncertainty factors given in Table 3.4 reflect the level of agreement between the Nayak *et al.* and the Gillotay and Simon studies.

CF_2Br_2 (Halon-1202): The recommendations provided here for the CF_2Br_2 cross sections and their temperature dependence in the $\lambda \geq 260$ nm region (given below) are based on the analysis provided by Papanastasiou *et al.* (2013) who reported absorption cross-section data in the long-wavelength region (300-325 nm; 210-296 K) that were corrected for Rayleigh scattering. For $\lambda < 260$ nm, the cross-section parameterization given in Burkholder *et al.* (1991) is recommended here. The uncertainty factors given in Table 3.4 are significantly lower than reported in JPL10-6 and encompass the range of the majority of the available experimental data.

CF_2BrCF_2Br (Halon-2402): The recommendations provided here for the CF_2BrCF_2Br cross sections and their temperature dependence are based on the studies reviewed in JPL10-6 together with the recent investigation and analysis by Papanastasiou *et al.* (2013) who reported absorption cross-section data in the long-wavelength region (300-325 nm; 250, 270, and 296 K) that were corrected for Rayleigh scattering. The 298 K cross sections recommended here are taken from JPL10-6 for $\lambda < 260$ nm and from Papanastasiou *et al.* for $\lambda \geq 260$ nm. For the temperature dependence at $\lambda < 260$ nm the parameterization of Gillotay *et al.* is recommended here. In the long-wavelength region, the cross-section parameterization reported in Papanastasiou *et al.* (given below) is recommended. The uncertainty factors given in Table 3.4 are significantly lower than reported in JPL10-6 and cover the range of the available experimental data, except in the long-wavelength region where the superseded data from Burkholder *et al.* (1991) fall outside the given range.

Absorption cross-section parameterizations for CF_2ClBr (Halon-1211), CF_2Br_2 (Halon-1202), and CF_2BrCF_2Br (Halon-2402) for wavelengths ≥260 nm and temperatures between 210 and 298 K as taken from Papanastasiou *et al.* (2013).

$$\ln\left(\sigma(\lambda,T)\right) = \sum_i A_i\left(\lambda - \bar{\lambda}\right)^i \times \left[1 + (296 - T)\sum_i B_i\left(\lambda - \bar{\lambda}\right)^i\right]$$

CF_2ClBr (Halon-1211)		
$\bar{\lambda} = 280.376$		
i	A_i	B_i
0	-48.3578	0.0002989
1	-0.1547325	8.5306×10^{-6}
2	-4.966942×10^{-4}	4.26×10^{-8}
3	1.56338×10^{-6}	-1.84×10^{-9}
4	3.664034×10^{-8}	1.284×10^{-11}
CF_2Br_2 (Halon-1202)		
$\bar{\lambda} = 287.861$		
i	A_i	B_i
0	-47.4178	0.0003173
1	-0.1567273	1.2323×10^{-5}
2	-2.624376×10^{-4}	2.68×10^{-8}
3	-6.78412×10^{-6}	-5.28×10^{-9}
4	1.261478×10^{-7}	6.99×10^{-11}
CF_2BrCF_2Br (Halon-2402)		
$\bar{\lambda} = 274.64$		
i	A_i	B_i
0	-48.3611	0.0001877
1	-0.1595	7.252×10^{-6}
2	-1.026×10^{-4}	2.917×10^{-7}
3	-1.334×10^{-5}	-1.725×10^{-9}
4	1.458×10^{-7}	-2.675×10^{-11}

NF_3 (Nitrogen trifluoride): JPL10-6 did not include an evaluation of the NF_3 UV absorption spectrum. The room temperature UV absorption spectrum has been reported by Makeev *et al.* (1975), Molina *et al.* (1995) (180-250 nm), Dillon *et al.* (2010) (184-226 nm), and Papadimitriou *et al.* (2013) (185-250 nm), where the wavelength range of the reported spectrum is given in parentheses. The spectrum reported by Makeev *et al.* seems to be in error and was not considered further. The agreement between the Molina *et al.*, Dillon *et al.*, and Papadimitriou *et al.* studies is good, to within ~5%, over the wavelength range most critical for atmospheric photolysis, 200 to 220 nm. Papadimitriou *et al.* also reported absorption cross-section data at 212, 231, 253, 273, and 296 K. The wavelength and temperature dependence parameterization reported by Papadimitriou *et al.*, see table below, is recommended here.

Absorption cross-section parameterization for NF_3 valid between 184.95 and 250 nm and the temperature range 212 to 296 K.

$$\log_{10}\sigma(\lambda,T) = \sum_i A_i\lambda^i + (296 - T)\sum_i B_i\lambda^i$$

NF_3 (Nitrogen trifluoride)		
i	A_i	B_i
0	-218.67	0.9261
1	4.03743	-0.0130187
2	-0.0295605	6.096×10^{-5}
3	9.596×10^{-5}	-9.75×10^{-8}
4	-1.3171×10^{-7}	9.76×10^{-12}
5	4.929×10^{-11}	–

3.4 Other Processes

Atmospheric heterogeneous loss processes involve chemical and physical interactions of gases with liquid and solid phases, i.e., clouds and aerosols. The composition of the condensed phases found in the atmosphere are multi-component where aqueous droplets, for example, may contain inorganic salts, sulfuric acid, and semi-volatile organics, while solid particles may consist of ice, soot, or mineral dust. Consequently, heterogeneous loss processes depend on the nature of the condensed phase, temperature, relative humidity, reactivity, and mass transport. For the majority of the molecules included in this report heterogeneous loss processes are expected to be minor, but are not well defined. Henry's Law (solubility) coefficients are evaluated in JPL10-6 and Staudinger and Roberts (2001) for a number of molecules considered in this report. Henry's Law coefficients used in Chapter 4 were not evaluated in this chapter.

Lu and Sanche (2001) and Lu (2009; 2010) have proposed that cosmic-ray induced heterogeneous chemistry may contribute to stratospheric loss of chlorofluorocarbons (CFCs). The proposed mechanism would, therefore, contribute to ozone depletion, particularly in the polar regions. The significance of this mechanism on stratospheric chemistry has been debated in the literature (Harris *et al.*, 2002; Müller, 2003; Patra and Santhanam, 2002). It has been shown that both observed stratospheric CFC distributions and tracer-tracer correlations of CFCs with long-lived species are not compatible with a significant destruction of CFCs on polar stratospheric clouds (PSC) (Grooß and Müller, 2011; Müller, 2003; Müller and Grooß, 2009). Thus, cosmic-ray induced heterogeneous reactions are not considered a significant stratospheric loss process for CFCs and not an alternative mechanism causing the Antarctic ozone hole (Grooß and Müller, 2011; Müller, 2003; Müller and Grooß, 2009).

3.5 Lifetimes, Uncertainties, and Ranges

The NASA/Goddard Space Flight Center (GSFC) two-dimensional (2-D) coupled chemistry-radiation-dynamics model was used to evaluate the impact of the kinetic and photochemical recommendations on atmospheric lifetimes. Model calculations were performed using input from the recommendations given in this report as well as those from JPL10-6 for comparison purposes. The GSFC 2-D model has been used in stratospheric ozone assessments (WMO, 2007; 2011), and in studies pertaining to the chemistry-climate coupling of the middle atmosphere. The residual circulation framework used in 2-D models has been shown to provide realistic simulations of atmospheric transport on long timescales (>30 days). As

demonstrated in recent studies, the model ozone, temperature, zonal wind, and long-lived tracer simulations are in good overall agreement with a variety of observations in reproducing transport-sensitive features in the meridional plane (Fleming *et al.*, 2011). The computational speed of the 2-D model allowed numerous sensitivity simulations to be performed as part of this evaluation as outlined in Table 3.5. The GSFC 2-D model is, therefore, a useful tool to evaluate the atmospheric lifetimes for the molecules included in this report, as well as the relative importance of the different atmospheric loss processes and the lifetime sensitivity to the recommended kinetic and photochemical parameters and their uncertainties. The GSFC 2-D model was also used in Chapter 5, "Model Estimates of Lifetimes", allowing for traceability between the 2-D and 3-D model calculated lifetimes.

The 2-D model calculations were used to (1) calculate local and global annually averaged lifetimes, (2) quantify the relative contributions of the reactive and photolytic loss processes to the local and global lifetimes, (3) compare lifetimes obtained using the SPARC and JPL10-6 recommended model input parameters, (4) evaluate the impact of Lyman-α photolysis (not included in JPL10-6) on calculated lifetimes, (5) quantify the range in calculated atmospheric lifetimes due to the uncertainties in the model input kinetic and photochemical parameters, and (6) evaluate the lifetime sensitivity to uncertainties in the O_2 and O_3 absorption cross sections.

The 2-D model results presented in this chapter are from steady-state simulations for year 2000 conditions of source gas loading, solar flux, and stratospheric aerosol density. These conditions are consistent with the year 2000 time slice model simulations and analysis presented in Chapter 5. The model tropospheric OH was specified from the monthly-varying OH field documented in Spivakovsky *et al.* (2000) following the methodology used in Chapter 5. Reaction with the OH radical is an important atmospheric removal process for many of the molecules included in this assessment, i.e., the hydrogen containing molecule lifetimes are largely determined by the rates of their OH reactions. Since the majority of the OH reactive loss occurs in the troposphere, specifying the tropospheric OH field in this manner was important for analysis of model simulations of the OH related loss rates and lifetimes. The lifetime sensitivity to the OH field is discussed further in Chapter 5. The stratospheric and mesospheric OH, and atmospheric $O(^1D)$ and Cl atom profiles are simulated by the model for all calculations presented in this chapter. Global annual averages are given here, consistent with the general methodology used to compute the lifetimes (Kaye *et al.*, 1994). Lifetimes are computed as the ratio of the global atmospheric burden to the vertically integrated annually averaged global total loss rate (Kaye *et al.*, 1994), consistent with the methodology used in the model simulations for Chapter 5.

Model results for CHF_2Cl, HCFC-22, obtained using the SPARC recommendations are given graphically here for example purposes, while a complete set of results for all the molecules is presented in the tables and graphical supplementary material. The calculated local lifetimes for the various loss processes as well as the total local lifetime are shown in Figure 3.3. The figure includes all of the loss processes, although not all make a significant contribution to the total local lifetime. To identify the wavelength regions of greatest importance in the photolytic loss, the photolytic loss was divided into Lyman-α and the wavelength ranges 169-190, 190-230, 230-286, and >286 nm. For HCFC-22, atmospheric loss in the troposphere is dominated by its reaction with the OH radical. In the middle to upper stratosphere reaction with $O(^1D)$ contributes to its loss with photolysis in the 190-230 nm wavelength region making a minor contribution. In the mesosphere above 65 km, HCFC-22 loss is dominated by Lyman-α photolysis.

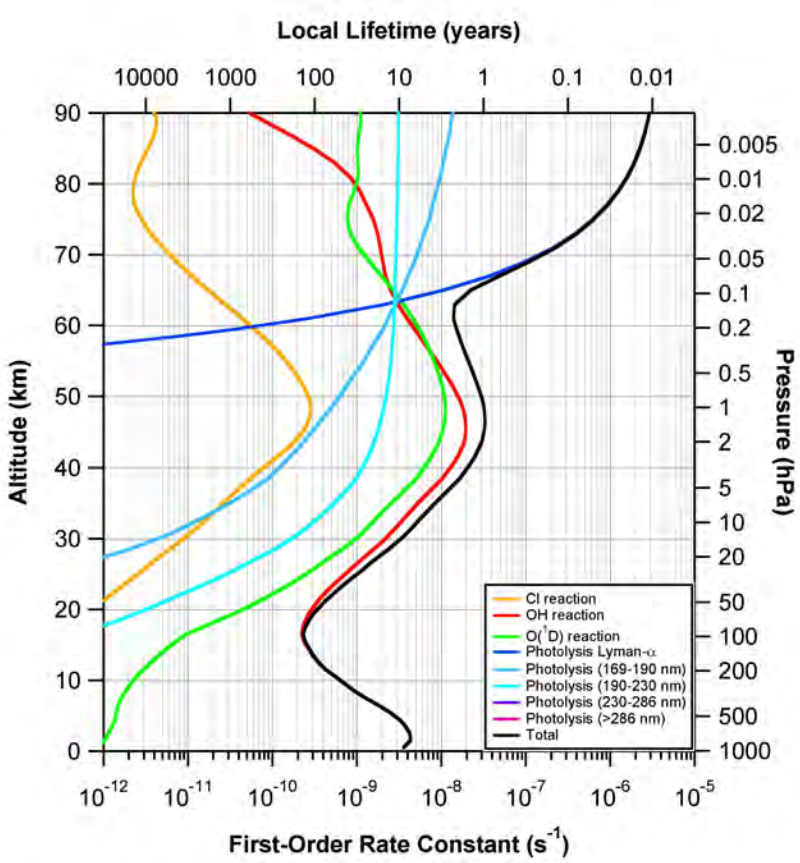

Figure 3.3. Global annually averaged local lifetimes for various gas-phase loss processes of CHF_2Cl (HCFC-22) calculated using the GSFC 2-D model for year 2000 steady state conditions.

The calculated atmospheric molecular loss rate and mixing ratio vertical profiles for HCFC-22 are shown in Figure 3.4. The molecular loss rate is greatest at Z = 0 and decreases significantly throughout the troposphere. The global annually averaged lifetime for HCFC-22 was calculated to be 12.2 years, while the lifetime obtained using the JPL10-6 parameters is slightly less, 12.0 years. The global lifetimes for each compound calculated using the SPARC and JPL10-6 recommended model input parameters are given in Tables 3.6 and 3.7. The differences in lifetimes obtained using the JPL10-6 and present recommended parameters are generally small, <5%, for most of the molecules. However, for CCl_4, the difference is substantial, 38.0 (JPL10-6) vs. 48.7 (SPARC) years, owing to the greater OH reactive loss obtained using the JPL10-6 recommended rate coefficient upper-limit for the OH + CCl_4 reaction. The rate coefficient upper-limit is significantly reduced in the present SPARC recommendation and, thus, represents a negligible loss process and in turn yields a longer and more representative lifetime. The lifetime difference is also large for Halon-2402, 13.9 (JPL10-6) vs. 27.8 (SPARC) years, due to the greater photolytic loss at wavelengths >286 nm obtained using the JPL10-6 recommendation and for CFC-115 (961 (JPL10-6) vs. 540 (SPARC) years) due to the change in its $O(^1D)$ rate coefficient. The lifetime differences for Halon-1211, Halon-1202, and HFC-227ea are less and on the order of ~20%.

Table 3.6 also gives the fractional contributions to the calculated lifetime from the photolytic and $O(^1D)$, OH, and Cl reactive losses for each molecule. The fractional contribution breakdown identifies the most critical loss processes for each molecule as well as potential focus areas for future laboratory studies. The fractional contributions obtained using the

present and JPL10-6 recommendations are also given graphically in Figure 3.5. The figure illustrates that photolysis is the dominant loss process for most of the species primarily removed in the stratosphere (including the Halons), while reaction with OH is the dominant atmospheric loss process for the hydrogen containing compounds. For example, for HCFC-22, OH reactive loss accounts for 98.2% of its global annually averaged loss, while $O(^1D)$ reaction contributes 1.4% and photolysis 0.4%.

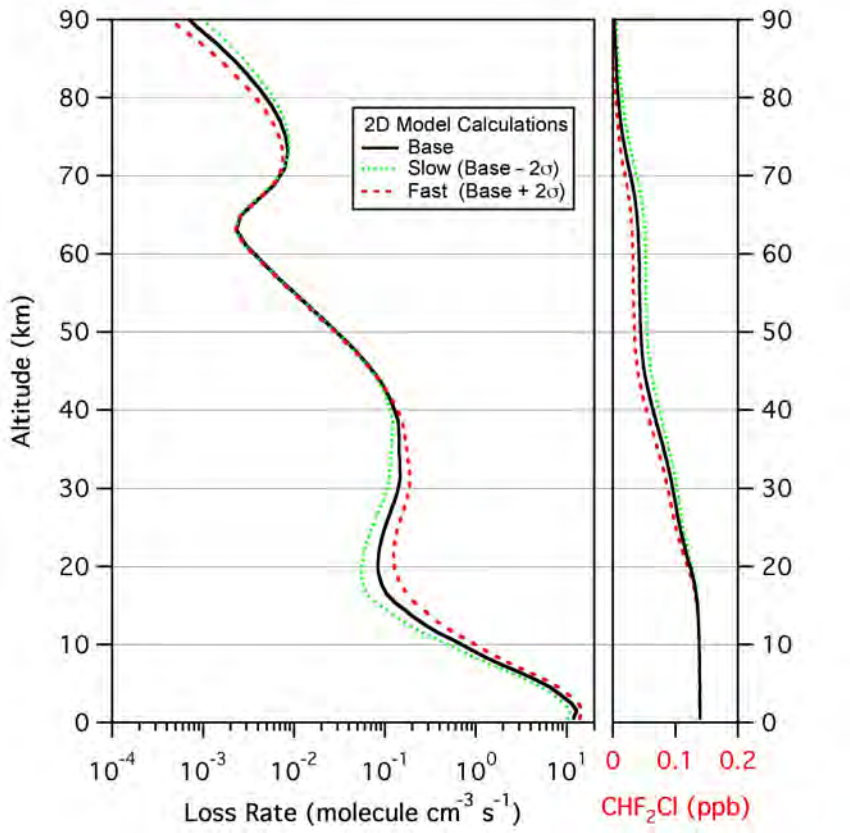

Figure 3.4. Global annually averaged vertical profile molecular loss rates and mixing ratios for CHF_2Cl (HCFC-22) calculated using the GSFC 2-D model and SPARC kinetic and photochemical parameter recommendations for year 2000 steady state conditions.

In summary, the key 2-D model global annually averaged findings include:

- For the hydrogen containing compounds, reaction with the OH radical is the dominant atmospheric removal process (>90% of the total loss) and occurs primarily in the troposphere for most of the molecules in this study.
- For N_2O (nitrous oxide), NF_3, the CFCs, and CCl_4, photolysis is a dominant loss process (37% for CFC-115, 70-75% for NF_3 and CFC-114, and >90% for the others,) with stratospheric photolysis in the 190-230 nm region accounting for >90% of the photolytic loss (75% of the photolytic loss for CFC-115).
- For the Halons, photolysis is the dominant loss process (>97%) with altitude dependent contributions from both the 190-230 and >286 nm wavelength regions.
- The $O(^1D)$ reactive loss is significant for CFC-114 (25%), CFC-115 (63%), N_2O (10%), and NF_3 (28.7%) but <6% for other molecules considered in this study.

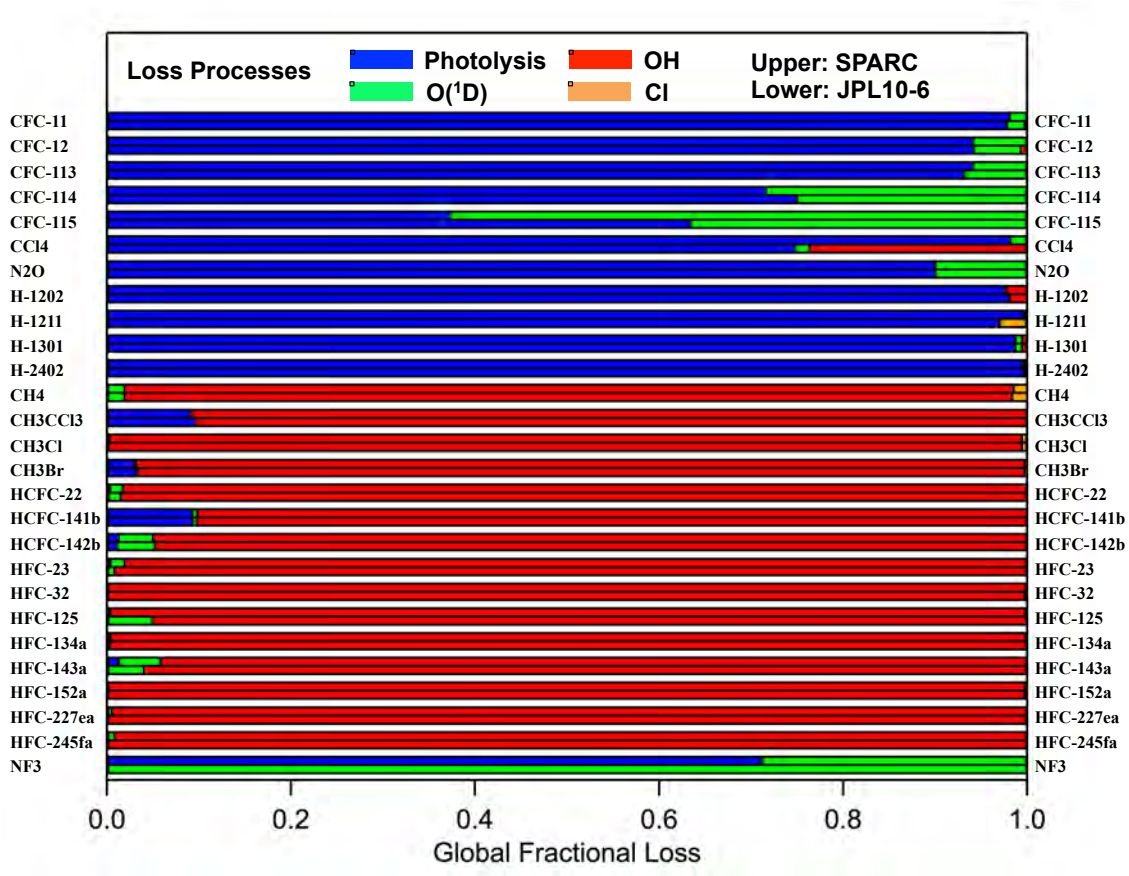

Figure 3.5. Summary of the global annually averaged fractional losses (see legend) obtained using the 2-D model with kinetic and photochemical input parameters from SPARC (upper bar) and JPL10-6 (lower bar).

- Overall, atmospheric loss due to Cl atom reaction is minor, <1.5% for CH_4 and <0.5% for all other molecules in this study.

An objective of this chapter was to evaluate the uncertainty (range) in calculated atmospheric lifetimes due to the uncertainties in the model input kinetic and photolytic parameters given in Tables 3.1 – 3.4. To do this, model simulations were made with the input parameters set to their 2-σ uncertainty lowest values (slow) and to their 2-σ uncertainty greatest values (fast) and compared with the baseline calculations presented above. However, a complication is that changes to the model input parameters impact all model calculated trace species including ozone. Changes in ozone modify the incident solar radiation in the atmosphere, which impacts the calculated lifetimes via changes in the photolysis of trace species, production of $O(^1D)$, and the concentration of stratospheric OH. To aid an evaluation of this feedback, two sets of model simulations were each made for the slow and fast scenarios: 1) all model constituents including ozone allowed to interact in standard fashion, and 2) as in 1), except with the molecules addressed in this report treated as non-interactive tracers so that changes to their kinetic and photolytic parameters will not impact ozone. Table 3.5 summarizes the model simulations performed.

The annually averaged ozone impacts of the slow and fast interactive simulations, using the SPARC model parameters, are shown in the top panels of Figure 3.6. The ozone change from the baseline calculation is generally small, <5%, but not negligible. In the slow case,

the change in ozone increases in the middle-upper stratosphere, but decreases in the troposphere and tropical lower stratosphere. For the fast case, the ozone changes from baseline are roughly equal and opposite to those in the slow case. The ozone changes in the mesosphere, above 60 kilometers (km), are generally small, <1%, and are not shown in Figure 3.6.

The vast majority of the ozone change in the slow/fast calculations is due to the changes in the kinetic parameters for the reactions of CH_4 with OH, $O(^1D)$, and Cl and the photolysis of N_2O and its reaction with $O(^1D)$. Changes in the kinetic and photolytic parameters of the other molecules included in this study have a minimal impact on ozone. Changes in the CH_4 reactions impact ozone via the inorganic chlorine (Cl_x) and odd hydrogen (HO_x) ozone-loss cycles in the stratosphere and the NO_x-induced ozone production cycle in the troposphere and lower stratosphere. The change in ozone due to the changes in the three CH_4 loss processes is shown in the middle panels in Figures 3.6. The net impact in the slow (fast) case yields ozone increases (decreases) of 1% in the upper stratosphere, ozone decreases (increases) of 1-2% in the upper troposphere-lower stratosphere, and ozone decreases (increases) of 6-7% in the ozone hole region.

Changes in the N_2O loss parameters impact stratospheric ozone via direct changes in the abundance of odd-oxygen ($O + O_3$) due to N_2O photolysis, and odd-nitrogen ($NO + NO_2$) due to the N_2O reaction with $O(^1D)$. The net impact on ozone is shown in the bottom panels in Figure 3.6. The net impact of the slow (fast) N_2O loss yields increases (decreases) in ozone of 4-5% in the global middle-upper stratosphere and polar lower stratosphere. Smaller ozone changes occur at lower altitudes that are likely caused by a "shielding" effect. In general, ozone increases at lower altitudes due to ozone depletion above are known in the literature as "self-healing" events and have been discussed previously (Harrison, 1975).

For almost all molecules, including the ozone feedback yielded a somewhat larger range of lifetimes between the slow and fast calculations. Exceptions to this are CFC-114 and CFC-115 that have weak tropospheric losses and large mesospheric losses. The ozone feedback had the largest impact on CFC-115, with lifetime differences of ~10% between the interactive and non-interactive cases. For compounds that have significant or dominant stratospheric losses (CFC-11, CFC-12, CFC-113, CFC-114, CCl_4, N_2O, and Halon-1301), the feedback effect is minor, with lifetime differences in the range 1.5 to 4%. For compounds that have a dominant tropospheric OH loss, the ozone feedback effect is small since tropospheric OH is specified in the model. For these compounds, the lifetime differences are <0.6% between the interactive and non-interactive cases.

Using the model calculations with the ozone feedback included, the uncertainty in the local lifetime was calculated from the slow and fast case results. Figure 3.7 shows the uncertainty in the local loss rate for HCFC-22 and a breakdown of the contribution from the different loss processes. The uncertainty at Z = 0 is ~18% due almost exclusively to the uncertainty in the OH + HCFC-22 reaction rate coefficient. The increase in the uncertainty with increasing altitude throughout the troposphere and lower stratosphere is due to the increased uncertainty in the rate coefficient at lower temperatures.

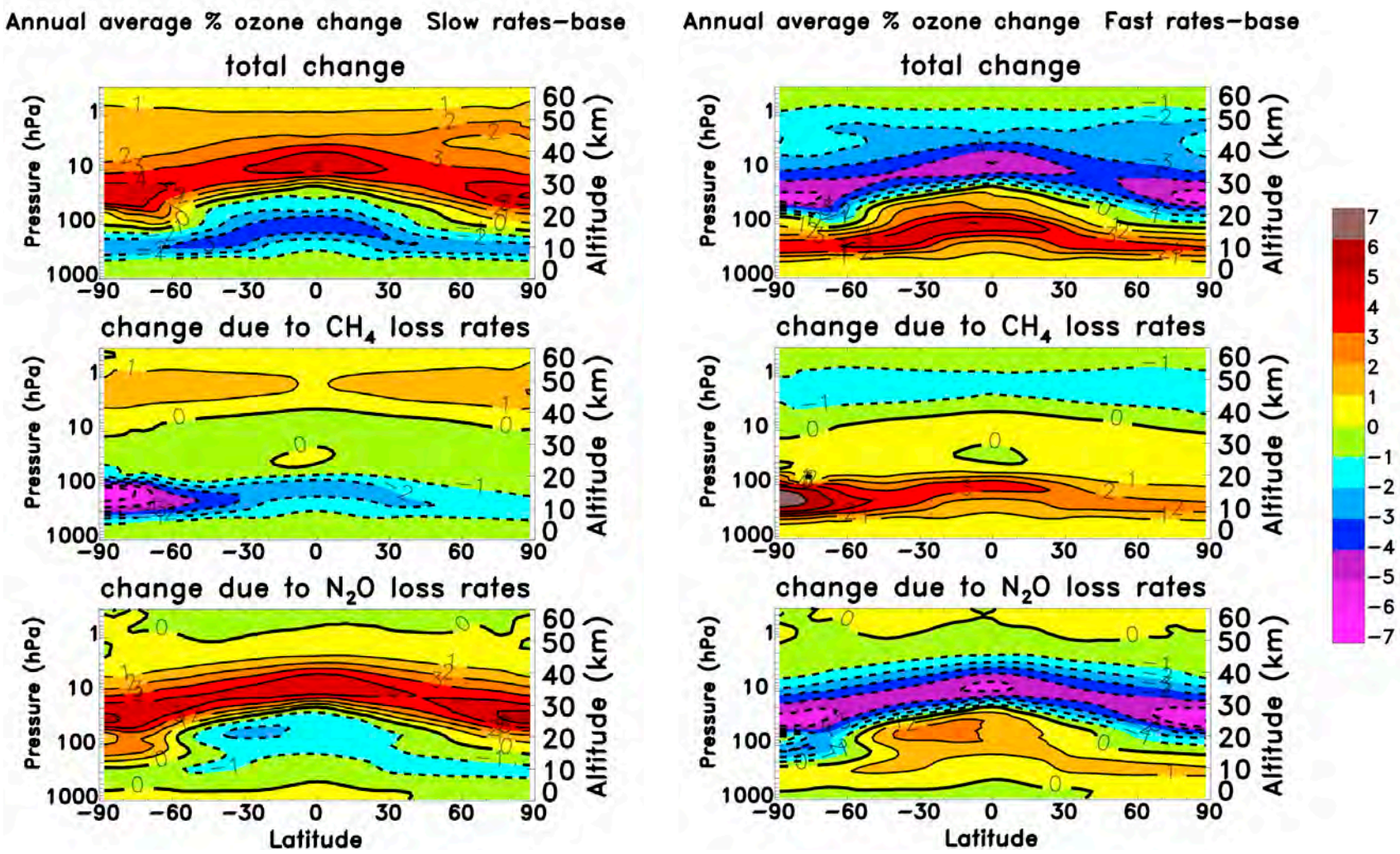

Figure 3.6. Annually averaged percentage ozone change in the slow and fast (see text) model simulations (top) for all 26 compounds, (middle) CH_4 only; (bottom) N_2O only. The ozone change is taken relative to the Baseline case using steady-state model simulations for year 2000 conditions as discussed in the text. The contour interval is ±1%.

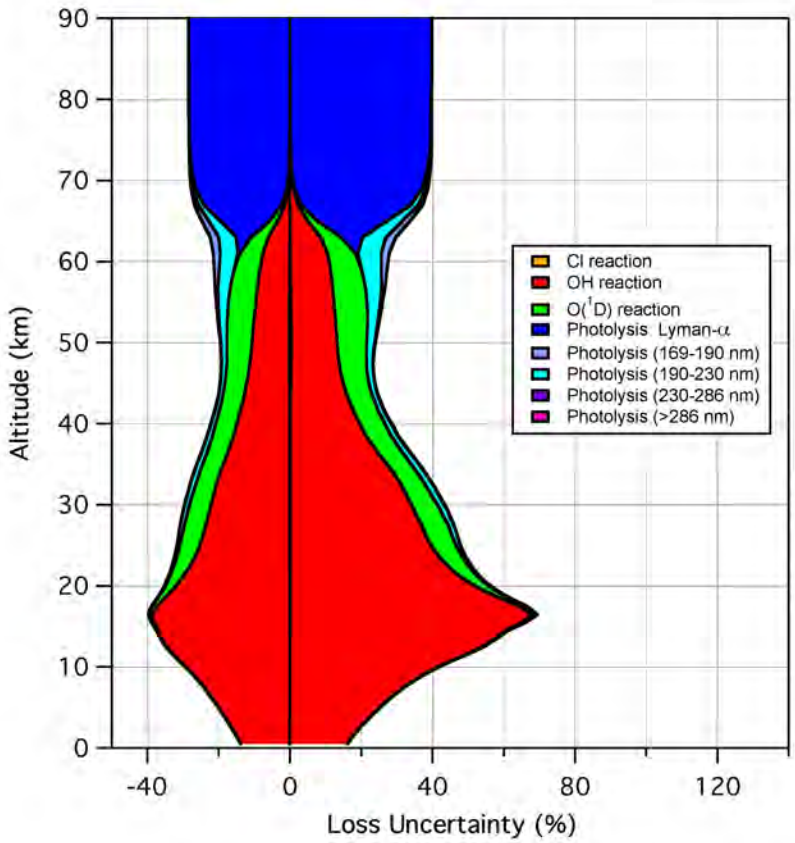

Figure 3.7. Uncertainty in the global annually average local loss rate from the GSFC 2-D model calculation with the SPARC recommended parameters and uncertainties for CHF_2Cl (HCFC-22).

The range in the HCFC-22 global lifetime computed from the fast (minimum lifetime) and slow (maximum lifetime) uncertainty limits with the ozone feedback included is 10.0 to 14.9 years, a ~±20% difference from the baseline lifetime value. The vertical molecular loss and mixing ratio profiles for the slow and fast cases are included in Figure 3.4 for comparison with the baseline calculation. The range in global lifetimes for all the molecules is given in Table 3.7. There is a wide variation in the lifetime ranges among the molecules; the percentage range is smallest, ~5-10%, for N_2O, CCl_4, and the CFCs (excluding CFC-115).

The 2-D model calculated lifetimes obtained using the SPARC and JPL10-6 input kinetic and photochemical parameters are also given graphically in Figure 3.8, where the whiskers represent the 2σ range in the calculated lifetime due solely to the estimated uncertainty in the input parameters.

Table 3.7 also gives the lifetimes separated by the troposphere (surface to the tropopause, seasonally and latitude-dependent), stratosphere, and mesosphere (<1 hPa). The lifetimes are computed using the global atmospheric burden and the loss rate integrated over the different atmospheric regions such that

$$\frac{1}{\tau_{Tot}} = \frac{1}{\tau_{Trop}} + \frac{1}{\tau_{Strat}} + \frac{1}{\tau_{Meso}}$$

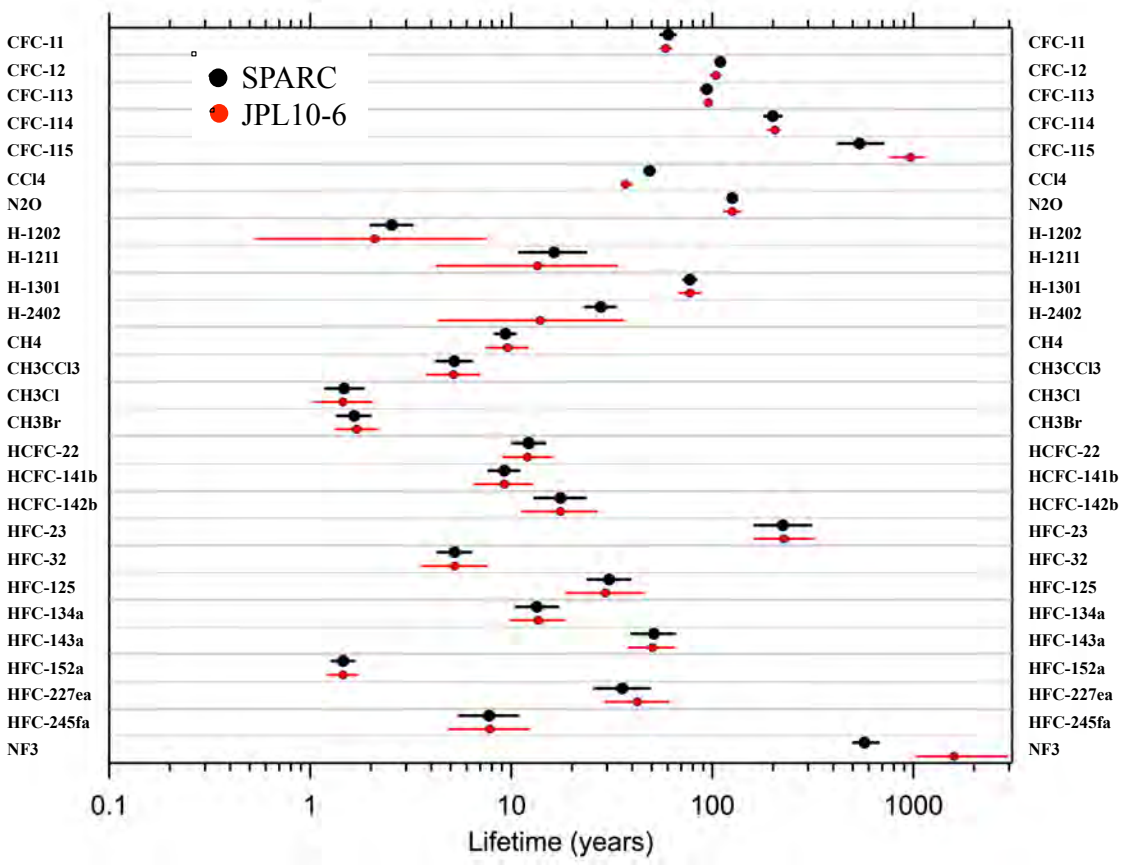

Figure 3.8. Summary of the global annually averaged lifetimes obtained using the 2-D model with kinetic and photochemical input parameters from SPARC (black, upper) and JPL10-6 (red, lower) values reported in Tables 3.6 and 3.7. The whisker error bars show the 2σ range in the calculated lifetime due solely to the uncertainty in the kinetic and photochemical input parameters.

Molecules with short tropospheric lifetimes reflect a dominant OH reactive loss, or for Halon-1211 and Halon-1202, a dominant photolysis loss at wavelengths >286 nm. Most molecules have very long mesospheric lifetimes (>10,000 years); CFC-114, CFC-115, HCFC-22, HCFC-142b, CH_4, and some of the HFCs have mesospheric lifetimes between 2,500 and 4,900 and years.

3.6 Lifetime Sensitivity to O_2 and O_3 UV Cross Sections

O_2 and O_3 absorption cross sections used in models are important in quantifying the amount of UV radiation incident at any point in the atmosphere, and in determining the concentration of ozone throughout the middle atmosphere. Uncertainties in the O_2 and O_3 cross sections therefore contribute to uncertainties in the calculated atmospheric lifetimes of trace species.

For the O_2 cross sections, uncertainties in the Schumann-Runge (S-R) bands (175-205 nm) and the Herzberg continuum (195-242 nm) arise from a combination of uncertainties in the laboratory measurements and the parameterization of the fine wavelength structure and temperature dependence of the S-R bands for use in atmospheric models. Total cross-section uncertainties in the S-R and Herzberg regions are estimated here to be in the range of 10 to 20% (2σ) based on the JPL10-6 data evaluation and Minschwaner *et al.* (2012). The O_3 UV

absorption cross-section uncertainty is taken here to be 4% (2σ), based primarily on the level of agreement among various laboratory measurements.

GSFC 2-D model simulations were used to evaluate the lifetime sensitivity to uncertainties in the O_2 and O_3 UV absorption cross sections. The model utilizes a look-up table calculated with the APL radiative transfer code to obtain the O_2 photolysis and incident solar radiation at each grid point as a function of wavelength (175-847.5 nm), solar zenith angle, overhead ozone column, and pressure (Anderson and Meier, 1979; Swartz *et al*., 1999). For the evaluation of uncertainties, new look-up tables were generated in which the cross sections were increased or decreased by a specified amount and then input into the 2-D model. Uncertainties of both ±10 and ±20% were applied to the O_2 cross sections. Model simulations were first performed with the O_2 cross sections perturbed simultaneously at all wavelengths. However, given the different spectral characteristics of, and atmospheric responses to the S-R and Herzberg regions, model calculations were also performed with the wavelength ranges <204 nm and >204 nm perturbed separately. For O_3, a cross-section uncertainty of ±4% (2σ) was used for all wavelengths, in both the look-up table and 2-D model chemistry. The wavelength bins and base cross sections are provided in the supplementary material. For Lyman-α and the wavelength range 169-175 nm, the O_2 photolysis and incident solar radiation at each grid point are calculated in the 2-D model separately from the look-up table. These wavelength regions have only minor contributions to the total global lifetime of the compounds addressed in this report and are not considered in this uncertainty analysis.

For the species primarily removed in the stratosphere, the lifetime changes due to the perturbations to the absorption cross sections are listed in Table 3.8; species removed primarily in the troposphere are not considered in this analysis since the 2-D model tropospheric OH is specified and therefore does not respond to changes in the O_2 and O_3 cross sections. The percentage change from the baseline case is indicated in parentheses in Table 3.8 (for reference, the baseline lifetimes are repeated from Tables 3.6 and 3.7). In general, reducing the O_2 and O_3 cross sections increases the incident solar flux and photolytic loss, thereby decreasing a compounds' lifetime. Conversely, increasing the cross sections leads to an increased lifetime. For the O_2 cross-section perturbations, the lifetime response is asymmetric for all compounds and wavelength ranges; i.e., reducing the cross sections results in a larger magnitude change (reduction) in lifetime compared with the corresponding response to increasing the cross sections. The magnitude of this asymmetry varies among the different compounds and wavelength ranges.

The results given in Table 3.8 show that since removal of most of the species is dominated by photolytic loss in the stratosphere, there is substantial lifetime sensitivity to uncertainties in the O_2 cross sections. The sensitivity is somewhat less for (1) CFC-115 and NF_3, which have substantial loss due to reaction with $O(^1D)$ and Lyman-α photolysis, and (2) Halon-1202 which has substantial tropospheric photolytic loss at wavelengths >286 nm. The lifetime sensitivity to the uncertainty in the O_3 cross sections (±4%) is small, with changes of less than ±1% for all the compounds. The results in Table 3.8 are based on free-running model simulations in which the O_3 and constituent profiles adjust to the O_2 and O_3 cross-section perturbations. Therefore, the lifetime responses for CFC-11 and CFC-12 are somewhat smaller than reported in Minschwaner *et al*. (2012), who used O_3 and CFC profiles fixed to observations.

The results in Table 3.8 illustrate that the lifetime responses to the O_2 cross-section perturbations are nearly linear; *i.e.*, the ±20% perturbations are roughly twice the magnitude of the ±10% perturbations. This is true for the perturbations made separately above and below 204 nm, and for all wavelength regions perturbed simultaneously. Perturbing the spectral region below 204 nm gives a larger lifetime response for all compounds, compared to perturbing the spectral region above 204 nm. The lifetime responses are combined, assuming the perturbations in the two O_2 wavelength regions and the O_3 perturbation are independent, as

$$\tau_{\text{Perturbed}} = \tau_{\text{Base}} \pm \sqrt{[\tau_{\text{Base}} - \tau^{\text{O}_2}_{<204\,nm}]^2 + [\tau_{\text{Base}} - \tau^{\text{O}_2}_{>204\,nm}]^2 + [\tau_{\text{Base}} - \tau^{\text{O}_3}_{\text{All}\,\lambda}]^2}$$

where τ_{Base} is the baseline lifetime, $\tau^{\text{O}_2}_{<204\,nm}$ and $\tau^{\text{O}_2}_{>204\,nm}$ are the lifetimes computed from the separate O_2 cross-section perturbations below and above 204 nm, respectively, and $\tau^{\text{O}_3}_{\text{All}\,\lambda}$ is the lifetime computed with the O_3 cross-section perturbation. The contribution of the O_3 cross-section perturbation to $\tau_{\text{Perturbed}}$ is small due to the weak lifetime sensitivity to the O_3 cross-section uncertainty. For all compounds, the range of $\tau_{\text{Perturbed}}$ is slightly smaller than that obtained from the model calculations with the O_2 cross sections perturbed at all wavelengths simultaneously. For example, for the ±20% O_2 cross-section perturbation for CFC-11, the range of $\tau_{\text{Perturbed}}$ is 49.8–67.8 years, compared to 47.8–70.8 years for all wavelengths perturbed simultaneously. This indicates that responses to the perturbations in the two wavelength regions are not fully independent, i.e., there is a small positive feedback effect present when perturbing the O_2 cross sections at all wavelengths simultaneously.

The recommended overall range in $\tau_{\text{Perturbed}}$ is given in Table 3.8 and was computed using the results from the ±20% O_2 cross-section perturbation below and above 204 nm. The uncertainties given in Table 3.8 as well as the lifetime uncertainties due to the kinetic and photochemical data for each molecule (Table 3.7) are used in Chapter 6 in the determination of the estimated overall lifetime uncertainty for each compound.

3.7 Conclusions and Future Directions

The most critical kinetic and photochemical processes that ultimately determine the atmospheric lifetimes of the compounds included in this report are identified by the fractional contributions and kinetic and photolytic lifetimes as given in Tables 3.6 and 3.7. The uncertainty in the kinetic and photochemical parameters was evaluated (see Tables 3.1 – 3.4 and the Supplementary Material for additional detail for each molecule) and the impact on atmospheric lifetimes was evaluated using 2-D model calculations, see Tables 3.6 and 3.7. Although there are no major gaps in the understanding of the atmospheric processing of these compounds, the 2-D atmospheric model calculations show that the recommended uncertainties in kinetic and photochemical parameters make a non-negligible contribution to the uncertainty (range) in calculated atmospheric lifetimes. The estimated uncertainties given in the SPARC recommendations, in general, lead to a reduction in the range of calculated lifetimes from those calculated using the NASA/JPL (JPL10-6) recommended kinetic parameters. The range in calculated lifetimes obtained for $CFCl_3$ (CFC-11), CF_2Cl_2 (CFC-12), CCl_4, and N_2O using the SPARC recommendations is between 5 and 10% (2σ uncertainty), while for CH_3CCl_3 (methyl chloroform), CH_3Cl, CH_3Br, CHF_2Cl (HCFC-22), and CH_3CCl_2F (HCFC-141b) it is ~20%, and the range is greater for CF_3CClF_2 (CFC-115), CBr_2F_2 (Halon-1202), $CBrClF_2$ (Halon-1211), CH_3CClF_2 (HCFC-142b), and several of the HFCs. Reducing uncertainties in kinetic and photochemical parameters, in general, is

desirable, and the results presented in this chapter and the Supplementary Material can be used to guide the direction of future studies. For example, the extension of rate coefficient data, in some cases, to the cold temperatures (~200 to 240 K) representative of the UT/LS would help reduce estimated uncertainties in calculated local lifetimes, which are currently based on an extrapolation of kinetic data obtained at higher temperatures. It was also shown that the existing uncertainties in the O_2 absorption cross sections in the Schumann-Runge bands between 190 and 204 nm contribute substantially to the absolute uncertainty in the lifetimes of molecules removed in the stratosphere by UV photolysis, e.g., CFCs. Studies that would reduce the present level of uncertainty in the O_2 absorption cross sections are therefore desired.

Table 3.1. Reaction rate coefficients and estimated uncertainties for the OH + compound gas-phase reactions.*

Compound	Chemical Formula	Temperature Range (K) **	*A* *	*E*/R (K)	*k*(298 K) *	*f*(298 K)	*g*	Footnotes
1. CFC−11	CCl_3F	–	*10*	*9695*	*<1 (-25)*	_	–	1,2
2. CFC−12	CCl_2F_2	–	*10*	*11910*	*<1 (-28)*	–	–	1,2
3. CFC−113	CCl_2FCClF_2	–	*10*	*>6220*	*<1 (-20)*	–	–	3,4
4. CFC−114	$CClF_2CClF_2$	–	*10*	*>6220*	<1 (-20)	–	–	3,4
5. CFC−115	CF_3CClF_2	–	*10*	*>6220*	*<1 (-20)*	–	–	3,4
6. Carbon Tetrachloride	CCl_4	–	*10*	*6220*	*<1 (-20)*	–	–	1,2
7. Nitrous Oxide	N_2O	–	–	–	*<5.0 (-17)*	–	–	3,a
8. Halon−1202	CBr_2F_2	–	*1*	*>2200*	*<5 (-16)*	–	–	5
9. Halon−1211	$CBrClF_2$	–	*1*	*>3500*	*<8 (-18)*	–	–	2,b
10. Halon−1301	$CBrF_3$	–	*1*	*>3600*	*<6 (-18)*	–	–	5
11. Halon−2402	$CBrF_2CBrF_2$	–	*1*	*>3600*	*<6 (-18)*	–	–	5
12. Methane	CH_4	195 – 300	1.85	1690	6.4 (-15)	1.05	50	2,c
13. Methyl Chloroform	CH_3CCl_3	233 – 379	1.64	1520	1.0 (-14)	1.10	50	5,6
14. Methyl Chloride	CH_3Cl	224 – 298	1.96	1200	3.5 (-14)	1.10	50	2,6,d
15. Methyl Bromide	CH_3Br	233 – 300	1.40	1150	3.0 (-14)	1.07	100	2,6,e
16. HCFC−22	$CHClF_2$	250 – 391	1.03	1600	4.8 (-15)	1.07	100	2,6
17. HCFC−141b	CH_3CCl_2F	250 – 400	1.25	1600	5.8 (-15)	1.07	100	5,6,f
18. HCFC−142b	CH_3CClF_2	223 – 400	1.30	1770	3.4 (-15)	1.15	50	5,6
19. HFC−23	CHF_3	252 – 298	0.52	2210	3.1 (-16)	1.15	100	5
20. HFC−32	CH_2F_2	222 – 384	1.70	1500	1.1 (-14)	1.07	100	5,6
21. HFC−125	CHF_2CF_3	220 – 364	0.60	1700	2.0 (-15)	1.10	100	5,6,g
22. HFC−134a	CH_2FCF_3	223 – 400	0.95	1600	4.4 (-15)	1.10	100	2,6,h
23. HFC−143a	CF_3CH_3	261 – 403	1.06	2010	1.25 (-15)	1.10	100	2,i
24. HFC−152a	CH_3CHF_2	210 – 300	0.87	975	3.3 (-14)	1.05	50	5,6,j
25. HFC−227ea	CF_3CHFCF_3	250 – 400	0.48	1680	1.7 (-15)	1.15	75	2,6,k
26. HFC−245fa	$CHF_2CH_2CF_3$	273 – 370	0.61	1330	7.0 (-15)	1.15	100	5,6
27. Nitrogen Trifluoride	NF_3	–	*10*	*>17500*	*<3 (-37)*	–	–	1,3,l

Footnotes

* Estimated values are given in italics; A is in units of 10^{-12} cm^3 molecule^{-1} s^{-1}; k(298 K) is in units of cm^3 molecule^{-1} s^{-1} and (-xx) represents $\times 10^{-xx}$; $k(T) = A \exp(-E/RT)$.

** Temperature range of available experimental data considered in the evaluation of the reaction rate coefficient parameters and uncertainty limits.

1 The recommendation given here was obtained by setting the pre-exponential factor (A) to 1×10^{-11} cm^3 molecule^{-1} s^{-1} and equating the activation energy (E) to the reaction endothermicity using the thermochemical parameters reported in JPL10-6 and IUPAC. The JPL10-6 recommendation was derived from experimentally determined rate coefficient upper limits.

2 A and/or E/R recommendation is revised from JPL10-6.

3 Not evaluated in JPL10-6.

4 The recommended kinetic parameters are taken to be equal to those for the OH + CCl_4 reaction.

5 A and E/R recommendation is unchanged from JPL10-6.

6 f(298 K) and/or g is revised from JPL10-6.

a Based on the study by Biermann *et al.* (1976), who measured a rate coefficient of 3.8×10^{-17} cm^3 molecule^{-1} s^{-1} at 298 K. A more conservative upper limit (4.0×10^{-16} cm^3 molecule^{-1} s^{-1}) was reported by Chang and Kaufman (1977b).

b Rate coefficient expression was estimated using an estimated Arrhenius A-factor and the rate coefficient upper-limit reported by Burkholder *et al.* (1991) at 373 K.

c A and/or E/R recommendation was taken from IUPAC data evaluation.

d The recommended k(298 K) was obtained from an average of the data of Hsu and DeMore (1994), Orkin *et al.* (2013), and Herndon *et al.* (2001). The recommended E/R was obtained from a fit to the data of Herndon *et al.* below 298 K.

e The recommended k(298 K) was obtained from an average of the data of Hsu and DeMore (1994) (recalculated based on the JPL10-6 recommended rate coefficient for the OH + CH_3CHF_2 reference reaction), Chichinin *et al.* (1994), Mellouki *et al.* (1992), and Zhang *et al.* (1992). The recommended value for E/R was derived from a fit to the data of Mellouki *et al.* below 300 K.

f The data from Lancar *et al.* (1993) at T<400K were used in the fit to obtain E/R.

g The recommended k(298 K) was obtained from an average of the data of Talukdar *et al.* (1991), DeMore (1993), and Young *et al.* (2009). The recommended value for E/R was taken from Talukdar *et al.*

h The present analysis differs from that given in JPL10-6 in that the three rate coefficients reported in DeMore (1993) were averaged in the determination of E/R.

i The present analysis differs from that given in JPL10-6 in that the DF-LMR results of Talukdar *et al.* (1991) were not included in the analysis for k(298K), although their LP-LIF results were included.

j The site specific rate coefficients were estimated by Kozlov *et al.* (2003) to be 33% reaction at the CH_3 group and 67% H atom abstraction from the CH_2F group.

k The recommended k(298 K) was obtained from an average of the results from the absolute rate studies of Nelson *et al.* (1993), Zellner *et al.* (1994), Zhang *et al.* (1994), and Tokuhashi *et al.* (2004) and the relative rate studies of Hsu and DeMore (1995) (recalculated based on the JPL10-6 recommended rate coefficients for the OH + CH_4 and OH + CHF_2CF_3 reference reactions) and Wallington *et al.* (2004) (recalculated based on the JPL10-6 recommended rate coefficient for the OH + C_2H_4 and OH + C_2H_2 reference reactions). The recommended value for E/R was based on a fit of the data below 400 K from Nelson *et al.* (1993), Zellner *et al.* (1994), Tokuhashi *et al.* (2004), and Hsu and DeMore (1995) after scaling to the recommended k(298 K) value.

l The rate coefficient parameters were estimated using a G3B3 quantum chemical method (Curtiss *et al.*, 2001) calculation of the reaction activation barrier, ~146 kJ mol^{-1}. Assuming a pre-exponential factor of 1×10^{-11} cm^3 $molecule^{-1}$ s^{-1} and E/R equal to the calculated activation barrier provides the basis of the recommendation.

Table 3.2. Reaction rate coefficients, reaction yields, and estimated uncertainties for the $O(^1D)$ + compound gas-phase reactions.*

Compound	Chemical Formula	Temperature Range (K) **	*A* *	*E*/R (K)	*k*(298 K) *	*f*(298 K)	*g*	Reaction Yield	Footnotes
1. CFC−11	CCl_3F	173 – 372	230	0	230	1.10	0	0.79 ± 0.04	1,2,3
2. CFC−12	CCl_2F_2	173 – 373	140	-25	157	1.15	0	0.76 ± 0.06	1,2,3,4
3. CFC−113	CCl_2FCClF_2	217 – 373	232	0	232	1.1	0	0.80 ± 0.04	2,3,4,5
4. CFC−114	$CClF_2CClF_2$	217 – 373	130	-25	142	1.1	0	0.80 ± 0.10	2,3,4,5
5. CFC−115	CF_3CClF_2	217 – 373	54	-30	60	1.15	0	0.84 ± 0.07	2,3,4
6. Carbon Tetrachloride	CCl_4	203 – 343	330	0	330	1.15	0	0.79 ± 0.04	1,2
7. Nitrous Oxide	N_2O	195 – 719	119	-20	127	1.1	25	0.39 (N_2 + O_2) 0.61 (2NO)	6
8. Halon−1202	CBr_2F_2	297	220	*0*	220	1.2	50	0.45 ± 0.06	6
9. Halon−1211	$CBrClF_2$	297	150	*0*	150	1.2	50	0.65 ± 0.04	6
10. Halon−1301	$CBrF_3$	297	100	*0*	100	1.2	50	0.40 ± 0.08	6
11. Halon−2402	$CBrF_2CBrF_2$	297	160	*0*	160	1.2	50	0.75 ± 0.07	6
12. Methane	CH_4	198 – 369	175	0	175	1.15	25	$1.0^{+0}_{-0.002}$	6
13. Methyl Chloroform	CH_3CCl_3	298	*325*	*0*	*325*	1.4	*0*	*0.9*	7,8
14. Methyl Chloride	CH_3Cl	298	260	*0*	260	1.3	50	0.91 ± 0.06	7,9
15. Methyl Bromide	CH_3Br	297	180	*0*	180	1.15	50	$1.0^{+0}_{-0.07}$	6
16. HCFC−22	$CHClF_2$	173 – 373	102	0	102	1.07	0	0.72 ± 0.06	2,3,4
17. HCFC−141b	CH_3CCl_2F	297	260	*0*	260	1.2	50	0.70 ± 0.05	6
18. HCFC−142b	CH_3CClF_2	217 – 373	200	0	200	1.1	0	0.75 ± 0.05	2,3,4
19. HFC−23	CHF_3	217 –372	8.7	-30	9.6	1.05	0	0.25 ± 0.05	2,3,4
20. HFC−32	CH_2F_2	298	51	*0*	51	1.2	50	0.30 ± 0.10	6
21. HFC−125	CHF_2CF_3	217 – 373	9.5	-25	10.5	1.07	0	0.70 ± 0.09	2,4,10
22. HFC−134a	CH_2FCF_3	297	49	*0*	49	1.15	50	0.35 ± 0.06	6
23. HFC−143a	CF_3CH_3	217 – 373	56	-20	60	1.2	0	0.65 ± 0.05	2,3,4
24. HFC−152a	CH_3CHF_2	297	175	*0*	175	1.2	50	0.55 ± 0.20	6
25. HFC−227ea	CF_3CHFCF_3	217 – 373	7.9	-70	10	1.1	0	0.72 ± 0.07	7,10
26. HFC−245fa	$CHF_2CH_2CF_3$	–	*150*	*0*	*150*	*1.3*	*0*	*0.5*	7
27. Nitrogen Trifluoride	NF_3	212 – 351	*20*	-44	*23*	*1.1*	*0*	$0.93^{+0.07}_{-0.21}$	2,4,11

Footnotes

* Estimated values are given in italics; A and k(298 K) are in units of 10^{-12} cm^3 $molecule^{-1}$ s^{-1}; $k(T) = A \exp(-E/RT)$.

** Temperature range of available experimental data considered in the evaluation of the reaction rate coefficient parameters and uncertainty limits.

1. Reactive yields taken from Feierabend *et al.* (2010).
2. Estimated uncertainty parameters revised from values reported in JPL10-6.
3. Recommended kinetic parameters and uncertainties based on evaluation of studies included in JPL10-6 as well as Baasandorj *et al.* (2013).
4. Kinetic parameters revised from values reported in JPL10-6.
5. Kinetic parameters taken from Baasandorj *et al.* (2011) and Baasandorj *et al.* (2013).
6. Kinetic parameters taken from JPL10-6.
7. Not evaluated in JPL10-6.
8. Nilsson *et al*. (2012) report a room temperature reactive rate coefficient, obtained using a relative rate method, of $(2.93 \pm 1.2) \times 10^{-10}$ cm^3 $molecule^{-1}$ s^{-1} (1σ error limit). The total rate coefficient given in the table was calculated assuming a 0.9 reaction yield.
9. Rate coefficient is an average of the values reported by Matsumi *et al.* (1993) and Force and Wiesenfeld (1981). The reaction yield was taken from Force and Wiesenfeld (1981).
10. Kinetic parameters taken from Baasandorj *et al.* (2013).
11. The recommended k(298 K) for the overall reaction is an average of the values derived from Arrhenius fits to the data of Zhao *et al.* (2010) and Dillon *et al.* (2011) and the value reported by Baasandorj *et al.* (2012) at 296 K. The recommended Arrhenius parameters are derived from a fit to these data after normalization to k(298 K). The recommended reaction yield is an average of the values reported by Zhao *et al.* (0.99) and Baasandorj *et al.* (2012) (0.87 +0.13/-0.15). The reaction yield is expected to be independent of temperature.

Table 3.3. Reaction rate coefficients and estimated uncertainties for the Cl + compound gas-phase reactions.*

Compound	Chemical Formula	Temperature Range (K) **	*A* *	*E*/R (K)	*k*(298 K) *	*f*(298 K)	*g*	Footnotes
1. CFC−11	CCl_3F	–	*100*	*8960*	*<8.7 (-24)*	–	–	1
2. CFC−12	CCl_2F_2	–	*100*	*11100*	*<5.2 (-27)*	–	–	1
3. CFC−113	CCl_2FCClF_2	–	*100*	*>5480*	*<1.0 (-18)*	–	–	2
4. CFC−114	$CClF_2CClF_2$	–	*100*	*>5480*	*<1.0 (-18)*	–	–	2
5. CFC−115	CF_3CClF_2	–	*100*	*>5480*	*<1.0 (-18)*	–	–	2
6. Carbon Tetrachloride	CCl_4	–	*100*	*5480*	*<1.0 (-18)*	–	–	1
7. Nitrous Oxide	N_2O	–	–	–	<1 (-17)			3
8. Halon−1202	CBr_2F_2	–	*100*	*9320*	*<2.6 (-24)*	–	–	1,a
9. Halon−1211	$CBrClF_2$	–	*100*	*6280*	*<7.1 (-20)*	–	–	1
10. Halon−1301	$CBrF_3$	–	*100*	*9290*	*<2.9 (-24)*	–	–	1
11. Halon−2402	$CBrF_2CBrF_2$	–	*100*	*9320*	*<2.6 (-24)*	–	–	1,a
12. Methane	CH_4	181 – 300	7.3	1280	1.0 (-13)	1.05	50	3
13. Methyl Chloroform	CH_3CCl_3	253 – 418	2.86	1716	9.03 (-15)	1.10	100	4,5,b
14. Methyl Chloride	CH_3Cl	222 – 300	19	1100	4.80 (-13)	1.07	50	4,5,c
15. Methyl Bromide	CH_3Br	213 – 300	14	1030	4.40 (-13)	1.05	50	3
16. HCFC−22	$CHClF_2$	298 – 430	5.57	2430	1.60 (-15)	1.08	100	3,5
17. HCFC−141b	CH_3CCl_2F	295 – 429	2.76	2140	2.10 (-15)	1.10	200	4,5,d
18. HCFC−142b	CH_3CClF_2	295 – 429	1.40	2420	4.10 (-16)	1.08	200	4,5,e
19. HFC−23	CHF_3	–	–	–	<5.0 (-16)	–	–	3
20. HFC−32	CH_2F_2	253 – 318	6.93	1590	3.34 (-14)	1.08	100	4,5,f
21. HFC−125	CHF_2CF_3	298	*1.8*	*2600*	3.0 (-16)	1.25	300	3,5
22. HFC−134a	CH_2FCF_3	253 – 300	0.98	1953	1.40 (-15)	1.10	200	4,g
23. HFC−143a	CF_3CH_3	281 – 368	9.7	3760	3.20 (-17)	2	300	4,5,h
24. HFC−152a	CH_3CHF_2	264 – 360	6.3	965	2.5 (-13)	1.10	100	4,i
25. HFC−227ea	CF_3CHFCF_3	298	*2.7*	*2600*	4.39 (-16)	1.30	300	j
26. HFC−245fa	$CHF_2CH_2CF_3$	298	*2.1*	*1700*	6.90 (-15)	1.30	300	k
27. Nitrogen Trifluoride	NF_3	–	*100*	*13200*	<1 (-29)	–	–	1,l

Footnotes

* Estimated values are given in italics; A is in units of 10^{-12} cm^3 molecule^{-1} s^{-1}; k(298 K) is in units of cm^3 molecule^{-1} s^{-1} and (-xx) represents $\times 10^{-xx}$; $k(T) = A \exp(-E/RT)$.

** Temperature range of available experimental data considered in the evaluation of the reaction rate coefficient parameters and uncertainty limits.

1 No experimental data available for this reaction. The reaction was not evaluated in JPL10-6. The recommendation given here was obtained by setting the pre-exponential factor (A) to 1×10^{-10} cm^3 molecule^{-1} s^{-1} and equating the activation energy (E) to the reaction endothermicity using the thermochemical parameters reported in JPL10-6 and IUPAC.

2 The recommended kinetic parameters are taken to equal those for the Cl + CCl_4 reaction.

3 A and E/R recommendation is unchanged from JPL10-6.

4 A and E/R recommendation is revised from JPL10-6.

5 f(298 K) and/or g is revised from JPL10-6.

a The rate coefficient upper-limit was estimated with E = 77.5 kJ mol^{-1}, which was obtained from an average of the values for the reaction of Cl with CH_3Br (77.8 kJ mol^{-1}) and CF_3Br (77.2 kJ mol^{-1}).

b The recommended k(298 K) was obtained from an average of the results from the relative rate studies of Platz *et al.* (1995) and Nilsson *et al.* (2009) and the absolute rate study of Talhaoui *et al.* (1996). The rate coefficient temperature dependence was obtained from a fit of the data from Talhaoui *et al.* (1996) and Nilsson *et al.* (2009) after scaling to the recommended k(298 K) value.

c The recommended k(298 K) is an average of the results from Manning and Kurylo (1977), Wallington *et al.* (1990), Beichert *et al.* (1995), Orlando (1999), and Bryukov *et al.* (2002). The rate coefficient temperature dependence was obtained from a fit of the data from Manning and Kurylo (1977), Wallington *et al.* (1990), Beichert *et al.* (1995), Orlando (1999), Bryukov *et al.* (2002), and Sarzyński *et al.* (2009) for temperatures <300 K.

d The recommended k(298 K) is an average of the results from Wallington and Hurley (1992), Tuazon *et al.*, (1992), Warren and Ravishankara (1993), and Talhaoui *et al.* (1996). The rate coefficient temperature dependence is based on a fit of the results from the studies of Warren and Ravishankara (<350 K) and Talhaoui *et al.* after scaling to the recommended k(298 K) value.

e The recommended k(298 K) is an average of the results from Wallington and Hurley (1992), Tuazon *et al.* (1992), and Talhaoui *et al.* (1996). The rate coefficient temperature dependence was taken from Talhaoui *et al.* (1996), which is the only available temperature dependent study.

f The recommended k(298 K) is an average of the results from Nielsen *et al.* (1992) and Nilsson *et al.* (2009). The rate coefficient temperature dependence was obtained from a fit of the data from Nielsen *et al.* (1992) and Nilsson *et al.* (2009) for temperatures <300 K after scaling to the recommended k(298 K) value.

g The recommended k(298 K) is an average of the data from Louis *et al.* (1997), Wallington and Hurley (1992), Tuazon *et al.* (1992), Kaiser (1993), and Nilsson *et al.*

(2009). The rate coefficient temperature dependence was obtained by fitting the T <300 K data from Louis *et al.* (1997), Kaiser (1993), and Nilsson *et al.* (2009) after scaling to match the recommended *k*(298 K) value.

h The recommended *k*(298 K) is an average of the results from the Tschuikow-Roux *et al.* (1985) and Nielsen *et al.* (1994) relative rate studies. The rate coefficient temperature dependence is based on the work of Tschuikow-Roux *et al.* (1985) combined with the rate expression for the Cl + CH_4 reaction recommended in this report.

i The recommended *A* and *E*/R values are for the total rate coefficient, i.e., loss of HFC-152a. The recommended *k*(298 K) was obtained from an average of an absolute rate and four relative rate studies, which are in good agreement. The temperature dependence was taken from Yano and Tschuikow-Roux (1986) where the site-specific rate coefficients are given as

$Cl + CH_3CHF_2 \rightarrow HCl + CH_3CF_2$; $k(T) = 6.3 \times 10^{-12} \exp(-965/T)$ cm^3 molecule^{-1} s^{-1}

$Cl + CH_3CHF_2 \rightarrow HCl + CH_2CHF_2$; $k(T) = 7.0 \times 10^{-12} \exp(-2400/T)$ cm^3 molecule^{-1} s^{-1}

j The recommended *k*(298 K) is the average of the relative rate determinations by Møgelberg *et al.* (1996) and *E*/R was estimated by comparison with compounds having similar reactivity at 298 K (e.g., HFC-125). The reaction was not evaluated in JPL10-6.

k The recommended *k*(298 K) was taken from Chen *et al.* (1997) and *E*/R was estimated by comparison with compounds having similar reactivity at 298 K (e.g., CH_3CCl_3). The reaction was not evaluated in JPL10-6.

l F atom abstraction from NF_3 by Cl is slightly exothermic (Gurvich *et al.*, 1989), ca. -11 kJ mol^{-1}. A G3B3 quantum chemical method (Curtiss *et al.*, 2001) calculation predicts an activation barrier (*E*/R) of ~110 kJ mol^{-1} for this reaction. Assuming a pre-exponential factor (*A*) of 1×10^{-10} cm^3 molecule^{-1} s^{-1} and this activation barrier provides the basis for the recommendation.

Table 3.4. Summary of Lyman-α (121.567 nm) absorption cross sections, σ(L-α), at 298 K and estimated cross-section uncertainties at Lyman-α and in the 169-190, 190-230, 230-286, and >286 nm wavelength regions.*

Compound	Chemical Formula	Lyman-α (121.567 nm)		*p*(298 K)/*w*				Footnotes
		σ(L-α, 298 K)**	*p*(298 K)	169-190 nm	190-230 nm	230-286 nm	>286 nm	
1. CFC−11	CCl_3F	9.8	1.2	1.10/60	1.10/120	1.30/–	–/–	1
2. CFC−12	CCl_2F_2	2.07	1.15	1.10/40	1.08/40	1.30/–	–/–	1
3. CFC−113	CCl_2FCClF_2	10	2.0	1.10/120	1.06/120	1.20/–	–/–	2
4. CFC−114	$CClF_2CClF_2$	3.6	1.3	1.14/60	1.14/60	–/–	–/–	1
5. CFC−115	CF_3CClF_2	0.457	3.0	1.14/–	1.30/–	–/–	–/–	1
6. Carbon Tetrachloride	CCl_4	3.7	1.2	1.10/120	1.06/60	1.20/–	–/–	3
7. Nitrous Oxide	N_2O	2.4	1.5	1.12/60	1.08/20	1.12/–	1.30/–	1
8. Halon−1202	CBr_2F_2	10	1.5	1.08/120	1.08/120	1.14/120	1.20/220	4
9. Halon−1211	$CBrClF_2$	7.75	1.5	1.10/500	1.10/500	1.14/220	1.40/220	4
10. Halon−1301	$CBrF_3$	2.5	1.4	1.16/220	1.08/120	1.20/120	1.30/–	1
11. Halon−2402	$CBrF_2CBrF_2$	*5*	2.0	1.14/120	1.10/120	1.14/60	1.30/220	4
12. Methane	CH_4	1.85	1.3	–/–	–/–	–/–	–/–	5,6
13. Methyl Chloroform	CH_3CCl_3	*7*	1.4	1.18/60	1.18/120	1.18/120	–/–	1
14. Methyl Chloride	CH_3Cl	8.8	1.15	1.06/60	1.12/120	1.24/–	–/–	1
15. Methyl Bromide	CH_3Br	3.2	1.3	1.06/60	1.06/60	1.10/60	–/–	1
16. HCFC−22	$CHClF_2$	1.76	1.4	1.10/30	1.26/60	–/–	–/–	1
17. HCFC−141b	CH_3CCl_2F	6.6	2.0	1.12/120	1.12/120	–/–	–/–	1
18. HCFC−142b	CH_3CClF_2	3.1	1.2	1.20/120	1.14/120	–/–	–/–	1
19. HFC−23	CHF_3	0.035	2.0	–/–	–/–	–/–	–/–	5,6
20. HFC−32	CH_2F_2	0.55	1.4	–/–	–/–	–/–	–/–	5
21. HFC−125	CHF_2CF_3	*0.035*	3.0	–/–	–/–	–/–	–/–	5
22. HFC−134a	CH_2FCF_3	*0.5*	2.0	–/–	–/–	–/–	–/–	6
23. HFC−143a	CF_3CH_3	1.75	2.0	–/–	–/–	–/–	–/–	5,6
24. HFC−152a	CH_3CHF_2	3.2	2.0	–/–	–/–	–/–	–/–	5
25. HFC−227ea	CF_3CHFCF_3	*0.035*	3.0	–/–	–/–	–/–	–/–	5
26. HFC−245fa	$CHF_2CH_2CF_3$	*1*	3.0	–/–	–/–	–/–	–/–	5
27. Nitrogen Trifluoride	NF_3	0.48	1.5	1.5/–	1.1/–	1.5/–	–/–	5

Footnotes

* p(298 K) and w are 2σ (95% confidence level) values where the uncertainty at temperature T (K) is given by $p(T) = p(298\ K)\exp(|w(1/T - 1/298)|)$.

** Absorption cross sections are in units of 10^{-17} cm^2 molecule^{-1}; estimated values are given in italics

1 The recommended cross sections and their wavelength and temperature parameterization are taken from JPL 10-6.

2 The absorption cross-section wavelength and temperature parameterization reported in JPL10-6 contains an error; a revised set of parameters was derived here.

3 The cross-section wavelength and temperature parameterization reported in JPL10-6 has been revised to include the parameterization between 200-230 nm reported in Rontu *et al.* (2010).

4 The recommended absorption cross sections at λ ≥260 nm are based on the parameterizations given in Papanastasiou *et al.* (2013).

5 Not included in JPL10-6 evaluation.

6 No UV spectral data are available. Photolysis at wavelengths >169 nm is expected to make a negligible contribution to the molecule's atmospheric loss.

Table 3.5. Summary of 2-D model simulations for year 2000 steady-state conditions.

Simulation	Input Kinetic and Photolytic Parameters	Model Conditions[a,b,c]
A	JPL10-6	Baseline
B	JPL10-6	2σ slow for all, interactive
C	JPL10-6	2σ fast for all, interactive
D	JPL10-6	2σ slow for all, non-interactive tracers
E	JPL10-6	2σ slow for all, non-interactive tracers
F	SPARC	Baseline
G	SPARC	2σ slow for all, interactive
H	SPARC	2σ fast for all, interactive
I	SPARC	2σ slow for CH_4 kinetics, Baseline for others, interactive
J	SPARC	2σ fast for CH_4 kinetics, Baseline for others, interactive
K	SPARC	2σ slow for N_2O kinetics and photolysis, Baseline for others, interactive
L	SPARC	2σ slow for N_2O kinetics and photolysis, Baseline for others, interactive
M	SPARC	2σ slow for all, non-interactive tracers
N	SPARC	2σ fast for all, non-interactive tracers
O	SPARC	2σ slow for all $O(^1D)$ reactions, 2σ fast for all photolysis, non-interactive tracers
P	SPARC	2σ fast for all $O(^1D)$ reactions, 2σ slow for all photolysis, non-interactive tracers

[a] all ≡ the kinetic and photolysis parameters for the compounds reported in this chapter (Tables 3.1 – 3.4)

[b] interactive ≡ the compounds allowed to interact with the other model constituents including ozone

[c] non-interactive ≡ the compounds treated as non-interactive tracers

Table 3.6. Fractional loss contributions and global annually averaged atmospheric lifetimes calculated using a 2-D model for 2000 steady-state conditions.*

Compound	Formula	hν (121.56 nm)	hν (169-190 nm)	hν (190-230 nm)	hν (230-286 nm)	hν (>286 nm)	hν Total	$O(^1D)$ Reactive Loss	OH Reaction	Cl Reaction	Lifetime (Years)
1. CFC−11	CCl_3F	<0.001	0.002	0.981	<0.001	–	0.982	0.018	–	–	60.2
		(–)	(0.001)	(0.977)	(<0.001)	(–)	(0.979)	(0.019)	(0.002)	(–)	(58.6)
2. CFC−12	CCl_2F_2	<0.001	0.029	0.913	<0.001	–	0.942	0.058	–	–	109.5
		(–)	(0.024)	(0.919)	(<0.001)	(–)	(0.943)	(0.051)	(0.006)	(–)	(103.7)
3. CFC−113	CCl_2FCClF_2	<0.001	0.013	0.930	<0.001	–	0.942	0.058	<0.001	<0.001	93.6
		(–)	(0.013)	(0.920)	(<0.001)	(–)	(0.933)	(0.067)	(–)	(–)	(95.4)
4. CFC−114	$CClF_2CClF_2$	0.008	0.055	0.654	–	–	0.717	0.283	<0.001	<0.001	199.7
		(–)	(0.059)	(0.692)	(<0.001)	(–)	(0.751)	(0.249)	(–)	(–)	(204.2)
5. CFC−115	CF_3CClF_2	0.063	0.028	0.283	–	–	0.374	0.626	<0.001	<0.001	539.9
		(–)	(0.062)	(0.573)	(–)	(–)	(0.635)	(0.365)	(–)	(–)	(960.7)
6. Carbon Tetrachloride	CCl_4	<0.001	<0.001	0.983	–	–	0.983	0.017	–	–	48.7
		(–)	(<0.001)	(0.749)	(<0.001)	(–)	(0.749)	(0.015)	(0.236)	(–)	(38.0)
7. Nitrous Oxide	N_2O	<0.001	0.012	0.888	<0.001	–	0.901	0.099	–	–	125.2
		(–)	(0.012)	(0.889)	(–)	(–)	(0.901)	(0.099)	(–)	(–)	(125.2)
8. Halon−1202	CBr_2F_2	<0.001	<0.001	0.057	<0.001	0.920	0.977	<0.001	0.023	<0.001	2.54
		(–)	(<0.001)	(0.042)	<0.001	(0.939)	(0.981)	(<0.001)	(0.019)	(–)	(2.09)
9. Halon−1211	$CBrClF_2$	<0.001	<0.001	0.419	<0.001	0.578	0.997	0.002	0.001	<0.001	16.3
		(–)	(<0.001)	(0.344)	(<0.001)	(0.627)	(0.970)	(0.001)	(0.029)	(–)	(13.5)
10. Halon−1301	$CBrF_3$	<0.001	<0.001	0.986	<0.001	0.002	0.988	0.007	0.005	<0.001	77.4
		(–)	(<0.001)	(0.986)	(<0.001)	(0.002)	(0.988)	(0.007)	(0.005)	(–)	(77.4)
11. Halon−2402	$CBrF_2CBrF_2$	<0.001	<0.001	0.724	<0.001	0.271	0.995	0.003	0.002	<0.001	27.8
		(–)	(<0.001)	(0.349)	(<0.001)	(0.648)	(0.997)	(0.002)	(0.001)	(–)	(13.9)
12. Methane	CH_4	<0.001	–	–	–	–	<0.001	0.019	0.966	0.015	9.32
		<0.001	(–)	(–)	(–)	(–)	(<0.001)	(0.019)	(0.965)	(0.016)	(9.56)
13. Methyl Chloroform	CH_3CCl_3	<0.001	<0.001	0.091	<0.001	–	0.091	<0.001	0.909	<0.001	5.19
		(–)	(<0.001)	(0.097)	(<0.001)	(–)	(0.097)	(–)	(0.903)	(<0.001)	(5.15)
14. Methyl Chloride	CH_3Cl	<0.001	<0.001	0.002	<0.001	–	0.003	0.001	0.991	0.005	1.47
		(–)	(<0.001)	(0.003)	(<0.001)	(–)	(0.003)	(–)	(0.992)	(0.005)	(1.45)
15. Methyl Bromide	CH_3Br	<0.001	<0.001	0.031	<0.001	<0.001	0.031	<0.001	0.966	0.003	1.65
		(–)	(<0.001)	(0.033)	(<0.001)	(<0.001)	(0.033)	(<0.001)	(0.964)	(0.003)	(1.70)
16. HCFC−22	$CHClF_2$	0.002	<0.001	0.002	–	–	0.004	0.014	0.982	<0.001	12.2
		(–)	(<0.001)	(0.002)	(–)	(–)	(0.003)	(0.013)	(0.984)	(<0.001)	(12.0)
17. HCFC−141b	CH_3CCl_2F	<0.001	0.001	0.093	<0.001	–	0.094	0.005	0.902	<0.001	9.2
		(–)	(0.001)	(0.093)	(<0.001)	(–)	(0.094)	(0.004)	(0.902)	(<0.001)	(9.20)
18. HCFC−142b	CH_3CClF_2	0.002	0.001	0.011	–	–	0.014	0.037	0.949	<0.001	17.5
		(–)	(0.001)	(0.011)	(–)	(–)	(0.012)	(0.041)	(0.947)	(<0.001)	(17.5)
19. HFC−23	CHF_3	0.005	–	–	–	–	0.005	0.015	0.980	–	223.8
		(–)	(–)	(–)	(–)	(–)	(–)	(0.009)	(0.991)	(–)	(226.4)
20. HFC−32	CH_2F_2	<0.001	–	–	–	–	<0.001	0.001	0.997	0.002	5.21
		(–)	(–)	(–)	(–)	(–)	(–)	(0.001)	(0.997)	(0.002)	(5.21)
21. HFC−125	CHF_2CF_3	<0.001	–	–	–	–	–	0.005	0.994	<0.001	30.6
		(–)	(–)	(–)	(–)	(–)	(–)	(0.050)	(0.950)	(<0.001)	(29.3)
22. HFC−134a	CH_2FCF_3	0.001	–	–	–	–	0.001	0.004	0.994	<0.001	13.4
		(–)	(–)	(–)	(–)	(–)	(–)	(0.004)	(0.996)	(<0.001)	(13.6)
23. HFC−143a	CF_3CH_3	0.014	–	–	–	–	0.014	0.045	0.941	<0.001	51.0
		(–)	(–)	(–)	(–)	(–)	(–)	(0.041)	(0.959)	(<0.001)	(50.1)
24. HFC−152a	CH_3CHF_2	<0.001	–	–	–	–	<0.001	0.001	0.996	0.003	1.45
		(–)	–)	(–	(–)	(–)	(–)	(0.001)	(0.997)	(0.002)	(1.45)
25. HFC−227ea	CF_3CHFCF_3	0.001	–	–	–	–	0.001	0.005	0.994	<0.001	35.6
		(–)	(–)	(–)	(–)	(–)	(–)	(–)	(1.0)	(–)	(42.3)
26. HFC−245fa	$CHF_2CH_2CF_3$	<0.001	–	–	–	–	<0.001	0.008	0.991	0.001	7.73
		(–)	(–)	(–)	(–)	(–)	(–)	(–)	(1.0)	(–)	(7.79)
27. Nitrogen Trifluoride	NF_3	0.063	0.100	0.549	0.001	0	0.713	0.287	–	–	569.2
		(–)	(–)	(–)	(–)	(–)	(–)	(1.0)	(–)	(–)	(1588)

* Model input kinetic and photochemical parameters from the present SPARC evaluation. The values obtained using the JPL10-6 evaluation parameters as model input are given in parenthesis.

Table 3.7. Summary of global annually averaged atmospheric lifetimes (years) calculated using a 2-D model for 2000 steady-state conditions.*

Compound	Formula	Lifetime (Total)	Lifetime Range **	% Range in Lifetime	Tropospheric	Stratospheric	Mesospheric
1. CFC−11	CCl_3F	60.2 (58.6)	54.3-66.3 (54.5-62.8)	± 10 (± 7)	1718 (1482)	62.4 (61.0)	>1e6 (>1e6)
2. CFC−12	CCl_2F_2	109.5 (103.7)	102.9-116.1 (96.6-110.7)	± 6.0 (± 7)	9879 (5944)	110.8 (105.6)	196500 (394400)
3. CFC−113	CCl_2FCClF_2	93.6 (95.4)	86.6-100.7 (90.4-98.4)	± 7.5 (± 4)	5708 (5661)	95.1 (97.1)	>1e6 (>1e6)
4. CFC−114	$CClF_2CClF_2$	199.7 (204.2)	178.3-223.9 (186.1-217.8)	± 11 (± 8)	15540 (18160)	218.4 (222.5)	2743 (2878)
5. CFC−115	CF_3CClF_2	539.9 (960.7)	414.8-717.1 (762-1144)	± 28 (± 20)	37420 (1.24e5)	664.4 (1158)	3119 (5914)
6. Carbon Tetrachloride	CCl_4	48.7 (38.0)	45.2-52.3 (35.6-40.3)	± 7.3 (± 6)	885.9 (137.7)	51.6 (52.4)	>1e6 (>1e6)
7. Nitrous Oxide	N_2O	125.2 (125.2)	118.1-132.3 (113.0-139.6)	± 5.7 (± 11)	10990 (11010)	127.5 (127.5)	19250 (19360)
8. Halon−1202	CBr_2F_2	2.54 (2.09)	1.96-3.26 (0.53-7.50)	± 26 (± 167)	2.74 (2.26)	35.9 (27.8)	>1e6 (>1e6)
9. Halon−1211	$CBrClF_2$	16.3 (13.5)	10.8-23.8 (4.18-34.0)	± 40 (± 110)	27.2 (20.3)	40.9 (40.1)	>1e6 (>1e6)
10. Halon−1301	$CBrF_3$	77.4 (77.4)	70.9-84.0 (67.7-87.9)	± 8.5 (± 13)	3343 (3338)	79.3 (79.3)	>1e6 (>1e6)
11. Halon−2402	$CBrF_2CBrF_2$	27.8 (13.9)	22.9-33.3 (4.32-36.4)	± 19 (± 115)	85.5 (22.5)	41.3 (36.6)	>1e6 (>1e6)
12. Methane	CH_4	9.32 (9.56)	8.17-10.6 (7.43-12.2)	± 13 (± 25)	9.92 (10.2)	159.6 (163.3)	4223 (4168)
13. Methyl Chloroform	CH_3CCl_3	5.19 (5.15)	4.17-6.44 (3.76-6.97)	± 22 (± 31)	5.76 (5.74)	53.1 (50.4)	>1e6 (>1e6)
14. Methyl Chloride	CH_3Cl	1.47 (1.45)	1.17-1.85 (1.02-2.05)	± 23 (± 35)	1.52 (1.49)	51.2 (52.9)	150300 (105500)
15. Methyl Bromide	CH_3Br	1.65 (1.70)	1.34-2.01 (1.32-2.18)	± 20 (± 25)	1.72 (1.78)	36.6 (38.2)	>1e6 (>1e6)
16. HCFC−22	$CHClF_2$	12.2 (12.0)	10.0-14.9 (9.00-16.0)	± 20 (± 29)	13.0 (12.7)	235.4 (232)	3175 (4900)
17. HCFC−141b	CH_3CCl_2F	9.2 (9.20)	7.6-11.1 (6.51-12.8)	± 19 (± 34)	10.3 (10.3)	84.2 (84.3)	>1e6 (>1e6)
18. HCFC−142b	CH_3CClF_2	17.5 (17.5)	12.9-23.6 (11.2-27.0)	± 31 (± 45)	19.0 (19.0)	233.3 (226.1)	2843 (3952)
19. HFC−23	CHF_3	223.8 (226.4)	159.4-313.3 (160.2-319.5)	± 34 (± 35)	238.8 (238.8)	4183 (4687)	23980 (60230)
20. HFC−32	CH_2F_2	5.21 (5.21)	4.24-6.37 (3.54-7.60)	± 20 (± 39)	5.41 (5.41)	142.2 (142)	5313 (6308)
21. HFC−125	CHF_2CF_3	30.6 (29.3)	23.7-39.5 (18.6-46.0)	± 26 (± 47)	32.4 (32.2)	593.3 (352.6)	9129 (5454)
22. HFC−134a	CH_2FCF_3	13.4 (13.6)	10.4-17.3 (9.80-18.6)	± 26 (± 32)	14.1 (14.3)	290.9 (296.4)	4295 (6772)
23. HFC−143a	CF_3CH_3	51.0 (50.1)	38.9-65.7 (38.0-65.4)	± 26 (± 27)	56.4 (54.4)	672.1 (677.7)	2555 (8517)
24. HFC−152a	CH_3CHF_2	1.45 (1.45)	1.26-1.67 (1.21-1.73)	± 14 (± 18)	1.50 (1.50)	47.6 (48.1)	46700 (48950)
25. HFC−227ea	CF_3CHFCF_3	35.6 (42.3)	25.6-49.4 (29.0-61.3)	± 33 (± 38)	37.7 (44.6)	673.4 (899.3)	9954 (15910)
26. HFC−245fa	$CHF_2CH_2CF_3$	7.73 (7.79)	5.44-10.9 (4.85-12.4)	± 35 (± 48)	8.13 (8.16)	162.1 (178.8)	4414 (6672)
27. Nitrogen Trifluoride	NF_3	569.2 (1588)	493.8-679.2 (1031-2951)	± 16 (± 60)	84150 (84150)	740.7 (1804)	2531 (15680)

* Model input kinetic and photochemical parameters from the present SPARC evaluation at the 2σ uncertainty limits. The calculated values obtained using the JPL10-6 evaluation recommended input parameters are given in parentheses.

** Using interactive model calculation; % range in lifetime is not symmetric; the value given is a rounded-off average.

Table 3.8. The range in global annually averaged atmospheric lifetimes obtained using a 2-D model for 2000 steady-state conditions with perturbations in the O_3 (±4%) and O_2 (±10 and ±20%) UV absorption cross sections.

Compound	Chemical Formula	Base Lifetime (yrs) *	O_3 Cross-Section Perturbation	O_2 Cross-Section Perturbation (±10%)			O_2 Cross-Section Perturbation (±20%)			Perturbation Lifetime Range / (% from Base) **
				All λ	<204 nm	>204 nm	All λ	<204 nm	>204 nm	
1. CFC-11	CCl_3F	60.2	59.9–60.5 (-0.5, +0.5)	54.2–65.7 (-10, +9.1)	55.8–64.1 (-7.3, +6.5)	58.3–61.7 (-3.2, +2.5)	47.8–70.8 (-21, +18)	50.8–67.3 (-16, +12)	55.8–62.9 (-7.3, +4.5)	49.8–67.8 (-17, +13)
2. CFC-12	CCl_2F_2	109.5	109–110 (-0.4, +0.4)	103–115 (-5.9, +5)	104–114 (-5, +4.1)	108–111 (-1.4, +1.4)	96.1–121 (-12, +11)	99–118 (-9.6, +7.7)	106–112 (-3.2, +2.3)	98.3–118 (-10, +8)
3. CFC-113	CCl_2FCClF_2	93.6	93.4–93.7 (-0.2, +0.1)	87.5–99 (-6.5, +5.8)	89.1–97.6 (-4.8, +4.3)	91.8–95 (-1.9, +1.5)	81.1–104 (-13, +11)	84–101 (-10, +7.9)	89.7–96.2 (-4.2, +2.8)	83.2–101 (-11, +8)
4. CFC-114	$CClF_2CClF_2$	199.7	200–200 (0, 0)	190–208 (-4.9, +4.2)	193–206 (-3.4, +3.2)	197–202 (-1.4, +1.2)	180–216 (-9.9, +8.2)	186–211 (-6.9, +5.7)	194–204 (-2.9, +2.2)	184–212 (-8, +6)
5. CFC-115	CF_3CClF_2	539.9	540–539 (0, -0.2)	525–552 (-2.7, +2.2)	530–548 (-1.8, +1.5)	535–544 (-0.9, +0.8)	509–563 (-5.7, +4.3)	519–555 (-3.9, +2.8)	530–548 (-1.8, +1.5)	517–557 (-4, +3)
6. Carbon Tetrachloride	CCl_4	48.7	48.4–49 (-0.6, +0.6)	42.9–54.1 (-12, +11)	45.1–51.8 (-7.4, +6.4)	46.1–50.8 (-5.3, +4.3)	36.9–59.2 (-24, +22)	41–54.4 (-16, +12)	42.8–52.4 (-12, +7.6)	39.0–55.5 (-20, +14)
7. Nitrous Oxide	N_2O	125.2	125–125 (0, 0)	118–131 (-5.7, +4.6)	120–129 (-4.1, +3.4)	123–127 (-1.7, +1.4)	111–138 (-11, +10)	115–133 (-8.1, +6.2)	120–129 (-4.1, +3)	114–134 (-9, +7)
8. Halon-1202	CBr_2F_2	2.54	2.52–2.57 (-0.8, +1.2)	2.50–2.57 (-1.6, +1.2)	2.50–2.57 (-1.6, +1.2)	2.50–2.54 (-1.6, 0)	2.45–2.59 (-3.5, +2)	2.47–2.61 (-2.7, +2.7)	2.53–2.53 (-0.4, -0.4)	2.46–2.61 (-3, +3)
9. Halon-1211	$CBrClF_2$	16.3	16.2–16.5 (-0.6, +1.2)	15.2–17.2 (-6.7, +5.5)	15.7–16.9 (-3.7, +3.7)	15.8–16.7 (-3.1, +2.5)	13.9–18 (-15, +10)	14.8–17.4 (-9.2, +6.7)	15.2–16.9 -6.7, +3.7)	14.4–17.5 (-12, +7)
10. Halon-1301	$CBrF_3$	77.4	77.2–77.7 (-0.3, +0.4)	71.5–82.7 (-7.7, +6.8)	74.1–80.4 (-4.3, +3.9)	74.6–79.8 (-3.6, +3.1)	65.2–87.7 (-16, +13)	70.2–82.8 (-9.4, +7)	71.2–81.7 (-8, +5.6)	67.9–84.3 (-12, +9)
11. Halon-2402	$CBrF_2CBrF_2$	27.8	27.6–28.1 (-0.7, +1.1)	24.8–30.6 (-11, +10)	26–29.4 (-6.5, +5.7)	26.4–28.9 (-5, +4)	21.5–33 (-23, +19)	23.8–30.7 (-14, +10)	24.6–29.7 (-12, +6.8)	22.7–31.2 (-18, +12)
12. Nitrogen Trifluoride	NF_3	569.2	569–569 (0, 0)	546–590 (-4.1, +3.7)	552–585 (-3, +2.8)	563–574 (-1.1, +0.8)	520–609 (-8.6, +7)	532–599 (-6.5, +5.2)	556–579 (-2.3, +1.7)	530–601 (-7, +6)

* The base lifetimes are from Tables 3.6 and 3.7.

** The percent change from the base lifetime is given in parentheses. The overall perturbation lifetime range recommended here, due to the O_3 and O_2 perturbations only, combines the uncertainties from the O_3 and O_2 (±20%) cross-section perturbations using the above and below 204 nm results (see text for details).

3.8 References

Addison, M. C., R. J. Donovan, and J. Garraway, Reactions of $O(^1D)$ and $O(^3P)$ with halogenomethanes, *Faraday Disc. Chem. Soc., 67*, 286-296, 1979.

Amimoto, S. T., A. P. Force, and J. R. Wiesenfeld, Ozone photochemistry: Production and deactivation of $O(2^1D_2)$ following photolysis at 248 nm, *Chem. Phys. Lett.*, *60*, 40-43, 1978.

Anderson, D. E., Jr., and R. R. Meier, Effects of anisotropic multiple scattering on solar radiation in the troposphere and stratosphere, *Appl. Opt., 18*, 1955-1960, 1979.

Atkinson, R., D. A. Hansen, and J. N. Pitts, Jr., Rate constants for the reaction of OH radicals with CHF_2Cl, CF_2Cl_2, $CFCl_3$, and H_2 over the temperature range 297-434 K, *J. Chem. Phys., 63*, 1703-1706, 1975.

Atkinson, R., G. M. Breuer, J. N. Pitts, Jr., and H. L. Sandoval, Tropospheric and stratospheric sinks for halocarbons: Photooxidation, $O(^1D)$ atom, and OH radical reactions, *J. Geophys. Res., 81*, 5765-5770, 1976.

Atkinson, R., D. L. Baulch, R. A. Cox, J. N. Crowley, R. F. Hampson, R. G. Hynes, M. E. Jenkin, M. J. Rossi, J. Troe, and T. J. Wallington, Evaluated kinetic and photochemical data for atmospheric chemistry: Volume IV - gas phase reactions of organic halogen species, *Atmos. Chem. Phys.*, *8*, 4141-4496, 2008.

Baasandorj, M., K. J. Feierabend, and J. B. Burkholder, Rate coefficients and ClO radical yields in the reaction of $O(^1D)$ with $CClF_2CCl_2F$, CCl_3CF_3, $CClF_2CClF_2$, and CCl_2FCF_3, *Int. J. Chem. Kinet.*, *43*, 1-9, 2011.

Baasandorj, M., B. D. Hall, and J. B. Burkholder, Rate coefficients for the reaction of $O(^1D)$ with the atmospherically long-lived greenhouse gases NF_3, SF_5CF_3, CHF_3, C_2F_6, c-C_4F_8, n-C_5F_{12}, and n-C_6F_{14}, *Atmos. Chem. Phys.*, *12*, 11753-11764, 2012.

Baasandorj, M., E. L. Fleming, C. H. Jackman, and J. B. Burkholder, $O(^1D)$ kinetic study of key ozone depleting substances and greenhouse gases, *J. Phys. Chem. A*, dx.doi.org/10.1021/jp310910f, 2013.

Beichert, P., J. L. Wingen, R. Vogt, M. J. Ezell, M. Ragains, R. Neavyn, and B. J. Finlayson-Pitts, Rate constants for the reactions of chlorine atoms with some simple alkanes at 298 K: Measurement of a self-consistent set using both absolute and relative rate methods, *J. Phys. Chem.*, *99*, 13156-13162, 1995.

Biermann, H. W., C. Zetzsch, and F. Stuhl, Rate constant for reaction of OH with N_2O at 298 K, *Ber. Bunsenges. Phys. Chem.*, *80*, 909-911, 1976.

Blitz, M. A., T. J. Dillon, D. E. Heard, M. J. Pilling, and I. D. Trought, Laser induced fluorescence studies of the reactions of $O(^1D_2)$ with N_2, O_2, N_2O, CH_4, H_2, CO_2, Ar, Kr and n-C_4H_{10}, *Phys. Chem. Chem. Phys.*, *6*, 2162-2171, 2004.

Bryukov, M. G., I. R. Slagle, and V. D. Knyazev, Kinetics of reactions of Cl atoms with methane and chlorinated methanes *J. Phys. Chem. A*, *106*, 10532-10542, 2002.

Burkholder, J. B., R. R. Wilson, T. Gierczak, R. Talukdar, S. A. McKeen, J. J. Orlando, G. L. Vaghjiani, and A. R. Ravishankara, Atmospheric fate of CF_3Br, CF_2Br_2, CF_2ClBr, and CF_2BrCF_2Br, *J. Geophys. Res.*, *96*, 5025-5043, 1991.

Cavalli, F., M. Glasius, J. Hjorth, B. Rindone, and N. R. Jensen, Atmospheric lifetimes, infrared spectra and degradation products of a series of hydrofluoroethers, *Atmos. Environ., 32,* 3767-3773, 1998.

Chang, J. S., and F. Kaufman, Kinetics of the reactions of hydroxyl radicals with some halocarbons: $CHFCl_2$, CHF_2Cl, CH_3CCl_3, C_2HCl_3, and C_2Cl_4, *J. Chem. Phys.*, *66*, 4989-4994, 1977a.

Chang, J. S., and F. Kaufman, Upper limits of the rate constants for the reactions of $CFCl_3$(F-ll), CF_2C1_2(F-12), and N_2O with OH. Estimates of corresponding lower limits to their tropospheric lifetimes, *Geophys. Res. Lett.*, *4*, 192-194, 1977b.

Chen, J., V. Young, and H. Niki, Kinetic and mechanistic studies for reactions of $CF_3CH_2CHF_2$ (HFC-245fa) initiated by H-atom abstraction using atomic chlorine, *J. Phys. Chem. A*, *101*, 2648-2653, 1997.

Chichinin, A., S. Teton, G. LeBras, and G. Poulet, Kinetic investigation of the OH + CH_3Br reaction between 248 and 390 K, *J. Atmos. Chem.*, *18*, 239-245, 1994.

Clyne, M. A. A., and P. M. Holt, Reaction kinetics involving ground $X^2\Pi$ and excited $A^2\Sigma^+$ hydroxyl radicals. Part 2. Rate constants for reactions of OH $X^2\Pi$ with halogenomethanes and halogenoethanes, *J. Chem. Soc. Faraday Trans. 2, 75*, 582-591, 1979.

Cronkhite, J. M., and P. H. Wine, Branching ratios for BrO production from reactions of O(^{1}D) with HBr, CF_3Br, CH_3Br, CF_2ClBr, and CF_2HBr, *Int. J. Chem. Kinet.*, 30, 555-563, 1998.

Curtiss, L. A., P. C. Redfern, K. Raghavachari, and J. A. Pople, Gaussian-3X (G3X) theory: Use of improved geometries, zero-point energies, and Hartree-Fock basis sets, *J. Chem. Phys.*, *114*, 108-117, 2001.

Davidson, J. A., H. I. Schiff, T. J. Brown, and C. J. Howard, Temperature dependence of the rate constants for reactions of O(^{1}D) atoms with a number of halocarbons, *J. Chem. Phys.*, *69*, 4277-4279, 1978.

DeMore, W. B., Rate constants for the reactions of OH with HFC-134a (CF_3CH_2F) and HFC-134 (CHF_2CHF_2), *Geophys. Res. Lett.*, *20*, 1359-1362, 1993.

Dillon, T. J., A. Horowitz, and J. N. Crowley, Cross-sections and quantum yields for the atmospheric photolysis of the potent greenhouse gas nitrogen trifluoride, *Atmos. Env.*, *44*, 1186-1191, 2010.

Dillon, T. J., L. Vereecken, A. Horowitz, V. Khamaganov, J. N. Crowley, and J. Lelieveld, Removal of the potent greenhouse gas NF_3 by reactions with the atmospheric oxidants O(^{1}D), OH and O_3, *Phys. Chem. Chem. Phys.*, *13*, 18600-18608, 2011.

Fang, T. D., P. H. Taylor, and B. Dellinger, Absolute rate measurements of the reaction of OH radicals with HCFC-21 ($CHFCl_2$) and HCFC-22 (CHF_2Cl) over an extended temperature range, *J. Phys. Chem., 100*, 4048-4054, 1996.

Feierabend, K. J., D. K. Papanastasiou, and J. B. Burkholder, ClO radical yields in the reaction of O(^{1}D) with Cl_2, HCl, chloromethanes and chlorofluoromethanes, *J. Phys. Chem. A*, *114*, 12052-12061, 2010.

Fleming, E. L., C. H. Jackman, R. S. Stolarski, and A. R. Douglas, A model study of the impact of source gas changes on the stratosphere for 1850-2100, *Atmos. Chem. Phys.*, *11*, 8515-8541, 2011.

Force, A. P., and J. R. Wiesenfeld, Collisional deactivation of $O(^1D_2)$ by the halomethanes. Direct determination of reaction efficiency, *J. Phys. Chem.*, *85*, 782-785, 1981.

Gillotay, D., and P. C. Simon, Ultraviolet absorption spectrum of trifluoro-bromo-methane, difluoro-dibromo-methane and difluoro-bromo-chloro-methane in the vapor phase, *J. Atmos. Chem.*, *8*, 41-62, 1989.

Gillotay, D., and P. C. Simon, Temperature-dependence of ultraviolet absorption cross-sections of alternative chlorofluoroethanes, *J. Atmos. Chem.*, *12*, 269-285, 1991.

Green, R. G., and R. P. Wayne, Relative rate constants for the reactions of $O(^1D)$ atoms with fluorochlorocarbons and with N_2O, *J. Photochem.*, *6*, 371-374, 1976/77.

Greenblatt, G. D, and A. R. Ravishankara, Laboratory studies on the stratospheric NO_x production rate, *J. Geophys. Res*., *95*, 3539-3547, 1990.

Grooß, J.-U., and R. Müller, Do cosmic-ray-driven electron-induced reactions impact stratospheric ozone depletion and global climate change?, *Atmos. Environ.*, *45*, 3508-3514, 2011.

Gurvich, L. V., I. V. Veyts, and C. B. Alcock, *Thermodynamic Properties of Individual Substances*, Fourth ed., Hemisphere Pub. Co., New York, 1989.

Handwerk, V., and R. Zellner, Kinetics of the reactions of OH radicals with some halocarbons ($CHClF_2$, CH_2ClF, CH_2ClCF_3, CH_3CClF_2, CH_3CHF_2) in the temperature range 260-370 K, *Ber. Bunsenges. Phys. Chem., 82,* 1161-1166, 1978.

Harris, N. R. P., J. C. Farman, and D. W. Fahey, Comment on "Effects of cosmic rays on atmospheric chlorofluorocarbon dissociation and ozone depletion", *Phys. Rev. Lett.*, *89*, 219801, 2002.

Harrison, H., Climatic Impact Assessment Program, 1975.

Heidner, R. F. I., and D. Husain, Electronically excited oxygen atoms, $O(2^1D_2)$. A time-resolved study of the collisional quenching by the gases H_2, D_2, NO, N_2O, NO_2, CH_4, and C_3O_2. Using atomic absorption spectroscopy in the vacuum ultraviolet, *Int. J. Chem. Kinet.*, *5*, 819-831, 1973.

Herndon, S. C., T. Gierczak, R. K. Talukdar, and A. R. Ravishankara, Kinetics of the reactions of OH with several alkyl halides, *Phys. Chem. Chem. Phys.*, *3*, 4529-4535, 2001.

Howard, C. J., and K. M. Evenson, Rate constants for the reactions of OH with ethane and some halogen substituted ethanes at 296 K, *J. Chem. Phys.*, *64*, 4303-4306, 1976.

Hsu, K. J., and W. B. DeMore, Rate constants for the reactions of OH with CH_3Cl, CH_2Cl_2, $CHCl_3$, and CH_3Br, *Geophys. Res. Lett.*, *21*, 805-808, 1994.

Hsu, K. J., and W. B. DeMore, Rate constants and temperature dependences for the reactions of hydroxyl radical with several halogenated methanes, ethanes, and propanes by relative rate measurements, *J. Phys. Chem.*, *99*, 1235-1244, 1995.

Hubrich, C., and F. Stuhl, The ultraviolet absorption of some halogenated methanes and ethanes of atmospheric interest, *J. Photochem.*, *12*, 93-107, 1980.

Jeong, K.-M., and F. Kaufman, Kinetics of the reaction of hydroxyl radical with methane and with nine Cl- and F-substituted methanes. I. Experimental results, comparisons, and applications, *J. Phys. Chem., 86,* 1808-1815, 1982.

Kaiser, E. W., Relative rate constants for reactions of HFC 152a, 143, 143a, 134a, and HCFC 124 with F or Cl atoms and for CF_2CH_3, CF_2HCH_2, and CF_3CFH radicals with F_2, Cl_2, and O_2, *Int. J. Chem. Kinet.*, *25*, 667-680, 1993.

Kaye, J. A., S. A. Penkett, and F. M. Ormond, Report on concentrations, lifetimes, and trends of CFCs, halons, and related species, NASA Reference Publication 1339, 1994.

Keller-Rudek, H., and G. K. Moortgat, MPI-Mainz-UV-VIS Spectral Atlas of Gaseous Molecules, http://www.atmosphere.mpg.de/spectral-atlas-mainz.

Kozlov, S. N., V. L. Orkin, and M. J. Kurylo, An investigation of the reactivity of OH with fluoroethanes: CH_3CH_2F (HFC-161), CH_2FCH_2F (HFC-152), and CH_3CHF_2 (HFC-152a), *J. Phys. Chem. A*, *107*, 2239-2246, 2003.

Lancar, I., G. Le Bras, and G. Poulet, Oxidation of CH_3CCl_3 and CH_3CFCl_2 in the atmosphere - Kinetic study of OH reactions, *J. Chim. Physique*, *90*, 1897-1908, 1993.

Louis, F., A. Talhaoui, J. P. Sawerysyn, M.-T. Rayez, and J.-C. Rayez, Rate coefficients for the gas phase reactions of CF_3CH_2F (HFC-134a) with chlorine and fluorine atoms: Experimental and ab initio theoretical studies, *J. Phys. Chem. A*, *101*, 8503-8507, 1997.

Lu, Q. B., Correlation between cosmic rays and ozone depletion, *Phys. Rev. Lett.*, *102*, 118501, 2009.

Lu, Q. B., Cosmic-ray-driven electron-induced reactions of halogenated molecules adsorbed on ice surfaces: Implications for atmospheric ozone depletion and global climate change, *Phys. Rep.*, *487*, 141-167, 2010.

Lu, Q. B., and L. Sanche, Effects of cosmic rays on atmospheric chlorofluorocarbon dissociation and ozone depletion, *Phys. Rev. Lett.*, *87*, 078501, 2001.

Makeev, G. N., V. F. Sinyanskii, and B. M. Smirnov, Absorption spectra of certain fluorides in the near ultraviolet region, *Doklady Phys. Chem.*, *222*, 452-455, 1975.

Manning, R., and M. J. Kurylo, Flash photolysis resonance fluorescence investigation of the temperature dependencies of the reactions of $Cl(^2P)$ atoms with CH_4, CH_3Cl, CH_3F, CH_3F, and C_2H_6, *J. Phys. Chem.*, *81*, 291-296, 1977.

Matsumi, Y., K. Tonokura, Y. Inagaki, and M. Kawasaki, Isotopic branching ratios and translational energy release of H and D atoms in reaction of $O(^1D)$ atoms with alkanes and alkyl chlorides, *J. Phys. Chem.*, *97*, 6816-6821, 1993.

Mellouki, A., R. K. Talukdar, A. -M. Schmoltner, T. Gierczak, M. J. Mills, S. Solomon, and A. R. Ravishankara, Atmospheric lifetimes and ozone depletion potentials of methyl bromide (CH_3Br) and dibromomethane (CH_2Br_2), *Geophys. Res. Lett.*, *19*, 2059-2062, 1992.

Minschwaner, K., L. Hoffmann, A. Brown, M. Riese, R. Müller, and P. F. Bernath, Stratospheric loss and atmospheric lifetimes of CFC-11 and CFC-12 derived from satellite observations, *Atmos. Chem. Phys. Discuss., 12*, 28733-28764, 2012.

Møgelberg, T. E., J. Sehested, M. Bilde, T. J. Wallington, and O. J. Nielsen, Atmospheric chemistry of CF_3CFHCF_3 (HFC-227ea): Spectrokinetic investigation of the $CF_3CFO_2CF_3$ radical, its reactions with NO and NO_2, and fate of the CF_3CFOCF_3 radicals, *J. Phys. Chem.*, *100*, 8882-8889, 1996.

Molina, L. T., P. J. Wooldridge, and M. J. Molina, Atmospheric reactions and ultraviolet and infrared absorptivities of nitrogen trifluoride, *Geophys. Res. Lett.*, *22*, 1873-1876, 1995.

Müller, R., Impact of cosmic rays on stratospheric chlorine chemistry and ozone depletion, *Phys. Rev. Lett.*, *91*, 058502, 2003.

Müller, R., and J. U. Grooß, Does cosmic-ray-induced heterogeneous chemistry influence stratospheric polar ozone loss?, *Phys. Rev. Lett.*, *103*, 228501, 2009.

Nayak, A. K., T. J. Buckley, M. J. Kurylo, and A. Fahr, Temperature dependence of the gas and liquid phase ultraviolet absorption cross sections of HCFC-123 (CF_3CHCl_2) and HCFC-142b (CH_3CF_2Cl), *J. Geophys. Res.*, 101, 9055-9062, 1996.

Nelson, D. D. J., M. S. Zahniser, and C. E. Kolb, OH reaction kinetics and atmospheric lifetimes of CF_3CFHCF_3 and CF_3CH_2Br, *Geophys. Res. Lett.*, *20*, 197-200, 1993.

Nielsen, O. J., T. Ellermann, E. Bartkiewicz, T. J. Wallington, and M. D. Hurley, UV absorption spectra, kinetics and mechanisms of the self-reaction of CHF_2O_2 radicals in the gas phase at 298 K, *Chem. Phys. Lett.*, *192*, 82-88, 1992.

Nielsen, O. J., E. Gamborg, J. Sehested, T. J. Wallington, and M. D. Hurley, Atmospheric chemistry of HFC-143a: Spectrokinetic investigation of the $CF_3CH_2O_2$ radical, its reactions with NO and NO_2, and the fate of CF_3CH_2O, *J. Phys. Chem.*, *98*, 9518-9525, 1994.

Nilsson, E. J. K., M. S. Johnson, O. J. Nielsen, E. W. Kaiser, and T. J. Wallington, Kinetics of the gas-phase reactions of chlorine atoms with CH_2F_2, CH_3CCl_3, and CF_3CFH_2 over the temperature range 253-553 K, *Int. J. Chem. Kinet.*, *41*, 401-406, 2009.

Nilsson, E. J. K., V. F. Andersen, O. J. Nielsen, and M. S. Johnson, Rate coefficients for the chemical reactions of CH_2F_2, $CHClF_2$, CH_2FCF_3 and CH_3CCl_3 with $O(^1D)$ at 298 K. *Chem. Phys. Lett.*, *554*, 27-32, 2012.

Orkin, V. L., and V. G. Khamaganov, Determination of rate constants for reactions of some hydrohaloalkanes with OH radicals and their atmospheric lifetimes, *J. Atmos. Chem., 16*, 157-167, 1993.

Orkin, V. L., V. G. Khamaganov, E. E. Kasimovskaya, and A. G. Guschin, Photochemical properties of some Cl-containing halogenated alkanes, *submitted to J. Phys. Chem.*, 2013.

Orlando, J. J., Temperature dependence of the rate coefficients for the reaction of chlorine atoms with chloromethanes, *Int. J. Chem. Kinet.*, *31*, 515-524, 1999.

Orlando, J. J., J. B. Burkholder, S. A. McKeen, and A. R. Ravishankara, Atmospheric fate of several hydrofluoroethanes and hydrochloroethanes: 2. UV absorption cross sections and atmospheric lifetimes, *J. Geophys. Res.*, *96*, 5013-5023, 1991.

Papanastasiou, D., N. Rontu Carlon, J. A. Neuman, E. L. Fleming, C. H. Jackman, and J. B. Burkholder, Revised UV absorption cross sections of CF_2Br_2, CF_2ClBr, and CF_2BrCF_2Br and ozone depletion potentials, *Geophys. Res. Lett.*, *40*, doi: 10.1002/grl.50121, 2013.

Papadimitriou, V. C., M. McGillen, E. L. Fleming, C. H. Jackman, and J. B. Burkholder, NF_3: UV absorption spectrum temperature dependence and the atmospheric lifetime implications, *Geophys. Res. Lett.*, *40*, doi: 10.1002/grl.50120, 2013.

Paraskevopoulos, G., D. L. Singleton, and R. S. Irwin, Rates of OH radical reactions. 8. Reactions with CH_2FCl, CHF_2Cl, $CHFCl_2$, CH_3CF_2Cl, CH_3Cl, and C_2H_5Cl at 297 K, *J. Phys. Chem., 85*, 561-564, 1981.

Patra, P. K., and M. S. Santhanam, Comment on "Effects of cosmic rays on atmospheric chlorofluorocarbon dissociation and ozone depletion", *Phys. Rev. Lett.*, *89*, 219803, 2002.

Platz, J., O. J. Nielsen, J. Sehested, and T. J. Wallington, Atmospheric chemistry of 1,1,1-trichloroethane: UV spectra and self-reaction kinetics of CCl_3CH_2 and $CCl_3CH_2O_2$ radicals, kinetics of the reactions of the $CCl_3CH_2O_2$ radical with NO and NO_2, and the fate of the alkoxy radical CCl_3CH_2O, *J. Phys. Chem.*, *99*, 6570-6579, 1995.

Rontu Carlon, N., D. K. Papanastasiou, E. L. Fleming, C. H. Jackman, P. A. Newman, and J. B. Burkholder, UV absorption cross sections of nitrous oxide (N_2O) and carbon tetrachloride (CCl_4) between 210 and 350 K and the atmospheric implications, *Atmos. Chem. Phys.*, *10*, 6137-6149, 2010.

Sander, S. P., J. Abbatt, J. R. Barker, J. B. Burkholder, R. R. Friedl, D. M. Golden, R. E. Huie, C. E. Kolb, M. J. Kurylo, G. K. Moortgat, V. L. Orkin, and P. H. Wine, *Chemical Kinetics and Photochemical Data for Use in Atmospheric Studies, Evaluation Number 17, JPL Publication 10-6,* Jet Propulsion Laboratory, California Institute of Technology 2011.

Sarzyński, D., A. A. Gola, A. Dryś, and J. T. Jodkowski, Kinetic study of the reaction of chlorine atoms with chloromethane in the gas phase, *Chem. Phys. Lett.*, *476*, 138-142, 2009.

Simon, P. C., D. Gillotay, N. Vanlaethem-Meuree, and J. Wisemberg, Temperature dependence of ultraviolet absorption cross-sections of chlorofluoroethanes, *Annales Geophysicae*, *6*, 239-248, 1988a.

Simon, P. C., D. Gillotay, N. Vanlaethem-Meuree, and J. Wisemberg, Ultraviolet absorption cross-sections of chloro and chlorofluoro-methanes at stratospheric temperatures, *J. Atmos. Chem.*, *7*, 107-135, 1988b.

Spivakovsky, C. M., J. A. Logan, S. A. Montzka, Y. J. Balkanski, M. Foreman-Fowler, D. B. J. Jones, L. W. Horowitz, A. C. Fusco, C. A. M. Brenninkmeijer, M. J. Prather, S. C. Wofsy, and M. B. McElroy, Three-dimensional climatological distribution of tropospheric OH: Update and evaluation, *J. Geophys. Res.*, *105*, 8931-8980, 2000.

Staudinger, J., and P. V. Roberts, A critical compilation of Henry's law constant temperature dependence relations for organic compounds in dilute aqueous solutions, *Chemosphere*, *44*, 561-576, 2001.

Swartz, W. H., S. A. Lloyd, T. L. Kusterer, D. E. Anderson, C. T. McElroy, and C. Midwinter, A sensitivity study of photolysis rate coefficients during POLARIS, *J. Geophys. Res., 104*, 26725-26735, 1999.

Talhaoui, A., F. Louis, P. Devolder, B. Meriaux, J. P. Sawerysyn, and M. T. Rayez, Rate coefficients of the reactions of chlorine atoms with haloethanes of type $CH_3CCl_{3-x}F_x$ (x = 0, 1, and 2): Experimental and ab initio theoretical studies, *J. Phys. Chem.*, *100*, 13531-13538, 1996.

Talukdar, R., A. Mellouki, T. Gierczak, J. B. Burkholder, S. A. McKeen, and A. R. Ravishankara, Atmospheric fate of CF_2H_2, CH_3CF_3, CHF_2CF_3, and CH_3CFCl_2: Rate coefficients for reactions with OH and UV absorption cross sections of CH_3CFCl_2, *J. Phys. Chem.*, *95*, 5815-5821, 1991.

Tokuhashi, K., L. Chen, S. Kutsuna, T. Uchimaru, M. Sugie, and A. Sekiya, Environmental assessment of CFC alternatives: Rate constants for the reactions of OH radicals with fluorinated compounds, *J. Fluor. Chem.*, *125*, 1801-1807, 2004.

Tschuikow-Roux, E., T. Yano, and J. Niedzielski, Reactions of ground state chlorine atoms with fluorinated methanes and ethanes, *J. Chem. Phys.*, *82*, 65-74, 1985.

Tuazon, E. C., R. Atkinson, and S. B. Corchnoy, Rate constants for the gas-phase reactions of Cl atoms with a series of hydrofluorocarbons and hydrochlorofluorocarbons at 298 ± 2 K, *Int. J. Chem. Kinet.*, *24*, 639-648, 1992.

Vranckx, S., J. Peeters, and S. Carl, A temperature dependence kinetic study of $O(^1D) + CH_4$: Overall rate coefficient and product yields, *Phys. Chem. Chem. Phys.*, *10*, 5714-5722, 2008.

Wallington, T. J., J. M. Andino, J. C. Ball, and S. M. Japar, Fourier transform infrared studies of the reaction of Cl atoms with PAN, PPN, CH_3OOH, HCOOH, CH_3COCH_3 and $CH_3COC_2H_5$ at 295 ± 2 K, *J. Atmos. Chem.*, *10*, 301-313, 1990.

Wallington, T. J., and M. D. Hurley, A kinetic study of the reaction of chlorine atoms with CF_3CHCl_2, CF_3CH_2F, $CFCl_2CH_3$, CF_2ClCH_3, CHF_2CH_3, CH_3D, CH_2D_2, CHD_3, CD_4, and CD_3Cl at 295 ± 2 K, *Chem. Phys. Lett.*, *189*, 437-442, 1992.

Wallington, T. J., M. D. Hurley, O. J. Nielsen, and M. P. S. Andersen, Atmospheric chemistry of $CF_3CFHCF_2OCF_3$ and $CF_3CFHCF_2OCF_2H$: Reaction with Cl atoms and OH radicals, degradation mechanism, and global warming potentials, *J. Phys. Chem. A*, *108*, 11333-11338, 2004.

Warren, R., T. Gierczak, and A. R. Ravishankara, A study of $O(^1D)$ reactions with CFC substitutes, *Chem. Phys. Lett., 183*, 403-409, 1991.

Warren, R. F., and A. R. Ravishankara, Kinetics of $Cl(^2P)$ reactions with CF_3CHCl_2, CF_3CHFCl, and CH_3CFCl_2, *Int. J. Chem. Kinet.*, *25*, 833-844, 1993.

Watson, R. T., G. Machado, B. Conaway, S. Wagner, and D. D. Davis, A temperature dependent kinetics study of the reaction of OH with CH_2ClF, $CHCl_2F$, $CHClF_2$, CH_3CCl_3, CH_3CF_2Cl, and $CF_2ClCFCl_2$, *J. Phys. Chem., 81*, 256-262, 1977.

Wine, P. H., and A. R. Ravishankara, Kinetics of $O(^1D)$ interactions with the atmospheric gases N_2, N_2O, H_2O, H_2, CO_2, and O_3, *Chem. Phys. Lett.*, *77*, 103-109, 1981.

WMO (World Meteorological Organization), *Scientific Assessment of Ozone Depletion: 2006, Global Ozone Research and Monitoring Project-Report* No. 50, 2007.

WMO (World Meteorological Organization), *Scientific Assessment of Ozone Depletion: 2010, Global Ozone Research and Monitoring Project-Report* No. 52, 2011.

Yano, T., and E. Tschuikow-Roux, Competitive photochlorination of the fluoroethanes CH_3CHF_2, CH_2FCH_2F and CHF_2CHF_2, *J. Photochem.*, *32*, 25-37, 1986.

Young, C. J., M. D. Hurley, T. J. Wallington, and S. A. Mabury, Atmospheric chemistry of CF_3CF_2H and $CF_3CF_2CF_2CF_2H$: Kinetics and products of gas-phase reactions with Cl atoms and OH radicals, infrared spectra, and formation of perfluorocarboxylic acids, *Chem. Phys. Lett.*, *473*, 251-256, 2009.

Zellner, R., G. Bednarek, A. Hoffmann, J. P. Kohlmann, V. Mors, and H. Saathoff, Rate and mechanism of the atmospheric degradation of 2 H-heptafluoropropane (HFC-227), *Ber. Bunsenges. Phys. Chem.*, *98*, 141-146, 1994.

Zhang, Z., S. Padmaja, R. D. Saini, R. E. Huie, and M. J. Kurylo, Reactions of hydroxyl radicals with several hydrofluorocarbons: The temperature dependencies of the rate constants for $CHF_2CF_2CH_2F$ (HFC-245ca), $CF_3CHFCHF_2$ (HFC-236ea), CF_3CHFCF_3 (HFC-227ea), and $CF_3CH_2CH_2CF_3$ (HFC-356ffa), *J. Phys. Chem.*, *98*, 4312-4315, 1994.

Zhang, Z., R. D. Saini, M. J. Kurylo, and R. E. Huie, A temperature dependent kinetic study of the reaction of the hydroxyl radical with CH_3Br, *Geophys. Res. Lett.*, *19*, 2413-2416, 1992.

Zhao, Z., P. L. Laine, J. M. Nicovich, and P. H. Wine, Reactive and non-reactive quenching of $O(^1D)$ by the potent greenhouse gases SO_2F_2, NF_3, and SF_5CF_3, *Proc. Nat. Acad. Sci.*, *107*, 6610-6615, 2010.

CHAPTER 4

Inferred Lifetimes from Observed Trace-Gas Distributions

Lead Authors:
Andreas Engel
Elliot L. Atlas

Co-Authors:
Peter F. Bernath
Harald Bönisch
Alex Brown
Johannes Laube
Kenneth R. Minschwaner
Stephen A. Montzka
Simon O'Doherty
Ronald G. Prinn
Matthew Rigby
Susan M. Schauffler
C. Michael Volk
Shari A. Yvon-Lewis

CHAPTER 4

Inferred Lifetimes from Observed Trace-Gas Distributions

Contents

4.1 Introduction

Atmospheric trends of trace gases are controlled by the balance of sinks (=losses) and sources (including direct emissions). One measure of the rate of loss of any atmospheric constituent is its atmospheric lifetime. A detailed discussion on the distinction between different ways of evaluating lifetimes (e.g., transient and steady-state lifetime) is given in Chapter 2. Species may have multiple different sink processes, and the combination of these processes determines the overall lifetime. For many long-lived species (e.g., chlorofluorocarbons (CFCs)), photochemical breakdown in the stratosphere is the main loss process and, in this case, the stratospheric lifetime becomes the overall atmospheric lifetime. In the troposphere, oxidation – often initiated by the hydroxyl radical (OH) – as well as wet and dry deposition processes are major loss processes. Some chemicals become destroyed in the hydrosphere or in soils, and these losses also must be considered to properly estimate their lifetimes. This chapter discusses the derivation of atmospheric lifetimes using atmospheric measurements of trace gases and model studies which are closely linked to atmospheric observations. Observations of global trace-gas mole fractions and their temporal change, of trace gas atmospheric distributions, and of the atmospheric mole fraction correlations in regions where destruction dominates atmospheric variability (e.g., in the stratosphere) can all be used to derive measurement-based lifetimes. They can also serve to constrain model estimates of atmospheric lifetimes and environmental impacts.

The atmospheric distribution of a trace gas, its temporal trends and its variability depend in part on the atmospheric lifetime. In the simplest case of a species whose emission into the atmosphere has stopped and which has no other sources, insight into a chemical's lifetime is provided by the e-folding time of the decrease of the atmospheric mole fraction. The most notable example of this is methyl chloroform, whose global mean mole fraction has decreased at an approximately constant exponential rate since 1998 (Montzka *et al.,* 2011). The e-fold time derived from exponential decay, however, is not generally the same as that derived for steady-state conditions, which is what models typically derive for trace gases. Lifetimes derived from observations are often affected by such temporal changes and are usually not steady-state lifetimes. Usually, even for species of anthropogenic origin that are no longer emitted in large amounts into the atmosphere, there will be some sources so that the simple e-folding time will seldom be a direct measure of the lifetime. In such cases a combination of different modeling techniques with observations of atmospheric mole fractions (see Section 4.3) can be used to derive optimal estimates of lifetimes of a trace gas. Note, however, that the lifetime derived in this way is usually not a steady-state lifetime but rather an average of the transient lifetimes over the time period considered for the respective study. In many cases the differences will be rather small, as discussed in the individual section of this chapter and in Chapter 2 and these calculated transient lifetimes can be transformed to yield steady-state lifetime estimates.

In this chapter we will present results from techniques that interpret atmospheric measurements of trace gases in different ways. Common to all methods is the need for well-calibrated, high-quality data. In Section 4.2 we thus present available tropospheric and stratospheric observations. The tropospheric measurements used in this report primarily rely on results from two global atmospheric monitoring networks (National Oceanic and Atmospheric Administration/Earth System Research Laboratory (NOAA/ESRL) and Advanced Global Atmospheric Gases Experiment (AGAGE)), though other network data are available for some of the gases evaluated here (e.g., the University of California at Irvine (UC Irvine) (http://cdiac.ornl.gov/trends/otheratg/blake/blake.html, the University of East

Anglia (UEA), and the SOGE (System for Observation of halogenated Greenhouse gases in Europe) networks). The section on stratospheric observations is subdivided into *in situ* data from high-altitude aircraft and from balloons (which are usually of high precision and accuracy but have a limited coverage) and satellite data (with less accuracy and higher absolute uncertainties but a much better spatial and temporal coverage). Section 4.3 then discusses the methods that rely on different combinations of observations with modeling work. In Section 4.4 we discuss the applicability of using tracer-tracer correlations observed in the stratosphere to infer relative and absolute stratospheric lifetimes, and we present results from this analysis of correlations. For the calculation of absolute lifetimes from the relative lifetimes of two tracers, the lifetime of one of the two tracers must be specified and the absolute lifetime of the other is reported relative to this specified lifetime. There is also an approach deriving absolute lifetimes from correlation analysis by using mean age as one of the tracers in the correlation (Volk *et al.,* 1997). The applicability of this method is discussed in more detail in Chapter 2 and will not be pursued any further in the present chapter.

4.2 Database of Atmospheric Observations

4.2.1 Tropospheric Observations

As discussed above, long-term observational records with consistent calibration are needed for the calculation of atmospheric lifetimes (Sections 4.3 and 4.4), to correct observed stratospheric tracer-tracer correlations for tropospheric trends, and to calculate global burdens. Where data from multiple sources are combined, care must be taken that these are intercalibrated well and are consistent with each other over time. Data from two atmospheric monitoring networks are often used for this purpose: the NOAA/ESRL (http://www.esrl.noaa.gov/) and AGAGE (http://agage.eas.gatech.edu/). Table 4.1 lists available data from these networks and others. Annual mean global mole fractions derived from these independent networks are typically within a few percent of each other for the more abundant chemicals (Montzka and Reimann, 2011).

Global tropospheric burdens of long-lived halocarbons and their changes over time are derived from atmospheric measurements of discrete air samples at multiple sites in each hemisphere at Earth's surface. The analysis of light passing through the atmosphere has also allowed trace-gas densities and their changes over time to be derived from satellites and from ground-based instrumentation (see Section 4.2.2). With either approach, measurements are conducted at remote sites to provide observational data for anthropogenically emitted gases that are representative of large atmospheric regions. Discrete measurements are conducted by collecting flasks and sending them to a central laboratory for analysis or by instruments located at remote sites that continually analyze samples as they are collected. Ground-based air sampling networks are designed to capture the predominant mole fraction gradients at Earth's surface so that an accurate estimate of global mean surface mole fractions can be derived. Because not all observation sites are shared by the main sampling networks, bringing data together from different networks can add substantially to our understanding of the surface distribution of a trace gas and provide a more accurate estimate of its true global mean mole fraction. Combining data from different networks is only useful if data from these networks are of comparable quality and if mole fraction differences between networks arising from standardization can be removed. In addition, for inverse techniques to provide accurate information about the distribution of sources (and potentially sinks), differences must be removed if the data are to be combined, so that distributions and time variations in the combined data record reflect true atmospheric gradients and variations.

Table 4.1. Summary of data availability from tropospheric monitoring networks (NOAA=NOAA/ESRL, USA; AGAGE=ALE/GAGE/AGAGE; UEA=University of East Anglia, UK; UCI=University of California, Irvine, USA in the table below). In the NOAA, AGAGE and UCI networks measurements are made at multiple sites in each hemisphere unless otherwise indicated. Dates indicate the year that the measurement started. Compounds are grouped into classes with removal primarily in the stratosphere or in the troposphere. CG=Cape Grim, Tasmania; TH=Trinidad Head/Cape Meares, California; JF=Jungfraujoch, Switzerland; MH=Mace Head/Adrigole, Ireland; CM=Cape Matatula, American Samoa; RP=Ragged Point, Barbados. (U) indicates uncalibrated.

Compound	Formula	NOAA	AGAGE	Notes
STRATOSPHERIC REMOVAL Species				
CFC-11	CCl_3F	1978[a]	1978	
CFC-12	CCl_2F_2	1978 [a]	1978	
CFC-113	CCl_2FCClF_2	1992 [b]	1982	CG in 1982, TH in 1984, CM and RP in 1985; and MH in 1987
CFC-114	$CClF_2CClF_2$	N.A.	2003	Includes a {constant} correction for co-elution of CFC-114a
CFC-115	CF_3CClF_2	2007 [c]	1998	AGAGE initially at MH and CG; more sites added in 2005
Carbon tetrachloride	CCl_4	1990 [a]	1978	CG, CM, RP in 1978, TH and MH in 1979
Nitrous oxide	$\mathbf{N_2O}$	1978 [a]	1978	
Halon-1211[d,e]	$CBrClF_2$	1992	1994	AGAGE at MH in 1994, CG in 1998 and JF in 2000; more sites added in 2005
Halon-1301[d,e]	$CBrF_3$	1989	1997	AGAGE initially at MH CG in 1998; JF in 2000; more sites added in 2005
Halon-2402[d,e]	$CBrF_2CBrF_2$	1995	2005	NOAA data before 2004 have substantial time gaps
TROPOSPHERIC REMOVAL Species				
Methane[f]	CH_4	1985	1985	TH in 1985, CG in 1986, MH and CM in 1987
Methyl chloroform	CH_3CCl_3	1990	1978	
Methyl chloride	CH_3Cl	1995	1998	AGAGE initially at MH and CG; more sites added in 2005
Methyl bromide	CH_3Br	1995	1998	AGAGE initially at MH and CG; more sites added in 2005
HCFC-22	$CHClF_2$	1992	1998	AGAGE initially at CG; MH in 1999; more sites added in 2005
HCFC-141b	CH_3CCl_2F	1992	199	AGAGE initially at MH; CG in 1998; more sites added in 2005
HCFC-142b	CH_3CClF_2	1992	1994	AGAGE initially at MH; CG in 1998; more sites added in 2005
Halon-1202[d,e]	CBr_2F_2	N.A.	N.A.	
HFC-23[e]	CHF_3	N.A.	2007	
HFC-32	CH_2F_2	2007 [c]	2005	
HFC-125	CHF_2CF_3	2007 [c]	1998	AGAGE initially at MH and CG; more sites added in 2005
HFC-134a	CH_2FCF_3	1994	1994	AGAGE at MH in 1994, CG in 1998; JF in 2000, more sites added in 2005
HFC-143a	CF_3CH_3	2007 [c]	2003	

HFC-152a	CH_3CHF_2	2000 [c]	1994	AGAGE at MH in 1994 and CG in 1998; more sites added in 2005
HFC-227ea	CF_3CHFCF_3	2007 [c]	2006	AGAGE initially at MH and CG; more sites added in 2007
HFC-245fa	$CHF_2CH_2CF_3$	N.A.	2006	AGAGE initially at MH and CG; more sites added in 2007
ADDITIONAL Species				
HFC-365mfc	$CF_3CH_2CF_2CH_3$	2007 [c]	2003	AGAGE initially at MH and JF; CG in 2004; more sites added in 2008
HFC-236fa	$CF_3CH_2CF_3$	N.A.	2006	AGAGE initially at MH and CG; more sites added in 2008
HFC-43-10mee	$CF_3CHFCHFCF_2CF_3$	N.A.	2010 [c] (U)	
CFC-13	$CClF_3$	2007 [c]	2003 [c] (U)	

Additional notes: **N.A.** indicates no measurements being made. NOAA data are derived with flask sampling and *in situ* instrumentation, depending on compound. NOAA results indicated in the table are derived from only flask measurements with the following exceptions: [a] Global means from NOAA are derived from a combination of flask and *in situ* measurements; the *in situ* measurements began in the late 1980s. [b] Global means from NOAA are derived from a combination of flask and *in situ* measurements; the *in situ* measurements began in 1999-2000. [c] Indicates that these data are currently unpublished. [d] Halons-1211 and -2402 are removed both in the troposphere and stratosphere. For Halon-1301 the stratosphere is the main loss region, while Halon-1202 is mainly removed in the troposphere. [e] UEA has CG data available for all four Halons and HFC-23 dating back to 1978 (partly from archived air samples). [f] Earlier CH_4 measurements are available from UCI dating back to 1978.

Although Table 4.1 provides information about on-going measurement records, i.e., chemicals for which measurements are being conducted on a regular basis to observe changes in atmospheric composition as they occur, other archives of air exist that allow an understanding of atmospheric changes in years before measurements began at these sites. One such air archive, the Cape Grim Air Archive, includes canister samples that were collected since 1978. Analysis of this air archive with present-day analysis techniques has provided an understanding of atmospheric composition changes in years since 1978 (e.g., Oram *et al.,* 1995; Maiss *et al.,* 1996; Prinn *et al.,* 2000). Other natural air archives also exist that have extended the measurement record into the early 1970s (e.g., Mühle *et al.,* 2010). Air trapped in consolidated snow (firn) or in ice bubbles has been extracted and atmospheric mole fractions of halocarbons have been measured as a function of depth (age) in snow and ice. The mean age of air samples collected from firn are up to ~100 years old (Severinghaus *et al.,* 2010). Although deriving an atmospheric history is less straightforward from firn or ice-bubble air than from air archived in canisters, past atmospheric changes can be reliably derived (e.g., Martinerie *et al.,* 2009; Buizert *et al.,* 2012).

4.2.2 Stratospheric Observations

Stratospheric observations of halocarbon mole fractions are important in several respects when determining lifetimes:

(i) the observed correlation slope between mole fractions of two species at or near the tropopause can be used to derive the relative lifetimes of two species (see Section 4.4),

(ii) the vertical distributions, which are a function of lifetime and growth rate, can be used to constrain model calculations which are used to derive lifetimes (see Chapter 5),

(iii) from global distributions of a tracer and modeled loss rates, the lifetime can be inferred (Section 4.3.4), and
(iv) stratospheric observations are needed to determine the stratospheric contribution to the total atmospheric burden of a species, which is needed to calculate the lifetime.

For determination of the slope of the correlation between two gases (point (i) above), high accuracies and sufficient data coverage are needed near the tropopause (see Chapter 2 and Section 4.4). Clearly, the slope correlation method requires simultaneous observations of at least two compounds. Moreover, observations with sufficient precision have only become available since the 1990s onward for most of the compounds considered here. Measurements can be made either *in situ* using high-flying aircraft or balloons as platforms or by remote sensing from space. Note that for the purpose of this section on stratospheric data the term *in situ* will include data from flask sampling techniques as well as from direct *in situ* measurements, as the characteristics of the data are similar.

4.2.2.1 *In Situ* Stratospheric Data

Due to the complexity involved with bringing instruments into the stratosphere, stratospheric *in situ* data are sporadic in time and do not have global coverage in space. Their main advantage is that they are often characterized by high spatial resolution and high data quality with systematic uncertainties that are usually rather small. In contrast to tropospheric observations which are available for many species on a regular basis, stratospheric *in situ* observations of a number of gases are available on campaign basis, i.e., only sporadic in time and space.

A number of publications focus on the stratospheric measurements of methane (CH_4) and nitrous oxide (N_2O) (Herman *et al.,* 1998, 2003; Park *et al.,* 2004; Spackman *et al.,* 2007) resulting in a broad database from a variety of campaigns, platforms and instruments. The most extensive data compilations for these two compounds are given by Andrews *et al.* (2001) and Greenblatt *et al.* (2002) who combine aircraft, balloon and (for the latter) satellite observations.

There are also publications reporting CFC-11 (CCl_3F) and/or CFC-12 (CCl_2F_2) mole fractions in the stratosphere. Examples are Ray *et al.,* 1999, 2002; Bujok *et al.,* 2001; Richard *et al.,* 2001; Jost *et al.,* 2002; Plumb *et al.,* 2003; Ehhalt *et al.,* 2007; Homan *et al.,* 2010, and Werner *et al.,* 2010. The other major ozone depleting compounds – carbon tetrachloride (CCl_4), methyl chloroform (CH_3CCl_3), and HCFC-22 ($CHClF_2$) – have been examined in Jobson *et al.,* 1999; Sen *et al.,* 1999; Toon *et al.,* 1999; and Park *et al.,* 2010. The most suitable data for stratospheric lifetime estimation for the latter five compounds in terms of data density and quality have been presented in Volk *et al.,* 1996, 1997; Moore *et al.,* 2003 (both excluding HCFC-22); Schauffler *et al.,* 2003; and Laube *et al*. (2013).

There are considerably less stratospheric data available for other compounds except for Halon-1211 ($CBrClF_2$) and CFC-113 (CCl_2FCClF_2), which have been measured frequently in the stratosphere since the 1990s (e.g., Volk *et al*., 1996, 1997; Wamsley *et al.,* 1998; Flocke *et al.,* 1999; and Moore *et al.,* 2003). There are only six papers reporting good quality data for Halon-1301 ($CBrF_3$) and/or CFC-115 ($CClF_2CF_3$) (Wamsley *et al.,* 1998; Schauffler *et al.,* 1999, 2003; Pfeilsticker *et al.,* 2000; Laube *et al.,* 2008, 2010a.)

Stratospheric observations of many of the remaining compounds are reported by Wamsley *et al.,* 1998 (methyl bromide (CH_3Br), Halon-2402 ($CBrF_2CBrF_2$)), Flocke *et al.,* 1999 (CFC-114 ($CClF_2CClF_2$) and Halon-2402), Schauffler *et al.,* 1999 (CH_3Br, Halon-2402), Schauffler *et al.,* 2003 (CFC-114, CFC-114a (CCl_2FCF_3), HCFC-141b (CH_3CCl_2F), HCFC-142b (CH_3CClF_2)) Ehhalt *et al.,* 2007 (CH_3Cl), Laube *et al.,* 2008, 2010a (CFC-114, CFC-114a, HCFC-141b, HCFC-142b, Halon-2402, Halon-1202 (CBr_2F_2)), Park *et al.,* 2010 (HCC-40 (CH_3Cl) and CH_3Br), Pfeilsticker *et al.,* 2000, and Sturges *et al.,* 2000 (Halon-2402, Halon-1202, CH_3Br). In addition, for other HFCs the only published observations are those of HFC-227ea (CF_3CHFCF_3) in Laube *et al.,* 2010b. No stratospheric data has yet been reported for a number of the compounds that were selected for evaluation in this report. One report for HFC-23 (CHF_3) is Oram *et al.,* 1998. The compounds for which there is no reported stratospheric data include HFC-32 (CH_2F_2), HFC-125 (CHF_2CF_3), HFC-134a (CH_2FCF_3), HFC-143a (CH_3CF_3), HFC-152a (CH_3CHF_2), and HFC-245fa ($CHF_2CH_2CF_3$).

4.2.2.2 Satellite Observations

Measurements of trace gases from satellites are obtained with techniques that employ two basic viewing geometries: nadir and limb-viewing sounders. Nadir sounders view the Earth's surface directly beneath the satellite sensor, while limb sounders look through an oblique slice of the atmosphere without viewing the surface. Nadir sounders such as IRIS, IMG, AIRS, TES and IASI are capable of measuring the total column of CFC-11, CFC-12, HCFC-22 and CH_4. Unfortunately these instruments do not have sufficient vertical resolution to be used for lifetime calculations. In contrast, limb sounders have sufficiently high vertical resolution to allow the calculation of the stratospheric lifetime of long-lived species from tracer-tracer correlations or from photolysis rate calculations. The instruments of primary interest for this study are ATMOS, CIRRIS-1A, CRISTA-2, CLAES, MIPAS, ACE, HIRDLS and MLS.

Atmospheric Trace Molecule Spectroscopy Experiment (ATMOS): ATMOS was designed to measure the volume-mixing ratio (VMR) of atmospheric constituents active in the infrared spectral region (IR). The ATMOS instrument was a Fourier transform spectrometer carried onboard NASA space shuttles on four occasions (1985, 1991, 1992 and 1993). ATMOS was capable of measuring vertical profiles of CFC-11, CFC-12, CCl_4, HCFC-22, CH_3Cl, N_2O and CH_4. Measurements of CH_3Cl, CFC-12, CFC-11, HCFC-22 and CCl_4 from ATMOS were first reported in Zander *et al.* (1987).

Measurements of N_2O, CFC-11, CFC-12 and CCl_4 VMRs from ATMOS were compared to those made by the NASA ER-2 aircraft during November 1994 (Chang *et al.,* 1996). The mean difference in CFC-11 VMRs between ATMOS and ER-2 was +4%, which is well within the uncertainty of the satellite measurements. Agreement for CFC-12 ranged between + 5% and – 6%, just a little outside the estimated ATMOS measurement precision of 5%. ATMOS measurements of CCl_4 were systematically higher (15%) than *in situ* measurements. In 2002 ATMOS version 3 data was released (Irion *et al.*, 2002). Retrievals in version 3 extended further into the troposphere than those in version 2, which has allowed better comparison with tropospheric *in situ* measurements. These comparisons showed good agreement for CFC-11, CFC-12, HCFC-22 and CH_3Cl although comparisons for CCl_4 showed that ATMOS VMRs remained high.

Cryogenic Infrared Radiance Instrumentation for Shuttle (CIRRIS): CIRRIS was designed to measure the atmospheric IR radiance from the troposphere to the lower thermosphere. The instrument was flown onboard the shuttle between April 28th and May 6th 1991. VMR profiles were retrieved for CFC-11 between 13 and 25 km and between 13 and 34 km for CFC-12 (Bingham *et al.,* 1997). Retrievals of atmospheric CCl_4 were also carried out using CIRRIS data between 10 and 20 km.

Cryogenic Infrared Spectrometers and Telescopes for the Atmosphere (CRISTA): CRISTA flew two missions onboard the Astronomical Shuttle Pallet Satellite (ASTRO-SPAS) in November 1994 (CRISTA-1) and in August 1997 (CRISTA-2). CRISTA analyzed IR emission from the Earth's limb for about 8 days during each flight. Vertical profiles from the upper troposphere to the lower thermosphere were retrieved from these measurements. CRISTA-2 was capable of measuring vertical profiles of CH_4, N_2O, CFC-11 and CFC-12 (Grossmann *et al.,* 2002). CFC-11 was retrieved between 8 and 28 km (Kuell *et al.,* 2005) and the VMRs agreed within the estimated errors with measurements made by the BONBON whole air sampler. Global CFC-11 VMR fields were produced on a 2 km x 5° latitude grid.

Cryogenic Limb Array Etalon Spectrometer (CLAES): CLAES on NASA UARS obtained global distributions of CFC-12 and CFC-11 in the stratosphere between October 1991 and May 1993. Seasonally varying dynamical features similar to those from N_2O and CH_4 were observed. These global distributions were compared and showed good agreement with the Goddard Space Flight Centre (GSFC) two-dimensional (2-D) model (Roche *et al.,* 1998). Instantaneous lifetimes were calculated for CFC-12 and N_2O using the global loss rates from four separate seasons and the mean atmospheric burden during this time. The calculated instantaneous lifetimes were 114 ± 22 years (CFC-12) and 118 ± 25 years (N_2O). These values led to steady-state lifetimes of 103 ± 25 years (CFC-12) and 117 ± 26 years (N_2O) (Minschwaner *et al.,* 1998). Section 4.3.4 of this chapter presents new results for the CFC-11 lifetime using this method applied to more recent satellite measurements.

Michelson Interferometer for Passive Atmospheric Sounding (MIPAS): MIPAS onboard ENVISAT was, until April 2012, capable of measuring the atmospheric concentration of CFC-11, CFC-12, HCFC-22, N_2O and CH_4. Retrievals carried out by Moore *et al.* (2006) calculated vertical profiles up to 24 km for CFC-11 and 27 km for CFC-12. HCFC-22 was also retrieved from MIPAS data producing a vertical profile up to a maximum altitude of 18 km. Hoffmann *et al.* (2005) also retrieved CFC-11 and CFC-12 from MIPAS with total errors of 7 to 10% in the upper troposphere and lower stratosphere. Hoffmann *et al.* (2008) carried out additional work on CFC-11 and satisfactory comparisons were made with retrievals from ATMOS, CRISTA and CIRRIS. Comparisons with the *in situ* High Altitude Gas Analyser (HAGAR) showed differences of less than 10% between HAGAR and MIPAS CFC-11.

Atmospheric Chemistry Experiment (ACE): ACE Fourier transform spectrometer (FTS) was launched onboard the satellite SCISAT-1 in August 2003(Bernath, 2006). ACE-FTS is capable of retrieving concentrations of CCl_4, CFC-11, CFC-12, CFC-113, CH_3Cl, HCFC-22, HCFC-141b, HCFC-142b, N_2O and CH_4. Carbon tetrachloride (CCl_4) was first retrieved from ACE observations for the 2004 global stratospheric chlorine budget derived by Nassar *et al.* (2006a) and a global distribution was determined by Allen *et al.* (2009). Brown *et al.* (2011) derived trends for 16 halogenated gases.

Validation of ACE-FTS version 2.2 (V.2.2) measurements of CFC-11 were made by comparison with balloon-borne FTS measurements (Mahieu *et al.,* 2008). Comparisons with the FIRS-2 instrument showed agreement to within 10% below 16 km. ACE-FTS measurements were also compared to the Mk-IV instrument, with agreement to 10% above 12 km and 20% below 12 km. CFC-11 was used in both the global stratospheric fluorine and chlorine budgets (Nassar *et al.* 2006a, 2006b). Validation of ACE-FTS V.2.2 measurements of CFC-12 also were made by comparisons with balloon-borne FTS measurements (Mahieu *et al.,* 2008) and the agreement is similar to the CFC-11 case. The retrieval method for CFC-113 was outlined by Dufour *et al.* (2005). This was the first retrieval of CFC-113 from a space-based instrument and was within 15% of surface mole fractions measured by AGAGE.

HCFC-141b is a new species available from the version 3.0 ACE-FTS retrieval. The retrieval method used by ACE for HCFC-142b was described by Dufour *et al.* (2005), who found that there was agreement to 15% between ground-based AGAGE and ACE measurements.

Other Satellites: Whilst active the High Resolution Dynamics Limb Sounder (HIRDLS) instrument retrieved both CFC-11 and CFC-12 (http://www.eos.ucar.edu/hirdls/data/). The Microwave Limb Sounder (MLS) retrieves both N_2O and CH_3Cl.

4.3 Combined Model/Observational Approaches

This section discusses different applications that use modeling in combination with observations and other relevant data to derive atmospheric lifetimes. The first application is inverse modeling to estimate lifetimes. Inverse modeling uses observational data measured at long-term monitoring sites (and potentially other relevant measurements) in combination with a transport model to infer emissions and/or lifetimes. For the study here, emissions are specified and a 2-D model is applied. This technique is used for the longer-lived species (lifetime more than 5 years) with predominately anthropogenic sources.

Forward modeling or global box modeling approaches can be applied to shorter-lived compounds with natural sinks and sources. For longer-lived compounds forward modeling can generally be used to check if lifetimes and assumed emissions are in agreement with the observed tropospheric time series. Global box modeling studies are discussed with respect to CH_3Cl, CH_3Br and CCl_4 in this report.

The inverse and forward modeling approaches require the use of independent bottom-up emission data. Industry reported production numbers are available up to the year 2007 from the Alternative Fluorocarbons Environmental Acceptability Study (AFEAS) for CFCs, HCFC-22, -124, -141b, and -142b, as well as for HFC-134a, -125, and -143a. However, AFEAS stopped their work as less than half of the global sales are now from companies reporting to AFEAS, so total emissions are not captured. Emissions used for this report are discussed in Section 4.3.1, and are consistent with modeling runs discussed in Chapter 5 of this report. No updated emission data were developed for this assessment.

The last approach used in this section will use global scale measurements of trace-gas distributions to estimate global atmospheric burdens. Global loss rates of the trace gas are then estimated from model calculations using recommended loss rates. The ratio of global burden to global loss rate is a direct measure of the instantaneous atmospheric lifetime at the time of the measurement.

4.3.1 Inverse Modeling

When combined with emissions estimates and knowledge of large-scale atmospheric chemistry and transport processes, trends in background mole fractions can be used to determine the overall lifetime of atmospheric constituents. Previous "inverse" estimates of the transient lifetimes of CFC-11, CFC-12, and CH_3CCl_3 have been made using AGAGE and NOAA measurements, emissions inventories and a simplified model of atmospheric transport and chemistry (Cunnold *et al.,* 1983, 1994; Prinn *et al.,* 2001, 2005).

Rigby *et al.* (2013) follow an approach similar to Cunnold *et al.* (1983), in which a two-dimensional chemical transport model (CTM) was used to simulate atmospheric mole fractions, which were compared to AGAGE and NOAA observations between 1978 and 2011. Using a Bayesian inverse method they combined the measurements and model to improve prior estimates of a set of parameters related to overall trace-gas lifetimes (stratospheric loss frequencies, OH concentrations, initial mole fractions and model transport parameters) in order to better match the observations. Lifetimes were estimated only for CFC-11, -12, -113, and CH_3CCl_3 as relatively robust emissions estimates were thought to exist for these compounds (McCulloch *et al.,* 2001; 2003, Rigby *et al.*, 2013). The lifetimes of other gases, with more poorly understood emissions (e.g., CCl_4, Xiao *et al.,* 2010a, Montzka and Reimann, 2011) were not estimated with this method.

4.3.1.1 Two-Dimensional Modeling of CFC and CH_3CCl_3 Mole Fractions

To simulate mole fractions at AGAGE and NOAA sampling sites, Rigby *et al.* (2013) used a 2-dimensional model of atmospheric transport and chemistry based on that of Cunnold *et al.* (1983, 1994). The model parameterizes the transport of trace gases between "boxes" with latitudinal boundaries at 30^oN, 0^oN and 30^oS and vertical boundaries at 200hPa and 500hPa. Initial estimates for the model transport parameters were taken from Cunnold *et al.* (1983, 1994) and the eddy diffusion parameters were subsequently adjusted in the inversion. Reaction rates of the gases with the tropospheric hydroxyl radical were taken from Chapter 3 recommendations. Stratospheric destruction was parameterized by loss frequencies in each of the four stratospheric boxes.

Emissions into the model were based on the methodology of McCulloch *et al.* (2001, 2003), who used surveys such as AFEAS, along with estimates of the consumption in all countries reported to the United Nations Environment Programme (UNEP) and assumptions about releases from banks to estimate global emissions. The estimates were compiled in 2006, and include projections to 2100, based on agreed phase-out schedules. These emissions were not adjusted in the Rigby *et al.* (2013) inversions. However, estimates of the influence of errors in the emissions on lifetimes were included in the derived uncertainty estimates.

4.3.1.2 Inverse Method

Rigby *et al.* (2013) used an inverse approach to estimate stratospheric loss frequencies for CFC-11, -12, and -113 at the same time as model transport parameters, OH concentrations and initial conditions. A non-linear (quasi-Newton) Bayesian inversion framework was used in which prior estimates of this set of parameters were provided, with estimates of their uncertainty. These parameters were subsequently adjusted in the inversion to bring the model prediction of the atmospheric mole fractions into better agreement with the observations, taking into account measurement and model uncertainties.

Initial estimates of the stratospheric loss frequencies of CFC-11, -12, and -113 were adjusted so that stratospheric lifetimes matched current World Meteorological Organization (WMO) recommendations (45, 100, and 85 years, respectively). The uncertainty in these stratospheric lifetimes was estimated from the range in overall lifetimes from previous photochemical model inter-comparison studies (Park *et al.,* 1999). The *a priori* global lifetime of CH_3CCl_3 was determined by the *a priori* global OH concentration (Spivakovsky *et al.*, 2000), assumptions about oceanic uptake (Butler *et al.*, 1991), and the assumed CH_3CCl_3 stratospheric loss frequencies (Naik *et al.*, 2000).

4.3.1.3 Lifetime Estimates and Optimized Mole Fractions

Two sets of inversions were performed, one using AGAGE data and another using NOAA data. Optimized mole fractions for the AGAGE inversion at the four surface boxes are shown in Figure 4.1. Optimized steady-state lifetimes are given in Table 4.2. Rigby *et al.* (2013) note that the influence of errors in estimated emissions is very large during the 1980s and 1990s, when emissions were high. Therefore, to minimize the influence of un-accounted emissions, the lifetimes presented below are the average taken from the time of peak burden onwards for each gas, until the end of 2011.

Rigby *et al.* (2013) estimate a steady-state lifetime for CFC-11 of 54 (42-73) years when AGAGE data were used and 52 (38-70) years when NOAA data were used (2-σ uncertainties). These estimates are somewhat longer than, but not significantly different from, the 45-year lifetime recommended in recent WMO reports (Prinn *et al.,* 1999). The uncertainties in these estimates include the influence of errors in the observations and *a priori* parameters, as well as an estimate of the influence of potentially biased emissions and calibration scales on the derived lifetimes (Rigby *et al.*, 2013).

Similarly to CFC-11, the Rigby *et al.* (2013) estimates of the lifetime of CFC-113 (109 (89-133) and 109 (86-140) years for AGAGE and NOAA, respectively) are longer than the values given in WMO Ozone Assessment Reports going back to the 1990s (85 years). However, they are in agreement with Volk *et al.* (1997), who estimated a lifetime of 112 ± 31 years (based on a lifetime for CFC-11 of 50 years) using observations of CFCs in the stratosphere. The steady-state lifetime of CFC-12 (111 (80-154) and 112 (78-160) years for AGAGE and NOAA, respectively) and CH_3CCl_3 (5.04 (4.78-5.33) years and 5.04 (4.71-5.42)) are consistent with recommended values in recent WMO assessments and other recently published estimates (e.g., Volk *et al.*, 1997, Prinn *et al.*, 2005).

The inversion method was also evaluated against output from the Whole Atmosphere Community Climate Model (WACCM) model (See Chapter 5). In this flux-based model calculation, mole fractions of several halocarbons at the AGAGE stations were used as the input to the inversion model together with the emissions used in the model. The resulting lifetimes calculated for CFC-11 were in very good agreement to the WACCM calculated lifetime, and lifetimes derived for CFC-12 and CH_3CCl_3 with the inversion were in good agreement (differences below 10%) with the model-derived values.

Table 4.2. *A priori* and optimized lifetimes (years) deduced using AGAGE and NOAA measurements. Figures in brackets indicate the 2-σ uncertainty ranges**.**

Species	**Lifetime (years)**		
	A priori	**AGAGE**	**NOAA**
CFC-11	45 (29-75) [1]	54 (42-73)	52 (38-70)
CFC-12	100 (71-170) [1]	111 (80-154)	112 (78-160)
CFC-113	85 (58-140) [1]	109 (89-133)	109 (86-140)
CH_3CCl_3	5.0 (2.8-10.5) [2]	5.04 (4.78-5.33)	5.04 (4.71-5.42)
CH_3CCl_3 with respect to OH loss	6.14 (4.0-11.6)	6.13 (5.24-7.39)	6.12 (5.23-7.37)

[1] Target global lifetime (WMO 2010 recommendation (Montzka and Reimann., 2011)) obtained by tuning initial stratospheric lifetime in the 12-box model. Uncertainty ranges are estimated based on Park *et al.*, 1999.

[2] 12-box model-calculated lifetimes based on OH concentrations from Spivakovsky *et al.* (2000), OH reaction rates recommended in Chapter 3 and stratospheric lifetimes from Naik *et al.,* 2000. Uncertainty range based on 100% uncertainty in OH concentration in each model semi-hemisphere.

4.3.1.4 Lifetimes of Gases Primarily Destroyed by Tropospheric OH

Using the tropospheric OH fields and transport parameters derived above, the 12-box model was used to simulate atmospheric concentrations of long-lived radiatively important trace gases that are primarily destroyed by tropospheric OH: CH_4, and the major HCFCs and HFCs. Simulations were performed from the time of peak CH_3CCl_3 burden to the end of 2011, and the mean steady-state lifetime of each gas during this period was estimated. Reaction rates with OH were taken from Chapter 3, and stratospheric lifetimes were taken from the 2-D model simulations in Chapter 3. Uncertainties in the derived lifetimes were due to the uncertainties in the tropospheric OH field, reaction rates and stratospheric lifetimes. The uncertainty in the derived OH field includes the measurement and modeling uncertainty propagated through the inversion and the uncertainty due to the prescribed CH_3CCl_3 stratospheric loss and oceanic uptake lifetimes and the CH_3CCl_3-OH reaction rate. This leads to an overall error in our OH estimates of approximately 13.8% (1 σ). The influence of uncertainties in OH, reaction rates, and stratospheric loss rates on the lifetimes of the related species was made by independently perturbing each term in the model, and tracking the resulting change in steady-state lifetime. Table 4.3 summarizes these calculations.

4.3.2 Other Models – Halons

While, in general, model-derived values of atmospheric lifetimes will be discussed in Chapter 5 of this report, there is one study which discusses the stratospheric lifetimes of Halons and in particular gives some insight into the stratospheric lifetimes of Halon-2402 and Halon-1202 (Newland *et al.*, 2012) which is closely linked to atmospheric observations. In this study a 2-D model approach using measured trends from the Cape Grim archive has also been applied to estimate the emissions and lifetimes of the four Halon species: Halon-1211, Halon-1301, Halon-2402, and Halon-1202 (Newland *et al.,* 2012). For the tropospheric lifetimes, the model was run to steady state with OH loss and photolysis active only in the troposphere, and the global burden of each trace gas was divided by the estimated global emission. Stratospheric lifetimes in Newland *et al.* (2012) were taken from Laube *et al.* (2013) for Halon-1211 and Halon-1301, and model parameters evaluated against available balloonborne

measurements of Halons in the stratosphere for Halons-2402 and -1202. The partial steady-state lifetimes for stratospheric loss derived in this way are 31 (27-37) years and 21 (18-26) years for Halons-2402 and -1202, respectively (see also Table 4.10).

Table 4.3. Lifetimes of CH_4 and the major HCFCs and HFCs based on the OH concentration derived in the 12-box model inversion, modeled stratospheric lifetimes and reaction rates from Chapter 3. The table shows both the global lifetime and lifetime with respect to tropospheric OH loss. 2-σ uncertainties are shown in parentheses.

Gas	Tropospheric OH lifetime (years)	Global lifetime (years)
CH_4	10.5 (8-15.1)	9.8 (7.6-13.8)
HCFC-22	13.2 (9.9-20.1)	12.4 (9.3-18.5)
HCFC-141b	10.7 (8-16.1)	9.4 (7.2-13.6)
HCFC-142b	19.4 (13.8-33.1)	17.7 (12.7-29.2)
HFC-23	244 (169-438)	228 (160-393)
HFC-32	5.65 (4.2-8.61)	5.4 (4-8.1)
HFC-125	32.5 (23.6-52.3)	30.5 (22.2-48.9)
HFC-134a	14.3 (10.4-23)	13.5 (9.9-21.2)
HFC-143a	57.2 (41.3-92.9)	51.4 (37.7-80.4)
HFC-152a	1.65 (1.26-2.39)	1.6 (1.2-2.2)
HFC-227ea	38.3 (26.7-67.6)	35.8 (25.4-60.7)
HFC-245fa	8.41 (5.8-15.31)	7.9 (5.5-13.8)

4.3.3 Global Box Models

Simple global box modeling has been used to examine the lifetimes of methyl bromide (Hu *et al.,* 2012; Yvon-Lewis and Butler, 2002; Yokouchi *et al.,* 2000; Yvon-Lewis and Butler, 1997; Yvon and Butler, 1996; Butler, 1994), methyl chloride (Hu *et al.,* 2013; Xiao *et al.,* 2010b; Yvon-Lewis and Butler, 2002) and carbon tetrachloride (Yvon-Lewis and Butler, 2002) (Table 4.4).

The global pseudo first order loss rate constants (k_{ocn}, k_{soil}, k_{OH}) are determined instantaneously for each month given the geographic distribution of degradation rate constants for that month. The degradation rate constants are not geographically constant and vary monthly. For the ocean, a 1° x1° grid of the ocean is used where the temperature and salinity determine the chemical loss rate constant, wind speeds determine gas exchange coefficients, and biological degradation rate constants based on the field measurements of biological degradation are applied (Butler, 1994; Yvon and Butler, 1996; Yvon-Lewis and

Butler, 1997; Yvon-Lewis and Butler, 2002; Yvon-Lewis *et al.*, 2009; Hu *et al.*, 2012, 2013). Especially for the soil and oceanic uptakes, the uncertainties due to the extrapolation of spot measurements to global uptake rates and in the case of the oceanic uptake the calculation of the air-sea-exchange coefficients are significant sources of uncertainties. The Henry's law coefficients that describe the equilibrium between concentrations in the liquid phase and the gas phase are smaller sources of uncertainties. Loss due to reaction with OH has a pseudo first order rate constant defined as k[OH] which varies by latitude and month (Atkinson *et al.*, 2006; Spivakovsky, 2000). The total loss rate is then averaged globally for the final lifetime calculation (Yvon-Lewis and Butler, 2002; Yvon-Lewis *et al.*, 2009; Hu *et al.*, 2012, 2013). For CH_3Br and CH_3Cl, a 1° x1° grid of soil biomes is used, and a degradation rate constant for that biome is applied according to time of year which indicates if the biome is considered frozen, snow covered or exposed (Yvon-Lewis and Butler, 2002; Yvon-Lewis *et al.*, 2009; Hu *et al.*, 2012, 2013). For CCl_4, the soil uptake rate constant is from other published soil uptake rates and the atmospheric burdens used with those rates (Montzka and Reimann, 2011 and references therein). All of these distributions vary monthly, and we can determine the global loss rate constant for each month. The loss rate constants are averaged over the year grid cell by cell, and then determine a global annual loss rate constant (Yvon-Lewis and Butler, 2002; Yvon-Lewis *et al.*, 2009; Hu *et al.*, 2012, 2013). As no assumptions about an equilibrium between sinks and sources are made in these calculations, the results are transient lifetimes, but they are expected to be very good proxies for the steady-state lifetimes.

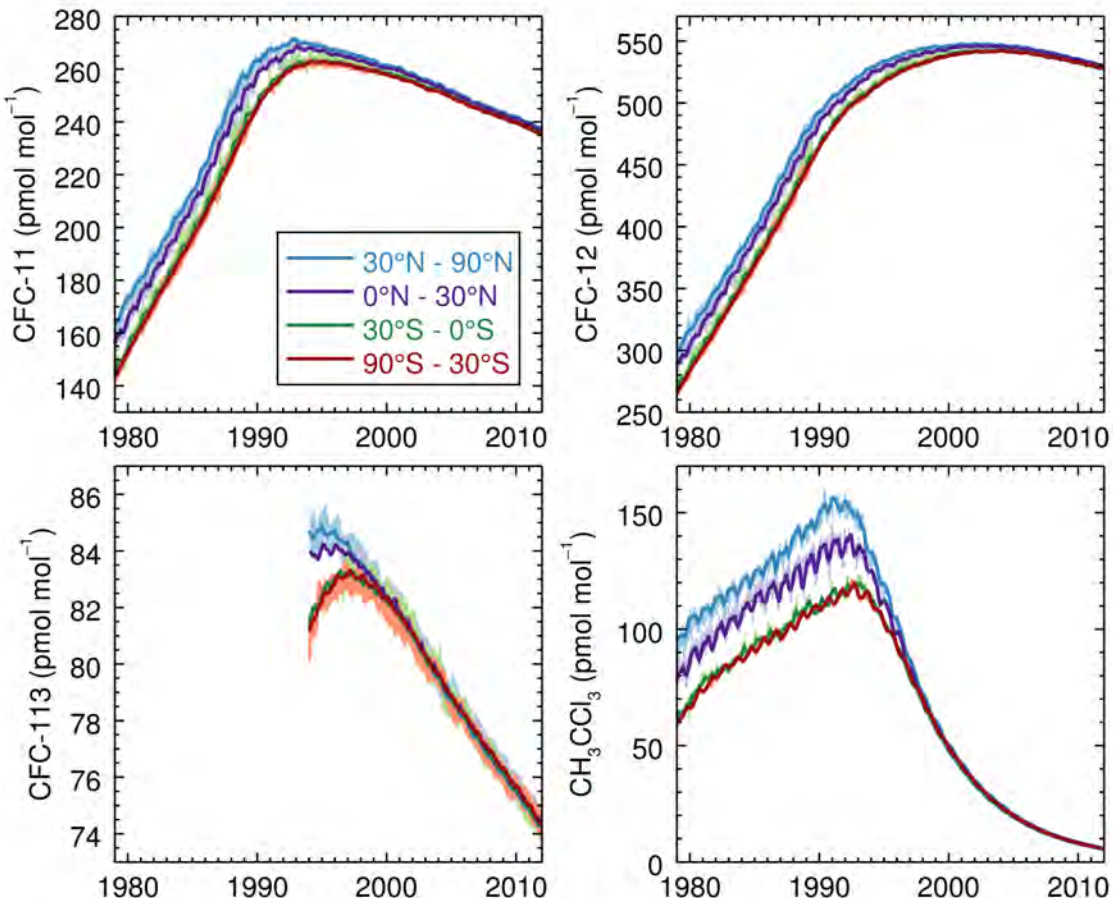

Figure 4.1. AGAGE measurements (shading), and optimized modeled mole fractions (solid lines) in the four surface semi-hemispheres for CFC-11, CFC-12, CFC-113 and CH_3CCl_3.

4.3.3.1 Methyl Bromide and Methyl Chloride

Atmospheric CH_3Cl and CH_3Br have many natural sources and sinks in common. Their common identified natural sources include the ocean, biomass burning, fungi, salt marshes, wetlands, rice paddies, mangroves and tropical rainforests (Hu *et al.,* 2010; Blei *et al.,* 2010; Yvon-Lewis *et al.,* 2009; Mead *et al.,* 2008a, b, Manley *et al.,* 2007; WMO, 2007, 2011; Lee-Taylor and Redeker, 2005; Dimmer *et al.,* 2001; Lee-Taylor and Holland, 2000; Rhew *et al.,* 2000; 2001; Rhew, 2011; Lobert *et al.,* 1999; Varner *et al.,* 1999; Watling and Harper, 1998; Moore *et al.,* 1996). Methyl bromide has the added anthropogenic source from fumigation uses (agricultural, structural and quarantine and pre-shipment (QPS)) (WMO, 2011). While the non-QPS anthropogenic emissions have been phased out as a result of the Montreal Protocol and its amendments, the QPS anthropogenic sources remain for CH_3Br.

Table 4.4. Published lifetimes of CH_3Br, CH_3Cl and CCl_4 from simple global box models. Numbers in parentheses are ranges reported in those studies.

Study	Lifetime (years)	Type of Model
Methyl Bromide		
Butler (1994)	1.2 (0.7-1.8)	Global box model
Yvon and Butler (1996)	0.8 (0.6-1.4)	Global box model
Yvon-Lewis and Butler (1997)	0.7 (0.6-0.9)	Global box model
Yokouchi *et al.* (2000)	1.0 (0.7-1.2)	Global box model
Hu *et al.* (2012)	0.8 (0.6-1.1)	Global box model
WMO (2011)	0.8	
Methyl Chloride		
Yvon-Lewis and Butler (2002)	1.3	Global box model
Xiao *et al.* (2010b)	1.0	(Inversion / Forward model)
Hu *et al.* (2013)	0.9 (0.7-1.1)	Global box model
WMO (2011)	1.0	
Carbon Tetrachloride		
WMO (1999)	35	
Yvon-Lewis and Butler (2002)	26	Global box model
WMO (2011)	20-30	(Adjustments to soil sinks and stratospheric lifetime)
WMO (2011)	26	
This Assessment	24 (19-40)	Global box model

Their shared identified sinks include degradation in the ocean, reaction with hydroxyl radicals (OH), photolysis in the stratosphere and uptake by soils (Butler, 1994; Yvon and Butler, 1996; Yvon-Lewis and Butler, 2002; WMO, 2003, 2007, 2011; Shorter *et al.,* 1995; Keene *et al.,* 1999; Keppler *et al.,* 2005). The total strength of known sinks outweighs the total strength of known sources by ~732 Gg yr^{-1} for CH_3Cl (Hu *et al.,* 2013) and ~35 Gg yr^{-1} for CH_3Br (WMO, 2011; Yvon-Lewis *et al.,* 2009). Forward models have been used to assess the strengths of these missing sources based on known sources and sinks (lifetimes).

Estimates of the budget and lifetime of CH_3Br have evolved over the years. In the early 1990s, when the oceans were first acknowledged as a sink for CH_3Br, Butler (1994) included oceanic uptake as an independent sink for CH_3Br in a box model reducing its estimated lifetime from 1.8 (Mellouki *et al.,* 1992) to 1.2 (0.7-1.8) years. Refinement of the oceanic sink and inclusion of a soil sink (Shorter *et al.,* 1995), further reduced the estimated lifetime to 0.8 (0.6-1.4) years (Yvon and Butler, 1996). In a subsequent update to this box model

approach, biological degradation in the oceans (King and Saltzman, 1997) was included reducing the estimated lifetime further to about 0.7 (0.6-0.9) years.

Hu *et al.* (2012) revised the box model of Yvon-Lewis and Butler (2002) to include separate coastal and open ocean regions, a finer resolution ocean, revised flux parameterization and additional degradation rate constant measurements. This increased the estimate of the partial atmospheric lifetime with respect to oceanic loss from 1.8 (Yvon-Lewis and Butler, 1997) to 3.1 (2.3-5) years but did not change the overall atmospheric lifetime estimate, 0.8 (0.7-0.9) years.

While CH_3Cl is known to share some of the same sources and sinks as CH_3Br and supplies the most natural chlorine to the stratosphere, the box and forward modeling studies of it are fewer (Table 4.4). The lifetime as determined using the box model of Yvon-Lewis and Butler (2002) was 1.3 years. The combined inversion and forward modeling of Xiao *et al.* (2010b) produced a lifetime estimate of 1.0 years which is in agreement with the recommendations given in WMO (2011) and WMO (2007). Hu *et al.* (2013) revised the box model of Yvon-Lewis and Butler (2002) to include separate coastal and open ocean regions, a finer resolution ocean, revised flux parameterization and revised solubility to improve the estimate of the partial atmospheric lifetime with respect to oceanic loss which reduced the atmospheric lifetime estimate to 1.2 years.

While there have been some variations in the predicted lifetimes of CH_3Cl and CH_3Br, the best estimates are 1.2 (0.7-1.3, 2 σ) years for CH_3Cl and 0.8 (0.6-1.1, 2 σ) years for CH_3Br.

4.3.3.2 Carbon Tetrachloride

The global box models applied here do not require source information, only sinks, to estimate atmospheric lifetimes and partial atmospheric lifetimes. The sinks for CCl_4 include loss in the stratosphere, degradation in the oceans (Butler *et al.*, 2011; Yvon-Lewis and Butler, 2002; Lee *et al.*, 1999; Krysell *et al.*, 1994) and degradation in soils (Rhew *et al.*, 2008; Liu, 2006; Happell and Roche, 2003). In Montzka and Reimann (2011), the partial atmospheric lifetime with respect to stratospheric loss "was taken to be 35 yr based on previous modeling and observational work". This stratospheric lifetime was quoted relative to a CFC-11 stratospheric lifetime of 45 years (see discussion in section 4.4.). A best estimate of the stratospheric loss lifetime for CCl_4 including the results of Laube *et al.* (2013) and Volk *et al.* (1997) is 42 years (this chapter, Section 4.4.4). Happell and Roche (2003) estimated a partial atmospheric lifetime with respect to a soil sink of 90 (50-418, 1 σ) years. As discussed in Montzka and Reimann (2011), the results of Rhew *et al.* (2008) and Liu (2006) indicate that the rate constants for the uptake by some biomes included in the Happell and Roche (2003) calculation were too large by a factor of 2. The revised soil sink partial lifetime is approximately 195 (108-907, 1 σ) years (Montzka and Reimann, 2011). The oceanic loss rate constant used in the model to determine the partial atmospheric lifetime with respect to oceanic loss is estimated based on observations of oceanic surface water undersaturations. The partial lifetime with respect to oceanic uptake was determined to be 94 (82-191, 1 σ) years (Yvon-Lewis and Butler, 2002) based on the cruise data available at the time. Using additional cruise data, Butler *et al.* (2011) revised the partial lifetime with respect to oceanic loss to 81 (71-167, 1 σ) years. Using this revised oceanic uptake along with the new best estimate for stratospheric loss of 42 years (31-59 years, 2 σ; cf. Section 4.4.4) and the soil sink of 195 years results in an estimated transient lifetime of 24 (18-40, 2 σ) years. This estimate is slightly smaller than previous estimates discussed in Montzka and Reimann

(2011) of 26 (23-33 years, 1 σ). As discussed in Montzka and Reimann (2011), a faster decline in atmospheric mixing ratios than shown in observations would be expected based on this lifetime and the estimated bottom-up emission. This discrepancy cannot be resolved by this new estimate of atmospheric lifetime of CCl_4.

4.3.4 Global Satellite Measurements and Modeled Loss Rates

The study of N_2O by Johnston *et al.* (1979) was one of the first to use global measurements in combination with modeled photolytic loss rates to examine the distribution of stratospheric loss for a long-lived gas, and to assess its transient lifetime. This work employed a global N_2O climatology built on a number of aircraft, balloon, and rocket measurements of stratospheric vertical profiles that spanned a range of latitudes. One aspect of this approach, in comparison with lifetimes based on 2- or 3-D model simulations, is that the trace-gas distribution was specified. This eliminated the need for a detailed analysis of winds, mixing, and dynamical parameterizations, and the calculated loss does not involve uncertainties associated with trace-gas transport

Later studies by Crutzen and Schmailzl (1983); Ko *et al.* (1991); and Minschwaner *et al.* (1993) incorporated the use of global N_2O data from the stratospheric and mesospheric sounder (SAMS) instrument on the Nimbus 7 satellite. The availability of higher precision global data and a wider array of species from the UARS mission led to revised estimates of stratospheric loss of both N_2O and CFC-12 (Minschwaner *et al.,* 1998), and estimated global steady-state lifetimes of 117 ± 26 (1 σ) years (N_2O) and 103 ± 25 (1-σ) years (CFC-12). In this section, new results are presented using this technique (Minschwaner *et al.,* 2013) with global CFC-11 and CFC-12 distributions determined from MIPAS, ACE, CRISTA-1 and CRISTA-2, and CLAES satellite measurements discussed in Section 4.2.2.2.

The transient lifetime for CFC-11 was calculated from its global atmospheric burden, *B*, divided by its global loss rate, *L*

$$T(t) = \frac{B(t)}{L(t)} \tag{4.1}$$

where both *B* and *L* are determined from the local concentrations $n(\phi,z,t)$, photolysis rates $J(\phi,z,t)$, and reaction rates with excited state atomic oxygen $k_1[O(^1D)]$

$$B(t) = 2\pi\, R_E^2 \int dz \int n(\varphi, z, t) \cos\varphi \, d\varphi \tag{4.2}$$

$$L(t) = 2\pi\, R_E^2 \int dz \int n(\varphi, z, t) \left\{ \mathrm{J}(\varphi, z, t) + k_1[\mathrm{O}(^1\mathrm{D})(\varphi, z, t)] \right\} \cos\varphi \, d\varphi \tag{4.3}$$

The above integrals are over altitude z and latitude ϕ (assuming zonal symmetry in the distribution and loss), and R_E is the Earth's radius.

As discussed above, the latitude and altitude distributions of CFC-11 and CFC-12 in Equations (4.2) and (4.3) are constrained from measurements. Results here involve global satellite observations from the following instruments: CFC-12 from CLAES between March 1992 and January 1993 (Nightingale *et al.,* 1996), CFC-11 from CRISTA-1 in November 1994 (Riese *et al.,* 1999) and from CRISTA-2 in August 1997 (Kuell *et al.,* 2005), CFC-11

from MIPAS between July 2002 and March 2004, CFC-12 from MIPAS between December 2002 and February 2003 (Hoffmann *et al.,* 2005, 2008), and both CFC molecules from ACE over the period 2006-2010 (Bernath *et al.,* 2005; Brown *et al.,* 2011). As shown below, the critical region where maximum calculated loss occurs for both CFCs is between 20 and 35 km altitude at low (+-30^o) latitudes (Figure 4.3).

Zonal averages for all three data sets were linearly interpolated onto a 1-km altitude grid from the surface to 50 km, and into latitudinal bins on a 5^o grid from 85°S to 85°N. Mole fractions above the top of vertical profiles were extrapolated to zero using cubic splines with matching gradients to the data at the uppermost valid measurement. Uncertainties in this extrapolation contribute to the overall uncertainty in lifetimes discussed below, although the magnitude of this error is small (<5%) in comparison with other uncertainties. At the bottom of vertical profiles, mole fractions extending down to 10 km altitude were linearly extrapolated where necessary up to the global/annual mean, tropospheric mole fraction at the time of each measurement (WMO, 2011). Mole fractions from 10 km to the surface were held constant at the 10-km value.

For CLAES CFC-12 and MIPAS CFC-11, mean seasonal distributions were constructed based on climatologies for four seasons: December-February, March-May, June-August, and September-November. The MIPAS CFC distributions incorporated adjustments to the altitude scale given in Hoffmann *et al.* (2008) by calculating geopotential heights using the native pressure grid from the MIPAS retrievals along with the temperature climatology discussed below. Corrections to the published altitudes were less than +0.5 km below 18 km, and between -0.2 and -1.8 km at higher altitudes. Global fields for ACE CFCs were constructed using one year of data in order to produce annual means with sufficient low latitude coverage. The MIPAS CFC-12 distribution is a mean over the months of December-February. For CRISTA-1 and 2 CFC-11, the data were assumed to represent means over +-70^o latitude for the months of November and August, respectively.

Figure 4.2 shows the MIPAS CFC-11 mean distribution for 2002-2004 along with the ACE annual mean 2008 climatology. Tropospheric levels of CFC-11 declined over the time between measurements by about 4%, which produces differences too small to be discerned in this figure and no corrections have been applied to account for such changes in the figure. The general stratospheric mole fraction patterns are similar for both distributions. The largest fractional differences between MIPAS and ACE occur at high latitudes below about 25 km altitude, although due to the pattern of loss presented below, such differences are not important for the CFC-11 lifetime. Above 20 km, MIPAS mole fractions are larger than ACE by 10-20% at all latitudes, and this difference is particularly conspicuous at low latitudes. Although smaller mole fractions in this region make it difficult to clearly see these differences in Figure 4.2, they do have a significant impact on the calculated lifetimes.

Photolysis frequencies (J-values) for CFC-11 and CFC-12 were calculated for each season, latitude, and altitude using the ultraviolet radiative transfer code described by Minschwaner *et al.* (1993). CFC absorption cross sections and the rate constants, k_1, for reactions with $O(^1D)$ were taken from the recommendations of Chapter 3 in this assessment. Effects of Lyman alpha photolysis near 121 nm were not considered due to its negligible contribution to overall photodissociation of CFC-11 and CFC-12 (discussed in Chapter 3). The distributions of $O(^1D)$ were modeled using steady-state photochemistry and calculated ozone photolysis frequencies. Climatologies of ozone (for UV opacity and for $O(^1D)$) and temperature (for incorporating temperature dependencies of reaction rates and cross sections) were adopted

from the UARS zonal means developed by Minschwaner *et al.* (1998). Comparisons between this ozone climatology and others derived from UARS instruments (Wang *et al.,* 1999; Grooß and Russell 2005) indicated a small bias of +3% in the low-latitude stratosphere in the Minschwaner *et al.* (1998) climatology, and ozone concentrations were decreased uniformly by 3% for these calculations. Solar irradiances in the wavelength range from 115 to 420 nm were specified from measurements during March 2004 from the Solar Radiation and Climate Experiment (SORCE) (Rottman *et al.,* 2006). For more details of the cross sections and photolysis calculations, see Minschwaner *et al.* (2013).

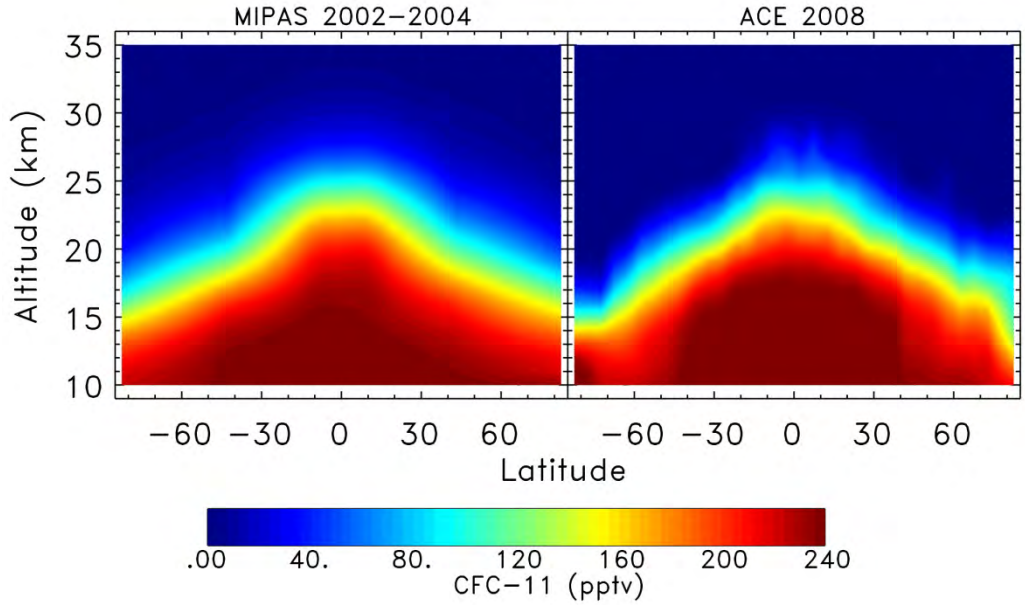

Figure 4.2. Zonal mean distributions of CFC-11 from MIPAS averaged over 2002-2004 (left), and from ACE for the 2008 mean (right).

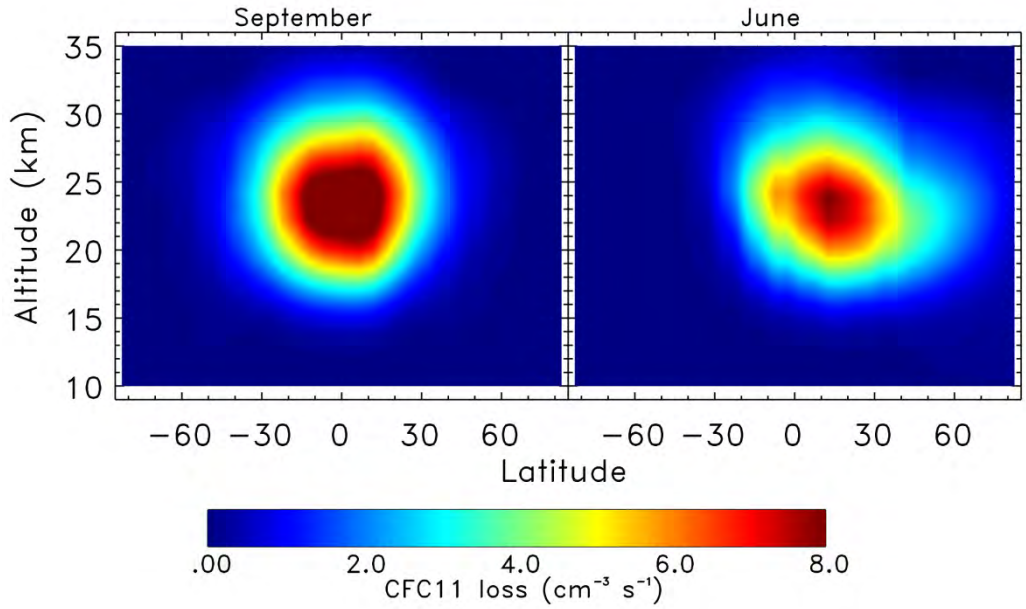

Figure 4.3. Loss rate for CFC-11 based on MIPAS distributions for September (left) and for June (right), in units of molecules cm^{-3} s^{-1}.

Calculated rates for stratospheric loss using MIPAS data are shown in Figure 4.3. Consistent with previous observationally based studies (Minschwaner *et al.,* 1993) and model results (Douglass *et al.,* 2008), CFC-11 loss is largest in the low latitude stratosphere between 20 and 28 km altitude. Globally integrated rates were found to be dependent on season; average removal rates are 12% larger during the equinoxes as compared to the solstices. These higher rates are primarily related to smaller solar zenith angles at low latitudes during equinox, with associated increases in actinic fluxes in the low latitude stratosphere where CFC-11 mole fractions are largest due to upwelling in the Brewer-Dobson circulation. An additional influence results from seasonal variations in ozone, with mole fractions slightly smaller in March than in June, which leads to greater penetration of solar radiation in March. Finally, there are seasonal changes in the MIPAS CFC-11 mole fractions that have about a 4% effect, although these act to oppose the impact of changes in actinic flux. For a fixed CFC-11 distribution, seasonal actinic flux and ozone changes produce larger variations of up to 16% in global loss rates.

The distribution of CFC-12 loss (not shown) also shows largest rates in the tropical stratosphere, but CFC-12 destruction is shifted upward about 6 km relative to CFC-11. Also, CFC-12 loss rates are 30-40% smaller than for CFC-11, which along with a larger global burden, translates to a longer lifetime for CFC-12 compared with CFC-11.

For both CFCs, the reaction $O(^1D)$ accounts for 4-8% of the total loss in the tropical stratosphere between 20 and 35 km. This reaction does become important to the destruction rate below 12 km and in the lower stratosphere at high latitudes, but these regions have a negligible impact on the global loss. Thus, the global sink for both CFCs is governed primarily by direct photodissociation.

Table 4.5 lists the sources of CFC-11 data and observation time periods used in this analysis, the global mean loss rates and burdens, and the transient and steady-state lifetimes derived from the measurements. All loss rates and burdens are based on calculated means over four seasonal values, with both CRISTA CFC-11 distributions held fixed and ACE values based on 4-year averages of the computed annual means. Table 4.5 also provides uncertainties in steady-state lifetimes based on an analysis of multiple sources of error and standard error propagation methods (Minschwaner *et al.,* 2013) applied to estimated 2σ uncertainties. The average fractional error in lifetime from a single dataset is about 55%. Uncertainties associated with CFC climatologies (33-41%) and with oxygen opacity between 185 and 220 nm (34% on photolysis loss) account for most of the uncertainty in lifetimes. Other primary sources of uncertainty are due to ozone opacity (16%) and CFC absorption cross sections (28% for CFC-11 and 14% for CFC-12 at the relevant stratospheric temperatures).

The steady-state lifetime of a long-lived gas, where emissions to the atmosphere exactly balance photochemical loss, will be different from its instantaneous lifetime if the mean tropospheric concentration is changing with time (which implies an imbalance between sources and sinks). This difference is due to the finite time lag between temporal changes in abundances for the stratosphere relative to the troposphere. For CFC-11, decreases in global mean tropospheric abundances during 1997-2010 were between -0.8%/yr and 1%/yr, indicating a larger stratospheric loss relative to tropospheric emissions. Assuming a mean time lag of 2 years for air to ascend through the tropical tropopause to 30 km altitude (Schoeberl *et al.,* 2008), steady-state lifetimes are 1.6% to 2% longer than transient lifetimes for the CRISTA-2, MIPAS, and ACE distributions. For CRISTA-1, 1994 marks the

approximate peak in tropospheric mole fraction and therefore the steady-state lifetime is nearly identical to the computed transient lifetime.

Table 4.5. Summary of CFC-11 lifetimes from satellite observations. While CRISTA-1 and CRISTA-2 are listed separately, they have been combined to one value for the calculation of the mean. All uncertainties given in this table represent 2σ ranges.

Instrument	Observation Period Used	Mean Global Burden (10^{34} molecules)	Mean Loss Rate (10^{25} molecules s^{-1})	Transient Lifetime (yr)	Steady-State Lifetime (yr)
CRISTA-1	Nov 1994	2.71	1.63	52.7	52.9 (33-140)
CRISTA-2	Aug 1997	2.64	1.39	60.0	60.7 (37-161)
MIPAS	2002-2004	2.50	2.24	35.4	36.1 (23-84)
ACE	2006-2010	2.38	1.67	45.2	46.1 (29-121)
Best Estimate					44.7 (30-91)

The multi-instrument mean CFC-11 steady-state lifetime is 44.7 (30-91) yr. The mean value is determined by an equal-weighted mean of the inverse lifetimes (as these, contrary to the lifetimes, exhibit symmetric uncertainties) based on CRISTA, MIPAS, and ACE datasets. Since the CRISTA-1 and CRISTA-2 data are from the same instrument with only minor differences in calibration and processing, the CRISTA results are not completely independent and are averaged first, before computing the multi-instrument mean that includes MIPAS and ACE results. Given the large number of tropical profiles from each dataset, differences in statistical errors between the three datasets are negligible. However, data that cover less than one month (CRISTA-1 and CRISTA-2) may be biased by seasonal changes in tropical CFC-11 profiles, which is estimated from MIPAS data to impact the derived lifetime by about 4%. A weighted mean lifetime that accounts for effects of this magnitude in the CRISTA datasets is shorter than the arithmetic mean by only 0.3 yr, thus an equal weighting is applied to the three datasets in computing the multi-instrument mean.

The large spread in CFC-11 lifetime derived from the four measurements (24.6 yr from minimum to maximum) results primarily from differences in low latitude mole fractions between 20 and 28 km altitude. This range in lifetime is also consistent with the estimated uncertainties due to stratospheric concentrations (33-41%). For the purposes of comparison, mean tropical profiles can be scaled to match tropospheric mole fractions for 1994, near the peak period of CFC-11 loading. Resulting differences between data sets are fairly large at 25 km, with the smallest mole fraction of 56 pmol mol^{-1} from CRISTA-2 and the largest of 100 pmol $mol^{-1}$from MIPAS. This broad range is reflected in the derived CFC-11 steady-state lifetimes, from 60.7 yr for the CRISTA-2 climatology, to 36.1 yr for the MIPAS climatology.

Table 4.6 lists the CFC-12 loss rates, burdens, and lifetimes derived from the three sets of measurements. CFC-12 abundances in the troposphere peaked around 2002-2003, and growth rates of +2.5%/yr for CLAES, zero for MIPAS, and -0.5%/yr for ACE have been adopted. Coupled with a mean age at 30-35 km in the tropics of 2.5 years, these growth rates were used to derive the steady-state lifetimes shown in Table 4.6. As indicated in the table, the variation between data sets for the CFC-12 steady-state lifetime is much smaller than for CFC-11, with a max-min spread of only 3.5 yr. This level of agreement may be fortuitous

given the 2-σ uncertainties of 32-51% due to stratospheric profile error sources. It should be noted that the reanalysis of CLAES CFC-12 data presented here includes revisions to the absorption cross section and ozone opacity in comparison to Minschwaner *et al.* (1998), leading to a small difference of about 3 yr in the derived lifetime. The multi-instrument mean CFC-12 steady-state lifetime (determined again as equal-weighted mean of the inverse lifetimes) is 106.6 (79-166) yr.

Table 4.6. Summary of CFC-12 lifetimes from satellite observations.

Instrument	Observation Period Used	Mean Global Burden (10^{34} molecules)	Mean Loss Rate (10^{25} molecules s^{-1})	Transient Lifetime (yr)	Steady-State Lifetime (yr)
CLAES	1992-1993	5.00	1.40	113.3	108.0 (76-185)
MIPAS	2002-2003	5.50	1.62	107.5	107.5 (69-250)
ACE	2006-2010	5.31	1.63	103.3	104.5 (71-201)
Best Estimate					106.6 (79-166)

Mean, steady-state lifetimes derived here 44.7 (30-91) yr for CFC-11 and 106.6 (79-166) yr for CFC-12) are in excellent agreement with the most recent WMO Ozone Assessment recommendations (45 yr for CFC-11 and 100 yr for CFC-12) (WMO, 2011). They deviate from the latter by only 1% and 7% for CFC-11 and CFC-12, respectively, i.e., much less than their uncertainties. The primary differences between CFC-11 and CFC-12 lifetimes in this analysis arise from differences in the absorption cross sections, which impact photolysis rates in Equation (4.3), and from differences in stratospheric vertical profiles, mainly within the tropical stratosphere below 35 km altitude. A major difficulty in calculating CFC-11 destruction relates to the very large vertical gradient in mole fraction. This large gradient complicates space-based observations that may have extended vertical fields of view, averaging kernels, or uncertainties in absolute altitude registration, and small errors in any of these quantities are magnified in calculated CFC-11 loss rates.

Loss rate calculations were also conducted using CFC-11 vertical profiles from model simulations of the GEOSCCM (see Chapter 5), using zonal and annual mean model outputs for 1997 and 2007. Table 4.7 compares CFC-11 global mean loss rates, burdens, and lifetimes. Differences between transient lifetimes calculated here and those based on model results range between 3 to 5%, with model lifetimes systematically longer by about 2 to 3 yr. These differences result from offsets in the calculations of global burdens (1-2%), and in global loss (2-3%). For global burdens, differences are likely related to longitudinal variations in tropospheric mole fraction and temperature (density) fields, since model CFC-11 burdens calculated using zonal mean fields produce nearly identical burdens as those for the satellite observation method shown in Table 4.7. However, modeled loss rates are unchanged between the 3-D and zonal mean cases, which suggests that loss rate differences shown in the table are more likely related to systematic differences in tropical ozone climatologies or in the treatment of oxygen opacity. In general, however, the level agreement in CFC-11 lifetimes from both methods is well within the magnitude of uncertainties noted previously in Table 4.5.

Table 4.7. Comparison of CFC-11 lifetime calculations. Sat Obs. Method refers to the calculation methods described in this section.

Method	Observation Period Used	Mean Global Burden (10^{34} molecules)	Mean Loss Rate (10^{25} molecules s^{-1})	Transient Lifetime (yr)
Sat Obs. Method	1997 mean	2.63	1.62	51.6
GEOSCCM	1997 mean	2.61	1.52	54.7
Sat Obs. Method	2007 mean	2.45	1.57	49.4
GEOSCCM	2007 mean	2.43	1.48	52.0

4.4 Lifetimes Derived from Stratospheric Tracer-Tracer Correlations

4.4.1 The Methods and Their Applicability

Tracer-tracer relations and tracer-mean age relations can be used to derive stratospheric lifetimes (which are equivalent to atmospheric lifetimes for 7 out of the 30 species mentioned in Table 4.1), i.e., the CFCs and Halon-1301; for Halon-1202 tropospheric loss is dominant and for Halon-1211 and 2402 tropospheric and stratospheric lifetimes are on the same order of magnitude (see e.g., Newland *et al.*, 2012 and references therein). The applicability of this approach is discussed in Chapter 2 from a theoretical point of view. Due to theoretical considerations, these methods require the tracer-tracer or tracer-mean-age slopes at the extratropical tropopause, best taken during the winter half year that dominates net transport (Plumb, 1996). From a practical point of view, the slope at the end point of the correlation curve can be difficult to measure and may be affected to some extent by variability of upper tropospheric tracer distributions and of cross-tropopause transport. These effects are likely to be small for correlations between two long-lived tracers (relative method), but may become more problematic for the (absolute) age-tracer method proposed by Volk *et al.* (1997), as age-tracers like SF_6 and CO_2 are not sufficiently well mixed in the troposphere. Even without these potential caveats, uncertainties of lifetimes derived from the absolute method are considerably larger than for the relative method (Volk *et al.,* 1997). Therefore, values derived with the absolute method will not be considered in this assessment report. The reader is referred to Chapter 2 for further discussion of the applicability of this method.

The tracer-tracer method (Plumb and Ko, 1992; Plumb, 1996) relates the slope of the relation between two long-lived tracers, χ_1 and χ_2, to the ratio of their respective fluxes through the tropopause (equaling their stratospheric sinks) and thus to the ratio of their stratospheric lifetimes:

$$\frac{\tau_1}{\tau_2} \cong \frac{\mathrm{d}\chi_2 B_1}{\mathrm{d}\chi_1 B_2}$$

where B_1 and B_2 are the global atmospheric burdens of the two tracers. As tracer-tracer relations are generally non-linear in the lower stratosphere, the accurate derivation of the slopes at the extratropical tropopause end-point of the relation presents a major challenge in

applying either method. Using near-global high-resolution aircraft data from the 1994 ASHOE/MAESA campaign, Volk *et al.* (1997) found the following measures to be essential to derive consistent slopes with transparent uncertainty estimates: (i) observations below the tropopause have to be excluded as spatial and temporal tropospheric variations result in tracer relations that are unrelated to τ, and (ii) an error-weighted orthogonal fitting routine has to be used in order to eliminate sensitivity of the slopes to switching X and Y axis. They then measured the slopes locally along the tracer relation (over tracer intervals corresponding to 2 years of age) and extrapolated these local (linear) slope results to the tropopause end point of the relation using a quadratic fit over a tracer interval corresponding to about 3 years of age. This procedure thus relies less on local information at the tropopause itself, where variations driven by tropospheric sources and transport (including seasonal variations) may become significant, but makes use of information across a major part of the lower stratosphere that is responsible for establishing the relation between the tracer fluxes and the tracer slopes; in addition the 3-year age range used for the final extrapolation also effectively averages over seasonal variations in stratospheric transport. Errors propagated through the complete procedure resulted in 1-σ uncertainties of the derived slopes at the tropopause of 5-10% for the tracer-tracer method.

A further obstacle in deducing lifetimes with this method is that most of the species involved have temporal trends in their atmospheric mole fractions. The slope is thus determined by a combination of chemical decay and temporal trends that need to be separated from each other. A method how to take these trends into account has been proposed by Volk *et al.* (1997) and was applied to the ASHOE/MAESA observations. A further method to detrend stratospheric observations, based on the knowledge of the tropospheric trend and the mean age of air has been suggested based on model work (Plumb *et al.,* 1999). One limitation of this latter approach is, however, that it relies on model calculations of the age spectrum and the chemical breakdown of trace gases in the stratosphere. While – in contrast to the method suggested by Volk *et al.* (1997) - this method would allow combining observations from different years, the associated uncertainties are expected to be rather high.

In this section, we will thus focus on investigations using the method suggested by Volk *et al.* (1997) that relies on determining a correction factor for the specific time of the measurements. The theoretical as well as the practical derivation of the correction factor is somewhat complex. In brief it makes use of (i) the observed tracer gradient with respect to age at the tropopause $d\chi/d\Gamma$, (ii) a quadratic fit to the non-linear time series of tropospheric mole fractions of the respective species during a 5-year period prior to the stratospheric observations, and (iii) a model-estimate of the width Δ of the stratospheric age spectrum (Hall and Plumb, 1994) relative to the mean age, i.e., the parameter Δ^2/Γ, which is roughly constant over the lower stratosphere according to three-dimensional (3-D) transport models. The growth correction factors C become particularly large for species that are very long-lived or for species that exhibit strongly non-linear growth, with the largest factors (in 1994) for CFC-113 (C=0.65+/-0.12) and CFC-12 (C=0.77+/-0.07). Results for the lifetimes using the relative method derived by Volk *et al.* (1997) are discussed in Sections 4.4.2 and 4.4.3, and are listed in Table 4.8 together with new results based on more recent observations (Laube *et al.,* 2013; Brown *et al.,* 2013).

4.4.2 Lifetime Estimates from *In Situ* Data

Only a few of the publications mentioned in Section 4.2.2 use *in situ* measurements to estimate stratospheric lifetimes. Exclusion of studies with limited precisions and thus

comparably high uncertainties (Kaye *et al.,* 1994; Avallone and Prather, 1997) reduces the number of studies. The most extensive evaluation is presented in Volk *et al.* (1997). All other studies rely to a large part on the methods developed in this work. The studies of Bujok *et al.,* 2001 and Laube *et al.,* 2010b focus on individual molecules only and estimate stratospheric lifetimes from correlation slopes against CFC-11 using the WMO reference lifetime of 45 years. Bujok *et al.,* 2001 derive an N_2O lifetime of 91±15 years, which is considerably lower than the 121±14 years estimated by Volk *et al.,* 1997 (based on 45 yr for CFC-11). Laube *et al.,* 2010b estimated the lifetime of HFC-227ea to be 370 years. However, this latter estimate revealed one of the limitations of the tracer-tracer correlation method. Very long stratospheric lifetimes result in correlation slopes close to zero, so that even small variations result in large uncertainty ranges (270 to 840 years in the case of HFC-227ea). The applicability of this method is thus currently very limited for several compounds of interest in this report, namely CFC-114, CFC-115, and HFC-23. Finally, the most recent work is that of Laube *et al.* (2013). Laube *et al.* (2013) combine *in situ* observations from the Geophysica aircraft and from balloons to derive burdens and tracer-tracer correlations. Ratios and their 2-σ uncertainty ranges of stratospheric lifetimes relative to CFC-11 derived from these studies are given in Table 4.8 along with the numbers recommended in the latest WMO Ozone Assessment (WMO, 2011) and results from the satellite-based study of Brown *et al.* (2013) discussed in the following section. We note that within the given 2-σ uncertainties (in most cases even within 1 σ), all values of the *in situ* studies agree with each other and with the values from WMO (2011).

Table 4.8. Overview of stratospheric lifetime ratios relative to CFC-11 and a combined best estimate (based on error weighted means) compared to those recommended in the most recent WMO Ozone Assessment (WMO, 2011) and (for N_2O) the IPCC Assessment (IPCC, 2007). Ranges indicate 2-σ uncertainties (the symmetric errors given in the original work by Volk *et al.* (1997) have been converted to asymmetric errors more accurately representing 2-σ uncertainties.)

	Volk *et al.*, 1997	**Laube *et al.*, 2013**	**Bujok *et al.*, 2001**	**Brown *et al.*, 2013**	**Best estimate**	**WMO 2011 [a] IPCC 2007**
Trace gas						
N_2O	2.70(2.18-3.54)		2.02 ±0.22	2.74(1.52-14.03)	2.70(2.20-3.50)	2.53[a]
CH_4	2.06(1.70-2.62)			4.33(2.36-25.94)		
CFC-12	1.92(1.54-2.56)	1.66 (1.36-2.15)		2.5(1.73-4.49)	1.91(1.65-2.27)	2.22
CFC-113	2.24(1.44-5.02)	1.37 (1.12-1.77)			1.56(1.28-1.98)	1.89
CFC-11	1.00	1.00		1.00		
CCl_4	0.72(0.59-0.93)	0.87 (0.66-1.28)		0.77 (0.49-1.81)	0.78(0.66-0.94)	0.78
CH_3CCl_3	0.76(0.58-1.11)	0.50 (0.29-1.86)			0.74(0.57-1.04)	0.87
Halon-1211	0.52(0.38-0.85)	0.61 (0.48-0.81)			0.58 (0.48-0.74)	
Halon-1301		1.37 (1.13-1.74)			1.37 (1.13-1.74)	1.44
HCFC-22		3.06 (1.31-∞)			3.06 (1.31-∞)	4.13
HCFC-141b		2.02 (0.82-∞)			2.02 (0.82-∞)	1.44
HCFC-142b		6.75 (1.39-∞)			6.75 (1.39-∞)	3.56
CH_3Cl				1.54 (0.53-∞)	1.54 (0.53-∞)	

4.4.3 Lifetime Estimates from Satellite Data

ACE-FTS satellite measurements from 2005 to 2010 have been used to calculate steady-state stratospheric lifetime ratios of CFC-12, CCl_4, CH_3Cl, N_2O and CH_4 relative to CFC-11 using the method described by Volk *et al.* (1997); (Brown *et al.,* 2013).

The data were divided into occultations made during stratospheric summer and winter from the Northern and Southern Hemispheres. Data were selected between 30^0 N/S and 70^0 N/S. These latitude bands were chosen so that data inside the polar vortex and the tropics would not be included. The data were separated using the following criteria: Northern Hemisphere Summer (May* – June – July – August – September – October*); Northern Hemisphere Winter (November – December – January – February – March – April); Southern Hemisphere Summer (November* – December – January – February – March – April*); and Southern Hemisphere Winter (May – June – July – August – September – October). [We note that months marked with * have been selected to increase the amount of data used in this study despite not being true stratospheric summer months.] These data were also divided by year, which produces 24 different data bins.

Mean correlation profiles were calculated using the mean mole fractions of both the correlating species (for example CFC-12) and CFC-11 calculated every 2 pmol mol^{-1} in the mole fraction of CFC-11. The error of each point was calculated from the standard deviation of the data within this 2-pmol mol^{-1} window. The derivation of the correlation slopes at the tropopause then followed nearly exactly the procedures described in Volk *et al.* (1997). First, the slope of the data in a window with width of 80 pmol mol^{-1} (of CFC-11) was calculated every 5 pmol mol^{-1} of CFC-11. A second-degree polynomial, weighted by the error of the points (1-σ error in the fit of the line), was then fit to the slope data and extrapolated to the tropopause using the VMR of CFC-11 retrieved by ACE-FTS at the tropopause. The tropopause slopes thus determined were corrected for the effects of tropospheric growth according to the method described in Volk *et al.* (1997) and outlined above (Section 4.4.1). The required slope of CFC-11 relative to the age of air at the tropopause was calculated from measurements made with instruments onboard the Geophysica aircraft in October 2009 and January 2010 by Laube *et al.* (2013). This value was scaled by the effective linear growth rate of CFC-11 between 2005 and 2010. Examples of the correlation plots produced in this study are presented in Figure 4.4.

An analysis of the altitude dependent systematic errors in ACE-FTS retrievals has not been carried out at this time. However, ACE-FTS occultations have been compared to data from other instruments such as the MK-IV and FIRS-2 balloon borne spectrometers (e.g., Mahieu *et al.,* 2008). Previous validation papers for N_2O, CH_4, CFC-11 and CFC-12 have not shown significant altitude dependent errors for the altitude range used in this study (Mahieu *et al.,* 2008; Velazco *et al.,* 2011). In addition to these comparisons, the profiles of CFC-11 and CFC-12 were compared to those from the SLIMCAT 3-D Chemical Transform Model (Brown *et al.,* 2011). The profiles used in this work showed that, whilst there were differences in the VMR from ACE-FTS and from SLIMCAT the overall shapes of the profiles were extremely similar. The differences between VMRs from ACE-FTS and other instruments (mentioned previously) can be used as a proxy for the systematic error, due to the fact that the full systematic errors associated with ACE-FTS retrievals are not known at this time. The methods described in this section were repeated using ACE-FTS VMR that were modified by the differences calculated in previous validation work. The values used to modify the VMRs were + 10% for CFC-11 and CFC-12 from the validation work of Mahieu

et al. (2008). Work by Velazco *et al.* (2011) also showed differences of + 10% for CH_4 and N_2O. The results of the reanalysis using these errors were combined with the statistical error.

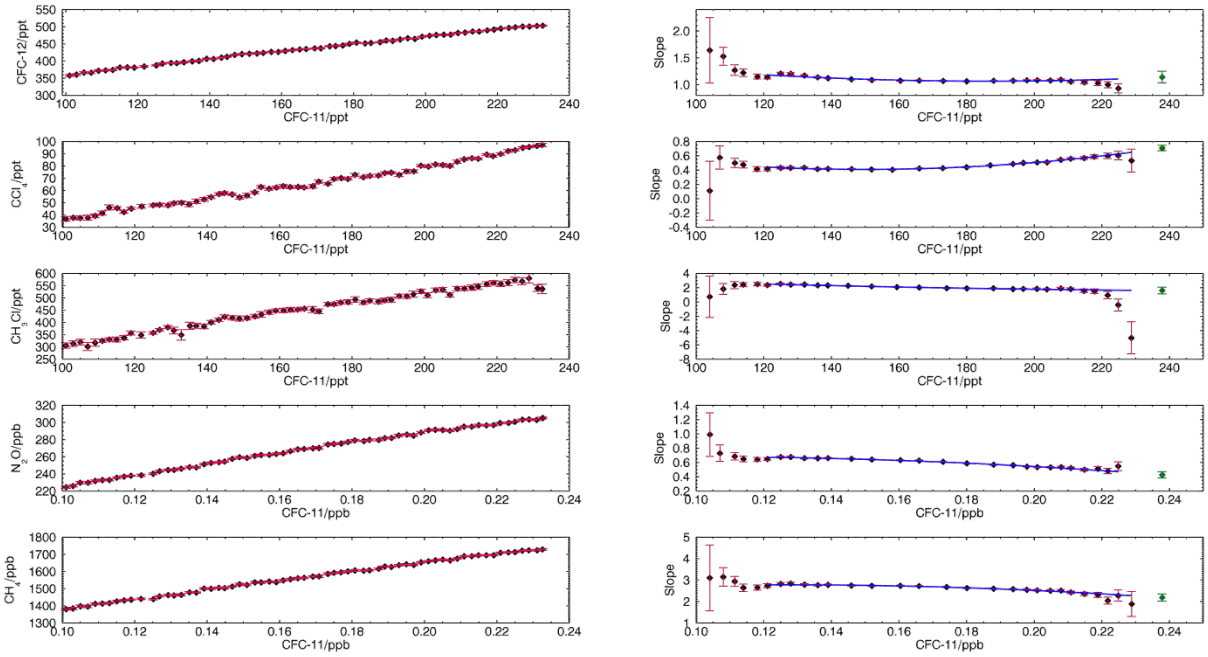

Figure 4.4. Correlations between the volume-mixing ratios of CFC-12, CCl_4, CH_4, CH_3Cl and N_2O and CFC-11 for the data from the Northern Hemisphere during the stratospheric winter of 2008. Left panels: The mean correlation curves. Each point represents the mean of the VMR, of both CFC-11 and CFC-12, in a window of 2 ppt of CFC-11. The error on these points is the standard deviation of the mean of the data within each 2 ppt window. Right panels: The local slope of data in an 80 ppt of CFC-11 window. The error on the points is the fitting error of this fit. The blue line is a second-degree polynomial fit to the local slopes. The green point is the extrapolated slope at the tropopause.

The remaining species, CH_3Cl and CCl_4, are more problematic than the other species. Previous validations of these species have shown large differences between ACE-FTS retrievals and the retrievals from other instruments. For example comparisons between ACE-FTS and the MK-IV instrument (Velazco *et al.,* 2011) found differences of 30% in the VMR retrievals of CH_3Cl. The errors on ACE-FTS retrievals of CCl_4 are estimated to be between 20 and 30% (Allen *et al.,* 2009). The estimation of systematic errors for the CCl_4 retrieval is complicated by the position of the spectral feature used to retrieve CCl_4 VMR. There is an interfering Q-branch of CO_2, the line mixing of which is not properly accounted for in the forward model. Similarly the Q-branch of CH_3Cl suffers from line mixing which is not properly included in the forward model. The effects of line mixing on both of these retrievals are most serious in the troposphere, where the density of the atmosphere is at its greatest. In the stratosphere, where the density of the atmosphere is lower, line mixing becomes less of a problem within the retrieval. Quantifying the effects of line mixing on the retrieved VMR is a research project in and of itself. In this work we have approximated the systematic errors to be - 30% for CH_3Cl (Velazco *et al.,* 2011) and + 20% for CCl_4 (Allen *et al.,* 2009). Once more lifetimes were calculated using VMR that had been modified by the corresponding systematic error. These errors represent the best attempt to quantify the effect of systematic

errors on the lifetimes of CCl_4 and CH_3Cl; however, due to the reasons outlined previously these errors may be different to those quoted here.

The lifetime ratios calculated from the tracer correlations show considerable spread between the individual hemisphere/season/year bins that is sometimes larger than expected from the estimated uncertainties. However, there are no systematic (seasonal, interhemispheric) variations apparent. Therefore, the mean lifetime of each species relative to CFC-11 was determined from the individual bins as error-weighted average of the individual inverse lifetimes (a quantity with symmetric uncertainties). These ratios are listed in Table 4.8 along with the results of the *in situ* studies.

4.4.4 Best Estimate of Lifetime Ratios

There are two systematic studies on lifetime ratios based on *in situ* measurements (Volk *et al.,* 1997 and Laube *et al.,* 2013) and one that is based on satellite observations (Brown *et al.,* 2013). As the two latter studies closely follow the methods (and even in detail the practical procedures) described in Volk *et al.* (1997) and summarized in Section 4.4.1, the three studies can be considered very consistent with each other regarding their methodology. Although there are notable differences for some species between the ratios derived by these studies, we emphasize that the results do agree within their 2-σ error uncertainties (with the exception of CH_4). These three independent studies all have strengths and weaknesses. While the Volk *et al.* (1997) study was carried out when atmospheric trends for CFC-12 and CFC-113 were quite large, the study by Laube *et al.* (2013) is based on a much smaller data set and only covers one season, and the Brown *et al.* (2013) study is based on satellite data which may be more prone to systematic uncertainties than *in situ* data. We therefore decided to base our recommendation on an error-weighted average of the three ratios (where the mean was again calculated for the inverse lifetimes, which exhibit symmetric uncertainties). As noted above, these studies all agree within their combined estimated error, with the exception of the studies by Volk *et al.* (1997) and by Brown *et al.* (2013) for the stratospheric lifetime of methane. We thus give no recommendation of the stratospheric lifetime of CH_4, as one or both of the studies must have unaccounted errors for this species. All our best estimates for the ratios of stratospheric lifetimes relative to CFC-11 are given in Table 4.8. The implications and the recommendations for atmospheric lifetimes based on observations are drawn in the following Section 4.5.

4.5 Conclusions

In this chapter different methods are applied to derive lifetimes of atmospheric trace gases based on their measurements in the atmosphere. Some of these methods rely on a combination of modeling and observations (Section 4.3) while relative lifetimes of some species can be deduced from stratospheric correlations (Section 4.4) directly. While this latter approach does not require an atmospheric model, it does rely on a complex conceptual framework and must also be applied with care. Common to all of these techniques is the need for high precision, high accuracy, and long-term internally consistent data from both the troposphere and the stratosphere. We note that the absolute method to derive stratospheric lifetimes from correlations between the mole fraction of a trace gas and its mean age (Volk *et al.,* 1997) is not considered here due to the larger uncertainties associated to this method (see also discussion in Chapter 2). All methods applied here rely on data from different time periods. As even steady-state atmospheric lifetimes are not constant in time, but may change e.g., due to changing chemistry or changing dynamics, there may be both interannual

variability and long-term changes in atmospheric lifetimes over the periods of investigations. However, the uncertainties in all the lifetimes derived here are significantly larger than any expected long-term changes, so we will assume in the following discussion that all values derived here can be compared and combined to yield best estimates.

As CFC-11 has traditionally been used as a reference species to derive lifetimes of other compounds, its stratospheric lifetime is of particularly high importance. WMO (1999) has recommended a change of the best estimate atmospheric lifetime from 50 years to 45 years based in part on values from inverse modeling (52 years, Cunnold *et al.,* 1997), from global loss calculated using balloon data (41.5 yr, Minschwaner *et al.,* 1993) and on the lifetime of 41±12 years derived from correlations between mean age and CFC-11 in the stratosphere (Volk *et al.,* 1997). New independent studies based on inverse modeling (Rigby *et al.,* 2013), comparable to the study of Cunnold *et al.* (1997) suggest a steady-state global CFC-11 lifetime of 53 (40-72, 2σ) years, averaged from inversions of AGAGE and NOAA data, respectively. The result is thus between current model estimates of 56 years (Douglass *et al.,* 2008) and the current WMO recommendation of 45 years. For CFC-12 Rigby *et al.* (2013) deduce a lifetimes of 111 (79-157, 2σ) years, again averaged from the inversions of AGAGE and NOAA data, respectively. The study by Rigby *et al.* (2013), while having significant uncertainties, suggests that the CFC-11 lifetime may be slightly longer than currently recommended, whereas the CFC-12 value of both studies, while being slightly higher than the WMO recommendation, is in good agreement with the current recommendation of 100 years. In the case of the inverse modeling improved independent estimates of emissions would allow to better constrain the lifetimes.

The second method used to derive global steady-state lifetimes of CFC-11 and CFC-12 is based on the combination of observed global distributions and calculated loss rates (Minschwaner *et al.,* 2013) and yields lifetimes of 45 (30-91, 2σ) years and 107 (79-166, 2σ) years for CFC-11 and CFC-12, respectively. This method relies on accurate information about the actinic flux, the temperature-dependent absorption cross section and the global distribution of the respective species, especially in the loss region. Due to the steeper gradient of the shorter-lived species CFC-11 in comparison to CFC-12, this method will work better for CFC-12 then for CFC-11. In order to reduce uncertainties in the future, better knowledge of actinic UV- fluxes in the tropical loss region, better information on absorption cross section and in particular for CFC-11 improved knowledge of the global distribution from well-validated satellite data with high vertical resolution are necessary.

Relative stratospheric lifetimes of two species can be derived based on the correlation observed between these species in the lower stratosphere. The results from such studies using both *in situ* and satellite data and the best estimate deduced from these studies are shown in Table 4.8. The currently recommended lifetimes of 100 years for CFC-12 and 45 years for CFC-11 would suggest a ratio of 2.22. This is in poor agreement with the results of the two *in situ* studies available (Volk *et al.,* 1997; and Laube *et al.,* 2013). Both these studies suggest that the ratio should be lower, i.e., 1.92 (1.54-2.56) (Volk *et al.,* 1997) and 1.66 (1.36-2.15) (Laube *et al.,* 2013). The ratio of 2.5 (1.73-4.49) based on satellite correlation studies (Brown *et al.,* 2013) is on the contrary higher than the WMO recommended lifetime ratio. Our best estimate of the lifetime-ratio between CFC-12 and CFC-11 is 1.91 (1.65-2.27). This ratio agrees with the ratio found from satellite observations and modeling of the loss rate (2.30) and from inverse modeling (2.08) within its 2σ range and within the combined 1σ ranges. Based on these ratios, we conclude that a lifetime of about 50 years for CFC-11 and 105 years for CFC-12 provides the best agreement with

observational data and observation-based studies. Taking into account all information available, including model studies from Chapter 5, a global steady-state lifetime of 52.3 (43-67, 2σ "most likely range" estimate) years is derived (see Chapter 6).

In the case of CFC-11 it must further be taken into account that some loss also occurs in the troposphere (e.g., Minschwaner *et al.*, 2013, see also discussion in Chapter 5). Using the model-derived tropospheric lifetime of 1870 years, we derive a stratospheric steady-state lifetime of 53.8 (44.3-68.8, 2σ) years, on which we base the following discussion. The stratospheric lifetime of CFC-12 derived from this is 103 (81-140) years. All uncertainties given are 2-σ uncertainties unless noted otherwise. The values given here will thus differ from the absolute values given in the original publications. Table 4.9 summarizes estimates of global lifetimes and Table 4.10 those for stratospheric lifetimes based on the results discussed in this chapter.

Global lifetimes for CFC-113 of 109 (89-133) and 109 (86-140) years are derived from inverse modeling (Rigby *et al.,* 2013), which is longer than the currently recommended value of 85 years. The correlation studies yield a best-estimate ratio of 1.56 (1.28-1.98) for the lifetime of CFC-113 relative to CFC-11. A direct comparison of vertical profiles of CFC-12 and CFC-113 (Laube *et al.,* 2010a, 2013) and cross sections (Sander *et al.,* 2011) suggests that CFC-113 should be shorter lived than CFC-12, as also currently recommended by WMO. Based on a stratospheric lifetime of 53.8 years of CFC-11 we derive a stratospheric lifetime of 84 (64-121) years, which is consistent with the inverse modeling within the estimated error.

Regarding CCl_4, the best estimate of the stratospheric lifetime is 42 (33-58) years, again based on a stratospheric lifetime of 53.8 years for CFC-11. This is slightly larger than the previous estimate of 35 years discussed in Montzka and Reimann (2011). Based on updated estimates of the other loss processes (oceanic uptake and degradation in soils) a new best estimate of the CCl_4 lifetime is 24 (18-40) years, which is slightly smaller than the value of 26 years suggested in Montzka and Reimann (2011). The discrepancy in emissions estimated using bottom-up and top-down-techniques (see discussion in Montzka and Reimann (2011)) cannot be resolved using this new estimate.

The main loss process for HCFC is reaction with OH radicals in the troposphere. Based on the tropospheric OH levels estimated from the inversion of CH_3CCl_3, on new recommendations for the OH reaction rate coefficients and on stratospheric lifetimes (see Chapter 3), the steady-state global lifetimes (see Tables 4.3 and 4.9) and the tropospheric lifetimes (Table 4.3) have been calculated for a range of HCFCs and HFCs. The resulting global lifetimes are 12.4, 9.4, and 17.7 years for HCFC 22, 141b, and 142b, respectively. One new study (Laube *et al.,* 2013) suggests that the stratospheric lifetime of HCFC-22 should be 3.06 (1.31-∞) times larger than that of CFC-11, i.e., 165 years (70-∞). The other HCFCs for which new result on the stratospheric lifetime are available are HCFC-141b and HCFC-142b, which should have stratospheric lifetime 2.02 (0.82-∞) and 6.75 (1.39-∞) times longer than that of CFC-11, respectively. Using the reference stratospheric lifetime of 53.8 years for CFC-11 results in stratospheric lifetimes of 109 (44-∞) and 363 (75-∞) years for HCFC-141b and HCFC-142b, respectively.

For Halon-1211, our best estimate for the stratospheric lifetime is 31 (24-45) years. Laube *et al.* (2013) further suggest that Halon-1301 should have a stratospheric lifetime that is 1.37 (1.13-1.74) times longer than that of CFC-11, i.e., 74 (56-106) years. Newland *et al.* (2012)

report model estimates of the stratospheric lifetimes for Halon-2402 and Halon-1202 of 31 (27-37) and 21 (18-26) years, respectively, which are consistent with stratospheric observations.

The best estimate for the stratospheric lifetime of CH_3CCl_3 is 0.74 (0.57-1.04) times that of CFC-11, resulting in a stratospheric lifetime of 40 (29-63) years. The inverse modeling by Rigby *et al.* (2013) suggests that the global lifetime of CH_3CCl_3 is 5.04 (4.75-5.37) years (average of inversion using NOAA and AGAGE data), in good agreement with the current WMO recommendation of 5.0 years.

While there have been some variations in the predicted lifetimes of CH_3Cl and CH_3Br, the overall ranges are 0.7-1.3 years for CH_3Cl and 0.6-1.1 years for CH_3Br, with best estimates being 0.9 and 0.8 (0.7-0.9) years respectively. New information is providing only small adjustments to the estimated lifetime. The current best estimates are unchanged from WMO (2011): 1 year for CH_3Cl and 0.8 year for CH_3Br.

Table 4.10 includes estimated lifetimes for N_2O, based on the observational lifetime methods discussed above. A value of 146 (111-212) years for the stratospheric lifetime is derived from the best estimate of the lifetime ratio studies. The IPCC 2007 recommendation of 114 years is near the low end of this range. A lifetime of 116 (85-181) years, based on CLAES N_2O observations with updated photochemical calculations (Minschwaner *et al.,* 1998, 2013), suggests about this lifetime and is consistent within the 2σ range of the correlation studies. The global steady-state lifetime of methane (CH_4) has been calculated to be 9.8 (7.6-13.8) years based on the tropospheric OH levels from the inversion of CH_3CCl_3 and recommendations for the OH reaction rate coefficients and stratospheric lifetimes from Chapter 3 of this report.

Reliable estimates of the atmospheric lifetimes of trace gases require high-quality observations as stated above. It should be ensured that these networks and continued stratospheric observations are maintained in order to provide the necessary reliable data for existing trace gases and also for new species as they appear. In addition air archives like the one from the Cape Grim observatory provide an invaluable database for future studies. Next to the knowledge of the temporal development of a species, good knowledge of the atmospheric loss and the sources to the atmosphere (both natural and anthropogenic emissions) are key in improving our knowledge on the atmospheric lifetimes of radiatively important or ozone depleting trace gases in the atmosphere. For this aspect, better estimates of emissions and better knowledge of the atmospheric chemistry and photochemistry are needed. Also, applying the methods used to derive information on atmospheric lifetimes from observation to model data may help in evaluating the methods used.

Table 4.9. Summary of estimated global lifetimes (years) (mean and 2-σ standard deviation) from various approaches described in this chapter, and previously recommended by WMO and IPCC. All values are steady-state lifetimes or have been adjusted for tracer transience, with the exception of the global box modeling results, which are, however, expected to be good proxies of the steady-state lifetimes.

	WMO 2011, IPCC 2007*	**WMO 1994**	**Inverse AGAGE and NOAA[b]**	**Global Box Model**	**Satellite derived[c]**	**Tracer Correlations[d] (best estimate)**
N_2O	114[*]				116 (85-181)	146 (111-212)
CH_4	12[*a]		9.8 (7.6-13.8)			
CFC-11	45	50	53 (40-72)		45 (30-91)	N.A.
CFC-12	100	102	111 (79-157)		107 (79-166)	103 (81-140)
CFC-113	85	85	109 (87-137)			84 (64-121)
CH_3CCl_3	5	5.4	5.04 (4.75-5.37)			
HCFC-22	11.9		12.4 (9.3-18.5)			
CH_3Br	0.8	1.3		0.8 (0.7-0.9)		
CH_3Cl	1	1.5		0.9		
CCl_4	26	42		24 (18-40)		
Halon-1301	65	65				74 (56-106)
HCFC-141b			9.4 (7.2-13.6)			
HCFC-142b			17.7 (12.7-29.2)			
HFC-23	222		228 (160-393)			
HFC-32	5.2		5.4 (4-8.1)			
HFC-125	28.2		30.5 (22.2-48.9)			
HFC-134a	13.4		13.5 (9.9-21.2)			
HFC-143a	47.1		51.4 (37.7-80.4)			
HFC-152a	1.5		1.6 (1.2-2.2)			
HFC-227ea	38.9		35.8 (25.4-60.7)			
HFC-245fa	7.7		7.9 (5.5-13.8)			

[a] In the case of CH_4 the given value is a response time, which is different from the steady-state lifetime.
[b] Only values for CFC-11, CFC-12, CFC-113 and CH_3CCl_3 are from inversion. The lifetimes given for other species in this column are from a forward run of the model using the OH fields derived from the CH_3CCl_3 inversion and stratospheric loss rates based on modeling work in Chapter 5.
[c] The satellite-derived values are the same as given in Table 4.10 for N_2O, CFC-12, and CFC-113, as these have no significant tropospheric loss.
[d] The values in this column are for the species from Table 4.10, for which the stratospheric lifetime is assumed to be equal to the global lifetime, i.e., tropospheric loss is negligible. All values based on an assumed stratospheric CFC-11 lifetime of 53.8 years.

Table 4.10. Best estimates of stratospheric lifetimes of trace-gases. The best estimate from the correlation studies is based on an assumed stratospheric CFC-11 lifetime of 53.8 (44.3-68.8) years and the average ratios shown in Table 4.8. Only data for CFCs are shown from the inversion studies, as the global and the stratospheric lifetimes are assumed to be equal for these species. All uncertainties are 2-σ errors. All values are representative of steady-state lifetimes.

	WMO 2011	WMO 1994	Inverse AGAGE and NOAA	Satellite derived	Tracer Correlations (best estimate)	2D Model checked for consistency with observations
N_2O	114*	120		116 (85-181)	146 (111-212)	
CH_4						
CFC-11	45	50			N.A.	
CFC-12	100	102	111 (79-157)	107 (79-166)	103 (81-140)	
CFC-113	85	85	109 (87-137)		84 (64-121)	
CH_3CCl_3	39				40 (29-63)	
HCFC-22	186				165 (70-∞)	
CH_3Br						
CH_3Cl					83 (28-∞)	
CCl_4	35				42 (33-58)	
Halon-1211					31 (24-45)	
Halon-1301	65	65			74 (56-106)	
Halon-2402						31 (27-37)
Halon-1202						21 (18-26)
HCFC-141b	64.9				109 (44-∞)	
HCFC-142b	160				363 (75-∞)	

4.6 References

Allen, N. D. C., P. F. Bernath, C. D. Boone, M. P. Chipperfield, D. Fu, G. L. Manney, D. E. Oram, G. C. Toon, and D. K. Weisenstein, Global carbon tetrachloride distributions obtained from the Atmospheric Chemistry Experiment (ACE), Atmos. Chem. Phys., 9, 7449-7459, 2009.

Andrews, A. E., K. A. Boering, S. C. Wofsy, B. C. Daube, D. B. Jones, S. Alex, M. Loewenstein, J. R. Podolske, and S. E. Strahan, Empirical age spectra for the midlatitude lower stratosphere from *in situ* observations of CO_2, *J. Geophys. Res.*, *106,* 10257-10274, 2001.

Avallone, L. M., and M. J. Prather, Tracer-tracer correlations: three-dimensional model simulations and comparisons to observations, *J. Geophys. Res.*, *102*, 19233-19246, 1997.

Atkinson, R., D. L. Baulch, R. A. Cox, J. N. Crowley, R. F. Hampson, R. G. Hynes, M. E. Jenkin, M. J. Rossi, J. Troe, and IUPAC Subcommittee, Evaluated kinetic and photochemical data for atmospheric chemistry: Volume II – gas phase reactions of organic species, *Atmos. Chem. Phys*., 6, 3625-4055, doi: 10.5194/acp-6-3625-2006, 2006.

Atkinson, R., D. L. Baulch, R. A. Cox, J. N. Crowley, R. F. Hampson, R. G. Hynes, M. E. Jenkin, M. J. Rossi, J. Troe, and T. J. Wallington, Evaluated kinetic and photochemical data for atmospheric chemistry, *Atmos. Chem. Phys*., 8, 4141-4496, 2008.

Bernath, P. F., Atmospheric Chemistry Experiment (ACE): Analytical chemistry from orbit, *Trends in Analytical Chemistry 2006, 25*, 647-54, 2006.

Bernath, P. F., C. T. McElroy, M. C. Abrams, C. D. Boone, M. Butler, C. Camy-Peyret, M. Carleer, C. Clerbaux, P.-F. Coheur, R. Colin, P. DeCola, M. DeMazière, J. R. Drummond, D. Dufour, W. F. J. Evans, H. Fast, D. Fussen, K. Gilbert, D. E. Jennings, E. J. Llewellyn, R. P. Lowe, E. Mahieu, J. C. McConnell, M. McHugh, S. D. McLeod, R. Michaud, C. Midwinter, R. Nassar, F. Nichitiu, C. Nowlan, C. P. Rinsland, Y. J. Rochon, N. Rowlands, K. Semeniuk, P. Simon, R. Skelton, J. J. Sloan, M.-A. Soucy, K. Strong, P. Tremblay, D. Turnbull, K. A. Walker, I. Walkty, D. A. Wardle, V. Wehrle, R. Zander, and J. Zou., Atmospheric Chemistry Experiment ACE): Mission overview, *Geophys. Res. Lett, 32*, L15S01, doi: 10.1029/2005GL022386, 2005.

Bingham, G. E., D. K. Zhou, B. Y. Bartschi, G. P. Anderson, D. R. Smith, J. H. Chetwynd, and R. M. Nadile, Cryogenic Infrared Radiance Instrumentation for Shuttle (CIRRIS-1A) Earth limb spectral measurements, calibration, and atmospheric O_3, HNO_3, CFC-12, and CFC-11 profile retrieval, *J. Geophys. Res.*, *102*, 3547-3558, 1997.

Blei, E., C. J. Hardacre, G. P. Mills, K. V. Heal, and M. R. Heal, Identification and quantification of methyl halide sources in a lowland tropical rainforest, *Atmos. Environ.*, *44*(8), 1005-1010, 2010.

Brown, A. T., C. M. Volk, M. R. Schoeberl, C. D. Boone, and P. F. Bernath, Stratospheric lifetimes of CFC-12, CCl_4, CH_4, CH_3Cl, and N_2O from measurements made by the Atmospheric Chemistry Experiment-Fourier Transform Spectrometer (ACE-FTS), *Atmos. Chem. Phys. Discuss*., 13, 4221–4287, doi:10.5194/acpd-13-4221-2013, 2013.

Brown, A. T., M. P. Chipperfield, C. Boone, C. Wilson, K. A. Walker, and P. F. Bernath, Trends in atmospheric halogen containing gases since 2004, *J. Quant. Spectrosc. Radiat. Trans*., *112,* 2552-2566, 2011.

Buizert, C., P. Martinerie, V. V. Petrenko, J. P. Severinghaus., C. M. Trudinger, E. Witrant, J. L. Rosen, A. J. Orsi, M. Rubino, D. M. Etheridge, L. P. Steele, C. Hogan, J. C. Laube, W. T. Sturges, V. A. Levchenko, Smith, A. M., Levin, I., Conway, T. J. Dlugokencky, E. J., Lang, P. M., Kawamura, K., T. M. Jenk, J. W. C. White, T. Sowers, J. Schwander, and T. Blunier, Gas transport in firn: Multiple-tracer characterisation and model intercomparison for NEEM, Northern Greenland, *Atmos. Chem. Phys.*, *12*, 4259-4277, doi: 10.5194/acp-12-4259-2012, 2012.

Bujok, O., V. Tan, E. Klein, R. Nopper, R. Bauer, A. Engel, M.-T. Gerhards, A. Afchine, D. S. McKenna, U. Schmidt, F. G. Wienhold, and H. Fischer, GHOST—A novel airborne gas chromatograph for *in situ* measurements of long-lived tracers in the lower stratosphere: Method and applications*, J. Atmos. Chem., 39*, 37-64, 2001.

Butler, J. H., The potential role of the ocean in regulating atmospheric CH_3Br. *Geophys. Res. Lett., 21*, 185-188, 1994.

Butler, J. H., J. W. Elkins, T. M. Thompson, and B. D. Hall, Oceanic consumption of CH_3CC1_3: Implications for tropospheric OH*, J. Geophys. Res., 96D*, 22347-22355, 1991.

Butler, J. H., S. A. Yvon-Lewis, J. M. Lobert, D. B. King, S. A. Montzka, J. W. Elkins, B. D. Hall, and V. Koropalov, A revised look at the oceanic sink for atmospheric CCl_4, *E.O.S. Trans. Fall Suppl*., A51A-0273, 2011.

Chang, A. Y., R. J. Salawitch, H. A. Michelsen, M. R. Gunson, M. C. Abrams, R. Zander, C. P. Rinsland, J. W. Elkins, G. S. Dutton, C. M. Volk, C. R. Webster, R. D. May, D. W. Fahey, R.-S. Gao, M. Loewenstein, J. R. Podolske, R. M. Stimpfle, D. W. Kohn, M. H. Proffitt, J. J. Margitan, K. R. Chan, M. M. Abbas, A. Goldman, F. W. Irion, G. L. Manney, M. J. Newchurch, and G. P. Stiller, A comparison of measurements from ATMOS and Instruments aboard the ER-2 aircraft: Halogenated gases, *Geophys. Res. Lett.*, *23*, 2393-2396, 1996.

Crutzen, P. J., and U. Schmailzl, Chemical budgets of the stratosphere, *Planet. Space Sci*., *31*, 1009-1032, 1983.

Cunnold, D. M., P. J. Fraser, R. F. Weiss, R. G, Prinn, P. G. Simmonds, B. R. Miller, F. N. Alyea, *et al.,* Global trends and annual releases of CCI_3F and CCI_2F_2 estimated from ALE/GAGE and other measurements from July 1978 to June 1991, *J. Geophys. Res.*, *99* (D1), 1107-1126, 1994.

Cunnold, D. M., R. G. Prinn, R. A. Rasmussen, P. G. Simmonds, F. N. Alyea, C. A. Cardelino, A. J. Crawford, P. J. Fraser, and R. D. Rosen, The Atmospheric Lifetime Experiment. 3. Lifetime methodology and application to three years of $CFCI_3$ data, *J. Geophys. Res., 88*, 8379-8400, 1983.

Cunnold, D. M., R. F. Weiss, R. G. Prinn, D. E. Hartley, P. G. Simmonds, P. J. Fraser, B. R. Miller, F. N. Alyea, and L. Porter, GAGE/AGAGE measurements indicating reductions in global emissions of CCl_3F and CCl_2F_2 in 1992-1994, *J. Geophys. Res., 102*, 1259-1269, 1997.

Dimmer, C. H., P. G. Simmonds, G. Nickless, and M. R. Bassford, Biogenic fluxes of halomethanes from Irish peatland ecosystems, *Atmos. Environ.*, *35* (2), 321-330, 2001.

Douglass, A. R., R. S. Stolarski, M. R. Schoeberl, C. H. Jackman, M. L. Gupta, P. A. Newman, J. E. Nielsen, and E. L. Fleming, Relationship of loss, mean age of air and the distribution of CFCs to stratospheric circulation and implications for atmospheric lifetimes*, J. Geophys. Res., 113*, D14309, doi: 10.1029/2007JD009575, 2008.

Dufour, G., C., D. Boone, and P. F. Bernath, First measurements of CFC-113 and HCFC-142b from space using ACE-FTS infrared spectra. *Geophys. Res. Lett.*, *32*, 4, 2005.

Ehhalt, D. H., F. Rohrer, D. R. Blake, D. E. Kinnison, and P. Konopka, On the use of nonmethane hydrocarbons for the determination of age spectra in the lower stratosphere, *J. Geophys. Res.*, *112*, D12208, doi: 10.1029/2006JD007686, 2007.

Flocke, F., R. L. Herman, R. J. Salawitch, E. Atlas, C. R. Webster, S. M. Schauffler, R. A. Lueb, R. D. May, E. J. Moyer, K. H. Rosenlof, D. C. Scott, D. R. Blake, and T. P. Bui, An examination of chemistry and transport processes in the tropical lower stratosphere using observations of long-lived and short-lived compounds obtained during STRAT and POLARIS, *J. Geophys. Res.*, *104*, 26625-26642, doi: 10.1029/1999JD900504, 1999.

Greenblatt, J. B., H.-J. Jost, M. Loewenstein, J. R. Podolske, D. F. Hurst, J. W. Elkins, S. M. Schauffler, E. L. Atlas, R. L. Herman, C. R. Webster, T. P. Bui, F. L. Moore, E. A. Ray, S. Oltmans, H. Vömel, J.-F. Blavier, B. Sen, R. A. Stachnik, G. C. Toon, A. Engel, M. Müller, U. Schmidt, H. Bremer, R. B. Pierce, B.-K. Sinnhuber, M. Chipperfield, and F. Lefevre, Tracer-based determination of vortex descent in the 1999/2000 Arctic winter, *J. Geophys. Res., 107*, doi: 10.1029/2001JD000937, 2002.

Grooß, J.-U., and J. M. Russell III, Technical note: A stratospheric climatology for O_3, H_2O, CH_4, NO_x, HCl, and HF derived from HALOE measurements, *Atmos. Chem. Phys.*, *5*, 2792-2807, 2005.

Grossmann, K. U., D. Offermann, O. Gusev, J. Oberheide, M. Riese, and R. Spang, The CRISTA-2 mission, *J. Geophys. Res.*, *107*, 8173, 2002.

Hall, T. M., and R. A. Plumb, Age as a diagnostic of stratospheric transport. *J. Geophys. Res.*, *99*, 1059-1069, 1994.

Happell, J. D., and M. P. Roche, Soils: A global sink of atmospheric carbon tetrachloride, *Geophys. Res. Lett., 30 (2),* 1088, doi: 10:1029/2002GL015957, 2003.

Herman, R. L., K. Drdla, J. R. Spackman, D. F. Hurst, P. J. Popp, C. R. Webster, P. A. Romashkin, J. W. Elkins, E. M. Weinstock, B. W. Gandrud, G. C. Toon, M. R. Schoeberl, H. Jost, E. L. Atlas, and T. P. Bui, Hydration, dehydration, and the total hydrogen budget of the 1999/2000 winter Arctic stratosphere, *J. Geophys. Res.*, *107*, doi: 10.1029/2001JD001257, 2003.

Herman, R. L., D. C. Scott, C. R. Webster, R. D. May, E. J. Moyer, R. J. Salawitch, Y. L. Yung, G. C. Toon, B. Sen, J. J. Margitan, K. H. Rosenlof, H. A. Michelsen, and J. W. Elkins, Tropical entrainment time scales inferred from stratospheric N_2O and CH_4 observations, *Geophys. Res. Lett.*, *25*, 2781-2784, 1998.

Hoffmann, L., R. Spang, M. Kaufmann, and M. Riese, Retrieval of CFC-11 and CFC-12 from Envisat MIPAS observations by means of rapid radiative transfer calculations, *Adv. Space Res., 36*, 915-921, 2005.

Hoffmann, L., M. Kaufmann, R. Spang, R. Müller, J. J. Remedios, C. M. Volk, T. von Clarmann, and M. Riese, Envisat MIPAS measurements of CFC-11: Retrieval, validation, and climatology, *Atmos. Chem. Phys.*, *8*, 3671-3688, 2008.

Homan, C. D., Volk, C. M., Kuhn, A. C., Werner, A., Baehr, J., Viciani, S., Ulanovski, A., and Ravegnani, F., Tracer measurements in the tropical tropopause layer during the AMMA/SCOUT-O3 aircraft campaign, *Atmos. Chem. Phys*., 10, 3615-3627, doi: 10.5194/acp-10-3615-2010, 2010.

Hu, L., S. A. Yvon-Lewis, Y. Liu, J. Salisbury, and J. E. O'Hern, Coastal emissions of methyl bromide and methyl chloride along the eastern Gulf of Mexico and east coast of the U.S., *Global Biogeochem. Cycles*, *24*, GB1007, doi: 10.1029/2009GB003514, 2010.

Hu, L., S. A. Yvon-Lewis, Y. Liu, and T. S. Bianchi, The ocean in near equilibrium with atmospheric CH_3Br, *Global Biogeochem. Cycles*, GB3016, doi: 10.1029/2011GB004272, 2012.

Hu, L., S. A. Yvon-Lewis, J. H. Butler, D. B. King, J. Lobert, and S. A. Montzka, An improved oceanic budget for methyl chloride, *J. Geophys. Res.*, 118, doi: 10.1029/2012JC008196, 2013.

IPCC (Intergovernmental Panel on Climate Change), *Climate Change 2007: The Physical Science Basis*, *Contribution of Working Group I to the Fourth Assessment Report of the Intergovernmental Panel on Climate Change*, edited by S. Solomon, D. Qin, M. Manning, Z. Chen, M. Marquis, K. B. Averyt, M. Tignor, and H. L. Miller, 996 pp., Cambridge University Press, Cambridge, U.K., and New York, NY, U.S.A., 2007.

Irion, F. W., M. R. Gunson, G. C. Toon, A. Y. Chang, A. Eldering, E. Mahieu, G. L. Manney, H. A., Michelsen, E. J. Moyer, M. J. Newchurch, G. B. Osterman, C. P. Rinsland, R. J. Salawitch, B. Sen, Y. L. Yung, and R. Zander, Atmospheric Trace Molecule Spectroscopy (ATMOS) Experiment Version 3 data retrievals, *Appl. Opt., 41*, 6968-6979, 2002.

Jobson, B. T., S. A. McKeen, D. D. Parrish, F. C. Fehsenfeld, D. R. Blake, A. Goldstein, S. Schauffler, and J. Elkins, Trace gas mixing ratio variability vs. lifetime in the troposphere and Stratosphere - Observations, *J. Geophys. Res., 104*, 16091-16113, 1999.

Johnston, H. S., O. Serang, and J. Podolske, Instantaneous global nitrous oxide photochemical rates, *J. Geophys. Res.*, *84,* 5077-5082, 1979.

Jost, H.-J., M. Loewenstein, J. B. Greenblatt, J. R. Podolske, T. P. Bui, D. F. Hurst, J. W. Elkins, R. L. Herman, C. R. Webster, S. M. Schauffler, E. L. Atlas, P. A. Newman, L. R. Lait, and S. C. Wofsy, Mixing events revealed by anomalous tracer relationships in the Arctic vortex during winter 1999/2000, *J. Geophys. Res.*, *107*, doi: 10.1029/2002JD002380, 2002.

Kaye, J., S. A. Penkett, and F. M. Ormond, *Report on Concentrations, Lifetimes, and Trends of CFCs, Halons, and Related Specie*s, NASA Reference Publication 1339, January, 247 pp., 1994.

Keene, W. C., M. A. K. Khalil, D. J. Erickson, III, A. McCulloch, T. E. Graedel, J. M. Lobert, M. L. Aucott, S. L. Gong, D. B. Harper, G. Kleiman, P. Midgley, R. M. Moore, C. Seuzaret, W. T. Sturges, C. M. Benkovitz, V. Koropalov, L. A. Barrie, and Y. F. Li, Composite global emissions of reactive chlorine from anthropogenic and

natural sources: Reactive Chlorine Emissions Inventory, *J. Geophys. Res.*, *104* (D7), 8429-8440, 1999.

Keppler, F., D. B. Harper, T. Röckmann, R. M. Moore, and J. T. G. Hamilton, New insight into the atmospheric chloromethane budget gained using stable carbon isotope ratios, *Atmos. Chem. Phys.*, *5* (9), 2403-2411, 2005.

King, D. B., and E. S. Saltzman, Removal of methyl bromide in coastal seawater: Chemical and biological rates, *J. Geophys. Res.*, *102* (C8), 18715-18721, 1997.

Ko, M. K. W., N. D. Sze, and D. K. Weisenstein, Use of satellite data to constrain the model-calculated atmospheric lifetime for N_2O: Implications for other grace gases, *J. Geophys. Res.*, *96*, 7547-7552, 1991.

Krysell, M., E. Fogelqvist, and T. Tanhua, Apparent removal of the transient tracer carbon tetrachloride from anoxic seawater, *Geophys. Res. Lett.*, *21* (23), 2511-2515, 1994.

Kuell, V., D. Offermann, M. Jarisch, B. Schaeler, A. Engel, H. Claude, H. G. J. Smit, A. Ebel, and H. Feldmann, Tropopause region temperatures and CFC 11 mixing ratios from CRISTA 2, *J. Geophys. Res., 110*, D16104, doi: 10.1029/2004JD005592, 2005.

Laube, J. C., A. Engel, H. Bönisch, T. Möbius, D. R. Worton, W. T. Sturges, K. Grunow, and U. Schmidt, Contribution of very short-lived organic substances to stratospheric chlorine and bromine in the tropics – a case study, *Atmos. Chem. Phys.*, *8*, 7325-7334, doi: 10.5194/acp-8-7325-2008, 2008.

Laube, J. C., A. Engel, H. Bönisch, T. Möbius, W. T. Sturges, M. Braß, and T. Röckmann, Fractional release factors of long-lived halogenated organic compounds in the tropical stratosphere, *Atmos. Chem. Phys.*, *10*, 1093-1103, doi: 10.5194/acp-10-1093-2010, 2010a.

Laube, J. C., P. Martinerie, E. Witrant, T. Blunier, J. Schwander, C. A. M. Brenninkmeijer, T. J. Schuck, M. Bolder, T. Röckmann, C. van der Veen, H. Bönisch, A. Engel, G. P. Mills, M. J. Newland, D. E. Oram, C. E. Reeves, and W. T. Sturges, Accelerating growth of HFC-227ea (1,1,1,2,3,3,3-heptafluoropropane) in the atmosphere, *Atmos. Chem. Phys.*, *10*, 5903-5910, doi: 10.5194/acp-10-5903-2010, 2010b.

Laube, J. C., A. Keil., H. Bönisch, A. Engel, T. Röckmann, C.M. Volk, and W. T. Sturges, Observation-based assessment of stratospheric fractional release, lifetimes, and Ozone Depletion Potentials of ten important source gases, *Atmos. Chem. Phys.,* 13, doi: 10.5194/acp-13-2779-2013, 2779-2791, 2013.

Lee, B.-S., J. L. Bullister, and F. A. Whitney, Chlorofluorocarbon CFC-11 and carbon tetrachloride removal in Saanich Inlet, an intermittently anoxic basin, *Marine Chem.*, *66*, 171-185, 1999.

Lee-Taylor, J. M., and E. A. Holland, Litter decomposition as a potential natural source of methyl bromide, *J. Geophys. Res.*, *105* (D7), 8857-8864, 2000.

Lee-Taylor, J., and K. R. Redeker, Reevaluation of global emissions from rice paddies of methyl iodide and other species, *Geophys. Res. Lett.*, *32*, L15801, doi: 0.1029/2005GL022918, 2005.

Liu, X.-F., Evidence of biodegradation of atmospheric carbon tetrachloride in soils: Field and microcosm studies, Ph.D. Thesis, 139pp. Columbia University, New York, NY U.S.A, 2006.

Lobert, J. M., W. C. Keene, J. A. Logan, and R. Yevich, Global chlorine emissions from biomass burning: Reactive Chlorine Emissions Inventory, *J. Geophys. Res.*, *104* (D7), 8373-8389, 1999.

Mahieu, E., P. Duchatelet, P. Demoulin, K. A. Walker, E. Dupuy, and L. Froidevaux, Validation of ACE-FTS v2.2 measurements of HCl, HF, CCl_3F and CCl_2F_2 using space-, balloon- and ground-based instrument observations, *Atmos. Chem. Phys., 8*, 6199-6221, 2008.

Maiss, M., L. P. Steele, R. J. Francey, P. J. Fraser, R. L. Langenfelds, N. B. A. Trivett, and I. Levin, Sulfur hexafluoride – a powerful new atmospheric tracer, *Atmos. Environ.*, *30,* 1621-1629, 1996.

Manley, S. L., N.-Y. Wang, M. L. Walser, and R. J. Cicerone, Methyl halide emissions from greenhouse-grown mangroves, *Geophys. Res. Lett.*, *34* (1), L01806, 2007.

Martinerie, P., E. Nourtier-Mazauric, J.-M. Barnola, W. T. Sturges, D. R. Worton, E. Atlas, L. K. Gohar, K. P. Shine, and G. P. Brasseur, Long-lived halocarbon trends and budgets from atmospheric chemistry modelling constrained with measurements in polar firn, *Atmos. Chem. Phys.*, *9*, 3911-3934, 2009.

McCulloch, A., P. Ashford, and P. M. Midgley, Historic emissions of fluorotrichloromethane (CFC-11) based on a market survey. *Atmos. Environ.*, *35* (26), 4387-4397. doi: 10.1016/S1352-2310(01)00249-7, 2001.

McCulloch, A., P. M. Midgley, and P. Ashford, Releases of refrigerant gases (CFC-12, HCFC-22 and HFC-134a) to the atmosphere. *Atmos. Environ.*, *37* (7), 889-902, doi: 10.1016/S1352-2310(02)00975-5, 2003.

Mead, M. I., I. R. White, G. Nickless, K.-Y. Wang, and D. E. Shallcross, An estimation of the global emission of methyl bromide from rapeseed (Brassica napus) from 1961 to 2003, *Atmos. Environ.*, 42 (2), 337-345, 2008a.

Mead, M. I., M. A. H. Khan, G. Nickless, B. R. Greally, D. Tainton, T. Pitman, and D. E. Shallcross, Leaf cutter ants: A possible missing source of biogenic halocarbons, *Environ. Chem.*, *5* (1), 5-10, 2008b.

Mellouki, A., R. K. Talukdar, A.-M. Schmoltner, T. Gierczak, M. J. Mills, S. Solomon and A. R. Ravishankara, Atmospheric lifetimes and ozone depletion potentials of methyl bromide (CH_3Br) and dibromomethane (CH_2Br_2), *Geophys. Res. Lett., 19* (22), 2279-2280, 1992.

Minschwaner, K., R. J. Salawitch, and M. B. McElroy, Absorption of solar radiation by O_2: Implications for O_3 and lifetimes of N_2O, $CFCl_3$, and CF_2Cl_2, *J. Geophys. Res.*, *98*, 10543-10561, 1993.

Minschwaner, K., R. W. Carver, B. P. Briegleb, and A. E. Roche, Infrared radiative forcing and atmospheric lifetimes of trace species based on observations from UARS, *J. Geophys. Res.*, *103*, 23243-23253, 1998.

Minschwaner, K., L. Hoffmann, A. Brown, M. Riese, R. Müller, and P. B. Bernath, Stratospheric loss and atmospheric lifetimes of CFC-11 and CFC-12 derived from satellite observations, *Atmos. Chem. Phys., 13,* 4253-4263, 2013.

Montzka, S. A., and S. Reimann (Coordinating Lead Authors), A. Engel, K. Krüger, S. O'Doherty, and W. T. Sturges (Lead Authors), Ozone-Depleting Substances (ODSs) and Related Chemicals, Chapter 1 in *Scientific Assessment of Ozone Depletion: 2010,*

Global Ozone Research and Monitoring Project–Report No. 52, 516 pp., World Meteorological Organization, Geneva, Switzerland, 2011.

Montzka, S. A., M. Krol, E. Dlugokencky, B. Hall, P. Jöckel, and J. Lelieveld, Small interannual variability of global atmospheric hydroxyl, *Science*, *331,* 67-69, 2011.

Moore, D. P., A. M. Waterfall, and J. J. Remedios, The potential for radiometric retrievals of halocarbon concentrations from the MIPAS-E instrument, *Adv. Space Res., 37*, 2238-2246, 2006.

Moore, F. L., J. W. Elkins, E. A. May, G. S. Dutton, R. E. Dunn, D. W. Fahey, R. J. McLaughlin, T. L. Thompson, P. A. Romashkin, D. F. Hurst, and P. R. Wamsley, Balloonborne *in situ* gas chromatograph for measurements in the troposphere and stratosphere, *J. Geophys. Res.*, *108* (D5), 8330, doi: 10.1029/2001JD000891, 2003.

Moore, R. M., W. Groszko, and S. J. Niven, Ocean-atmosphere exchange of methyl chloride: Results from NW Atlantic and Pacific Ocean studies. *J. Geophys. Res., 101,* 28529-28538, 1996.

Mühle, J., A. L. Ganesan, B. R. Miller, P. K. Salameh, C. M. Harth, B. R. Greally, M. Rigby, L. W. Porter, L. P. Steele, C. M. Trudinger, P. B. Krummel, S. O'Doherty, P. J. Fraser, P. G. Simmonds, R. G. Prinn, and R. F. Weiss, Perfluorocarbons in the global atmosphere: tetrafluoromethane, hexafluoroethane, and octafluoropropane, *Atmos. Chem. Phys.,* 10 (11), 5145-5164, *10.5194/*acp-10-5145-2010, 2010.

Naik, V., A. K. Jain, K. O. Patten, and D. J. Wuebbles, Consistent sets of atmospheric lifetimes and radiative forcings on climate for CFC replacements: HCFCs and HFCs, *J. Geophys. Res.*, *105* (D5), 6903-6914, doi: 10.1029/1999JD901128, 2000.

Nassar, R., P. F. Bernath, C. D. Boone, C. Clerbaux, P. F. Coheur, G. Dufour, L. Froidevaux, E. Mahieu, J. C. McConnell, S. D. McLeod, D. P. Murtagh, C. P. Rinsland, K. Semeniuk, R. Skelton, K. A. Walker, and R. Zander, A global inventory of stratospheric chlorine in 2004, *J. Geophys. Res.-Atmos., 111*, 13, doi: 10.1029/2006JD007073, 2006a.

Nassar, R., P. F. Bernath, C. D. Boone, S. D. McLeod, R. Skelton, and K. A. Walker, A global inventory of stratospheric fluorine in 2004 based on Atmospheric Chemistry Experiment Fourier transform spectrometer (ACE-FTS) measurements. *J. Geophys. Res.-Atmos., 111*, 10, 2006b.

Newland, M. J., C. E. Reeves, D. E. Oram, J. C. Laube, W. T. Sturges, C. Hogan, and P. J. Fraser, Southern hemispheric halon trends and global halon emissions, 1978-2011, submitted to *Atmos. Chem. Phys. Discuss.,* Sept., 2012.

Nightingale, R. W., Q. E. Roche, J. B. Kumer, J. L. Mergenthaler, J. C. Gille, S. T. Massie, P. L. Bailey, D. P. Edwards, M. R. Gunson, G. C. Toon, B. Sen, J.-F. Blavier, and P. S. Connell, Global CF_2Cl_2 measurements by UARS cryogenic limb array etalon spectrometer: Validation by correlative data and a model, *J. Geophys. Res.*, *101*, 9711-9736, 1996.

Oram, D. E., C. E. Reeves, S. A. Penkett, and P. J. Fraser, Measurements of HCFC−142b and HCFC−141b in the Cape Grim air Archive: 1978–1993, *Geophys. Res. Lett.*, *22* (20), 2741-2744, doi: 10.1029/95GL02849, 1995.

Oram, D. E., W. T. Sturges, S. A. Penkett, A. McCulloch, and P. J. Fraser, Growth of fluoroform (CHF_3, HFC−23) in the background atmosphere, *Geophys. Res. Lett.*, *25* (1), 35-38, doi: 10.1029/97GL03483, 1998.

Park, J. H., M. K. W. Ko, C. H. Jackman, R. A. Plumb, J. A. Kaye, and K. H. Sage, (Eds.), *Models and Measurements Intercomparison II*, Hampton, VA, National Aeronautics and Space Administration, 1999.

Park, S., E. L. Atlas, R. Jiménez, B. C. Daube, E. W. Gottlieb, J. Nan, D. B. A. Jones, L. Pfister, T. J. Conway, T. P. Bui, R.-S. Gao, and S. C. Wofsy, Vertical transport rates and concentrations of OH and Cl radicals in the Tropical Tropopause Layer from CO_2 and halocarbons, *Atmos. Chem. Phys. 10*, 6669, 2010.

Park, S. Y., E. L. Atlas, and K. A. Boering, Measurements of N_2O isotopologues in the stratosphere: Influence of transport on the apparent enrichment factors and the isotopologue fluxes to the troposphere, *J. Geophys. Res.*, *109*, D01305, doi: 10.1029/2003JD003731, 2004.

Pfeilsticker, K., W. T. Sturges, H. Bösch, C. Camy-Peyret, M. P. Chipperfield, A. Engel, R. Fitzenberger, M. Müller, S. Payan, and B.-M. Sinnhuber, Lower stratospheric organic and inorganic bromine budget for the Arctic winter 1998/99, *Geophys. Res. Lett.*, *27*(20), 3305-3308, doi: 10.1029/2000GL011650, 2000.

Plumb, I. C., P. F. Vohralik, and K. R. Ryan, Normalization of correlations for atmospheric species with chemical loss, *J. Geophys. Res., 104*, 11723-11732, 1999.

Plumb, R. A., A "tropical pipe" model of stratospheric transport, *J. Geophys. Res.*, *101*, 3957-3972, 1996.

Plumb, R. A., and M. K. W. Ko., Interrelationships between mixing ratios of long-lived stratospheric constituents, *J. Geophys. Res.*, *97*, 10145-10156, 1992.

Plumb, R. A., W. Heres, J. L. Neu, N. Mahowald, J. del Corral, G. C. Toon, E. Ray, F. Moore, and A. E. Andrews, Global tracer modeling during SOLVE: High latitude descent and mixing, *J. Geophys. Res., 107*, 8309, doi: 1029/2001JD01023, 2002 (printed 108, D5, 2003).

Prinn, R. G., R. Zander (Lead Authors), D. M. Cunnold, J. W. Elkins, A. Engel, P. J. Fraser, M. R. Gunson, M. K. W. Ko, E. Mahieu, P. M. Midgley, J. M. Russell III, C. M. Yolk, and R. F. Weiss, Long-lived ozone-related compounds, in D. L. Albritton, P. J. Aucamp, G. Mégie, and R. T. Watson, editors, *Scientific Assessment of Ozone Depletion, Global Ozone Research and Monitoring Project, Report No. 44*, Chapter 1, World Meteorological Organization, 1999.

Prinn, R. G., R. F. Weiss, P. J. Fraser, P. G. Simmonds, D. M. Cunnold, F. N. Alyea, S. O'Doherty, P. Salameh, B. R. Miller, J. Huang, R. H. J. Wang, D. E. Hartley, C. Harth, L. P. Steele, G. Sturrock, P. M. Midgley, and A. McCulloch, A history of chemically and radiatively important gases in air deduced from ALE/GAGE/AGAGE, *J. Geophys. Res.*, *115*, 17751-17792, doi: 10.1029/2000JD900141, 2000.

Prinn, R. G., J. Huang, R. F. Weiss, D. M. Cunnold, P. J. Fraser, P. G. Simmonds, A. McCulloch, C. Harth, P. Salameh, S. O'Doherty, R. H. Wang, L. Porter, and B. R. Miller. Evidence for substantial variations of atmospheric hydroxyl radicals in the past two decades, *Science, 292,* 1882-8, ISSN 0036-8075, doi: 10.1126/science.1058673. URL http://www.ncbi.nlm.nih.gov/pubmed/11337586, 2001.

Prinn, R. G., J. Huang, R. F. Weiss, D. M. Cunnold, P. J. Fraser, P. G. Simmonds, A. McCulloch, C. Harth, S. Reimann, P. Salameh, R. H. Wang, L. W. Porter,

B. R. Miller, and P. B. Krummel, Evidence for variability of atmospheric hydroxyl radicals over the past quarter century, *Geophys. Res. Lett., 32,* L07809, doi: 10.1029/2004GL022228, 2005.

Ray, E. A., F. L. Moore, J. W. Elkins, G. S. Dutton, D. W. Fahey, H. Vömel, S. J. Oltmans, and K. H. Rosenlof, Transport into the Northern Hemisphere lowermost stratosphere revealed by *in situ* tracer measurements, *J. Geophys. Res.*, *104* (D21), 26565-26580, 1999.

Ray, E. A., F. L. Moore, J. W. Elkins, D. F. Hurst, P. A. Romashkin, G. S. Dutton, and D. W. Fahey, Descent and mixing in the 1999–2000 northern polar vortex inferred from *in situ* tracer measurements, *J. Geophys. Res.*, *107*, doi: 10.1029/2001JD000961, 2002.

Reeves, C. E., Atmospheric budget implications of the temporal and spatial trends in methyl bromide concentration, *J. Geophys. Res.*, *108*, 4343, doi: 10.1029/2002JD002943, 2003.

Rhew, R. C., Sources and sinks of methyl bromide and methyl chloride in the tallgrass prairie: Applying a stable isotope tracer technique over highly variable gross fluxes, *J. Geophys. Res.*, *116* (G3), G03026, doi: 10.1029/2011jg001704, 2011.

Rhew, R. C., B. R. Miller, and R. F. Weiss, Natural methyl bromide and methyl chloride emissions from coastal salt marshes, *Nature*, *403* (6767), 292-295, 2000.

Rhew, R. C., B. R. Miller, M. K. Vollmer, and R. F. Weiss, Shrubland fluxes of methyl bromide and methyl chloride, *J. Geophys. Res., 106*, 20875-20882, 2001.

Rhew, R. C., B. R. Miller, and R. F. Weiss, Chloroform, carbon tetrachloride and methyl chloroform fluxes in southern California ecosystems, *Atmos. Environ.*, *42* (30), 7135-7140, doi: 10.1016/j.atmosenv.2008.05.038, 2008.

Richard, E. C., K. C. Aikin, A. E. Andrews, B. C. Daube, Jr., C. Gerbig, S. C. Wofsy, P. A. Romashkin, D. F. Hurst, E. A. Ray, F. L. Moore, J. W. Elkins, T. Deshler, and G. C. Toon, Severe chemical ozone loss inside the Arctic polar vortex during winter 1999-2000 inferred from *in situ* airborne measurements, *Geophys. Res. Lett.*, *28*, 2197-2200, doi: 10.1029/2001GL012878, 2001.

Riese, M., R. Sprang, P. Preusse, M. Ern, M. Jarisch, D. Offermann, and K. U. Grossmann, Cryogenic Infrared Spectrometers and Telescopes for the Atmosphere (CRISTA) data processing and atmospheric temperature and trace gas retrieval, *J. Geophys. Res.*, *104*, 16349-16367, 1999.

Rigby, M., R. G. Prinn, S. O'Doherty, S. A. Montzka, A. McCulloch, C. M. Harth, J. Mühle, P. K. Salameh, R. F. Weiss, D. Young, P. G. Simmonds, B. D. Hall, G. S. Dutton, D. Nance, D. J. Mondeel, J. W. Elkins, P. B. Krummel, L. P. Steele, and P. J. Fraser, Re-evaluation of the lifetimes of the major CFCs and CH_3CCl_3 using atmospheric trends,
Atmos. Chem. Phys., 13, 2691-2702, 2013.

Roche, A. E., R. W. Nightingale, J. B. Kumer, J. L. Mergenthaler, C. H. Jackman, and E. L. Fleming, Distribution and seasonal variation of CFCs in the stratosphere: Comparison of satellite global data and a 2-D model, *Adv. Space Res., 21*, 1383-1391, 1998.

Rottman, G. J., T. N. Woods, and W. McClintock, SORCE Solar UV Irradiance Results, *Adv. Space Res*., *37*, 2, 201-208, doi: 10.1016/j.asr.2005.02.072, 2006.

Sander, S. P., J. Abbatt, J. R. Barker, J. B. Burkholder, R. R. Friedl, D. M. Golden, R. E. Huie, C. E. Kolb, M. J. Kurylo, G. K. Moortgat, V. L. Orkin and P. H. Wine, *Chemical Kinetics and Photochemical Data for Use in Atmospheric Studies, Evaluation No. 17*, JPL Publication 10-6, Jet Propulsion Laboratory, Pasadena, http://jpldataeval.jpl.nasa.gov/, 2011.

Schauffler, S. M., E. L. Atlas, D. R. Blake, F. Flocke, R. A. Lueb, J. M. Lee-Taylor, V. Stroud, and W. Travnicek, Distributions of brominated organic compounds in the troposphere and lower stratosphere, *J. Geophys. Res.*, *104* (D17), 21513-21536, doi: 10.1029/1999JD900197, 1999.

Schauffler, S. M., E. L. Atlas, S. G. Donnelly, A. Andrews, S. A. Montzka, J. W. Elkins, D. F. Hurst, P. A. Romashkin, G. S. Dutton, and V. Stroud, Chlorine budget and partitioning during the Stratospheric Aerosol and Gas Experiment (SAGE) III Ozone Loss and Validation Experiment (SOLVE), *J. Geophys. Res.*, *108* (D5), 4173, doi: 10.1029/2001JD002040, 2003.

Schoeberl, M. R., A. R. Douglass, R. S. Stolarski, S. Pawson, S. E. Strahan, and W. Read, Comparison of lower stratospheric tropical mean vertical velocities, *J. Geophys. Res.*, *113,* D24109, doi: 10.1029/2008JD010221, 2008.

Sen, B., G. B. Osterman, R. J. Salawitch, G. C. Toon, J. J. Margitan, J.-F. Blavier, A. Y. Chang, R. D. May, C. R. Webster, R. M. Stimpfle, G. P. Bonne, P. B. Voss, K. K. Perkins, J. G. Anderson, R. C. Cohen, J. W. Elkins, G. S. Dutton, D. F. Hurst, P. A. Romashkin, E. L. Atlas, S. M. Schauffler, and M. Loewenstein, The budget and partitioning of stratospheric chlorine during the 1997 Arctic summer, *J. Geophys. Res., 104* (D21), 26653-26665, doi: 10.1029/1999JD900245, 1999.

Severinghaus, J. P., M. R. Albert, Z. R. Courville, M. A. Fahnestock, K. Kawamura, S. A. Montzka, J. Mühle, T. A. Scambos, E. Shields, C. A. Shuman, M. Suwa, P. Tans, and R. F. Weiss, Deep air convection in the firn at a zero-accumulation site, central Antarctica*, Earth and Planet. Sci. Lett.*, *293*, 359-367, 2010.

Shorter, J. H., C. E. Kolb, P. M. Crill, R. M. Kerwin, R. W. Talbot, M. E. Hines, and R. C. Harriss, Rapid degradation of atmospheric methyl bromide in soils, *Nature, 377*, 717-719, 1995.

Spackman, J. R., E. M. Weinstock, J. G. Anderson, D. F. Hurst, H.-J. Jost, and S. M. Schauffler, Aircraft observations of rapid meridional transport from the tropical tropopause layer into the lowermost stratosphere: Implications for midlatitude ozone, *J. Geophys. Res.*, *112*, D12308, doi: 10.1029/2006JD007618, 2007.

Spivakovsky, C. M., J. A. Logan, S. A. Montzka, Y. J. Balkanski, M. Foreman-Fowler, D. B. A. Jones, L. W. Horowitz, *et al.,* Three-dimensional climatological distribution of tropospheric OH: Update and evaluation, *J. Geophys. Res.*, *105* (D7), 8931-8980, doi: 10.1029/1999JD901006, 2000.

Sturges, W. T., D. E. Oram, L. J. Carpenter, A. Engel, and S. A. Penkett, Bromoform as a source of bromine to the stratosphere, *Geophys. Res. Lett., 27*, 2081-2084, 2000.

Sturges, W. T., H. P. McIntyre, S. A. Penkett, J. Chappellaz, J. Barnola, R. Mulvaney, E. Atlas, and V. Stroud, Methyl bromide, and other brominated methanes, and methyl iodide in polar firn air, *J. Geophys. Res., 106*, 1595-1606, 2001.

Toon, G. C., J.-F. Blavier, B. Sen, J. J. Margitan, C. R. Webster, R. D. May, D. W. Fahey, R. Gao, L. Del Negro, M. Proffitt, J. Elkins, P. A. Romashkin, D. F. Hurst, S. Oltmans,

E. Atlas, S. Schauffler, F. Flocke, T. P. Bui, R. M. Stimpfle, G. P. Bonne, P. B. Voss, and R. C. Cohen, Comparison of MkIV balloon and ER-2 measurements of atmospheric trace gases, *J. Geophys. Res.*, *104*, 26779-26790, 1999.

Trudinger, C. M., D. M. Etheridge, G. A. Sturrock, P. J. Fraser, P. B. Krummel, and A. McCulloch, Atmospheric histories of halocarbons from analysis of Antarctic firn air: Methyl bromide, methyl chloride, chloroform, and dichloromethane, *J. Geophys. Res.*, *109*, D22310, doi: 10.1029/2004JD004932, 2004.

Varner, R. K., P. M. Crill, and R. W. Talbot, Wetlands: A potentially significant source of atmospheric methyl bromide and methyl chloride, *Geophys. Res. Lett.*, *26* (16), 2433-2435, doi: 10.1029/1999gl900587, 1999.

Velazco, V. A., G. C. Toon, J.-F. L. Blavier, A. Kleinböhl, G. L. Manney, W. H. Daffer, P. F. Bernath, K. A. Walker, and C. Boone, Validation of the Atmospheric Chemistry Experiment by noncoincident MkIV balloon profiles, *J. Geophys. Res., 116,* D06306, doi: 10.1029/2010jd014928, 2011.

Volk, C. M., J. W. Elkins, D. W. Fahey, R. J. Salawitch, G. S. Dutton, J. M. Gilligan, M. H. Proffitt, M. Loewenstein, J. R. Podolske, K. Minschwaner, J. J. Margitan, and K. R. Chan, Quantifying transport between the tropical and midlatitude lower stratosphere, *Science, 272,* 1763-1768, 1996.

Volk, C. M., J. W. Elkins, D. W. Fahey, G. S. Sutton, J. M. Gilligan, M. Loewenstein, J. R. Podolske, K. R. Chan, and M. R. Gunson, Evaluation of source gas lifetimes from stratospheric observations, *J. Geophys. Res.*, *102* (D21), 25543-25564, 1997.

Wamsley, P. R., J. W. Elkins, D. W. Fahey, G. S. Dutton, C. M. Volk, R. C. Myers, S. A. Montzka, J. H. Butler, A. D. Clarke, P. J. Fraser, L. P. Steele, M. P. Lucarelli, E. L. Atlas, S. M. Schauffler, D. R. Blake, F. S. Rowland, W. T. Sturges, J. M. Lee, S. A. Penkett, A. Engel, R. M. Stimpfle, K. R. Chan, D. K. Weisenstein, M. K. W. Ko, and R. J. Salawitch, Distribution of halon-1211 in the upper troposphere and lower stratosphere and the 1994 total bromine budget, *J. Geophys. Res, 103*, 1513-1526, 1998.

Wang, H. J., D. M. Cunnold, L. Froidevaux, and J. M. Russell, A reference model for middle atmosphere ozone in 1992-1993, *J. Geophys. Res.*, *104*, 21629-21643, 1999.

Watling, R., and D. B. Harper, Chloromethane production by wood-rotting fungi and an estimate of the global flux to the atmosphere, *Mycol. Res.*, *102* (7), 769-787, 1998.

Werner, A., C. M. Volk, E. V. Ivanova, T. Wetter, C. Schiller, H. Schlager, and P. Konopka, Quantifying transport into the Arctic lowermost stratosphere, *Atmos. Chem. Phys.*, *10*, 11623-11639, www.atmos-chem-phys.net/10/11623/2010/, doi: 10.5194/acp-10-11623-2010, 2010.

WMO, *Scientific Assessment of Ozone Depletion: 1998, Global Ozone Research and Monitoring Project–Report No. 44*, Geneva, Switzerland, 1999.

WMO, *Scientific Assessment of Ozone Depletion: 2002, Global Ozone Research and Monitoring Project–Report No. 47*, 498 pp., Geneva, Switzerland, 2003.

WMO, *Scientific Assessment of Ozone Depletion: 2006, Global Ozone Research and Monitoring Project - Report No. 50*, Geneva, Switzerland, 2007.

WMO, *Scientific Assessment of Ozone Depletion: 2010, Global Ozone Research and Monitoring Project - Report No. 52*, 516 pp., Geneva, Switzerland, 2011.

Xiao, X., R. G. Prinn, P. J. Fraser, R. F. Weiss, P. G. Simmonds, S. O'Doherty, B. R. Miller, P. K. Salameh, C. M. Harth, P. B. Krummel, A. Golombek, L. W. Porter, J. H. Butler, J. W. Elkins, G. S. Dutton, B. D. Hall, L. P. Steele, R. H. J. Wang, and D. M. Cunnold, Atmospheric three-dimensional inverse modeling of regional industrial emissions and global oceanic uptake of carbon tetrachloride, *Atmos. Chem. Phys.*, *10* (21), 10421-10434, doi: 10.5194/acp-10-10421-2010, 2010a.

Xiao, X., R. G. Prinn, P. J. Fraser, P. G. Simmonds, R. F. Weiss, S. O'Doherty, B. R. Miller, P. K. Salameh, C. M. Harth, P. B. Krummel, L. W. Porter, J. Mühle, B. R. Greally, D. Cunnold, R. Wang, S. A. Montzka, J. W. Elkins, G. S. Dutton, T. M. Thompson, J. H. Butler, B. D. Hall, S. Reimann, M. K. Vollmer, F. Stordal, C. Lunder, M. Maione, J. Arduini, and Y. Yokouchi, Optimal estimation of the surface fluxes of methyl chloride using a 3-D global chemical transport model, *Atmos. Chem. Phys.*, *10*, 5515-5533, doi: 10.5194/acp-10-5515-2010, 2010b.

Yokouchi, Y., T. Machida, L. A. Barrie, D. Toom-Sauntry, Y. Nojiri, Y. Fujinuma, Y. Inuzuka, H. Li, H. Akimoto, and S. Aoki, Latitudinal distribution of atmospheric methyl bromide: Measurements and modeling, *Geophys. Res. Lett., 27* (5), doi: 10.1029/1999GL010884, 2000.

Yvon, S. A., and J. H. Butler, An improved estimate of the oceanic lifetime of atmospheric CH3Br, *Geophys. Res. Lett., 23,* (1), 53-56, 1996.

Yvon-Lewis, S. A., and J. H. Butler, The potential effect of oceanic biological degradation on the lifetime of atmospheric CH_3Br, *Geophys. Res. Lett.*, *24* (10), 1227-1230, 1997.

Yvon-Lewis, S. A., and J. H. Butler, Effect of oceanic uptake on atmospheric lifetimes of selected trace gases, *J. Geophys. Res.-Atmos.*, *107* (D20), 2002.

Yvon-Lewis, S. A., E. S. Saltzman, and S. A. Montzka, Recent trends in atmospheric methyl bromide: Analysis of post-Montreal Protocol variability, *Atmos. Chem. Phys.*, *9* (16), 5963-5974, 2009.

Zander, R., C. P. Rinsland, C. B. Farmer, and R. H. Norton, Infrared spectroscopic measurements of halogenated source gases in the stratosphere with the ATMOS instrument, *J. Geophys. Res.*, *92*, 9836-9850, 1987.

CHAPTER 5

Model Estimates of Lifetimes

Lead Authors:
Martyn Chipperfield
Qing Liang

Co-Authors:
Luke Abraham
Slimane Bekki
Peter Braesicke
Sandip Dhomse
Glauco Di Genova
Eric L. Fleming
Steven Hardiman
Daniela Iachetti
Charles H. Jackman
Douglas E. Kinnison
Marion Marchand
Giovanni Pitari
Eugene Rozanov
Andrea Stenke
Fiona Tummon

Contributors:
Jérémie Burgalat
David Cugnet
Stacey M. Frith
Charlotte Pascoe
Matthew Rigby

CHAPTER 5

Model Estimates of Lifetimes

Contents

5.1 Introduction

We discuss how to use three-dimensional (3-D) Chemistry Climate Model (CCM) simulations to estimate atmospheric lifetimes of trace gases, their variability and trends, and to understand the controlling chemical and dynamical processes. We examine the model-estimated lifetimes and uncertainties in the context of the empirically derived values (Chapter 4) and uncertainty estimates in kinetics (Chapter 3). One advantage of CCMs is that they provide a useful tool to extend our current knowledge into the future to quantify how lifetimes will change in a future climate with a recovering ozone layer and a changing circulation and oxidation capacity – processes that are key in determining the lifetimes of Ozone Depleting Substances (ODSs).

The abundance of a species in the atmosphere depends on its rate of emission and its rate of chemical (and/or physical) loss, i.e., its lifetime. CCMs participating in current ozone assessment efforts use mixing ratio boundary conditions (MBC) to simulate the evolution of ODSs and greenhouse gases (GHGs) in the atmosphere, by prescribing surface concentration scenarios at the lowest model layer. Estimated lifetimes are used to predict the rate at which ODSs and GHGs will be removed from the atmosphere, and therefore scenarios used for modelling the future atmosphere. These boundary conditions largely control the time evolution of the atmospheric burden of the source gases, therefore impacting projections for the recovery of the ozone layer. They also affect projections of radiative forcing and climate change. Over the past few years significant doubts have been raised over some of the tabulated lifetimes of major ODSs provide in, for example, World Meteorological Organization/United Nations Environment Programme (WMO/UNEP) Assessments (e.g., Douglass *et al*., 2008; Liang *et al*., 2008). CCMs provide an essential tool, with which we can examine the consistency between annual change in the integrated atmospheric amount, the computed atmospheric loss and the input of ODSs to the atmosphere implied by the MBCs. We can also use CCMs to investigate differences that arise from using flux boundary conditions (FBCs) to specify the input of ODSs and GHGs.

Various definitions of lifetime have been introduced in Chapter 2. The model-calculated lifetime depends on input boundary conditions. In a simulation with time-dependent boundary conditions, dividing the atmospheric abundance of a trace gas by its atmospheric loss yields the instantaneous atmospheric lifetime. This lifetime can differ from the lifetime derived in steady-state conditions when the surface flux (implied by MBC or specified by FBC) is balanced by atmospheric removal. We will use two types of model simulations, transient and steady-state (timeslice) runs, and auxiliary ODS tracers to discuss the difference and connection between instantaneous lifetime and steady-state lifetime, as well as the impact of trends and atmospheric distributions on lifetime.

The atmospheric partial lifetime, τ_{atmos}, of a trace gas is calculated in a model using the globally integrated sum of its loss rate at all locations weighted by the local number density. Note that except for species that have surface losses, i.e., CCl_4, CH_3CCl_3, CH_4, CH_3Cl, CH_3Br, the atmospheric partial lifetime τ_{atmos} is the equivalent of global atmospheric lifetime τ for the majority of the species assessed in this report. Aside from uncertainty associated with kinetic rates (as discussed in Chapter 3), uncertainty in lifetime estimates can also arise from variations in representing transport and chemical processes in a model. For stratospheric removal (SR) species that are removed mainly by ultraviolet (UV) photolysis with maximum loss in the stratosphere, their lifetimes depend not only on the photolysis rate, but are also affected by how fast the atmospheric circulation moves air through the maximum

loss region. The destruction of tropospheric removal (TR) species is dominated by reaction with hydroxyl radical (OH) with the majority of the loss in the troposphere within 30°N/S of the equator. Therefore, species in each group require different validation of the mechanisms for their atmospheric removal.

We present lifetime estimates from six CCMs and one two-dimensional (2-D) model from groups worldwide (Table 5.1) for present day and 2100 conditions. The CCMs participated in the Chemistry-Climate Model Validation Activity (CCMVal) for the WCRP's (World Climate Research Programme) SPARC (Stratospheric Processes and their Role in Climate) Project (Eyring *et al.,* 2005) and so the key processes which impact lifetimes (e.g., photolysis, stratospheric circulation) have already been evaluated extensively (e.g., Waugh and Eyring, 2008; Morgenstern *et al.,* 2010; Butchart *et al.,* 2011; SPARC CCMVal, 2010). CCMVal has provided a framework for model evaluation and a focus of ongoing model improvement by research groups. For the lifetime assessment, we will focus on processes of particular relevance to model estimates of ODS lifetimes and evaluate CCMs in three major areas (i) photolysis, (ii) thermal reactions, (iii) atmospheric transport to address how differences in dynamical and photochemical processes in various models influence their lifetime estimates.

We aim to provide the best model lifetime estimates for the present day as well as to quantify how future climate change may affect these lifetimes. The remainder of this chapter is structured to cover three main areas: (i) experiment design, (ii) model evaluation, and (iii) lifetime estimates. Section 5.2 describes how simulations for the lifetime experiments are formulated. The main results of model evaluation are contained in Section 5.3. Section 5.4 discusses our model-based estimates of the lifetimes based on different model experiments and tracers. Section 5.5 discusses our results and Section 5.6 contains our summary and recommendations.

5.2 Model Descriptions and Experiments

This section summarizes the details of the participating models and describes the experiments performed.

5.2.1 Participating Models

Lifetime calculations in this chapter are conducted using results from six three-dimensional (3-D) CCMs and one two-dimensional CCM, GSFC2D (Chapter 3). The GSFC2D serves as a bridge between Chapter 3 and Chapter 5 to examine (i) how well does the GSFC2D performance compare with the 3-D models, and (ii) how should the uncertainty in kinetics derived in Chapter 3 be translated into 3-D CCM calculated atmospheric lifetimes. Model simulations conducted for this assessment used the same kinetic recommendations from JPL 10-6 (Sander *et al*., 2011) and are driven with the same surface GHG and ODS boundary conditions, and sea surface temperatures (except GSFC2D – see Appendix A). However, models differ in dynamical schemes, e.g., advection, convection, cloud parameterisation, as well as the inclusion of various atmospheric processes, e.g., solar cycle, quasi-biennial oscillation (QBO). In this chapter we attribute the differences in model-calculated lifetimes to variances due to model transport. A short description of each 3-D CCM model and the GSFC2D model is given in Appendix A (Section 5.7). The six 3-D CCMs contributing results to this chapter all participated in SPARC CCMVal-2. The report from this activity, SPARC CCMVal (2010), provides a detailed description of these models and contains a

detailed process-based evaluation. Here we concentrate mostly on evaluation of chemical and dynamical aspects critical to lifetime calculations.

Table 5.1. List of CCMs and 2-D model contributing to this chapter.

Model	Institutes	Researchers	Reference
GEOSCCM	NASA GSFC, USA	Q. Liang A.R. Douglass S. Frith	Pawson *et al.* (2008)
GSFC2D	NASA GSFC, USA	E. Fleming C. Jackman	Fleming *et al.* (2011)
LMDZrepro	CNRS, France	S. Bekki M. Marchand J. Burgalat D. Cugnet	Jourdain *et al*. (2008)
SOCOL	PMOD-WRC, ETH, Switzerland	E. Rozanov A. Stenke F. Tummon	Egorova *et al.* (2005)
UMUKCA	U. Cambridge, UK Met Office, UK U. Leeds, UK	P. Braesicke N.L. Abraham J.A. Pyle S. Hardiman N. Butchart S. Dhomse	Morgenstern *et al.* (2009)
ULAQ	U. L'Aquila, Italy	G. Pitari D. Iachetti G. Di Genova E. Mancini	Pitari *et al.* (2002)
WACCM	NCAR, USA	D. Kinnison	Garcia *et al.* (2007)

5.2.2 Description of Lifetime Experiments

We use a number of model simulations and types of tracers to investigate the relationships between surface fluxes, atmospheric burden, removal rates and lifetime.

5.2.2.1 Model Simulations

The model simulations considered here consist of a transient simulation from 1960-2010 (TRANS) and two timeslice simulations with 2000 conditions (TS2000) and 2100 conditions (TS2100) to calculate present-day and future lifetimes, respectively. Simulations TRANS and TS2000 allow us to compare lifetimes calculated in a full transient experiment with a steady-state experiment. All models participating in the lifetime assessment were required to use the same mixing boundary conditions for greenhouse gases from Coupled Model Intercomparison Project (CMIP) Representative Concentration Pathways (RCP) Scenario 4.5, ODSs according to WMO (2011), and HFCs based primarily on Velders *et al.* (2009). All model simulations used in this chapter, including the GSFC2D simulations, were conducted with the same chemical kinetics and photolysis rates recommended by JPL 10-6 (Sander *et al*., 2011). Note that some differences may arise due to ambiguity in JPL recommendations. Sea surface temperatures and sea ice concentrations in all six 3-D CCMs are prescribed as

monthly mean boundary conditions following the global sea ice concentration and sea surface temperature (HadISST1) data set provided by the UM Met Office Hadley Centre (Rayner *et al.*, 2003). We present here a brief description of simulation setup for this assessment. For more detailed information about model simulations see Appendix B and the individual model descriptions for any deviations from the prescribed setup in Appendix A.

TRANS is a 50-year transient run from 1960 to 2010, based on the definition of the REF-B1 simulation used in CCMVal-2 (SPARC CCMVal, 2010, Chapter 2). It is important to point out that while REF-B1 was a transient simulation with stratosphere-only chemistry schemes, the TRANS simulations from four (SOCOL, ULAQ, WACCM, UMUKCA) of the six 3-D CCMs were run with stratosphere-troposphere coupled chemistry. All forcings in this simulation are taken from observations, and are mostly identical to those described by Eyring *et al.* (2006) and Morgenstern *et al.* (2010) for REF-B1. This transient simulation includes all anthropogenic and natural forcings based on changes in trace gases, solar variability, volcanic eruptions, quasi-biennial oscillation (QBO), and sea surface temperatures/sea ice concentrations (SSTs/SICs). Models that do not include a detailed tropospheric chemistry scheme prescribed their tropospheric OH values to the 3-D monthly OH documented in Spivakovsky *et al.* (2000). For models that have coupled stratosphere-troposphere chemistry schemes, emissions of ozone and aerosol precursors are from the RCP 4.5 Scenario (Lamarque *et al.*, 2011).

TS2000 is a 30-year timeslice simulation for 2000 conditions, designed to diagnose steady-state lifetimes and to facilitate the comparison of model output against constituent observations from various measurement datasets. This simulation is conducted with prescribed GHG, ODS, and HFC surface boundary conditions for 2000, but individual models were run with either repeating or interannually varying solar variability, volcanic eruptions, quasi-biennial oscillation (QBO), and sea surface temperatures/sea ice concentrations (SSTs/SICs) for 2000 conditions. In general the final 20 years are used for analysis.

TS2100 is a 30-year timeslice simulation, driven with 2100 conditions, to diagnose steady-state lifetimes in a future climate with a recovered stratospheric ozone layer and a faster Brewer-Dobson circulation. This simulation was conducted with prescribed GHG, ODS, and HFC surface boundary conditions for 2100, but individual models were ran with either repeating or interannually varying solar variability, quasi-biennial oscillation (QBO), and sea surface temperatures/sea ice concentrations (SSTs/SICs) for 2100 conditions. In general the final 20 years are used for analysis.

One of the key factors dominates the lifetime of TR species is the tropospheric OH abundance. OH is produced in the troposphere mainly through reaction of $O(^1D)$ with H_2O with photodissociation of acetone, peroxides, carbonyls and HONO being important in particular regions (IPCC, 2007). The local abundance of OH involves most of the fast photochemistry in the troposphere and is controlled by a delicate balance between its sources and sinks. The concentration of OH responds to changes in tropospheric carbon monoxide (CO), methane (CH_4), water (H_2O), ozone (O_3), nitrogen oxides (NO_x), as well as overhead O_3 column (e.g., Spivakovsky *et al.,* 2000). The seven models participating in this assessment can be divided into three groups depending upon how tropospheric OH is treated. Models that do not include a detailed tropospheric chemistry scheme, GEOSCCM and GSFC2D, prescribed their tropospheric OH with a recommended 3-D monthly values documented in Spivakovsky *et al.* (2000). SOCOL, ULAQ, UMUKCA, and WACCM have

fully coupled stratosphere-troposphere chemistry schemes and calculate interactive OH in the troposphere. Although tropospheric OH in LMDZrepro is forced with OH taken from a full-chemistry simulation of the TOMCAT 3-D tropospheric CTM (Savage *et al.,* 2004), chemical loss of ODSs is not calculated below 400 hPa. Therefore, we exclude LMDZrepro in the lifetime calculation for all TR species. A detailed evaluation of the performance of CCMs in tropospheric chemistry has yet to be conducted in the ongoing SPARC Chemistry-Climate Modelling Initiative (CCMI). A full evaluation of modelled OH and the related fast photochemistry is beyond the scope of this assessment and difficult due to a shortage of OH observations. In this assessment, we only seek to demonstrate how ranges in simulated OH abundance in models can impact the uncertainty in lifetimes of TR species. In addition, we seek to use CCMs to address how tropospheric OH responds to climate changes under 2100 conditions, including a recovered stratospheric O_3 layer, changes in CH_4 and H_2O, as well as changes in cloudiness. Therefore, models that calculate interactive tropospheric OH were asked to use the same NO_x and non-methane hydrocarbon emissions in TS2100 as TS2000. This chapter also examines how changes in kinetic losses rates due to increasing atmospheric temperature in 2100 impact the lifetime of TR species.

5.2.2.2 Auxiliary ODS tracers

Two additional sets of ODS tracers are embedded in the CCM simulations, but uncoupled from the full chemistry scheme. One set of tracers is calculated with realistic surface emission flux boundary conditions (FBC) and the other with prescribed constant boundary conditions (CONST). Although the FBC and CONST tracers are driven with different boundary conditions, they are destroyed in the atmosphere with the same kinetics as the corresponding full chemistry MBC tracers. Note that potential biases in simulated FBC concentrations do not affect the simulated ozone layer through modified ozone depletion.

FBC tracers. For four high priority species that have ready-to-use bottom up emission estimates, we include their FBC tracers in the CCM simulations: $CFCl_3$(CFC-11)_FBC, CF_2Cl_2(CFC-12)_FBC, CH_3CCl_3_FBC, $CHClF_2$(HCFC-22)_FBC. These FBC tracers are initialised with similar conditions to the MBC tracers at the start of the simulation and evolve with geographically resolved surface emission fluxes released and atmospheric losses via photolysis and thermal reactions with atomic oxygen (first excited state, $O(^1D)$) and OH.

***CONST tracer*s**. Five constant tracers are embedded in the simulations: CFC-11_CONST, CFC-12_CONST, N_2O_CONST, CH_3CCl_3_CONST, and CH_4_CONST. These tracers are lost with the same kinetics as the MBC tracers but have a prescribed constant 100 pptv surface boundary condition.

We use the combination of MBC, FBC, and CONST tracers from the same model runs to examine how surface emission trends, atmospheric abundance and trace gas distribution impact atmospheric lifetime.

5.3 Model Evaluation and Analysis

To illustrate the importance of chemical loss in different regions, Figure 5.1 shows the annually averaged zonal mean loss rates of six ODSs with lifetimes ranging from ~5 years (methyl chloroform (CH_3CCl_3)) to ~120 years (nitrous oxide (N_2O)). CFC-11, CFC-12, and N_2O are SR species with chemical loss occurring solely in the stratosphere. The shorter lived of these (CFC-11) is destroyed lower in the stratosphere compared to the longer-lived species

CFC-12 and N_2O. Although $CBrClF_2$ (Halon-1211) is also primarily destroyed via photolysis, the majority of its loss occurs in the troposphere as it can be removed by photolysis at UV wavelengths up to 320 nm. CH_4 and CH_3CCl_3 are TR species with most of their loss occurring in the troposphere. There are small contributions from stratospheric loss, more so in the case of CH_3CCl_3. For all species, about 75-95% of the atmospheric removal occurs between 60°N-60°S with >50% of the loss occurring in the tropics (within 30° of the equator). Therefore, in this chapter, we focus mainly on model intercomparison and evaluation in the tropical region.

5.3.1 PhotoComp Results

SPARC CCMVal (2010) described the experiments and results from 'PhotoComp 2008', an off-line photolysis rate intercomparison for the CCMVal-2 CCMs. Photolysis is one of the most important processes included in a CCM and is critical for an accurate assessment of the lifetime of most of the species considered in this report. PhotoComp 2008 was a systematic evaluation of the photolysis codes as used in the CCMs by comparison with standalone reference models.

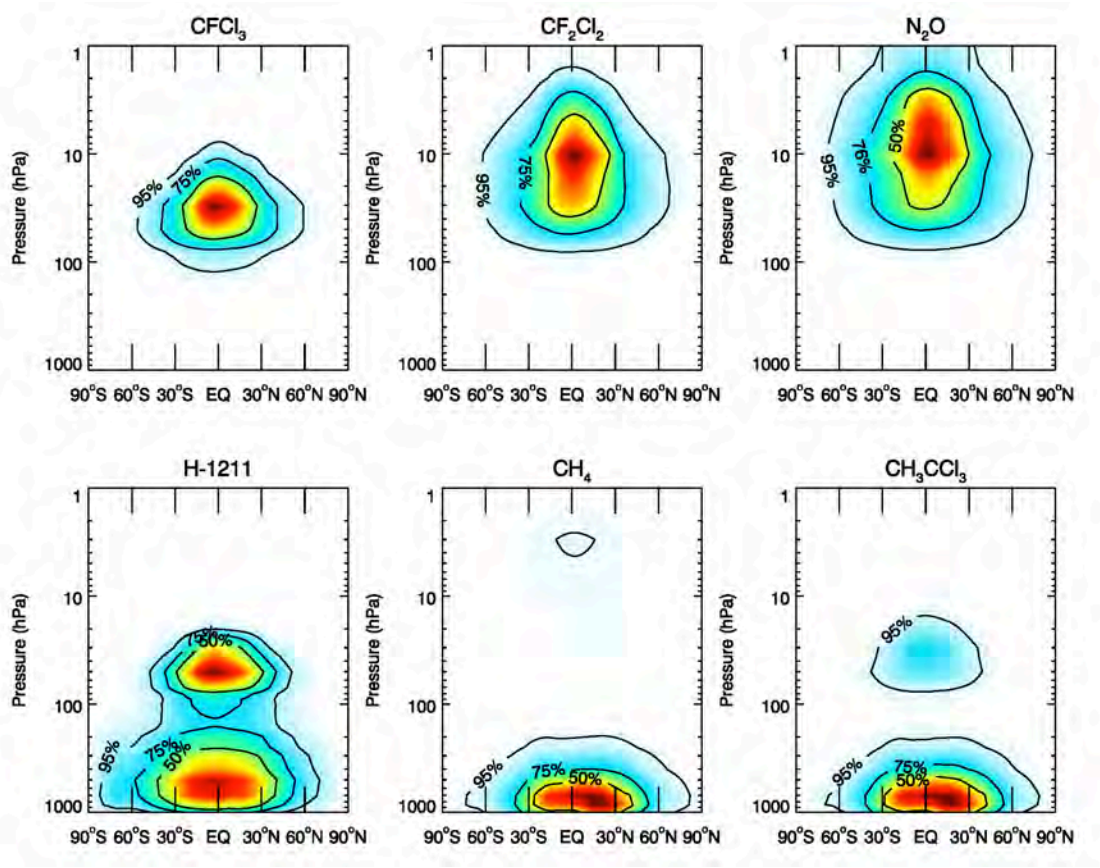

Figure 5.1. Example latitude-pressure cross sections of zonally integrated annual loss rates of $CFCl_3$, CF_2Cl_2, N_2O, Halon-1211, CH_4 and CH_3CCl_3 between 2000-2005 from the WACCM TRANS simulation, with warm colours indicating faster loss rates. The solid contours outline the regions within which 95%, 75% and 50% of the loss occurs.

Not all of the CCMVal-2 CCMs participated in PhotoComp 2008. Only 8 out of the 17 CCMs were able to take part, along with some reference codes. In terms of the models contributing to this assessment the list included GEOSCCM, LMDZrepro, SOCOL, and WACCM. Therefore, a key process for the evaluation of atmospheric lifetimes remained unevaluated for some models participating here. The PhotoComp tests have now been applied to the remaining 3-D models used here (see below).
The CCMs that did participate in PhotoComp 2008 showed a wide range of skill in calculating photolysis rates (SPARC CCMVal (2010) Figure 6-6). GEOSCCM, LMDZrepro and WACCM were consistently in the 0.9 – 1.0 (90-100%) range. NIWA-SOCOL and SOCOL had some occasional problems that could be due either to the radiative transfer solutions or to cross-section implementations.

PhotoComp 2011

The CCMVal project aimed at producing methods for evaluating models that could be archived and returned to in the future as models improve. In this spirit we have used the procedure for PhotoComp 2008 and used it to run new tests for models that did not participate as part of CCMVal-2. This updated intercomparison, PhotoComp 2011, involved the models listed in Table 5.2.

There were three parts to the PhotoComp 2008 photolysis comparison that are described in detail in Chapter 6 of SPARC CCMVal (2010). Parts 1 and 2 have been used for PhotoComp 2011. Briefly, these experiments are:

Part 1 is a basic test of all J-values for high sun (SZA = 15°) over the ocean (albedo = 0.10, Lambertian). Part 1a: Clear sky (only Rayleigh scattering) and no aerosols. Part 1b: Pinatubo aerosol in the stratosphere. Part 1c: Stratus cloud in the troposphere. The primary atmosphere was specified in terms of pressure layers, mean temperature, and column O_3 in each layer. Absorption by NO_2 or other species was not included in calculating optical depths.

Table 5.2. Models contributing to CCMVal PhotoComp 2011. The six CCMs are indicated in bold. Italics indicate new participants compared to PhotoComp 2008.

Group	Model	Label	P1a	P1b	P1c	P2a	P2n	P2m	P3	Participants
GSFC, USA	FastJX	GFJX	√	√	√	√	√	√	√	H. Bian
GSFC, USA	**GEOSCCM**	GEOS	√			√	√	√		R. Kawa R. Stolarski
CNRS, France	**LMDZrepro** (TUV4.1)	LMDZ	√	√	√	√	√	√	√	S. Lefebvre S. Bekki
PMOD-WRC / ETH, CH NIWA, NZ	**SOCOL**	SOCOL	√		√	√	√	√		F. Tummon D. Smale E. Rozanov
UCI, USA	FastJX & UCIref	UCIJ UClr	√	√	√	√	√	√	√	M. Prather
U. L'Aquila	***ULAQ***	*ULAQ*	√	√	√	√	√	√	√	G. Pitari G. Di Genova D. Iachetti
U. Cambridge Met Office	***UMUKCA***	*UKCA*	√			√	√	√		P. Braesicke P. Telford
NCAR, USA	**WACCM**	WACC	√			√	√	√	√	D. Kinnison

Part 2 tests the simulation of a spherical atmosphere and twilight conditions that are critical to the polar regions. It used the same atmosphere as Part 1 without clouds or aerosols and assumed equinox (solar declination = 0°) and latitude of 84°N. The surface SZA (not including refraction) therefore varies from 84º (noon) to 96° (midnight). J-values were reported at noon, midnight, and the 24-hour average (integrating as done in the CCM).

Figures 5.2 and 5.3 show results for species relevant to this lifetimes assessment from PhotoComp 2011 for Part 1a and Part 2 (84^{o}), respectively. The plots show results from the six CCMs listed in Table 5.2, along with three of the reference models used in PhotoComp 2008 between 100 hPa and 1 hPa, a key region of loss for most stratospheric removed species considered here. Overall the level of agreement in the photolysis rates shown is good and the model-model spread is significantly less than seen in SPARC CCMVal (2010). This is due to the iterative improvement in some of the models shown and the removal of some of the outlying models from CCMVal-2. For the high priority species it is interesting to note that the spread in the J rates for CFC-12 is larger than for CFC-11, where the models show an extremely good level of agreement. Other species for which there is a relatively large spread in J rates in the upper stratosphere include HCFC-22, CCl_2FCClF_2 (CFC-113) and CH_3Cl (HCC-40). For the species that are photolysed at short wavelengths, SOCOL produces J rate profiles that tend to differ from other models. Their photolysis rates of CFC-12 and N_2O carry on increasing significantly with height at the top of the region studied (0.01 hPa, not shown). At lower altitudes the agreement is better, but SOCOL does underestimate the photolysis rate of CF_3CClF_2 (CFC-115) and, to some extent, N_2O in the middle stratosphere compared to other models.

Overall, these results show that the models used in this report to evaluate lifetimes calculate accurate and consistent photolysis rates thereby increasing confidence in the model results.

5.3.2 Fast Chemistry Evaluation

No new evaluation of the fast chemistry in the models has been performed for this report. Therefore, we summarize how the participating models performed in the SPARC CCMVal (2010). WACCM was among the group of models that performed very well in the tests using a Photochemical Steady-State (PSS) model to evaluate the models' radical chemistry. GEOSCCM also scored relatively well, giving confidence in the formulation of the model. LMDZrepro and UMUKCA obtained marks in the middle of the range of CCMs. Overall the ULAQ and SOCOL models did not score so highly at that time. However, these two models have been updated since CCMVal-2 (see Appendix A) and so we would expect improvements.

5.3.3 Model Circulation Tests: Mean Age and Comparison with Observations

Figures 5.4 and 5.5 show the stratospheric modelled age-of-air from the CCMs used in this report for 2000 conditions and comparison with values derived from balloon and aircraft observations. For the analysis here the modelled age was set to zero at the tropical tropopause. This procedure had the largest impact on UMUKCA which otherwise produced a tropopause age with a value of around 0.5 years; the shift of reference for the other models was smaller than this. In the lower stratosphere (50 hPa) the CCMs tend to agree well with each other and with the observed variation in age from the tropics to the poles. One exception is SOCOL, which produces mean age-of-air about 1 year younger than the

observations at high latitudes. The models show a large variation in age in the mid and upper stratosphere. At around 50 km SOCOL, WACCM, LMDZrepro, GEOSCCM and UMUKCA produce ages that are 1-2 years younger than ULAQ and GSFC2D. The balloon observations used in Figure 5.5 only provide data up to ~30km but tend to show the models with the older ages are more realistic. Figure 5.5 also shows the gradient in mean age between the northern mid-latitudes and the tropics. This diagnostic tests the recirculation rate of air in the tropical upwelling and mid-latitude downwelling branches of the Brewer-Dobson circulation. The Brewer Dobson circulation itself has transition, shallow and deep branches with vertical ranges of 100-70, 70-30 and above 30 hPa, respectively (Lin and Fu, 2013). ULAQ and UMUKCA have the strongest gradients in mean age and these correspond well with observations. GEOSCCM, GSFC2D, LMDZrepro and WACCM have gradients which are slightly too weak while in SOCOL the gradient is far too week. Overall these results show that ULAQ, GEOSCCM, GSFC2D, LMDZrepro and WACCM have reasonable circulations. UMUKCA appears to have a slow stratospheric circulation, but the slow recirculation into the tropics maintains the young age there. In SOCOL the circulation is too fast.

5.3.4. Online Chemical Diagnostics

The rates of chemical processes which lead to the loss of ODS in the atmosphere have been compared in the lifetime experiments. The fluxes through photolysis, OH and $O(^1D)$ reactions were archived and are intercompared here.

To illustrate the skill of each model in simulating the vertical distribution of species which are factored into the loss rates, we compare ODS vertical profiles with balloon and satellite measurements (Figures 5.6 and 5.7). Figure 5.6 compares the tropical vertical profiles of CFC-11, CFC-12, N_2O, and CH_4 with the annual mean climatology from the Atmospheric Chemistry Experiment (ACE) satellite measurements. Figure 5.7 compares the vertical profiles of CFC-11, CFC-12, N_2O, CH_4, and Halon-1211 with three balloon measurements collected at Ft. Sumner (34.5^{o}N, 104.2^{o}W) in October 2002, September 2003 and 2004. All seven models capture the observed vertical gradients fairly well. The SOCOL model shows consistently higher concentrations in the stratosphere than the other models for all species. This implies more efficient transport of ODSs from the tropical tropopause entrance to the mid and upper stratosphere where maximum loss of the long-lived ODSs occurs, consistent with the younger age-of-air in this model. The UMUKCA model in general performs well, but shows higher CFC-12 and N_2O in the tropical middle stratosphere, related to a weak circulation. Halon-1211 in the UMUKCA model is notably lower than the other models throughout most of the troposphere and stratosphere. For Halon-1211 that has significant removal in the troposphere, such a bias is consistent with the model's (unadjusted) age-of-air being too old at the tropical tropopause.

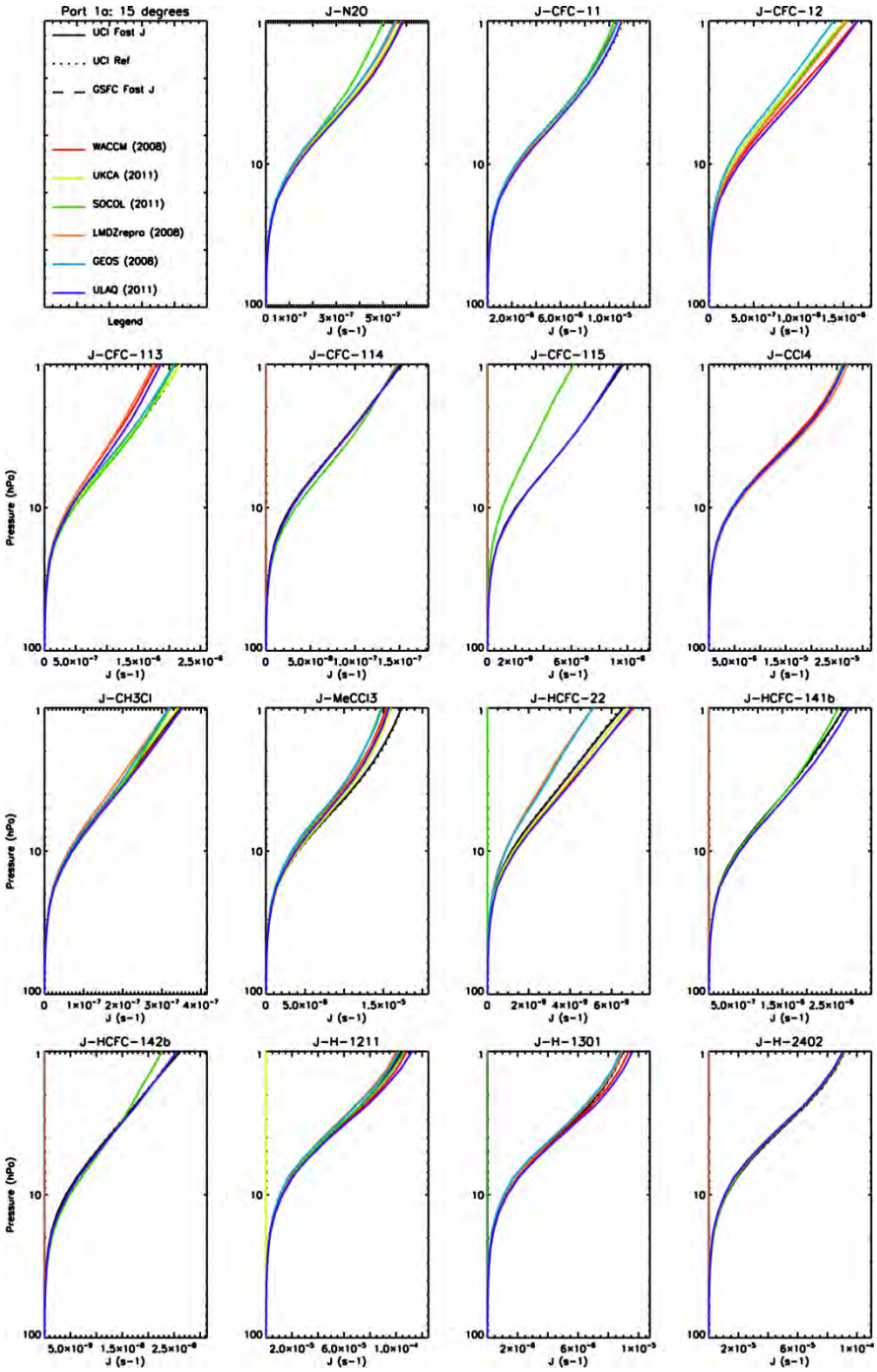

Figure 5.2. Comparison of modelled photolysis rates at 15° (PhotoComp 2011 Part 1a) between 100 hPa and 1 hPa from the WACCM, UMUKCA, GEOSCCM, SOCOL, LMDZrepro and ULAQ CCMs used in this report and 3 reference models from SPARC CCMVal (2010). Note that not all models show results for all species. GSFC2D did not perform PhotoComp tests.

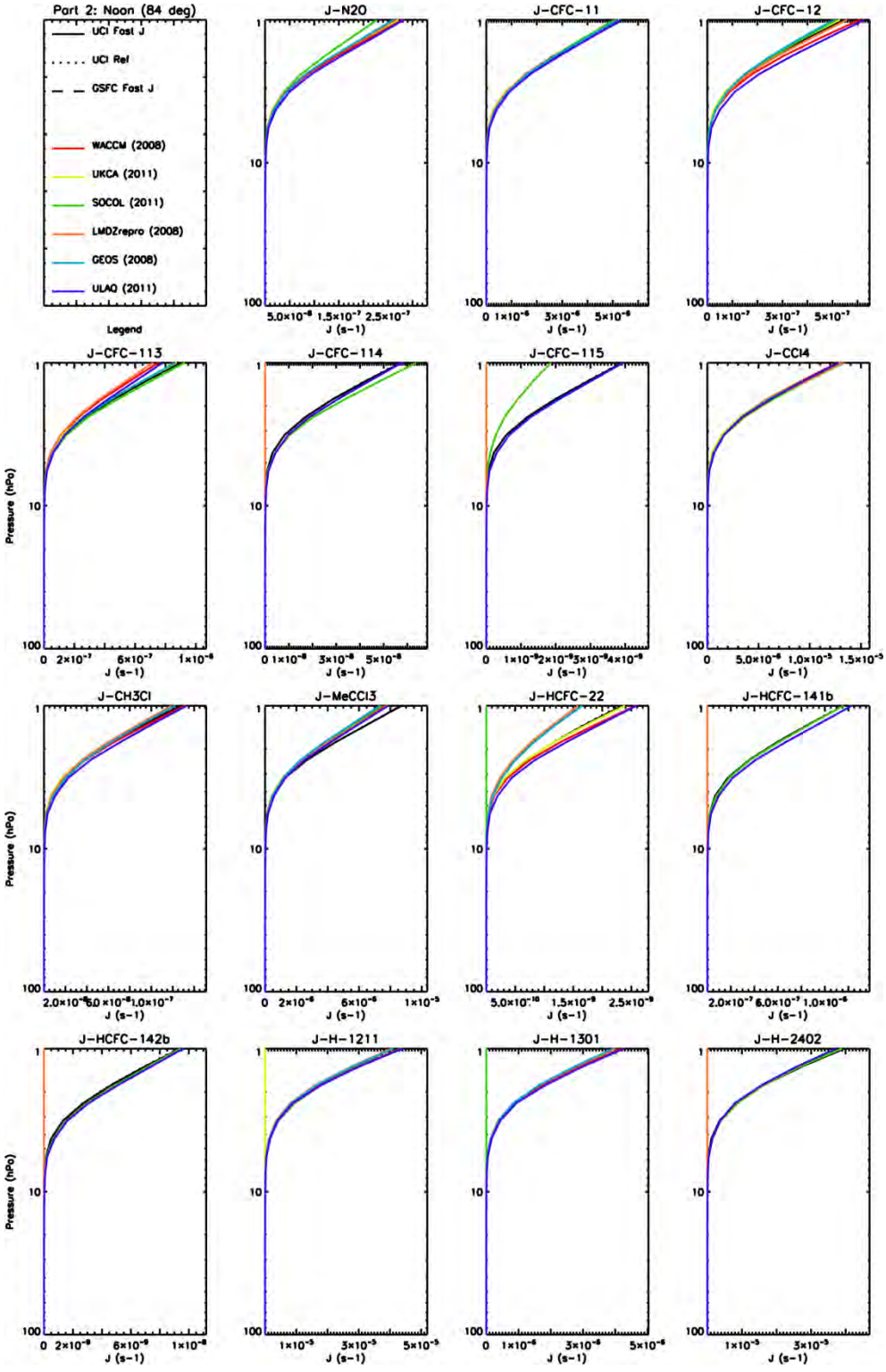

Figure 5.3. As Figure 5.2, but for 84^{o} (PhotoComp 2011 Part 2).

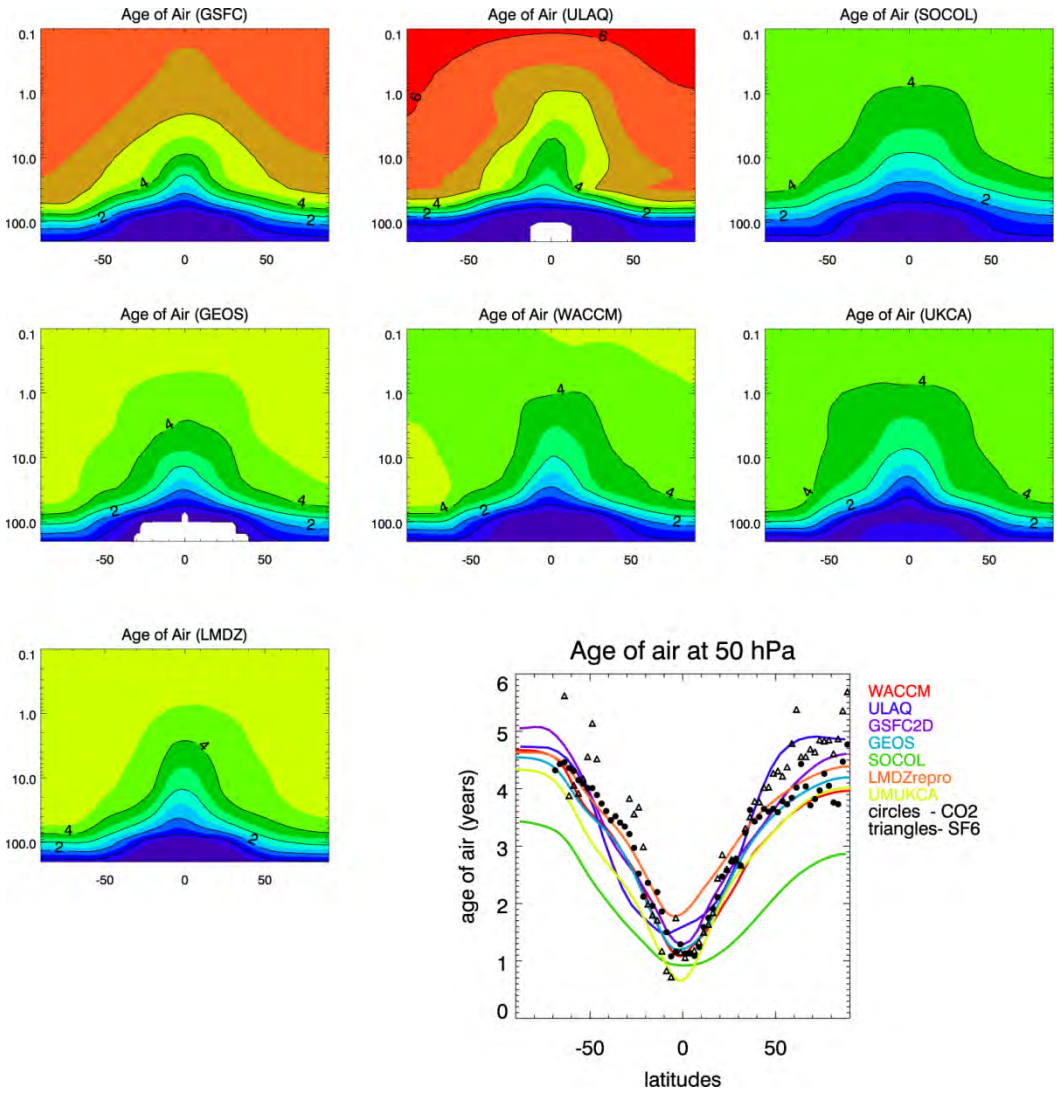

Figure 5.4. Mean age-of-air (years) calculated from present-day CCM simulations. The mean age was calculated using the last 15 years of the TS2000 runs. The lower right panel compares the mean age with observations at 50 hPa and derived age-of-air from CO_2 (filled circles) and SF_6 (triangles) measurements as described in Hall *et al.,* (1999).

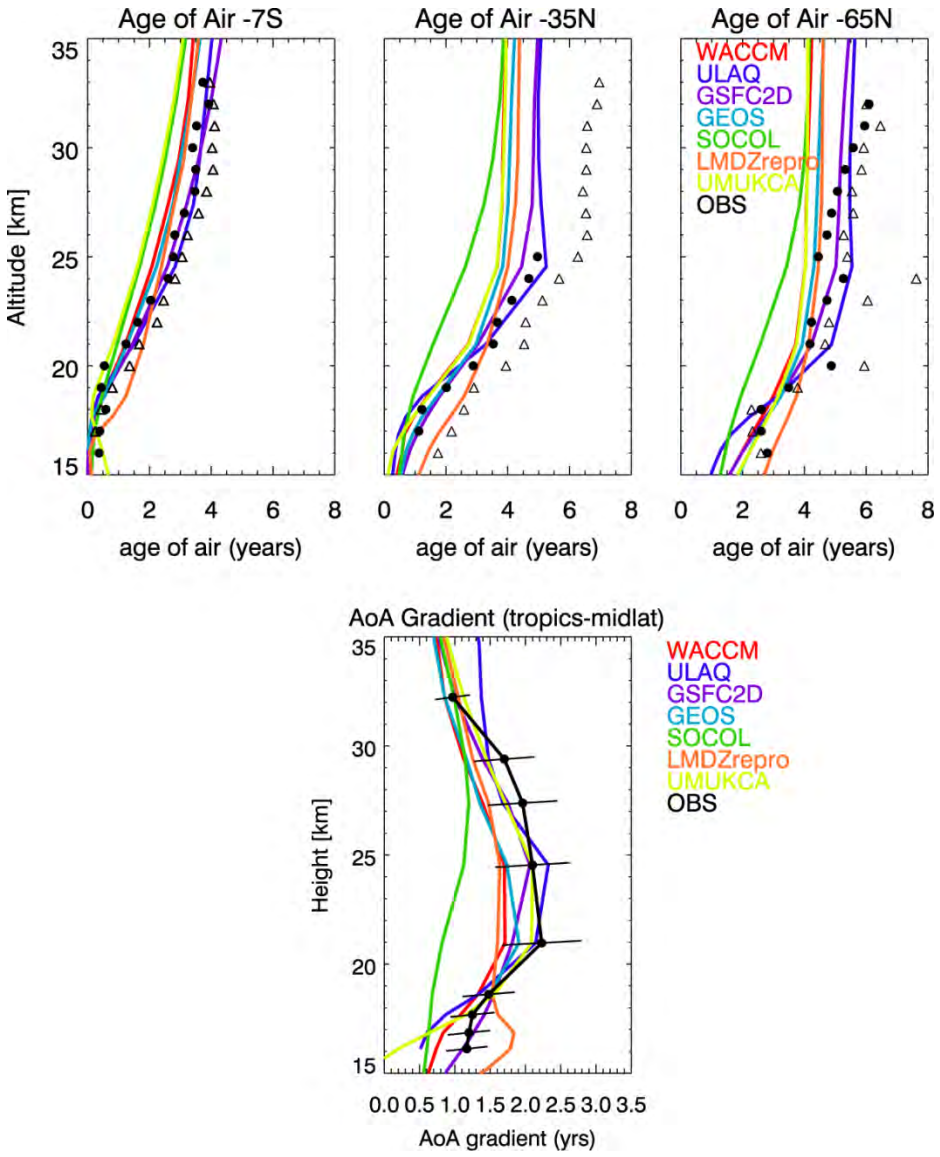

Figure 5.5. (Top) Mean age-of-air from present day CCM simulations for (a, left) 7°S, (b, centre) 35°N and (c, right) 65°N. The ages are 15-year averages of the model zonal mean output from TS2000 runs. The panels also show estimates derived from observations. (Bottom) Mean age gradient between northern midlatitudes (35°N-45°N) and tropics (10°S – 10°N) from model runs and observations with ±25% uncertainties (see Figure 5.5 from SPARC CCMVal (2010)).

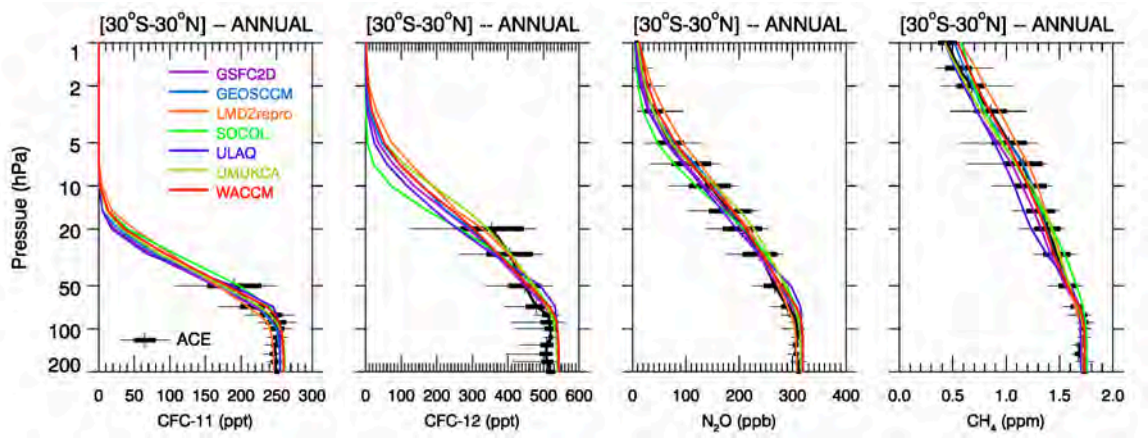

Figure 5.6. Comparison of tropical annual mean CFC-11, CFC-12, N_2O, and CH_4 profiles from the TRANS CCM simulations with ACE Climatology.

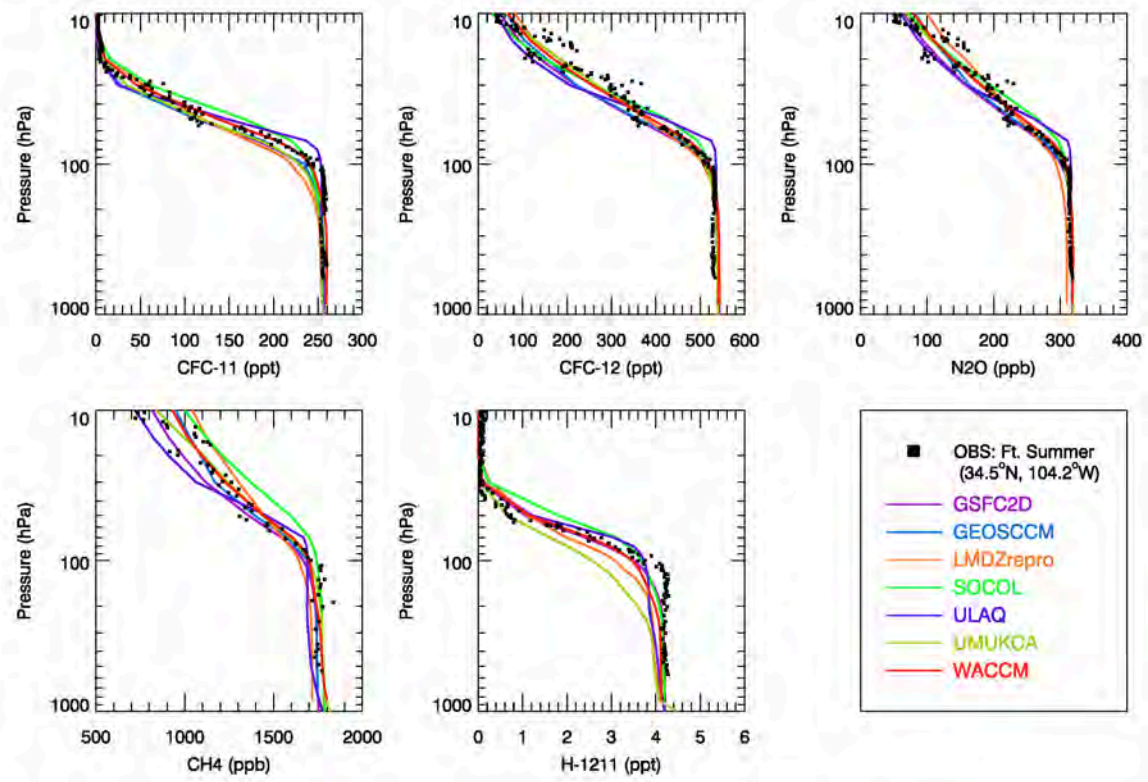

Figure 5.7. Comparison of ODS profiles from the TRANS CCM simulations with balloon measurements obtained at Ft. Sumner (34.5°N, 104.2°W) in Sep/Oct 2002-2004. Models are sampled at the closest location in the corresponding month.

5.3.4.1 Comparison of J[ODS]

Figure 5.8 compares the mean rate of the photolysis reactions from run TS2000 in the tropics. Overall, the seven models show a fair level of agreement in the magnitude of the loss rate and the altitude where maximum loss occurs. The SOCOL model shows rates consistently larger than the other models. A further comparison of the mean J rates in the tropical stratosphere (Figure 5.A1) shows that while the SOCOL model displays higher J values for some of the ODSs between 1-10 hPa, its J values between 10-100 hPa are not notably different from the other models. The higher photolysis loss fluxes in the SOCOL model (Figure 5.8) are mostly due to higher modelled ODS concentrations, a result of its faster circulation. Note that Halon-1202 is removed by photolysis at UV wavelengths up to 340 nm and Halon-1211 and Halon-2402 are removed by photolysis at UV wavelengths up to 320 nm, so a major part of the removal of these halons occurs in the troposphere. The SOCOL model differs significantly from the other four models that carry these halons in its loss rates in the troposphere, possibly due to the absence of long wavelength photolysis.

5.3.4.2 Comparison of k[ODS][OH]

Figure 5.9 compares the mean rate of the OH reactions from run TS2000 in the tropics for species significantly affected by this process. The models exhibit significant differences in the loss rates due to OH, particularly below 500 hPa where more than half of the loss occurs. The simulated OH loss rates near the surface differ by as much as a factor of 2-3 among individual models. Since all models use the same prescribed surface concentrations for the TR species, and are driven by the same sea surface temperature, this implies the difference in the OH loss rates is most likely due to differences in modelled OH.

As a further check, we compare the modelled OH concentration from all participating models (Figures 5.10 and 5.11, and Table 5.3). As explained in Section 5.2.2.1, two of the participating models (GEOSCCM and GSFC2D) use the same prescribed OH in the troposphere (Spivakovsky *et al.,* 2000) while SOCOL, ULAQ, UMUKCA and WACCM calculate interactive tropospheric OH based on surface emissions of NO_x and non-methane hydrocarbons (NMHC). Table 5.3 lists the global mean tropospheric OH concentrations ($[OH]_{GM}$) from all models and compares with previous published values. The global mean tropospheric OH (below 200 hPa) for present-day conditions ranges from 1.01×10^6 molecules/cm^3 to 1.30×10^6 molecules/cm^3 among models, with the four CCMs that calculate their own 'full chemistry' displaying $[OH]_{GM}$ higher than 1.20×10^6 molecules/cm^3. While previous reported OH concentrations show significant differences due to differences in model domain and spatial resolution (Lawrence *et al*., 2001), the majority of the published $[OH]_{GM}$ range from 0.94×10^6 to 1.0×10^6 molecules/cm^3 for $[OH]_{GM}$ below 200hPa. A detailed comparison of zonal mean distribution (Figure 5.10) and tropical mean vertical profiles of OH (Figure 5.11) suggests all models show higher OH concentrations than Spivakovsky *et al*. (2000). The modelled OH mixing ratios in the lower tropical troposphere, where OH loss plays a critical role in determining the atmospheric lifetime of TR species, differ by a factor of two between individual models. Even when models produce similar $[OH]_{GM}$, they still display significant differences in OH abundance at different altitudes. Interestingly, though the GEOSCCM and GSFC2D models both use the same prescribed OH in the troposphere, their modelled OH differ slightly from each other and from the prescribed OH fields. As prescribed OH is input into models in units of molecules/cm^3, this difference likely reflects model variations in online temperature and pressure fields used in the unit conversions between mole mixing ratio and concentration units for the other model species.

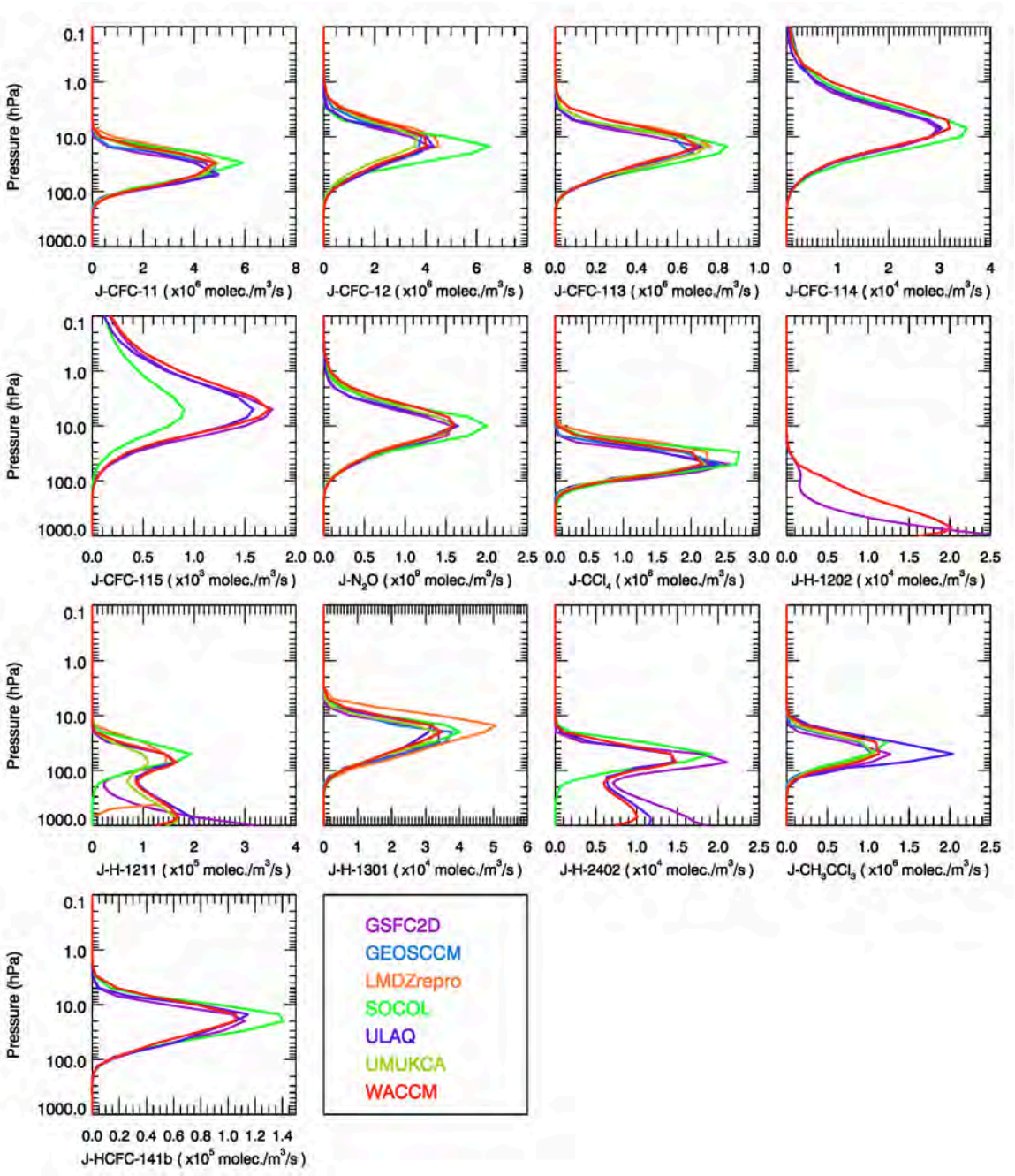

Figure 5.8. Comparison of modelled 30-year mean photolytic loss fluxes J[ODS] from the TS2000 simulation averaged between 30°S-30°N.

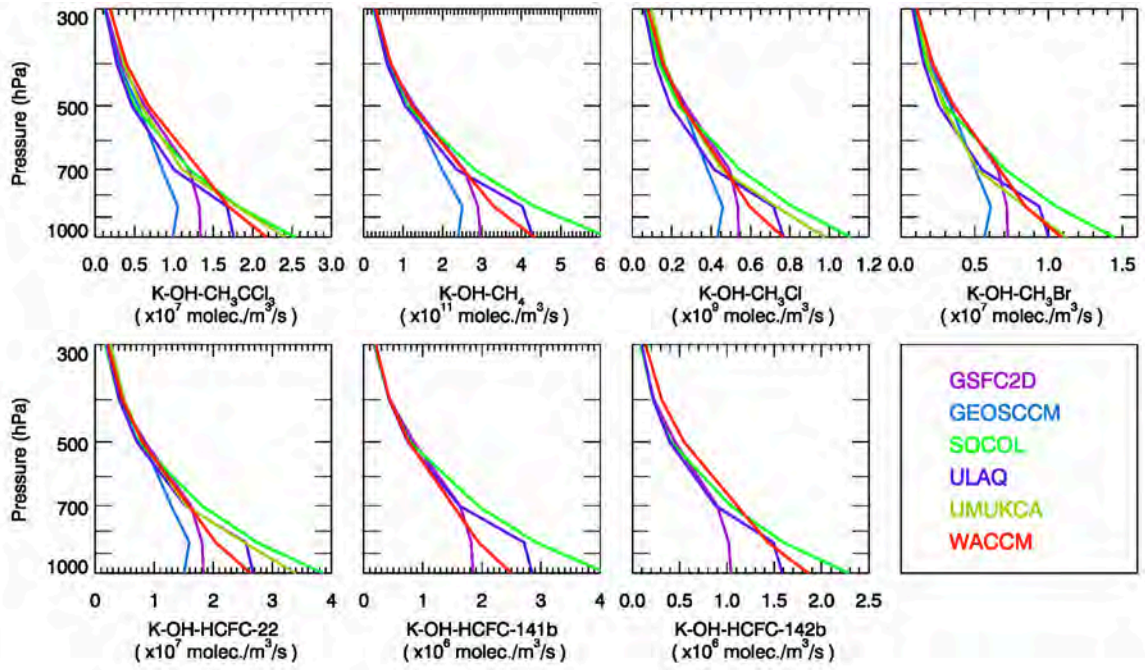

Figure 5.9. Comparison of modelled 30-year mean k[ODS][OH] loss fluxes from the TS2000 simulation averaged between 30°S-30°N.

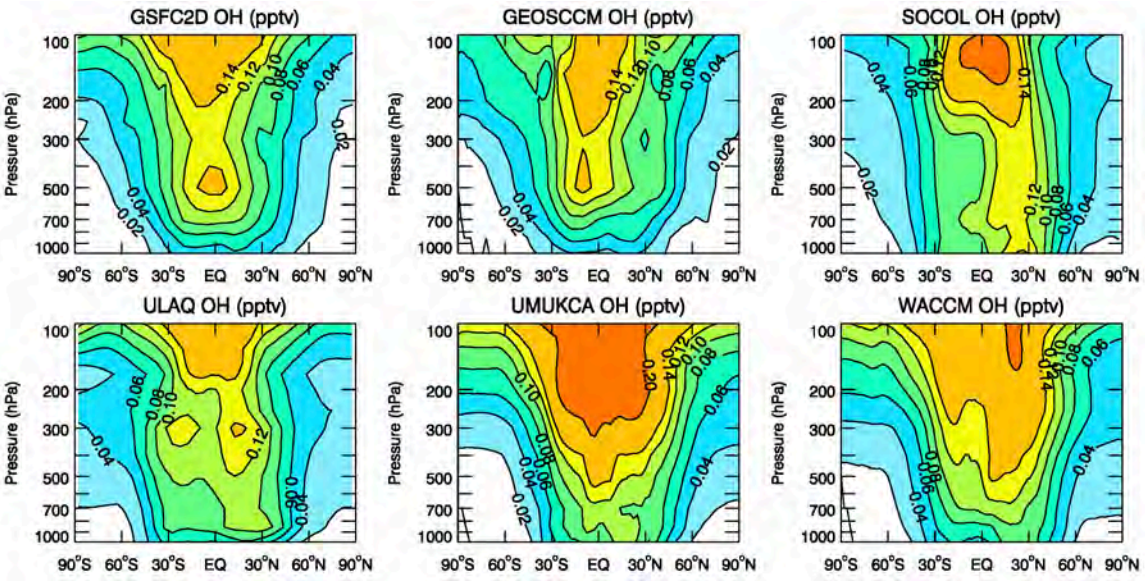

Figure 5.10. Comparison of modelled zonal mean OH (pptv) from the TS2000 simulation for the GSFC2D, GEOSCCM, SOCOL, ULAQ, UMUKCA and WACCM models.

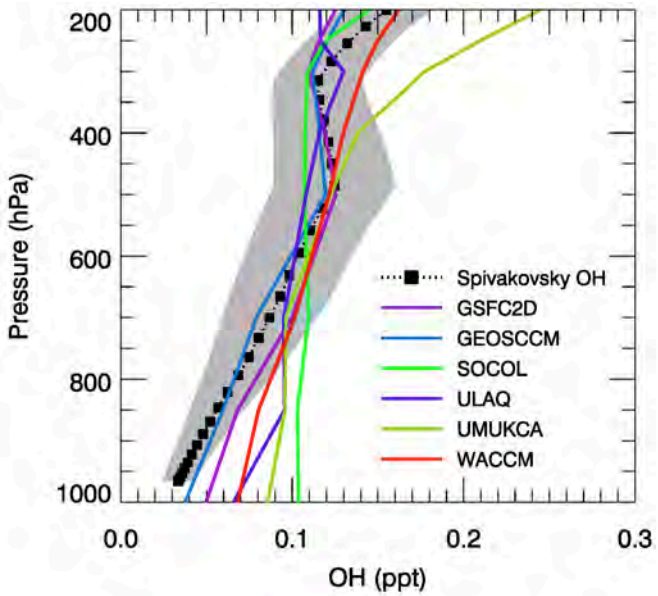

Figure 5.11. Comparison of tropical [30°S-30°N] mean OH profiles from the GSFC2D, GEOSCCM, SOCOL, ULAQ, UMUKCA and WACCM models. Mean tropical OH profile and 1-σ variance (gray shading) from Spivakovsky TS2000 simulations for *et al*. (2000) is also shown.

Table 5.3. Global mean tropospheric OH concentrations ($x10^6$ molecules/cm^3, mass weighted). Results for the 2000s and 2100s are calculated using the final 10 years of model output from the TS2000 simulations and results for the 1960s are 10-year averages between 1960-1969 from the TRANS simulations.

$[OH]_{GM}$	Published values *	GSFC2D	GEOSCCM	SOCOL	ULAQ	UMUKCA	WACCM
2000s (below 100 hPa)	**0.7 – 1.24**	0.91	0.87	1.07	0.99	1.22	1.07
2000s (below 200 hPa)	**0.94 – 1.0**	1.05	1.01	1.26	1.20	1.30	1.23
1960s (below 200 hPa)	N/A	1.05	1.01	1.25	1.25	1.28	1.14
2100s (below 200 hPa)	N/A	1.05	1.01	1.08	1.25	1.37	1.30

* The published values of mass weighted OH concentration adapted from Lawrence *et al.* (2001):
a) Spivakovsky *et al*. (1990): 0.8 $x10^6$ molecules/cm^3 below 100 hPa
b) Prather and Spivakovsky (1990): 0.8 $x10^6$ molecules/cm^3 below 100 hPa
c) Crutzen and Zimmermann (1991): 0.7 $x10^6$ molecules/cm^3 below 100 hPa
d) Prinn *et al*. (1995): 0.97 $x10^6$ molecules/cm^3 below 200 hPa
e) Wang *et al*. (1998): 1.0 $x10^6$ molecules/cm^3 below 200 hPa
f) Prinn *et al*. (2001): 0.94 $x10^6$ molecules/cm^3 below 200 hPa
g) Poisson *et al*. (2000): 1.24 $x10^6$ molecules/cm^3 below 100 hPa
h) Spivakovsky *et al*. (2000): 1.16 $x10^6$ molecules/cm^3 below 100 hPa within ±32° latitude and up to 200 hPa outside that region.

More recent published values since Lawrence *et al.* (2001):
i) Krol *et al.* (2003): $1.03x10^6$ molecules/cm^3
j) Prinn *et al*. (2005): $1.10x10^6$ molecules/cm^3
k) Bousquet *et al*. (2005): $0.99x10^6$ molecules/cm^3
l) Wang *et al*. (2008): $1.06x10^6$ molecules/cm^3

5.3.4.3 Comparison of k[ODS][O(^{1}D)]

Reaction with O(^{1}D) provides a minor loss mechanism for many of the ODSs and accounts for as much as ~10-40% of the total atmospheric loss for some species, e.g., CFC-114, CFC-115, and N_2O. Figure 5.12 compares the mean loss flux of the O(^{1}D) reactions from run TS2000 in the tropics. Models show a large spread in loss fluxes for all CFCs in the peak loss regions with differences of ~30-40% with respect to model mean values for four of the five CFCs and a factor of 4 for CFC-115. This large spread is mainly the result of the spread of modelled k[O(^{1}D)] rates (Figure 5.A2). While all models show a consistent and similar logarithmic dependence of k[O(^{1}D)] rates as a function of pressure, the actual rates differ by as much as 30-60% for CFC-11, CFC-12, CFC-113, and CFC-114 between models. The SOCOL and ULAQ models show $k_{O1D\text{-}CFC115}$[O(^{1}D)] rates 3-4 times higher than those from the GSFC2D and WACCM. Instead of a reaction rate constant of $1.5\text{x}10^{-11}$ cm^{-3} molecule s^{-1} ($0.3\times5.0\times10^{-11}$ cm^{-3} molecule s^{-1}, for 30% reaction) recommended by JPL 10-6, the full 5.0×10^{-11} cm^{-3} molecule s^{-1} (reaction + quenching) rate was used in the SOCOL and ULAQ models. The models agree fairly well in calculated $k_{O1D\text{-}N2O}$[O(^{1}D] and $k_{O1D\text{-}CH4}$[O(^{1}D)]. UMUKCA shows reasonable $k_{O1D\text{-}ODS}$[O^{1}D] rates for all species except N_2O; the UMUKCA $k_{O1D\text{-}N2O}$[O(^{1}D] rate is only half of those from the other models due to an implementation error.

5.4 Model Lifetime Calculations

We calculate the atmospheric lifetime, τ_{atmos}, of an ODS by dividing its global burden, B (moles), with its global integrated loss, L (moles/yr). The global burden is calculated as:

$$B = \int q_{i,j,k} \cdot \frac{\rho_{i,j,k} A_{i,j} dz_k}{mw_{air}} = -\frac{1}{g \cdot mw_{air}} \int q_{i,j,k} A_{i,j} dp_k \qquad (5.1)$$

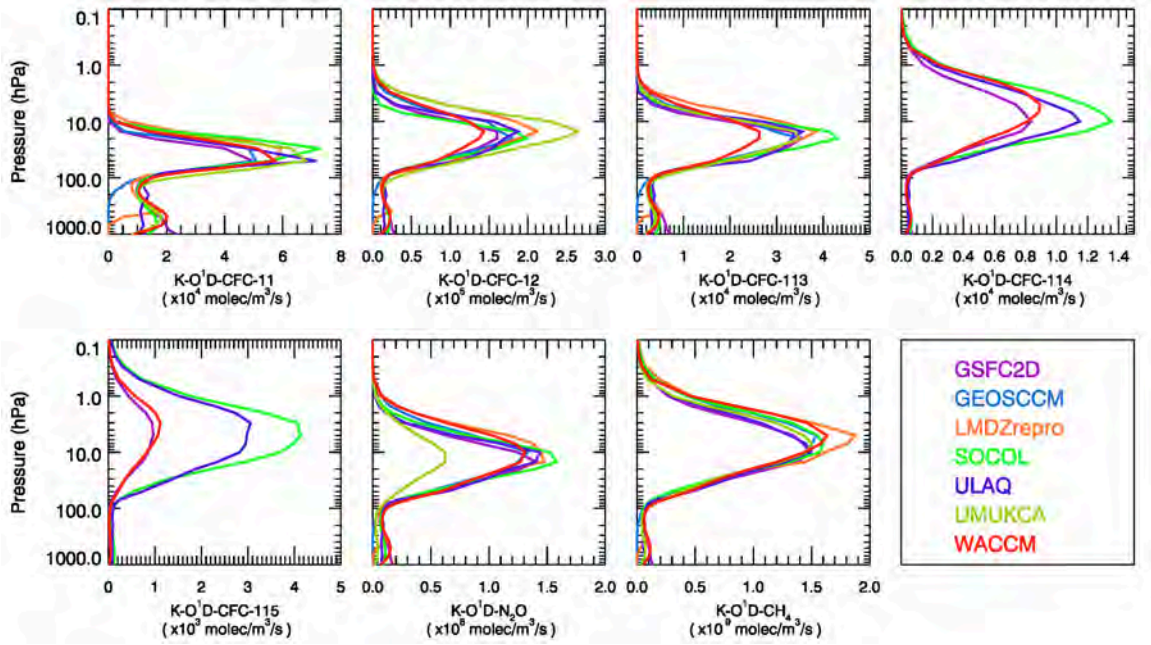

Figure 5.12. Comparison of modelled 30-year mean k[ODS][O(^{1}D)] reaction rates from the TS2000 simulation averaged between 30°S-30°N.

Similarly, L can be calculated as

$$L = -\frac{1}{g \cdot mw_{air}} \int (J_{i,j,k} + k_{i,j,k}) A_{i,j} dp_k \tag{5.2}$$

where $q_{i,j,k}$ is the mole mixing ratio and $\rho_{i,j,k}$ is air mass density at a model grid box (the *i*-th grid in the longitude dimension, *j*-th in the latitude and *k*-th in the vertical) and $A_{i,j}$ is area of grid box. $J_{i,j,k}$ and $k_{i,j,k}$ are photolytic loss rates (mole/mole/s) and thermal loss rates, respectively. dz_k is vertical thickness, and dp_k is the pressure thickness of the grid box. g is gravity and mw_{air} is the molecular weight of air.

5.4.1 Present-Day Lifetime Estimates

5.4.1.1 Evolution of Lifetimes from 1960s to Present

Figure 5.13 shows the time evolution of modelled instantaneous τ_{atmos} of seven high-priority species (CFC-11, CFC-12, CCl_4, N_2O, CH_4, CH_3CCl_3, HCFC-22) from the TRANS run. Time series of modelled instantaneous τ_{atmos} for all species of interest are included in Appendix D Figures 5.A3 to 5.A5. Note that while the TRANS run extends from 1960-2010, only the results between 1960-2006 are shown. This is because the TRANS runs from SOCOL and LMDZrepro stop in 2006 and the missing lifetime values from these two models result in a misleading increase in multi-model mean lifetime between 2006-2010. Overall, the model calculations clearly show a decrease in lifetime for all SR species. A primary reason for the decrease in the calculated lifetimes of CFCs and other man-made ODSs is the diminishing imbalance between surface fluxes and atmospheric losses as the atmosphere approaches steady-state conditions (Martinerie *et al.,* 2009). The contrast in lifetime between CFC MBC and CONST tracers, shown in Figure 5.14, clearly demonstrates that the main cause of the decrease in CFC-11 and CFC -12 lifetimes can be attributed to trends in their atmospheric concentrations. A secondary cause of the decrease in lifetime of the SR species is likely due to the combination of higher-altitude O_3 depletion that increases photolytic destruction and the speed-up of the Brewer-Dobson circulation. The CONST tracers implemented in the GEOSCCM and WACCM models suggest that the changes in photolysis and circulation together explain a decrease of ~5 years (~8% with respect to the ~57-58 years in the 2000s) in CFC-11 lifetime and ~7 years (~7% with respect to the ~93-96 years in the 2000s) in CFC-12 lifetime between the 1960s and the 2000s. Changes in atmospheric concentrations lead to a decrease of ~15 years in CFC-11 lifetime and ~30 years in CFC-12 lifetime. The small difference between the lifetimes of N_2O and its CONST tracer implies that the lifetime of N_2O is not affected by the relatively small change in its atmospheric concentration. The ~7 years (6% with respect to a 115-year lifetime in the 2000s) small decrease in N_2O lifetime from the 1960s to the 2000s is mainly due to changes in photolysis and atmospheric circulation. The instantaneous τ_{atmos} of the SR species also display significant interannual variations with year-to-year 1-σ variance of ±3-5%.

Box 5.1. The Impact of Topography on Lifetime Calculations

While differences in modelled transport and photochemistry lead to variations in calculated atmospheric lifetimes, significant differences may also arise due to differences in model output methods used to calculate atmospheric burden. Table 5.4 compares the steady-state global CFC-11 burden, $\boldsymbol{B}_{CFC\text{-}11}$, from the TS2000 simulation from all seven models. The calculated $\boldsymbol{B}_{CFC\text{-}11}$ varies by ~9% (with respect to a multi-model mean of 4.34×10^{10} moles) between models despite all using the same prescribed MBC condition and outputting data on the same pressure levels. The three CCMs, LMDZrepro, SOCOL and ULAQ, that do not report missing values in atmospheric concentrations when output grid points fall below model terrain all give relatively high $\boldsymbol{B}_{CFC\text{-}11}$. The GSFC2D model, which has a surface pressure extending down to 1013 hPa everywhere, also yields a similarly high $\boldsymbol{B}_{CFC\text{-}11}$. The relatively coarse vertical output resolution in the troposphere (1000, 850, 700, 500, 400, 300hPa, in compliance with the CCMVal-2 output format) requested for this assessment appears to be inadequate for an accurate burden calculation. Therefore, the three 3-D CCMs (GEOSCCM, UMUKCA, and WACCM) that account for topography in model output also yield a 0.17×10^{10} mole difference in their atmospheric burden due to detailed differences in how topography is treated on output layers.

Since SR species are uniformly mixed in the troposphere, it is possible to simply account for the topography effect on the burden calculation by assuming a constant atmospheric mixing ratio at all model grid points below 400 hPa and applying the following mass correction factor, α, to the calculated burden below 400 hPa:

$$\alpha = \frac{985hPa - 400hPa}{1013hPa - 400hPa} = 0.954$$

where 985 hPa is the global mean surface pressure. The topography-corrected $\boldsymbol{B}_{CFC\text{-}11}$ for all seven models is given in Table 5.4.

For TR species, the topography effect applies to both the burden and the loss calculation. Since the above correction is only valid when mixing ratios or losses are uniform in the troposphere, it is not feasible to apply a similar correction for the TR species. However, our calculation (not shown) suggests that for these species, the topography impact on loss and burden approximately cancel with each other with the calculated lifetime accurate within ~1%.

For model lifetimes reported in this chapter, we apply the topography correction to all SR species and halons, for both MBC tracers and CONST tracers. No correction is done for the FBC tracers, as these are not uniformly mixed in the troposphere. This results in a slight difference in calculated lifetimes between MBC tracers and their corresponding FBC tracers.

Table 5.4. The original and topography-corrected global burdens of CFC-11 from the TS2000 runs.

	GSFC2D (76 layers)	GEOSCCM	LMDZ-repro [a]	SOCOL [a]	ULAQ [a]	UMUKCA	WACCM
$\boldsymbol{B}_{CFC\text{-}11}$ ($\times10^{10}$ moles)	4.46	4.15	4.35	4.54	4.48	4.22	4.32
Topography-corrected $\boldsymbol{B}_{CFC\text{-}11}$ ($\times10^{10}$ moles)	4.31	4.25	4.27	4.40	4.36	4.29	4.34

[a] 3-D CCMs with topography not accounted for in model output.

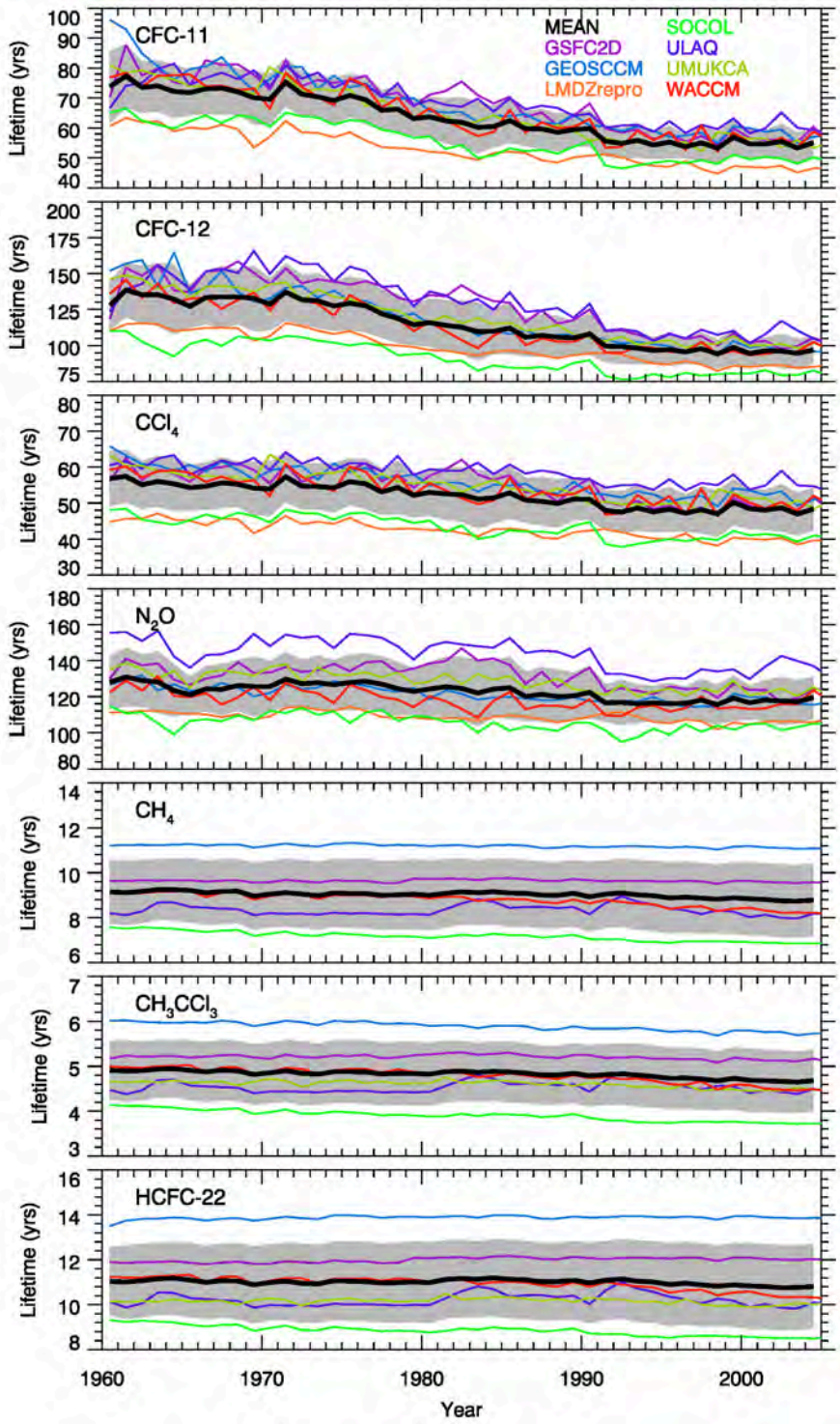

Figure 5.13. Time evolution of modelled atmospheric lifetimes (yrs) of seven high priority species between 1960 and 2006 from the TRANS simulations. Model mean lifetimes (thick black lines) and 1-σ variance (gray shading) are also shown.

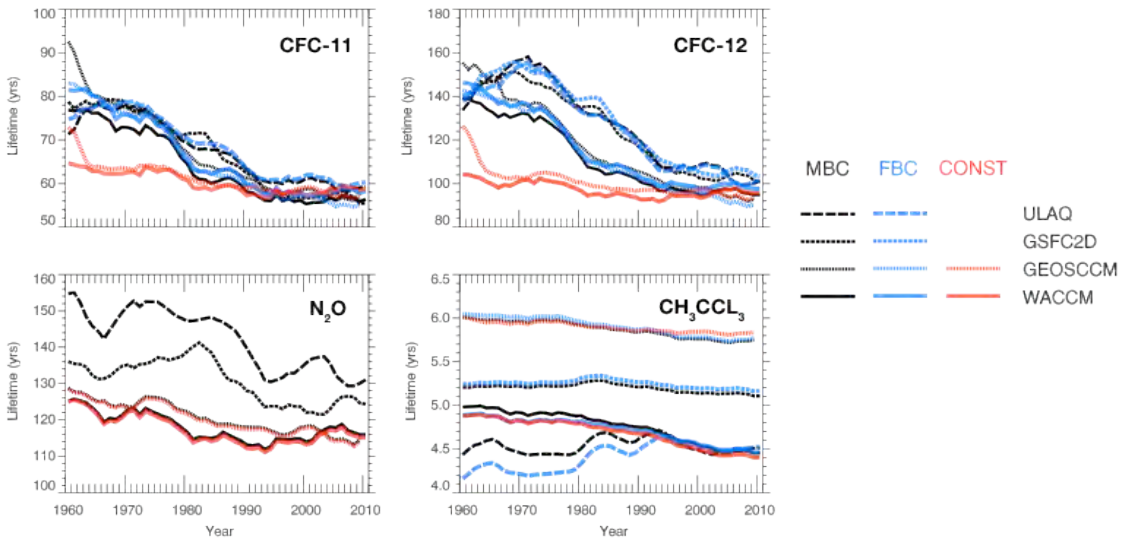

Figure 5.14. Time evolution of modelled atmospheric lifetimes of MBC CFC-11, CFC-12, N_2O, and CH_3CCl_3 (black lines) between 1960 and 2010 from the TRANS simulations and their corresponding FBC (blue lines) and CONST (red lines) tracers when available. For better visualization, the lifetimes are smoothed with a 5-year running mean filter.

While FBC tracers show significant differences in atmospheric distributions and total burden compared to MBC tracers in the same model (Figure 5.15), their modelled lifetimes are not notably different from the lifetime of MBC tracers. A detailed comparison between the 2000 steady-state lifetime and instantaneous lifetime of MBC, FBC, CONST tracers is shown in Table 5A-1 in Appendix C. Note that the instantaneous lifetimes in 2000 for all seven high priority species are not statistically different from their year 2000 steady-state lifetimes, despite their different trends in atmospheric concentrations (decreasing trends for CFC-11, CFC-12, CH_3CCl_3, CCl_4, and increasing trends for N_2O, CH_4 and HCFC-22).

The time dependencies of the lifetimes of TR species vary between models as they differ in how OH is treated or calculated in the troposphere. While GSFC2D (prescribed OH), ULAQ, and UMUKCA (interactive OH) show little trend between 1960 and 2010, SOCOL and WACCM display a ~5-10% decrease in the lifetime of three high priority TR species, CH_4, CH_3CCl_3, and HCFC-22. GEOSCCM shows a ~5% decrease in $\tau_{atmos,CH3CCl3}$, a smaller decrease in the lifetime of $\tau_{atmos,CH4}$, and little change in $\tau_{atmos,HCFC-22}$. The decrease in calculated $\tau_{atmos,CH3CCl3}$ in GEOSCCM (prescribed OH) mostly reflects the lifetime response to a warmer tropical troposphere while the decrease in SOCOL and WACCM (interactive OH) is likely due to the combined impact of a warmer troposphere and increases in OH concentrations (Table 5.3). The slightly different responses in CH_4, CH_3CCl_3, and HCFC-22 lifetimes in GEOSCCM are most likely due to differences in the trends of their atmospheric concentrations between 1960 and 2010, but this difference is less noticeable in WACCM and SOCOL as lifetime changes due to a warmer troposphere and changing OH are more dominant.

Figure 5.14 also shows the differences in calculated lifetime between the MBC, FBC and CONST tracers for CH_3CCl_3. In contrast to SR species where all models show consistent differences between each type of tracer, the differences in lifetime of CH_3CCl_3 between models overwhelm the differences between different types of tracers within a given model.

This implies that the main uncertainty in model-calculated lifetime of the TR species is dominated by the models' skill in simulating atmospheric OH (see Section 5.3.4.2).

5.4.1.2 Present-Day Steady-State Lifetimes

Table 5.5 lists the steady-state τ_{atmos} of ODSs and their substitutes for 2000 conditions from all models. The models agree fairly well in lifetime estimates for many SR species, with calculated lifetimes in general within 10% of the multi-model mean. Lifetimes of several major SR species, e.g., CCl_4, CFC-11, CFC-12, N_2O, from the SOCOL and LMDZrepro models are lower than the other models, most likely due to their fast tropical ascent (see Sections 5.3.3 and 5.4.3). The modelled steady-state τ_{atmos} of TR species differ greatly among models, with the range of estimates varying between 30%-40% for all species, mainly due to differences in modelled OH. One major caveat of the model mean lifetimes of HFCs is that these lifetime estimates are based on only two models (GSFC2D and GEOSCCM), both with prescribed OH fields. It is important to point out in addition to differences in OH, variations in air temperature, particularly in the tropical lower troposphere, can also exert a minor impact on the lifetime against loss by OH via their effects on thermal reaction rates. An increase in air temperature of 3K can lead to loss rate increases, therefore lifetime decreases, by as much as 3-5% for some of the temperature-sensitive species, e.g., HCFC-22, CH_4, CH_3CCl_3. However, for simulations conducted for this lifetimes assessment, since all 3-D CCMs are driven with the same sea surface temperature, variation in TR lifetimes due to differences in air temperature is minimized.

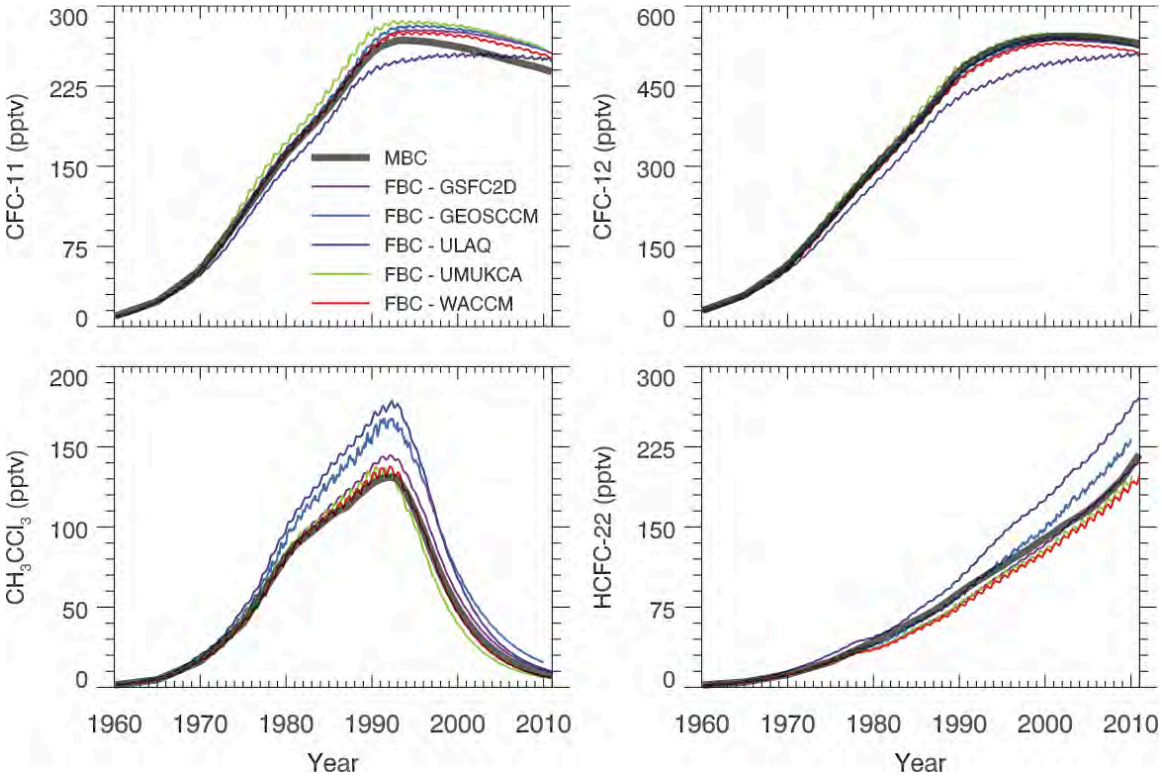

Figure 5.15. Time evolution of global mean surface concentration (pptv) of the modelled FBC tracers (dotted lines) compared with the prescribed MBC tracer scenario between 1960 and 2010 from the TRANS simulations.

Table 5.5. Steady-state τ_{atmos} (yrs) for Year 2000 from the TS2000 model runs**.** For best-estimate lifetimes for all targeted species, refer to Tables 6-1, 6-2 and 6-3 in Chapter 6.

Species	Chemical Formula	Model Mean	GSFC2D	GEOSCCM	LMDZ-repro	SOCOL	ULAQ	UMUKCA	WACCM
CFC-11	CCl_3F	**55.3**	58.6	58.3	49.1	50.8	58.6	56.8	56.9
CFC-12	CCl_2F_2	**94.7**	103.7	96.0	88.2	84.1	99.4	101.5	93.1
CFC-113	CCl_2FCClF_2	**87.3**	95.4	88.9	81.1	80.5	92.8	87.4	87.4
CFC-114	$CClF_2CClF_2$	**189**	204	--	--	169	205	--	184
CFC-115	CF_3CClF_2	**991** [a,b]	961	--	--	*	*	--	1022
CCl_4	CCl_4	**48.6**	50.7 [c]	52.2	42.0	41.4	54.3	52.0	51.3
N_2O	N_2O	**115**	125	117	105	107	127	*	112
Halon-1202	CBr_2F_2	**1.8**	2.1	--	--	--	--	--	1.6
Halon-1211	$CBrClF_2$	**11.5**	13.5	--	--	--	9.8	12.3	11.0
Halon-1301	$CBrF_3$	**72.2**	77.4	72.8	66.0	67.1	78.0	74.7	71.4
Halon-2402	$CBrF_2CBrF_2$	**14.5**	13.9	--	--	--	13.9	--	15.9
CH_4	CH_4	**8.7**	9.6	11.1	--	7.3	8.2	--	8.4
CH_3CCl_3	CH_3CCl_3	**4.6**	5.2	5.8	--	4.0	4.1	4.3	4.6
CH_3Cl	CH_3Cl	**1.3**	1.5	1.7	--	1.1	1.2	1.1	1.3
CH_3Br	CH_3Br	**1.5**	1.7	1.9	--	1.3	1.4	1.4	1.5
HCFC-22	$CHClF_2$	**10.7**	12.0	14.0	--	9.1	10.1	9.5	10.6
HCFC-141b	CH_3CCl_2F	**8.0**	9.2	--	--	7.1	7.8	--	8.1
HCFC-142b	CH_3CClF_2	**14.2**	17.5	--	--	13.6	14.7	--	12.2
HFC-23	CHF_3	**242**	226	260	--	--	--	--	--
HFC-32	CH_2F_2	**5.5**	5.2	5.9	--	--	--	--	--
HFC-125	CHF_2CF_3	**31.3**	29.3	33.7	--	--	--	--	--
HFC-134a	CH_2FCF_3	**14.4**	13.6	15.4	--	--	--	--	--
HFC-143a	CF_3CH_3	**53.2**	50.1	56.8	--	--	--	--	--
HFC-152a	CH_3CHF_2	**1.5**	1.5	1.6	--	--	--	--	--
HFC-227ea	CF_3CHFCF_3	**45.3**	42.4	48.6	--	--	--	--	--
HFC-245fa	$CHF_2CH_2CF_3$	**7.8**	7.8	--	--	--	--	--	--

[a] We calculate the mean lifetime of CFC-115 as the average of the GSFC2D and WACCM lifetimes as SOCOL and ULAQ specified a too large reaction rate constant for $O(^1D)$ and CFC-115 in their calculations.

[b] The CFC-115 lifetime calculated in Chapter 5 is significantly higher than the value in Chapter 6 (540 yr) due to differences in CFC-115 photolysis rates in the JPL 10-6 recommendation and the SPARC Lifetime recommendation (Chapter 3).

[c] The CCl_4 lifetime from GSFC2D is the τ_{phot}, instead of the τ_{atmos} which includes loss against photolysis and OH listed in Chapter 3.

In Table 5.6 we summarize the present-day model mean steady-state τ_{atmos} and 1-σ variance of the targeted species. The model mean lifetimes and their variances are calculated from the inverse of the mean and the variance of all available modelled loss rates. Partial lifetimes in different regions of the atmosphere, stratosphere vs. troposphere, and partial lifetimes associated with different loss processes, i.e., photolysis, reaction with OH, $O(^1D)$ and Cl, are also listed. The model mean lifetime estimates for CFC-11, CCl_4 and all four halons are significantly different from the WMO (2011) values. Considering the large range of modelled lifetime for the TR species, the modelled mean lifetimes of the TR species agree fairly well with the values given in WMO (2011). Photolytic destruction is the dominant loss process for all SR species with reaction with $O(^1D)$ as a minor loss channel for CFCs and N_2O. Reaction with $O(^1D)$ is particularly important for CFC-114 and CFC-115, accounting for 27% and 38% of their global loss, respectively. Although photolysis is the predominant removal process for Halons, for three (H-1202, H-1211, and H-2402) of the four targeted, the majority of the removal occurs in the troposphere. Removal of the TR species occurs primarily through reaction with OH, with photolysis, reaction with $O(^1D)$ and Cl being two minor loss channels for individual species.

5.4.1.3 Global OH Abundance Inferred from CH_3CCl_3

The 2-D model inverse method has been traditionally used with surface observations of CH_3CCl_3 to derive the atmospheric lifetime of CH_3CCl_3 and global mean OH abundance (e.g., Prinn *et al*., 1995, 2001; Montzka *et al*., 2011; Rigby *et al*., 2013). However, it is difficult to conclude whether the inferred OH concentration is representative of the true atmosphere due to a shortage of OH observations. Since CH_3CCl_3_FBC mimics well the long-term as well as short-term variations of CH_3CCl_3 in the atmosphere (Wang *et al*., 2008), one useful application is to substitute surface CH_3CCl_3 observations with 3-D CCM-modelled CH_3CCl_3_FBC in the 2-D model (see Chapter 4 and Rigby *et al*., 2013) to derive the corresponding lifetime and OH abundance. Table 5.7 compares the 2-D model inversely derived τ_{OH} and $[OH]_{GM}$ using surface CH_3CCl_3_FBC from WACCM and GEOSCCM as pseudo-observational constraints with those calculated directly using model output. The close agreement between the 2-D model inferred and 3-D CCM calculated τ_{OH} and $[OH]_{GM}$ confirms the robustness of the 2-D model inverse method and the inferred $[OH]_{GM}$ of 1.09×10^6 molecules/cm^3 is likely representative of the true global OH abundance. This is consistent with the findings in Wang et al. (2008), who inversely derived OH using a 3-D chemistry transport model and CH_3CCl_3 observations. They found that the global OH abundance can be well constrained in a Bayesian inverse approach and reported a similar $[OH]_{GM}$ of 1.06×10^6 molecules/cm^3 between 1988 and 1994.

Table 5.6. Present-day modelled steady-state τ_{atmos} (yrs). SR species whose WMO (2011) lifetimes are less (or more) than model mean – (+) 1-σ variance are highlighted in bold. For best-estimate lifetimes for all targeted species, refer to Tables 6.1, 6.2, and 6.3 in Chapter 6.

Species	WMO (2011)	Model Mean τ_{atmos}	Model Variance % (yrs)	τ_{strat}	τ_{trop}	τ_{phot}	τ_{OH}	τ_{O1D}	τ_{Cl}
CFC-11	45	**55.3**	8% (4.2)	57.0	1870	56.4	--	2930	--
CFC-12	100	94.7	8% (7.3)	95.5	11600	100	--	1750	--
CFC-113	85	87.3	6% (5.5)	88.4	7620	92.9	--	1460	--
CFC-114	190	189	10% (18.0)	191	19600	261	--	684	--
CFC-115	1020	991[a]	4% (43.1)	997	126000	1590	--	2610	--
CCl_4[b]	35	**48.6**	12% (5.6)	50.6	1230	48.7	--	--	--
N_2O	114[c]	115	8% (9.0)	116	15600	127	--	1180	--
Halon-1202	2.9	**1.8**	21% (0.4)	15.3	2.0	1.8	--	10600	--
Halon-1211	16	**11.5**	14% (1.6)	33.5	17.3	11.5	--	8040	--
Halon-1301	65	**72.2**	7% (4.7)	73.5	4490	73.3	--	5260	--
Halon-2402	20	**14.5**	8% (1.1)	33.8	25.1	14.4	--	6790	--
CH_4	8.7[c]	8.7	16% (1.4)	152	9.3	--	8.9	462	598
CH_3CCl_3	5	4.6	14% (0.6)	37.7	5.2	45.8	5.1	--	--
CH_3Cl	1.5[d]	1.3	14% (0.2)	30.4	1.3	436	1.3	--	259
CH_3Br	1.9[d]	1.5	14% (0.2)	26.3	1.6	51.8	1.6	5180	466
HCFC-22	11.9	10.7	15% (1.6)	161	11.3	4090	10.8	654	--
HCFC-141b	9.2	8.0	11% (0.8)	72.3	8.9	91.5	8.8	1720	--
HCFC-142b	17.2	14.2	15% (2.1)	212	15.3	1510	14.8	398	--
HFC-23	222	242	[*]*15% (36.9)*	4420	256	--	244	31100	--
HFC-32	5.2	5.5	[*]*15% (0.8)*	124	5.8	--	5.5	5210	2110
HFC-125	29	31.3	[*]*15% (4.8)*	351	34.5	--	32.8	705	--
HFC-134a	13.4	14.4	[*]*15% (2.2)*	267	15.3	--	14.5	3100	--
HFC-143a	47.1	53.2	[*]*15% (8.1)*	612	58.3	--	55.6	1230	--
HFC-152a	1.5	1.5	[*]*15% (0.2)*	39.0	1.6	--	1.5	2600	401
HFC-227ea	38.9	45.3	[*]*15% (6.9)*	782	48.0	--	45.3	--	--
HFC-245fa	7.7	7.8	[*]*15% (1.2)*	149	8.2	--	7.8	--	--

[a] The CFC-115 lifetime calculated in Chapter 5 is significantly higher than the value in Chapter 6 (540 yr) due to differences in CFC-115 photolysis rates in the JPL 10-6 recommendation and the SPARC Lifetime recommendation (Chapter 3).

[b] The CCl_4 lifetime from models is τ_{phot}, compared with τ_{atmos} from WMO (2011), which accounts for losses due only to photolysis and reaction with OH.

[c] CH_4 lifetime from IPCC (2007) which includes both atmospheric and soil sinks. The soil sink accounts for <10% of the total loss.

[d] The τ_{atmos} which are listed instead of τ.

[*] For HFCs, since results are only from two models, both driven with the same prescribed OH fields, we adopted the largest variance (15%) calculated for the TR species with reaction with OH being the predominant loss, HCFC-22, as model variance.

Table 5.7. The comparison of the 2-D model inferred lifetimes and $[OH]_{GM}$ with 2-σ uncertainties (in parentheses) using CH_3CCl_3_FBC from WACCM and GEOSCCM as pseudo-observational constraints with those calculated directly using model output. CH_3CCl_3 lifetimes and $[OH]_{GM}$ (2-σ uncertainties shown in parentheses) derived using surface observations from Chapter 4 are also shown.

	Observation-derived (Chapter 4)	GEOSCCM		WACCM	
		3-D CCM	2-D inverse model	3-D CCM	2-D inverse model
$[OH]_{GM}$ ($\times 10^6$ molecules/cm^3)	1.09 (1.02-1.16)	1.01	0.96 (0.90-1.02)	1.21	1.29 (1.21-1.37)
τ_{atmos} (yrs)	5.4 (5.1-5.7)	5.8	6.1 (5.8-6.5)	4.6	4.7 (4.5-5.0)
τ_{OH} (yrs)	6.2 (5.8-6.6)	6.7	7.1 (6.7-7.5)	5.0	5.3 (5.0-5.6)
τ_{strat} (yrs)	43	46.5	46.5	46.7	46.7

5.4.2 Relative Lifetimes from Tracer-Tracer Correlations

For SR species under steady-state conditions tracer-tracer correlations can be used to derive relative lifetimes (see Chapter 2 for the theory and Chapter 4 for applications to observations). The relative lifetime of two tracers is given by:

$$\frac{\tau_2}{\tau_1} = \frac{q_2}{q_1}\frac{dq_1}{dq_2} \tag{5.3}$$

where q_1 and q_2 are volume mixing ratios. We have derived relative lifetimes from simulation TS2000 by correlating model tracers with respect to CFC-11 ($CFCl_3$). For this we analyzed the last 15 years of the run when the steady-state assumption should be valid. The method is illustrated by Figure 5.16. To evaluate the lifetime using Equation (5.3) mean tracer values at/below 100 hPa in the tropics and extra-tropics were used. Table 5.8 shows the derived relative stratospheric lifetimes, along with the corresponding absolute lifetime assuming a lifetime of $CFCl_3$ of 55 years, which is close to the model mean in Table 5.5. Results for CH_4 are also included; at steady state this method gives an estimate of the stratospheric lifetime of TR tracers such as this.

The relative lifetimes shown in Table 5.8 show a generally good level of agreement between the models. For example, ignoring UMUKCA, the relative lifetime of CFC-12 varies from 89.7 years in WACCM to 97.9 years in LMDZrepro. This range is a lot narrower than the range of absolute lifetimes of 84.1 to 103.7 given in Table 5.5. This is also the case for CFC-113 (84.2-89.1 yrs versus 80.5-95.4 yrs), CCl_4 (45.1-48.4 yrs versus 41.4-54.3 yrs), Halon 1301 (68.2-74.3 yrs versus 66.0-78.0 yrs) and N_2O (108.9-118.8 yrs versus 105–127 yrs). Also, while LMDZrepro, for example, generally produces low absolute lifetimes in Table 5.5, this is not the case for the relative lifetimes. Evidently, the models are showing a greater degree of overall self-consistency in the relative SR lifetimes. Relative lifetimes depend more strongly on chemical loss processes, and are less sensitive to differences in stratospheric circulation. Halons 1211 and 2402 have significant tropospheric loss, as does CH_4. The tracer-tracer correlation method will diagnose stratospheric lifetimes (compare to Table 5.6). However, the method appears to produce a wide range in values and more work is needed to test the usefulness of this approach for TR species.

Table 5.8. Relative steady-state τ_{atmos} for year-2000 conditions for high priority SR species from the TS2000 model simulations, derived from tracer-tracer correlations compared to CFC-11 ($CFCl_3$). Values in parentheses are the corresponding lifetime assuming τ_{CFCl3}=55 yrs. Also shown are results for the stratospheric lifetime of CH_4. For best-estimate lifetime for all targeted species, please refer to Tables 6-1, 6-2 and 6-3 in Chapter 6.

Species	GSFC2D	GEOSCCM	LMDZrepro	SOCOL	ULAQ	UMUKCA	WACCM
CFC-12	1.65 (90.1)	1.68 (92.4)	1.78 (97.9)	1.64 (90.2)	1.67 (91.9)	1.99 (109.5)	1.63 (89.7)
CFC-113	1.53 (84.2)	1.56 (85.8)	1.62 (89.1)		1.56 (85.8)	1.67 (91.9)	1.54 (84.7)
CFC-114	3.14 (172.7)				3.30 (181.5)		3.23 (177.7)
CFC-115	14.3 (786.5)						20.4 (1122.0)
CCl_4	0.87 (47.9)	0.88 (48.4)	0.86 (47.3)	0.82 (45.1)	0.88 (48.4)	0.87 (47.9)	0.88 (48.4)
N_2O	1.98 (108.9)	2.04 (112.2)	2.16 (118.8)	2.11 (116.1)	2.10 (115.5)	2.34 (128.7)	1.97 (108.4)
Halon-1211	0.69 (38.0)		0.63 (34.7)		0.37 (20.4)	[a]	0.57 (31.4)
Halon-1301	1.27 (69.9)	1.24 (68.2)	1.35 (74.3)	1.31 (72.1)	1.31 (72.1)	0.89 (49.0)	1.25 (68.8)
Halon-2402	0.63 (34.7)			0.63 (34.7)	0.45 (24.8)		0.64 (35.2)
CH_4	2.28 (125.4)	2.74 (150.7)	3.06 (168.3)	3.18 (174.9)	1.27 (69.9)	2.26 (124.3)	2.48 (136.4)

[a] Derived UMUKCA stratospheric lifetime by this method is very short (<10 years).

The relative lifetimes derived for UMUKCA appear to differ significantly from the other models. For UMUKCA it seems that the tracer-tracer correlations in the lower stratosphere do not produce such a compact correlation compared to other models (see Figure 5.16). This may be due to processing output from native model levels to pressure levels for analysis or may be due to the semi-Lagrangian advection scheme used in UMUKCA and the impact of this scheme on advected tracers as discussed by Morgenstern *et al*., (2009). Therefore, the objectively fitted slope of this UMUKCA line deviates from that which would fit the outer envelope of the tracer-tracer correlation plot and lead to a relative lifetime more consistent with the other models. This behaviour might be related to the larger offset seen in the mean age-of-air in the tropical upper troposphere/lower stratosphere (which is reset to zero at the tropical tropopause for analysis of all models in any case).

Clearly, the lifetime of a SR tracer depends on the rate of circulation of the species through the stratosphere, i.e., in the Brewer-Dobson circulation. The rate of this stratospheric circulation is illustrated by the age-of-air (see Section 5.3.3.1). In this section we explore the quantitative relationship between the derived lifetimes and age-of-air for individual models.

5.4.3 Variation of SR Species Lifetimes with Modelled Age-of-Air

Figure 5.17 shows correlation plots of derived lifetimes with stratospheric mean age-of-air for selected SR species (not including results from LMDZrepro – see below). For this analysis the mean age-of-air for each model has been reset to zero at the tropical tropopause (see Section 5.3.3.1). Overall there is a positive correlation: Models with older mean age-of-air give longer lifetimes. The correlation is relatively compact for the CFCs, CCl_4 and N_2O (r > 0.81). Overall, this confirms the results of relative lifetimes discussed above and shows the

influence of modelled mean age-of-air on the lifetimes of SR species. Given an observational estimate of the mean age-of-air in the stratosphere, the correlations in Figure 5.17 could be used to derive an optimal atmospheric lifetime.

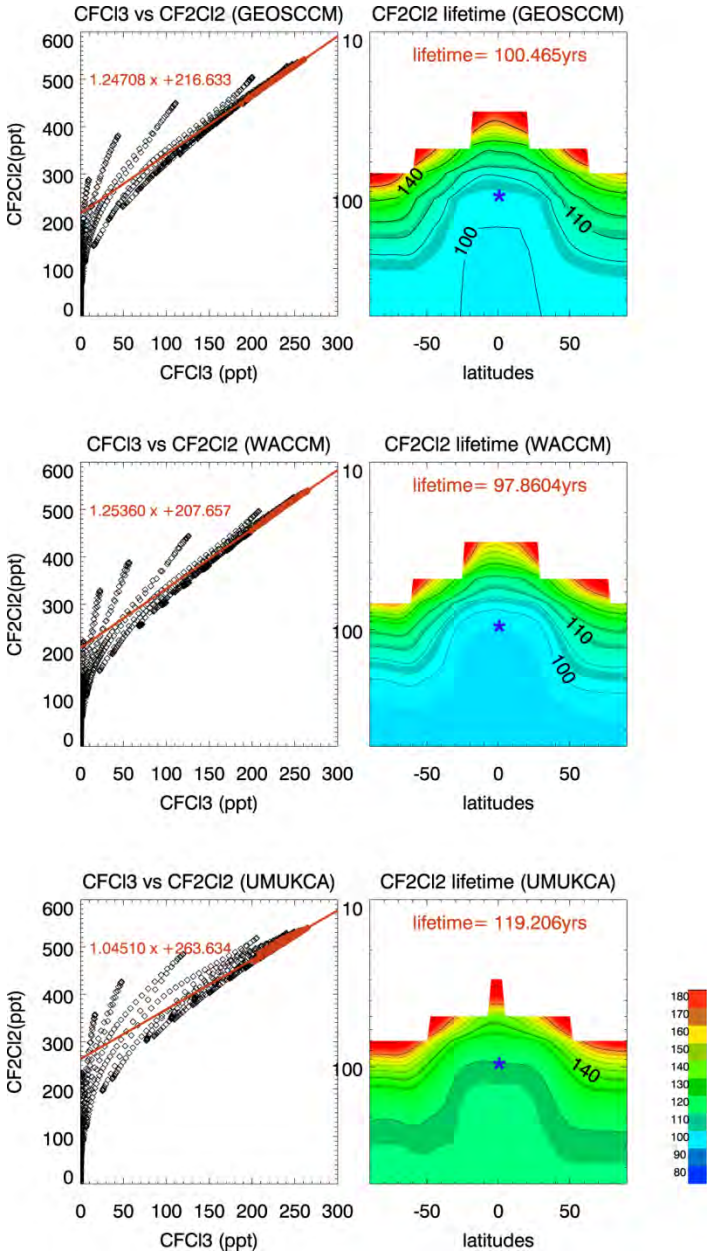

Figure 5.16. Example plots showing the calculation of relative lifetime for CFC-12 (CF_2Cl_2) from tracer-tracer correlation plots for the GEOSCCM, WACCM and UMUKCA models. Results are shown for average of last 15 years of the TS2000 runs. The left panels show the CFC-12 (CF_2Cl_2) vs. CFC-11 ($CFCl_3$) correlation plot. The points in orange (selected as the points between 60°S and 60°N, below 100 hPa and within 30% of the maximum tracer values in this region) are fitted to a straight line (equation in panel). The right panels show the example relative lifetime of CF_2Cl_2 evaluated using Equation (5.3) (see text) and an assumed approximate CFC-11 lifetime of 60 years. See text for more accurate model-based estimates. The lifetime at 100 hPa in the tropics (location of blue star) is shown in the right panels and used in Table 5.8.

As noted above Figure 5.17 does not include results from LMDZrepro. The equivalent figure which also includes these results is given in Appendix D Figure 5.A6. With results from LMDZrepro included, the correlation between lifetime and age is a lot less strong, for example for CFC-11 *r* decreases from 0.87 to 0.22. Evidently, the transport in LMDZrepro in the critical region for SR species loss cannot be represented by the simple metric of global mean age-of-air. Figure 5.18 shows the correlation between modeled lifetimes and the difference in mean age between two levels in the tropical lower stratosphere for CFC-11 and CFC-12. The chosen altitudes span the lower stratosphere up to an altitude above the main loss region for each species. This quantity is therefore a measure of the time taken for air to ascend through this loss region, allowing for vertical advection and mixing between the tropics and mid-latitudes (i.e., recirculation of ascending air). In Figure 5.18 the models display a better correlation than in Figure 5.A6, i.e., modeling the correct mean ascent rate through the tropical lower-mid stratosphere is key. The better models have the larger age difference, i.e., they have values that approach the observed difference. Although LMDZrepro gives a reasonable overall simulation of stratospheric age-of-air (Figure 5.4), the metric in Figure 5.18 shows that the model has a fast ascent rate in the key loss region, which leads to short modelled lifetimes.

5.4.4 Variation of TR Species Lifetimes and OH

While all participating models show a fair level of agreement in their estimated atmospheric lifetime of SR species, modelled lifetimes of TR species display a large range, mainly due to differences in their representation of OH in the troposphere. Figure 5.19 plots the derived partial atmospheric lifetimes of TR species against tropospheric mean OH, $[OH]_{trop}$. There is a clear anti-correlation between modelled lifetime and $[OH]_{trop}$ (r = -0.91 to -0.95). The differences in detail in the modelled OH distributions (interactive or specified) appear to play a secondary role in determining the lifetime, compared to the simple overall tropospheric mean OH.

We conducted two sensitivity TS2000 simulations with the GSFC2D model, differing from TS2000 by increasing and decreasing the prescribed OH field by 20%, to investigate the impact of OH abundance on the lifetimes of the TR species. Results suggest that lifetimes of TR species respond rather linearly to the OH abundance. A 20% increase in OH leads to ~16% decrease in TR species lifetimes against OH on average, while a 20% decrease leads to ~19% increase in lifetime against OH. Although all three simulations were run with the same MBC at the surface, the change in OH leads to a slight decrease (increase) in tropospheric ODS concentrations in the high-OH (low-OH) simulation. The asymmetric response is due to a smaller relative change in ODS concentrations in the high-OH simulation than in the low-OH simulation. The slightly larger relative response in the low-OH case implies higher efficiency in ODS-destruction at lower OH concentrations.

Figure 5.20 plots the OH partial lifetimes, τ_{OH}, of CH_4, HCFC-22, CH_3Cl, and CH_3Br against τ_{OH} of CH_3CCl_3 from all available models as well as the observation-derived τ_{OH} from Chapter 4. While models differ greatly in their calculated lifetime of TR species against OH, τ_{OH} of a TR species is tightly correlated with that of CH_3CCl_3 (r = 0.991-0.996), independent of differences in OH abundances in individual models. The multi-model regression slope of τ_{OH} of a TR species against $\tau_{OH,CH3CCl3}$ agrees well with the reverse ratio of their thermal reaction rates with OH, $k_{OH\text{-}CH3CCl3}/k_{OH\text{-}TR}$, at 272K, as noted in Spivakovsky *et al*. (2000). An important implication of this is that it is possible to derive τ_{OH} of a TR species by scaling up $\tau_{OH,CH3CCl3}$ using the ratio of thermal reaction rates.

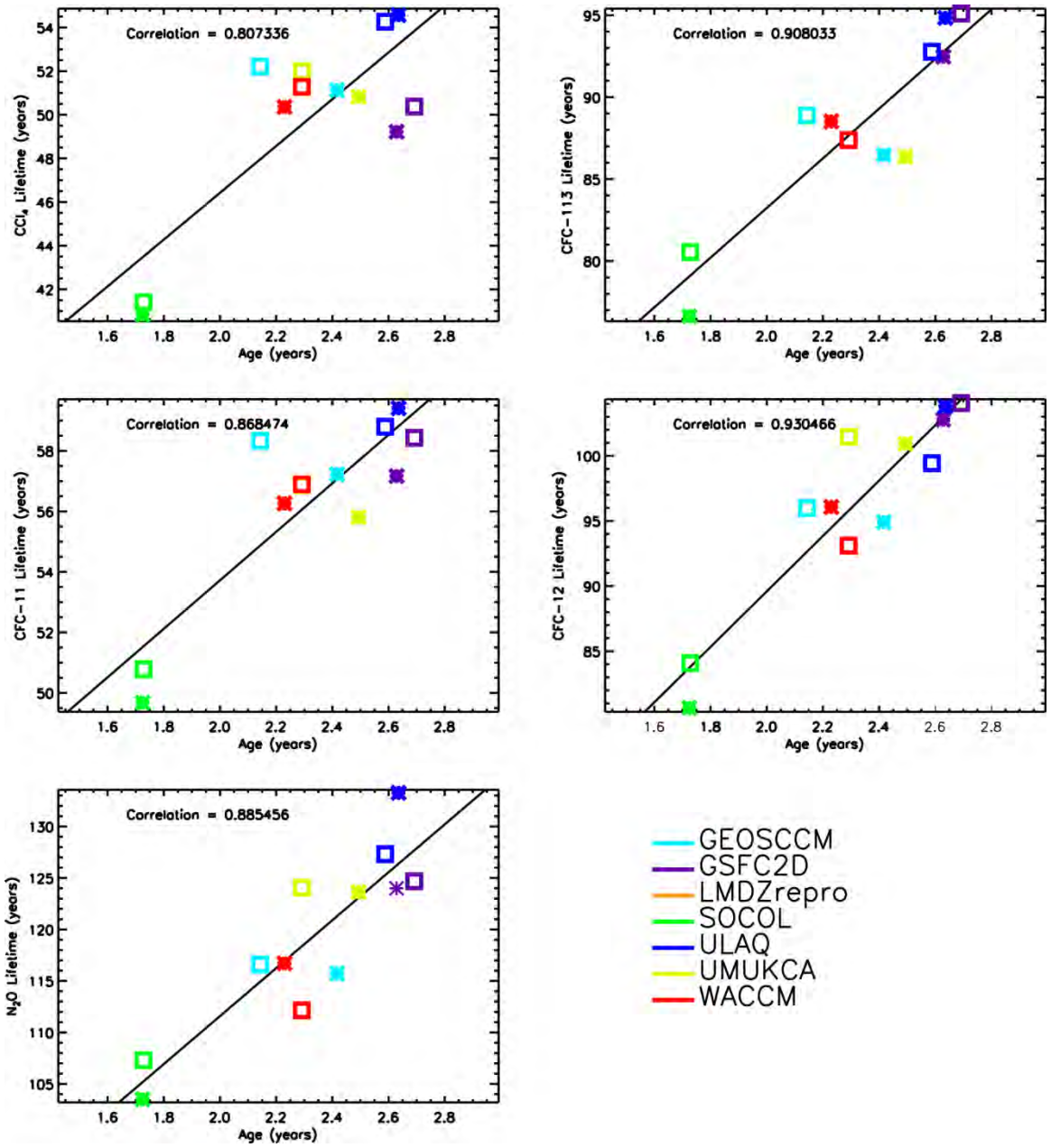

Figure 5.17. Correlation of modelled lifetimes (yrs) with the global mass-weighted average of stratospheric mean age-of-air from 100 hPa to 1 hPa (yrs) for (a) CCl_4, (b) CFC-113, (c) CFC-11, (d) CFC-12 and (e) N_2O. Results are shown from runs TS2000 (square) and TRANS (asterisk). Note that results from LMDZrepro are not included – see Figure 5.A6 in Appendix D.

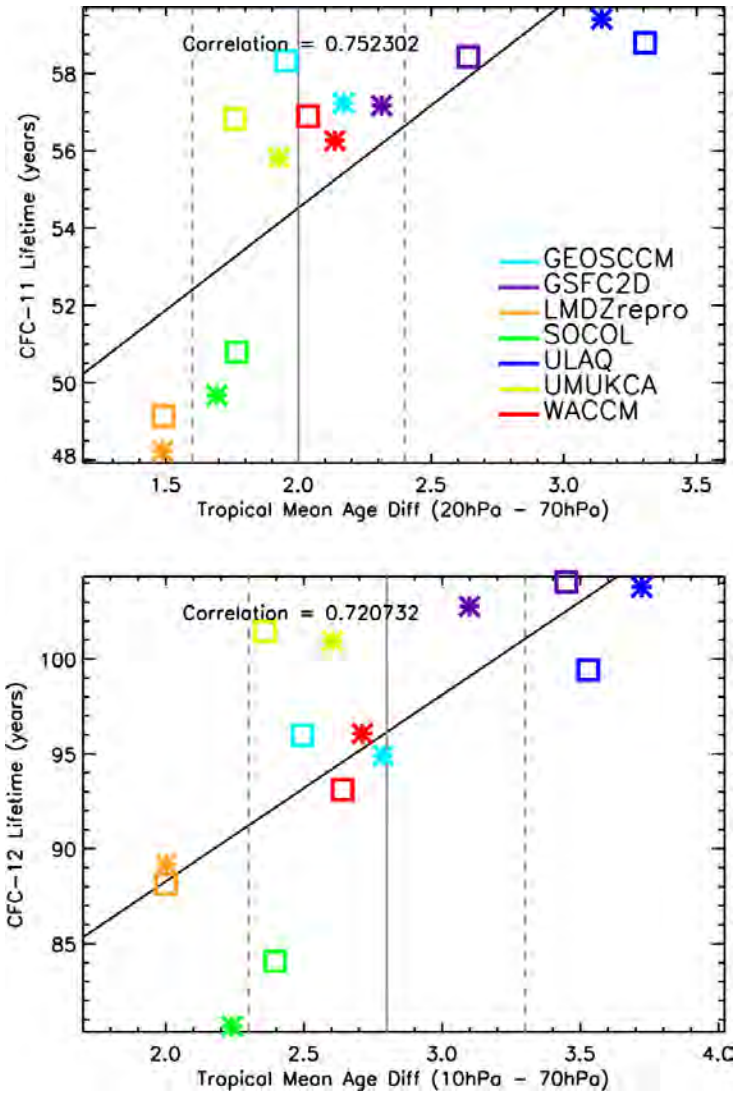

Figure 5.18. Correlation of modelled lifetimes (yrs) with the difference in mean age-of-air between two levels in the tropics for (a, top) CFC-11 (age difference between 70 hPa and 20 hPa), and (b, bottom) CFC-12 (age difference between 70 hPa and 10 hPa). Results are shown from runs TS2000 (square) and TRANS (asterisk). Also shown are estimates of the observed tropical mean age difference (vertical solid line) and its uncertainty (dashed vertical lines).

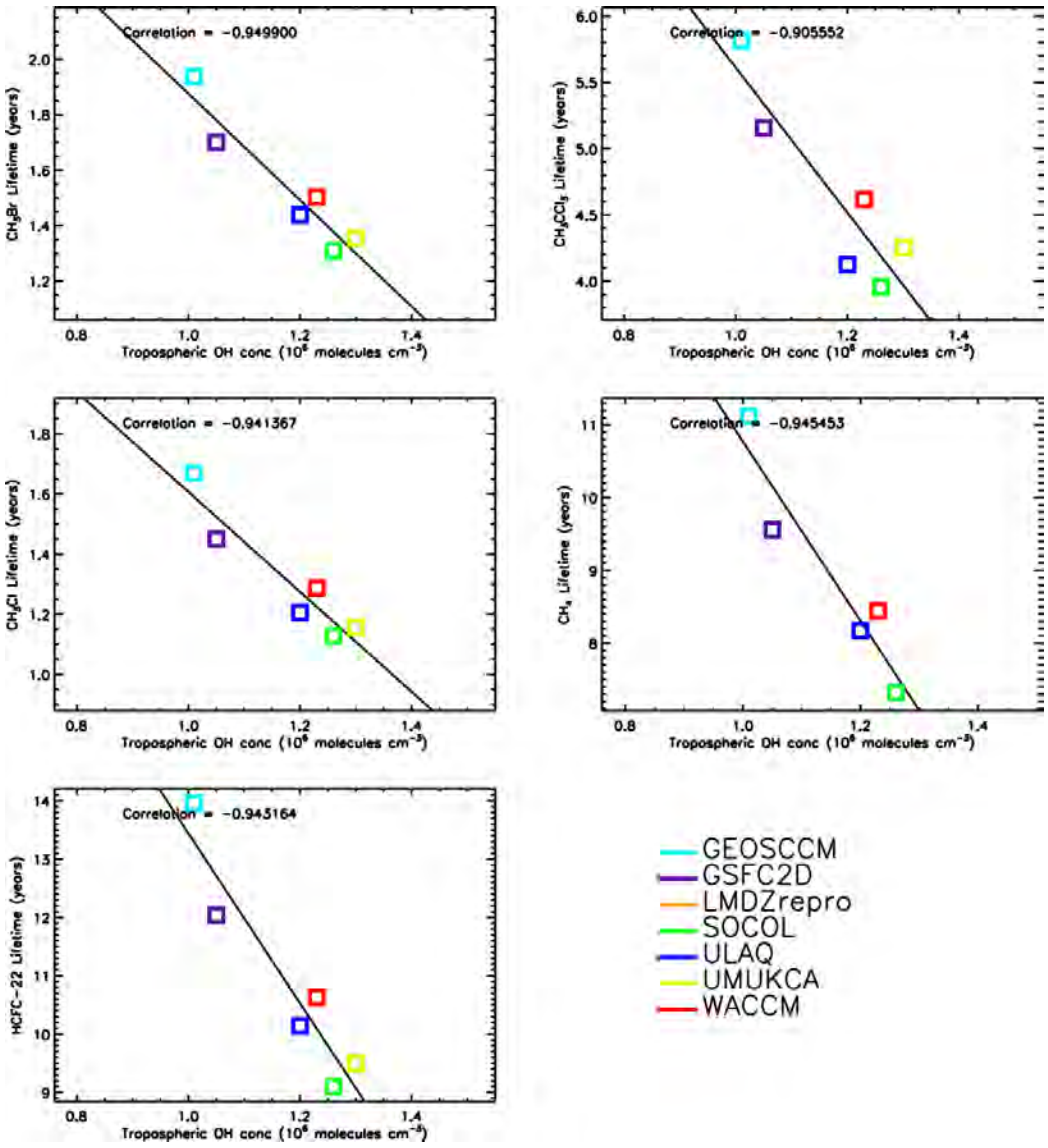

Figure 5.19. Correlation of modelled lifetimes (yrs) with tropospheric mean OH concentration (x 10^6 molecules cm^{-3}) for (a) CH_3Br (b) CH_3CCl_3, (c) CH_3Cl, (d) CH_4 and (e) HCFC-22. Results are shown from TS2000 runs (square). Results from LMDZrepro were not used for TR species and are not plotted here.

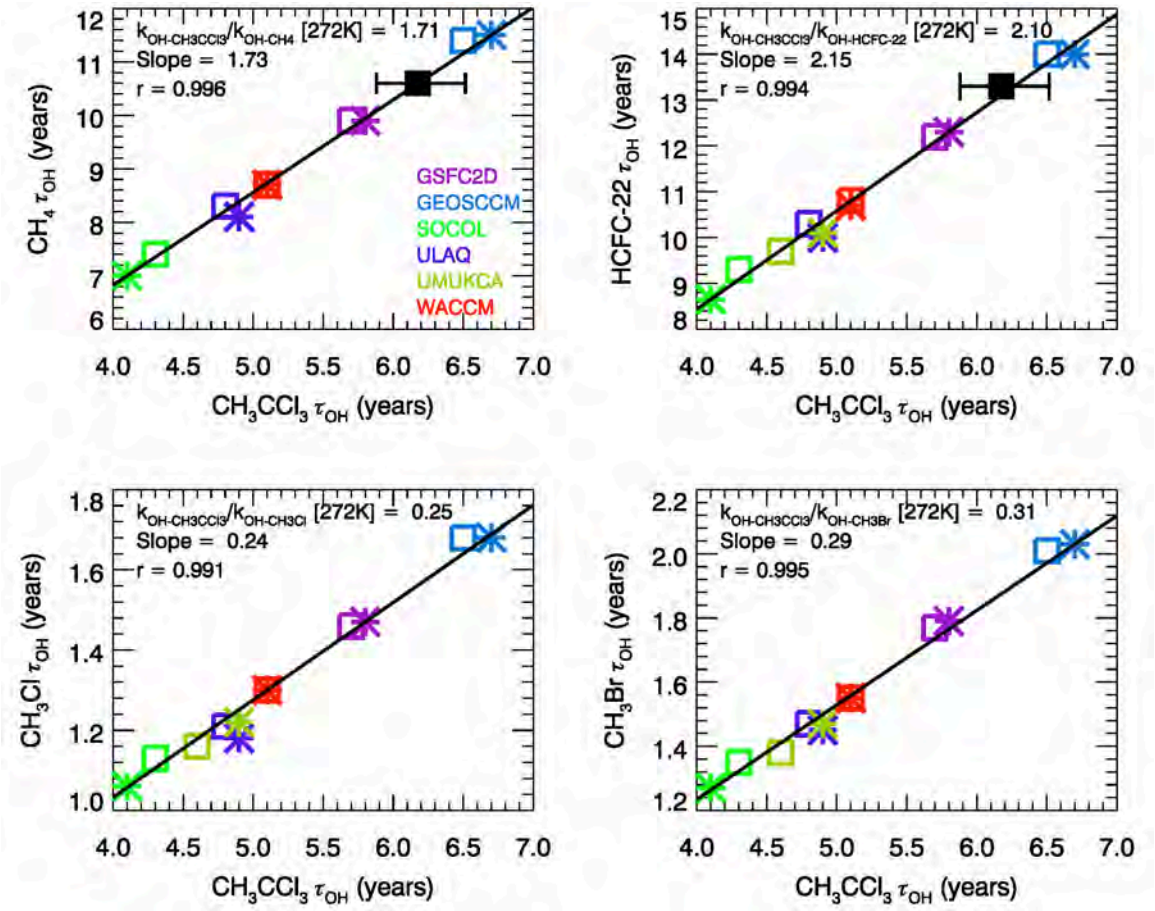

Figure 5.20. Correlation of modelled OH partial lifetimes (yrs) for (a) CH_4, (b) HCFC-22, (c) CH_3Cl, and (d) CH_3Br with modelled OH partial lifetime of CH_3CCl_3. Results are shown from runs TS2000 (squares) and TRANS (asterisks). Results from the 2-D inverse model used in Chapter 4 are also shown for CH_4 and HCFC-22 (black filled squares with horizontal bars indicating 2-σ uncertainty).

5.4.5 Future Lifetimes Estimates

Atmospheric changes are expected to modify tracer lifetimes in various ways in the future atmosphere. For example, a speed-up in the Brewer-Dobson circulation (BDC) in the critical region for stratospheric loss would be expected to lead to a reduction in the lifetime of photolytically removed species. Lin and Fu (2013) analysed the BDC changes in CCMVal-2 model experiments and found that while models consistently simulated an acceleration of both the shallow and deep branches of the BDC, the acceleration of the deep branch (i.e., above 30 hPa) was much smaller. They also noted significant differences between models. For the TR species, a future climate would lead to changes in tropospheric OH (e.g., through humidity changes) and air temperature, thus affecting the atmospheric lifetimes. For this assessment run TS2100 can be used to investigate how lifetimes may change due to these processes. Recall, however, that not all models have interactive tropospheric OH.

Table 5.9 compares the lifetimes for the TS2000 and TS2100 runs for six models that have conducted both runs. The six participating models predict different responses in future atmospheric lifetimes of SR species. GEOSCCM, SOCOL, and UMUKCA show a decrease

in lifetimes in most of the SR species while WACCM show a slight increase in all SR species. The future lifetime changes predicted by the GSFC2D and ULAQ are somewhat mixed, with increases for some and decreases in the others. A comparison of change in mean age-of-air between the simulations for 2100 and 2000 suggests that all models, except WACCM, show a speeding up of the Brewer-Dobson circulation although the magnitude of this change varies (Figure 5.21). GEOSCCM, GSFC2D, and SOCOL show only a small decrease in mean age (~1-3 months) while UMUKCA and ULAQ show larger changes. WACCM shows a slight speed-up (~0-1 month) of the shallow branch of the Brewer-Dobson circulation but a slow-down (~0-2 months) of the deep branch of the Brewer-Dobson circulation. However, such a weak change in circulation in WACCM might not be statistically significant. On the other hand, all models predict a decrease in photolysis (J) rates under 2100 conditions with the recovered ozone layer and a cooler stratosphere, though the relative changes in J rates vary among models and species. ULAQ and UMUKCA predict the strongest reduction in J rates, e.g., ~13% decrease in $J_{CFC\text{-}11}$ in the tropical lower stratosphere between 10-100 hPa with respect to the 2000 conditions, while GSFC2D, WACCM and GEOSCCM show a much weaker reduction of 5-6%. SOCOL displays a medium response of ~9% reduction in the corresponding $J_{CFC\text{-}11}$ rate. From a multi-model mean perspective, the decrease in lifetime due to a faster Brewer-Dobson circulation cancels with the increase in lifetime due to weaker photolysis. Therefore, the atmospheric lifetimes for SR species under 2100 conditions do not change significantly from the lifetimes under 2000 conditions.

With the exception of SOCOL, all models predict shorter lifetimes for TR tracers. The decrease in TR species lifetimes in GSFC2D and GEOSCCM is due to increases in air temperature while the decreases in ULAQ, UMUKCA, and WACCM are due to a combined impact of increasing OH (Table 5.3) and increasing air temperature. For all the models that calculate tropospheric OH interactively, the SOCOL model is the only model that predicts a decrease in $[OH]_{GM}$ from 1.26×10^6 molecules/cm^3 in 2000 to 1.08×10^6 molecules/cm^3 in 2100, therefore leading to an increase in lifetimes of TR tracers. However, the marked difference between its simulated OH concentration and vertical profile under present day conditions and the other models, as well as the previously published results, raises questions over the robustness of such a response.

It is important to point out that our projection of how lifetimes of ODSs will change in a future climate is dependent upon the choice of GHGs scenario used to drive the TS2100 run, as higher levels of CH_4 and CO_2 from RCP 6.5 (the more likely scenario) or RCP 8.5 will lead to a different response in atmospheric circulation, ozone concentration, as well as OH abundance, therefore a different future lifetime for both the SR and TR species.

5.5 Synthesis

The model results for the individual high priority species (Tables 5.5 and 5.6) indicate:

- **CFC-11**: Lifetime is ~23% larger than given in WMO (2011).
- **CFC-12**: The models overall show a similar lifetime to that given in WMO (2011) (5% smaller).
- **N_2O**: The models show a very similar lifetime to that given in WMO (2011).
- **CCl_4**: Modelled atmospheric lifetime is ~39% larger than that given in WMO (2011).
- **CH_3CCl_3**, **CH_4, HCFC-22**: Modelled lifetimes are similar to previous estimates and models show a large range of lifetime estimates.

Table 5.9. Steady state τ_{atmos} for 2000 and 2100 conditions from the TS2000 and TS2100 model simulations. For best-estimate lifetime for all targeted species, refer to Tables 6-1, 6-2, and 6-3 in Chapter 6.

Species	Model Mean		GSFC2D		GEOSCCM		SOCOL		ULAQ		UMUKCA		WACCM	
	2000[a,b]	**2100**	**2000**	**2100**	**2000**	**2100**	**2000**	**2100**	**2000**	**2100**	**2000**	**2100**	**2000**	**2100**
CFC-11	**56.5**	**55.2**	58.6	57.7	58.3	54.7	50.8	49.3	58.6	57.6	56.8	55.2	56.9	57.7
CFC-12	**95.8**	**95.3**	103.7	103.5	96.0	90.6	84.1	81.9	99.4	104.2	101.5	98.8	93.1	96.7
CFC-113	**88.5**	**87.8**	95.4	94.4	88.9	83.4	80.5	79.1	92.8	96.6	87.4	85.5	87.4	90.6
CFC-114	**189**	**193**	204	206	--	--	169	171	205	205	--	--	184	192
CFC-115	**991**	**1015**	961	981	--	--	--	--	--	--	--	--	1022	1052
CCl_4	**49.9**	**48.6**	50.7	49.9	52.2	48.7	41.4	40.2	54.3	52.9	52.0	50.4	51.3	51.8
N_2O	**117**	**118**	125	125	117	111	107	107	127	132	--	--	112	118
H1202	**1.8**	**2.0**	2.1	2.5	--	--	--	--	--	--	--	--	1.6	1.6
H1211	**11.5**	**11.9**	13.5	13.4	--	--	--	--	9.8	10.0	12.3	13.5	11.0	11.4
H1301	**73.4**	**73.1**	77.4	76.8	72.8	68.6	67.1	66.1	78.0	79.2	74.7	76.2	71.4	73.5
H2402	**14.5**	**14.8**	13.9	14.0	--	--	--	--	13.9	14.2	--	--	15.9	16.4
CH_4	**9.2**	**8.7**	9.6	9.2	11.1	10.6	7.3	8.1	8.2	7.5	--	--	8.4	8.0
CH_3CCl_3	**5.2**[c]	**4.9**	5.2	4.9	5.8	5.6	4.0	--	--	--	--	--	4.6	4.4
CH_3Cl	**1.3**	**1.3**	1.5	1.4	1.7	1.6	1.1	1.3	1.2	1.1	1.1	1.1	1.3	1.2
CH_3Br	**1.6**	**1.5**	1.7	1.6	1.9	1.9	1.3	1.5	1.4	1.3	1.4	1.3	1.5	1.4
HCFC-22	**11.0**	**10.5**	12.0	11.5	14.0	13.4	9.1	9.9	10.1	9.4	9.5	9.2	10.6	10.0
HCFC-141b	**8.3**	**7.9**	9.2	8.8	--	--	7.1	7.8	7.8	7.3	--	--	8.1	7.7
HCFC-142b	**14.5**	**13.6**	17.5	16.6	--	--	13.6	15.2	14.7	13.6	--	--	12.2	11.5
HFC-23	**242**	**229**	226	213	260	247	--	--	--	--	--	--	--	--
HFC-32	**5.5**	**5.3**	5.2	5.0	5.9	5.7	--	--	--	--	--	--	--	--
HFC-125	**31.3**	**30.1**	29.3	28.1	33.7	32.4	--	--	--	--	--	--	--	--
HFC-134a	**14.4**	**13.8**	13.6	13.0	15.4	14.8	--	--	--	--	--	--	--	--
HFC-143a	**53.2**	**50.7**	50.1	47.5	56.8	54.3	--	--	--	--	--	--	--	--
HFC-152a	**1.5**	**1.4**	1.5	1.4	1.6	--	--	--	--	--	--	--	--	--
HFC-227ea	**45.3**	**40.3**	42.4	40.3	48.6	--	--	--	--	--	--	--	--	--
HFC-245fa	**7.8**	**7.5**	7.8	7.5	--	--	--	--	--	--	--	--	--	--

[a] Model mean lifetimes for 2000 listed in this table are calculated without LMDZrepro results for a meaningful comparison with the 2100 lifetimes.
[b] The lifetime of all TR species for 2000 and 2100 conditions are calculated without SOCOL results.
[c] The CH_3CCl_3 lifetimes from ULAQ and UMUKCA in 2100 are not realistic due to very low concentrations of CH_3CCl_3 in the TS2100 run, therefore we exclude CH_3CCl_3 lifetimes from these two models in this comparison.

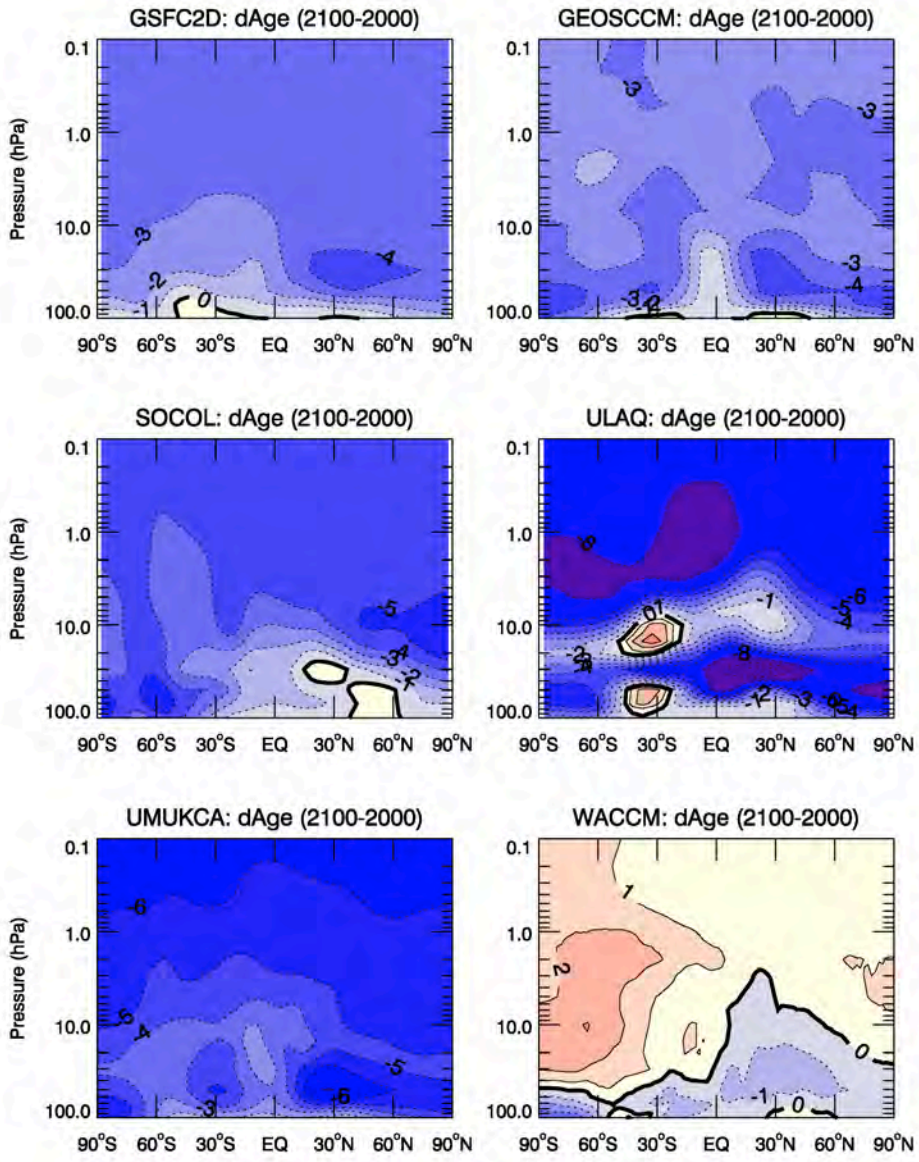

Figure 5.21. Difference in mean age-of-air (months) between CCM runs for 2100 and 2000 conditions. (Note: LMDZrepro did not perform TS2100 run and so is not included here).

Other SR species with notable results:

- **Halon-1202, Halon-1211, and Halon-2402**: Modelled lifetimes are significantly smaller (~30%) than given in WMO (2011).
- **Halon-1301**: Lifetime longer (11%) than that given in WMO (2011).

Other TR species with notable results:

- **CH_3Br**: Lifetime smaller (20%) than given in WMO (2011).
- **HCFC-141b** and **HCFC-142b**: Modelled lifetimes are shorter (13-17%) than given in WMO (2011).
- **HFC-143a**: Lifetime longer than that given in WMO (2011).
- **HFC-227ea**: Lifetime longer than that given in WMO (2011).

5.6 Summary

This chapter has analysed results from seven global models (six 3-D CCMs and a 2-D model) which were run with the same standard photochemical data. We diagnosed both instantaneous and steady-state lifetimes for species with sinks mainly in the troposphere (tropospheric removal, TR) and stratosphere (stratospheric removal, SR) for present-day and 2100 conditions. The key results are:

Quantification of Lifetimes

- The transient lifetimes of, for example, CFC-11 and CFC-12 before the 1990s are larger than steady-state lifetimes but decrease to approach the steady-state lifetime after this time. N_2O, CH_3CCl_3, and CH_4 show little differences between transient and steady-state lifetimes. The strong variations in CFC emissions over this period cause this difference.
- Flux Boundary Condition (FBC) tracers show similar lifetimes to Mixing Ratio Boundary Condition (MBC) tracers within the same model, despite significant differences in their atmospheric distributions and total burden.
- Species that are destroyed in the stratosphere show a range of model-calculated lifetimes. The lifetimes show a clear correlation with the simulated tropical mean age profile, which depends on the Brewer-Dobson circulation. In particular, the tropical ascent rate through the altitudes of large loss is critical to the calculated lifetimes with faster ascent rates produce shorter lifetimes.
- Species that are predominantly removed by OH show a large range of lifetime estimates between models. However, for many models the large range of lifetimes show a good straight-line correlation with the simple metrics of global mean tropospheric OH and CH_3CCl_3 lifetime.
- A global mean OH abundance of 1.09×10^6 molecules/cm^3 has been inferred using CH_3CCl_3 observations in the 2-D inverse model. This is likely representative of the true global mean OH because the results were confirmed by using observationally derived surface CH_3CCl_3 from the flux boundary condition tracer in the WACCM and GEOSCCM simulations as pseudo-observational constraints to derive τ_{OH} and $[OH]_{GM}$ in the inverse model (Chapter 4). This implies that the four 3-D CCMs that calculate OH interactively with full tropospheric chemistry have high-biased tropospheric OH, thus shorter TR lifetimes.
- Overall best model estimates have been calculated using the multi-model mean. Species for which the new mean modelled lifetimes show a significant increase with respect to WMO (2011) and IPCC (2007) are CFC-11, CCl_4, Halon-1301, HFC-143a, and HFC-227ea.
- Species for which the new mean modelled lifetimes show a significant decrease with respect to WMO (2011) and IPCC (2007) are Halon-1202, Halon-1211, Halon-2402, CH_3Br, HCFC-141b, and HCFC-142b.
- For 2100 some models indicate a speed-up of the Brewer-Dobson circulation and a younger age-of-air. However, for other models the circulation change is not so clear. A thicker (recovered) ozone layer in 2100 leads to reduced photolysis. These two processes lead to cancelling effects in the models and hence there is no clear trend in the lifetimes of SR tracers between 2000 and 2100. However, these impacts will depend on the future GHG scenario used.

- For a 2100 atmosphere the majority of models indicate a decrease in TR species lifetime due to the combined impact of increasing OH and increasing air temperature. Similar to the SR species, these impacts are likely to vary when a different future GHG scenario is used.

Modelling Recommendations

From a modelling point of view, recommendations for future assessments are:

- The runs presented here are the first attempts at running ODSs with flux boundary conditions (FBC) in long-term assessment simulations. Modelled distributions vary between the MBC and FBC tracers. This shows that models will diverge significantly if assessments adopt FBCs for future runs. Another complication is that full emission and sink information will be needed for all halocarbons. That information is likely not yet available so FBCs might be used for a subset of species at most.
- Scenarios which predict the future evolution of ODSs, and which are used in MBC model simulations, should be updated using new lifetimes.

5.7 Appendix A: Model Description and Updates Since CCMVal-2

SPARC CCMVal (2010) provided a comprehensive description of the CCMs used in this report. Since SPARC CCMVal (2010) the models have evolved and this section provides a brief summary of the key updates and improvements.

GEOSCCM

For this assessment, we use the GEOS CCM V2 that couples the GEOS-5 GCM version Fortuna 2-4 with an updated stratospheric chemistry module originally described by Douglass and Kawa (1999). The photochemical scheme includes all important gas-phase reactions for the stratosphere (Douglass and Kawa, 1999). The model uses a flux-form semi-Lagrangian dynamical core (Lin, 2004). Moist processes in GEOS-5 are represented using a convective parameterisation and prognostic cloud scheme. Convection is parameterised using the relaxed Arakawa Schubert (RAS) scheme developed by Moorthi and Suarez (1992). The simulations are run with spatial resolution of 2° latitude by 2.5° longitude and 72 layers extending from the surface to 0.01 hPa.

Changes since CCMVal-2 (SPARC CCMVal 2010):

- The chemical kinetics and photolysis rates were updated to the recommendations of JPL 10-6 (Sander *et al*., 2011).
- Two very-short-lived bromocarbons, CH_2Br_2 and $CHBr_3$, are added and interact with full stratospheric chemistry scheme.
- The model now uses 3-D monthly mean OH from Spivakovsky *et al.* (2000) in the troposphere instead of the original zonal mean OH archived in a previous tropospheric full chemistry Chemical Transport Model (CTM) simulation from GEOS-Chem.
- For this assessment, GEOSCCM added HFC-23, HFC-32, HFC-134a, HFC-143a, HFC-125, HFC-152a, and HFC-245fa to the chemistry scheme.

LMDZrepro

For this assessment we use a new version of the LMDZrepro CCM which couples the LMDZ-CM5 GCM version, developed for the CMIP5 exercise (Szopa *et al*., 2012; Dufresne *et al*., 2012), with an updated version of the REPROBUS chemistry module (Jourdain *et al*., 2008). The dynamical part of the LMDZ GCM is based on a finite-difference formulation of the primitive equations of meteorology on a staggered and stretchable (the Z of LMDZ standing for zoom) longitude-latitude grid. The radiation scheme is inherited from the European Centre for Medium-Range Weather Forecasts (Fouquart and Bonnel, 1980; Morcrette *et al*., 1986). The photolysis rates are calculated off-line with the Tropospheric and Ultraviolet Visible (TUV) radiative model (Madronich and Flocke, 1998). The dynamical effects of the subgrid-scale orography are parameterised according to Lott (1999). Turbulent transport in the planetary boundary layer is treated as a vertical eddy diffusion (Laval *et al*., 1981) with counter-gradient correction and dry convective adjustment. The surface boundary layer is treated according to Louis (1979). A statistical cloud scheme is used to predict the cloud properties with a different treatment for convective clouds (Bony and Emanuel, 2001) and large-scale condensation (Hourdin *et al.*, 2006). Vapour and liquid water, and atmospheric trace species are advected with a monotonic second-order finite volume scheme (Hourdin and Armengaud, 1999). Instead of using the recommended tropospheric 3-D monthly mean OH from Spivakovsky *et al*. (2000), the model calculates tropospheric OH. However, the model is forced below 400 hPa by 3-D monthly mean 1990s

climatologies of NO_x, CO and O_3 taken from a simulation by a well-established 3-D tropospheric CTM, the TOMCAT model (Savage *et al*., 2004).

Changes since CCMVal-2 (SPARC CCMVal 2010):

- The number of hybrid sigma-pressure vertical levels has been reduced from 50 in the stratospheric version of LMDZ (Lott *et al*., 2005) to 39, with 15 levels above 20 km. The top layer is about at the same altitude as the CCMVal-2 L50 version and is fine enough to resolve the propagation of the mid-latitude waves in the stratosphere and to produce sudden stratospheric warming.
- The horizontal resolution has been increased from 96 points in longitude by 72 in latitude (3.75^o x 2.5^o) to 96 points in longitude by 95 in latitude (3.75^o x 1.9^o).
- The chemical kinetics and photolysis rates were updated according to the latest recommendations in the JPL 10-6 evaluation (Sander *et al*., 2011).

SOCOL

For this assessment SOCOL v3.0 was used. In contrast to its predecessor SOCOL v2.0 described by Schraner *et al.* (2008) and evaluated in SPARC CCMVal-2 report (SPARC CCMVAL 2010), the new version exploits MA-ECHAM5 instead of MA-ECHAM4 as the underlying GCM. The advection of the chemical species is calculated by the flux-form advection scheme of Lin and Rood (1996) instead of the hybrid scheme by Zubov *et al.* (1999). From a technical point of view, the coupling between GCM and CTM has been much simplified. The chemical module has been transferred from Fortran77 to Fortran95 and completely rewritten according to the ECHAM5 infrastructure. In contrast to the previous versions, the model can be executed in parallel mode, which enables a substantial reduction of the wall clock time. ECHAM5 includes several changes in the model physics and numerics.

A new parameterization of stratiform clouds has been developed, including a separate treatment of cloud water and cloud ice, advanced cloud microphysics and a statistical model for the calculation of the cloud cover. The description of coupling processes between land surface and atmosphere has been improved, including a new data set of land surface data. Water vapour, cloud variables, and chemical species are transported by a flux-based, mass-conserving, and shape-preserving transport scheme (Lin and Rood, 1996) instead of the semi-Lagrangian approach used in ECHAM4. The shortwave radiation code is basically the same as in ECHAM4; however, the spectral resolution has been increased from 2 to 6 bands. The new longwave radiation code is based on k-correlated scheme and the number of spectral intervals has been increased to 16. The chemical scheme remains the same, but the reaction rates were updated using the latest JPL evaluation (Sander *et al.,* 2011). Preliminary analysis of the 26-year long model run results shows substantial improvement of the transport-related model quantities such as total inorganic chlorine and methane over the southern high latitudes in October and tropical water vapour tape recorder speed.

ULAQ

For this report the ULAQ model was updated in the following ways:

- Vertical resolution: 126 log-pressure levels from the surface (1000 hPa) to 0.04 hPa, with an approximate pressure altitude increment of 568 m.
- Horizontal resolution: T21 (5.6^o x 5.6^o).

- Species cross sections were updated using JPL 10-6 (Sander *et al.*, 2011) recommendations. Schumann-Runge bands are treated following the parameterisation of Minschwaner *et al.* (1993) based on (fixed-T) ODF formulation. As an alternative, the ULAQ-CCM can also use the SRB parameterisation of Allen and Frederick (1982). Diurnal averages are calculated with a 5-point Gaussian quadrature.
- Photolysis and solar heating rates are calculated with a new radiative transfer module, covering wavelengths from Lyman-alpha up to the solar NIR. Solar heating rates are calculated for O_3, O_2, NO_2, SO_2, H_2O, CO_2, aerosols. Radiative transfer is treated with a two-stream delta-Eddington approximation model (Toon *et al.,* 1989). Sphericity is included by means of Chapman functions (Dahlback and Stamnes, 1991). Refraction is treated with an iterative ray-tracing technique (Gallery *et al.,* 1983) in a simple exponential refraction model. Rayleigh-scattering cross sections are calculated with the WMO-1985 approximation. Aerosol and cirrus cloud extinction values are passed daily from the ULAQ-CCM aerosol module to the radiative module, with appropriate values of Q-ext, g, and single scattering albedo, given the calculated size distribution of the particles. Warm clouds are not included. Surface albedo is taken from MERRA 2-D hourly averaged data (http://gdata1.sci.gsfc.nasa.gov). Sun-earth distance is calculated daily as a function of orbit eccentricity. Solar cycle is included. Top-of-atmosphere solar fluxes are taken from the CCMVal web page and are carefully integrated on the wavelength bins used in the ULAQ model.
- Upper tropospheric cirrus ice particle formation is included via homogeneous and heterogeneous freezing (Kärcher and Lohmann, 2002).

UMUKCA

The current model is a further development of the version described in Morgenstern *et al.* (2009). Both the Unified Model (UM) climate model and the UKCA stratospheric chemistry module have been updated. The current version of the climate model is 7.3 as compared to 6.1 for CCMVal-2 (SPARC CCMVal 2010). It runs at a horizontal resolution of 3.75^o x 2.5^o (Arakawa C grid) with 60 levels in the vertical (hybrid geometric height coordinate), ranging from the surface up to approximately 84 km. The model solves the three-dimensional equations of motion, with vertical velocity being a prognostic quantity. Consequently monthly mean diagnostics on pressure levels are processed from the monthly mean pressure and the monthly mean of a quantity on model levels. Many physical parameterisations (including convection) have been changed between 6.1 and 7.3. For more details see Hewitt *et al.* (2011), which describes the HadGEM3 modelling framework from which the atmospheric model used in this intercomparison is derived.

The chemistry has been extended to meet the requirements of the lifetime assessment, including rate updates following JPL 10-6 recommendations. The stratospheric chemistry used in CCMVal-2 distinguished between two chlorine (CFC-11 and CFC-12) and one bromine (CH_3Br) source gas. Contributions from other species were 'lumped' into these three gases. The current version considers explicitly seven chlorine (CCl_4, CFC-11, CFC-12, CFC-113, HCFC-22, CH_3CCl_3, CH_3Cl) and five bromine (H-1211, H-1301, CH_3Br, CH_2Br_2, $CHBr_3$) source gases. Photolysis for all species is now calculated using Fast-Jx (Neu *et al.*, 2007; Telford *et al.*, 2013). The radiative transfer calculations in the climate model use the trace gas distributions determined by the interactions of transport and chemistry.

WACCM

The Whole-Atmosphere Community Climate Model, Version 4 (WACCM4) is a comprehensive numerical model, spanning the range of altitude from the Earth's surface to the lower thermosphere (Garcia *et al.,* 2007). WACCM4 is a fully interactive model, wherein the radiatively active gases (CO_2, H_2O, N_2O, CH_4, CFCs, HCFCs, halons, NO, O_3) affect heating and cooling rates and therefore dynamics. WACCM4 is based on the software framework of the National Center for Atmospheric Research's Community Atmospheric Model, version 4 (CAM4), which is contained in the Community Earth System Model (CESM) version 1.0.3.

Changes since CCMVal-2 (SPARC CCMVal 2010):

- The gas-phase chemical reaction and photolysis rates were updated to the recommendations of JPL 10-6 (Sander *et al*., 2011).
- The chemical mechanism has been expanded to include a detailed representation of tropospheric chemistry (Emmons *et al.,* 2010). The WACCM version used in CCMVal-2 had 59 species and 234 chemical reactions. The mechanism used in this report contains 144 species and 443 chemical reactions.
- Time-dependent surface emissions for CO, NO, and non-methane hydrocarbons were taken from the IPCC ACCMIP emission inventory (Lamarque *et al*., 2011).
- In CCMVal-2 the WACCM mechanism included 10 organic halogens: CH_3Cl, CFC-11, CFC-12, CFC-113, HCFC-22, CCl_4, CH_3CCl_3, H-1211, H-1301, and CH_3Br. For this report an additional eight organic halogens were added: CFC-114, CFC-115, HCFC-141b, HCFC-142b, CH_2Br_2, $CHBr_3$, Halon-1202, and Halon-2402.

GSFC2D

The NASA/Goddard Space Flight Center (GSFC) two-dimensional (2-D) model was originally developed in the 1980s for studies pertaining to the chemistry of the middle atmosphere and has been used in stratospheric assessments since 1989. The specified transport version of the model, in which the transport and temperature fields are derived offline from meteorological data, was originally described in Douglass *et al*. (1989) and Jackman *et al*. (1990) with subsequent updates discussed in Considine *et al*. (1994); Jackman *et al*. (1996); and Fleming *et al*. (1999, 2007). The model now uses the year-to-year transport and temperature fields for 1979-2010 derived from the MERRA meteorological analyses. The coupled version of the model, in which the chemistry, radiation, and dynamics are computed interactively, was originally discussed in Bacmeister *et al*. (1995) and Rosenfield *et al*. (1997). This version of the model has recently undergone significant improvements (Fleming *et al*., 2011) and simulates long term (1960-2100) changes in stratospheric ozone, temperature, and age-of-air that are in good agreement with the GEOSCCM. Both versions of the model are used in this assessment.

Both the specified transport and coupled versions of the model use the same chemistry solver and kinetic and photochemical calculations. While neither model version was included in CCMVal-2 (SPARC CCMVal, 2010), several of the model components are very similar to those used in the GEOSCCM which was evaluated in CCMVal-2. These components include: the infrared (IR) radiative transfer scheme (Chou et al., 2001); the photolytic calculations (Anderson and Lloyd, 1990; Jackman *et al*., 1996); and the microphysical model for polar stratospheric cloud (PSC) formation (Considine *et al*., 1994). The chemistry solver includes all gas-phase reactions important for the stratosphere and computes a full diurnal

cycle for 35 fast chemical constituents. This scheme was shown to be in good agreement with photochemical steady state box model calculations (Park *et al*., 1999). The latest JPL 10-6 recommendations are used for the photolytic cross sections and reaction rate constants (Sander *et al*., 2011). The model domain extends from the ground to approximately 92 km, with a grid resolution of 4° latitude by 1 km altitude.

5.8 Appendix B: Description of Model Simulations

TRANS is a 50-year transient run from 1960 to 2010, based on the definition of the REF-B1 simulation used in CCMVal-2 (SPARC CCMVal, 2010, Chapter 2). All forcings in this simulation are taken from observations, and are mostly identical to those used by Eyring *et al.* (2006) and Morgenstern *et al.* (2010) for REF-B1. This transient simulation includes all anthropogenic and natural forcings based on changes in trace gases, solar variability, volcanic eruptions, QBO, and SSTs/SICs.

- **GHGs** (N_2O, CH_4, and CO_2) Coupled Model Intercomparison Project (CMIP) RCP 4.5 Scenario.
- **ODS** (CFC-11, CFC-12, CFC-113, CFC- 114, CFC-115, CH_3CCl_3, HCFC-22, HCFC-141b, HCFC-142b, Halon-1211, Halon-1202, Halon-1301, and Halon-2402) are prescribed at the surface according to Table 5A-3 (baseline A1 scenario) of WMO (2011).
- **HFCs** (HFC-23, HFC-32, HFC-125, HFC-134a, HFC-143a, HFC-152a, HFC-245fa), except HFC-23, are from high scenario A1 of Velders *et al.* (2009) merged with AGAGE measurements in 2010. HFC-23 between 1978 and 2009 is from the annual global mean in Table 3 of Miller *et al.* (2010).
- **SST and SICs** are prescribed as monthly mean boundary conditions following the observed global SIC and SST data set HadISST1 (Rayner *et al.,* 2003).
- **Solar variability**. Daily spectrally resolved solar irradiance data from 1 January 1950 to 31 Dec 2006 (in $W/m^2/nm$) are provided at http://www.geo.fu-berlin.de/en/met/ag/strat/research/SOLARIS/Input_data/index.html. The data are derived with the method described by Lean *et al.* (2005). Each modelling group was required to integrate the data over the individual wavelength intervals used in their radiation and photolysis schemes.
- **The QBO**: Models that do not produce an internally generated QBO were asked externally impose a QBO.
- **Aerosol Surface Area Densities (SADs)** from observations are considered in TRANS (Eyring *et al.,* 2010, Morgenstern *et al.,* 2010).
- **Emission of ozone and aerosol precursors** (CO, NMVOC, NO_x and SO_2) are from Representative Concentration Pathways (RCP) Scenario 4.5 (Lamarque *et al*., 2011).
- **Tropospheric OH:** Models that do not include a detailed tropospheric chemistry scheme were asked to use to prescribe their tropospheric OH values to the 3-D monthly OH documented in Spivakovsky *et al.* (2000).

TS2000 is a 30-year timeslice simulation for 2000 conditions, designed to diagnose steady-state lifetimes and to facilitate the comparison of model output against constituent observations from various measurement datasets.

- **GHGs, ODSs, and HFCs:** The surface concentrations of GHGs are based on CMIP RCP4.5 Scenario while the surface halogens are based on Table 5A-3 of WMO (2010) for the year 2000. The surface concentrations of HFCs are from the A1 scenario of Velders *et al.* (2009) for the year 2000. All ODSs, GHGs and HFCs repeat every year.
- **Emission of ozone and aerosol precursors** (CO, NMVOC, NO_x and SO_2) are from the RCP4.5 Scenario and are repeating annually.
- **Tropospheric OH:** Models that do not include a detailed tropospheric chemistry scheme are asked to use OH fields of Spivakovsky *et al.* (2000) in the troposphere.

TS2100 is a 30-year timeslice simulation for 2100 conditions, designed to diagnose steady-state lifetimes in a future climate with recovered stratospheric ozone layer and a faster Brewer-Dobson circulation.

- **GHGs, ODSs, and HFCs:** The surface concentrations of GHGs and ODSs are based on projections of the CMIP RCP4.5 Scenario and Table 5A-3 of WMO (2011) for the year 2100, respectively. There are no projections available for HFCs in 2100 and no recommendation was made for this experiment.
- **Ozone and aerosol precursors, and tropospheric OH:** OH in the troposphere is controlled by a delicate balance between its sources and sinks and responds to changes in tropospheric concentrations of CO, CH_4, H_2O, O_3, NO_x, as well as overhead O_3 column. In this assessment, we only seek to address how OH responds to climate changes, i.e., changes in O_3 column, H_2O and CH_4, under 2100 conditions. Therefore, models that calculate realistic tropospheric OH were asked to use the same precursors emissions as run TS2000. Models which do not include a detailed tropospheric chemistry scheme were asked to use OH fields of Spivakovsky *et al.* (2000) in the troposphere.

FBC tracer emissions

- **Annual global emission**: The surface emissions used in TRANS are time-dependent annual bottom up emissions computed using time series of data on production and sales into various end-use categories having different release functions (McCulloch *et al.,* 2001, 2002).
- **Emission distribution:** The geographical resolved distribution is based on the distribution of 1986 for CFC-11 and CFC-12, 1990 for HCFC-22 and CH_3CCl_3 for 1950-1995. From 1995 to 2010, the distribution is calculated using the geographical resolved fractionation of 2000 for CFC-11 and CFC-12. The calculated global emissions were distributed among countries using the distribution of individual national fractions of the world total Gross Domestic Product **(**McCulloch *et al.,* 2001, 2002**)**. Within each country, emissions were distributed to individual grid squares using a population distribution (McCulloch *et al.,* 2001, 2002; AFEAS, 2001).
- **Surface emission for TS2000:** Surface emissions of year 2000 are used repeatedly for the entire 30-year simulation. Due to the difference in source vs. sink balance for each species, individual FBC tracers evolve differently, with CFC-11_FBC and CH_3CCl_3_FBC behaving as trace gases with an increasing trend and CFC-12_FBC and HCFC-22_FBC behaving as time-decaying tracers.
- **Surface emission for TS2100:** All emissions of the above four species become zero (or have a very small value) in 2100. Models used zero emissions for all four FBC tracers repeatedly for the entire simulation.

5.9 Appendix C

Table 5.A1. Comparison of model steady-state lifetime (τ_{ss}) from the TS2000 simulation with the transient lifetime ($\tau_{transient}$) for MBC high priority species and their FBC and CONST tracers in year 2000 from the transient simulation. Note part of the differences in the lifetimes between the FBC and MBC tracers are due to the unaccounted topography impact on the FBC tracers as discussed in Box 5.1.

Species		GSFC2D	GEOSCCM	LMDZ -repro	SOCOL	ULAQ	UMUKCA	WACCM
CFC-11	τ_{SS}	58.6	58.3	49.1	50.2	58.6	56.8	56.9
	$\tau_{transient, MBC}$	56.6	60.0	47.0	49.5	58.2	56.3	55.1
	$\tau_{transient, FBC}$	60.0	58.7	--	--	60.6	61.4	55.2
	$\tau_{transient, CONST}$	--	60.4	--	--	--	--	57.1
CFC-12	τ_{SS}	103.7	96.0	88.2	84.1	99.4	101.5	93.1
	$\tau_{transient, MBC}$	102.1	98.5	85.0	80.5	101.4	99.9	93.3
	$\tau_{transient, FBC}$	99.1	96.1	--	--	105.0	109.7	93.0
	$\tau_{transient, CONST}$	--	97.5	--	--	--	--	92.1
CCl_4	τ_{SS}	50.7	52.2	42.0	41.4	54.3	52.0	51.3
	$\tau_{transient, MBC}$	49.2	53.5	40.0	41.0	53.8	51.2	50.1
N_2O	τ_{SS}	125	117	105	107	127	--	112
	$\tau_{transient, MBC}$	124	120	--	105	130	--	113
	$\tau_{transient, CONST}$	--	119	--	--	--	--	112
CH_3CCl_3	τ_{SS}	5.2	5.8	--	4.0	4.1	4.3	4.6
	$\tau_{transient, MBC}$	5.2	5.8	--	3.7	4.5	4.5	4.6
	$\tau_{transient, FBC}$	5.2	5.8	--	--	4.5	4.5	4.6
	$\tau_{transient, CONST}$	--	--	--	--	--	4.5	4.5
CH_4	τ_{SS}	9.6	11.1	--	7.3	8.2	--	8.4
	$\tau_{transient, MBC}$	10.0	11.2	--	6.9	8.5	--	8.4
	$\tau_{transient, CONST}$	--	10.9	--	--	--	--	8.5
HCFC-22	τ_{SS}	12.0	14.0	--	9.1	10.1	9.5	10.6
	$\tau_{transient, MBC}$	12.4	13.9	--	8.5	10.3	9.9	10.1
	$\tau_{transient, FBC}$	12.4	14.0	--	--	11.7	9.8	10.3

5.10 Appendix D: Additional Figures

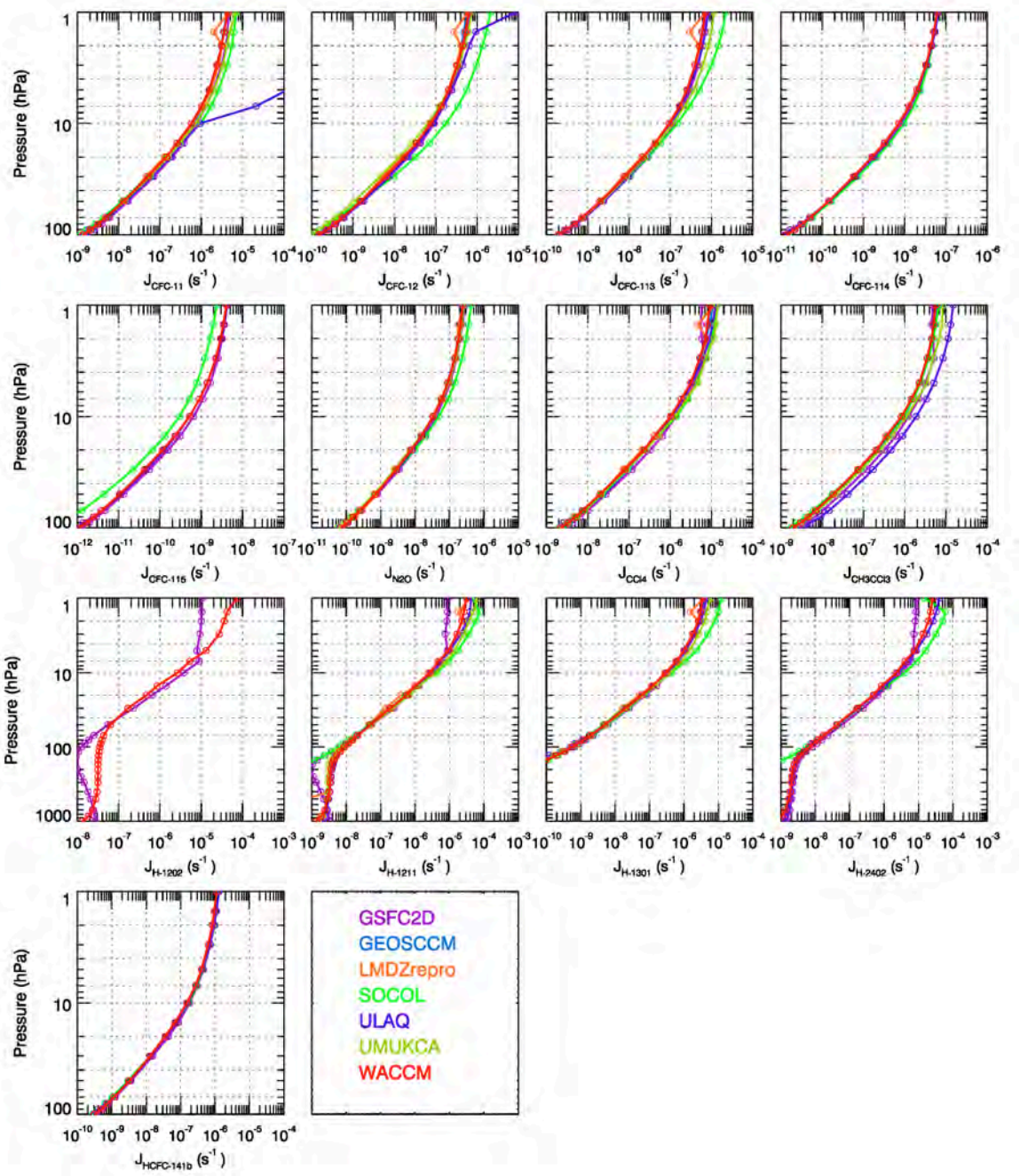

Figure 5.A1. Comparison of modelled 30-year mean J_{ODS} rates from the TS2000 simulation averaged between 30°S-30°N.

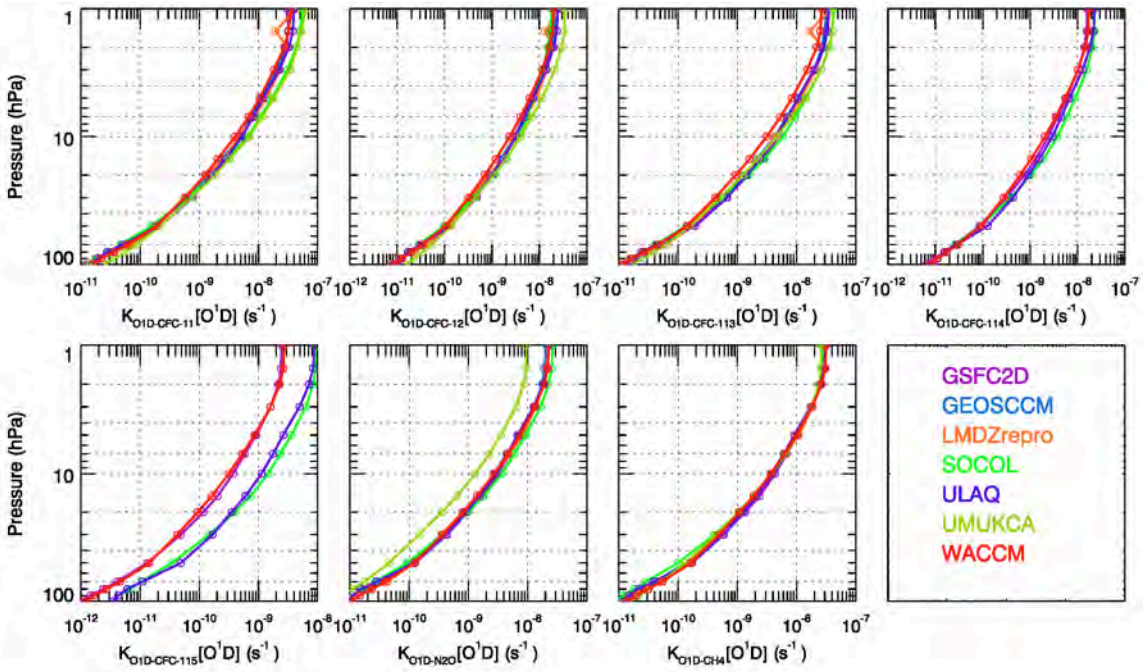

Figure 5.A2. Comparison of modelled 30-year mean $k_{O1D\text{-}ODS}[O^1D]$ rates from the TS2000 simulation averaged between 30°S-30°N.

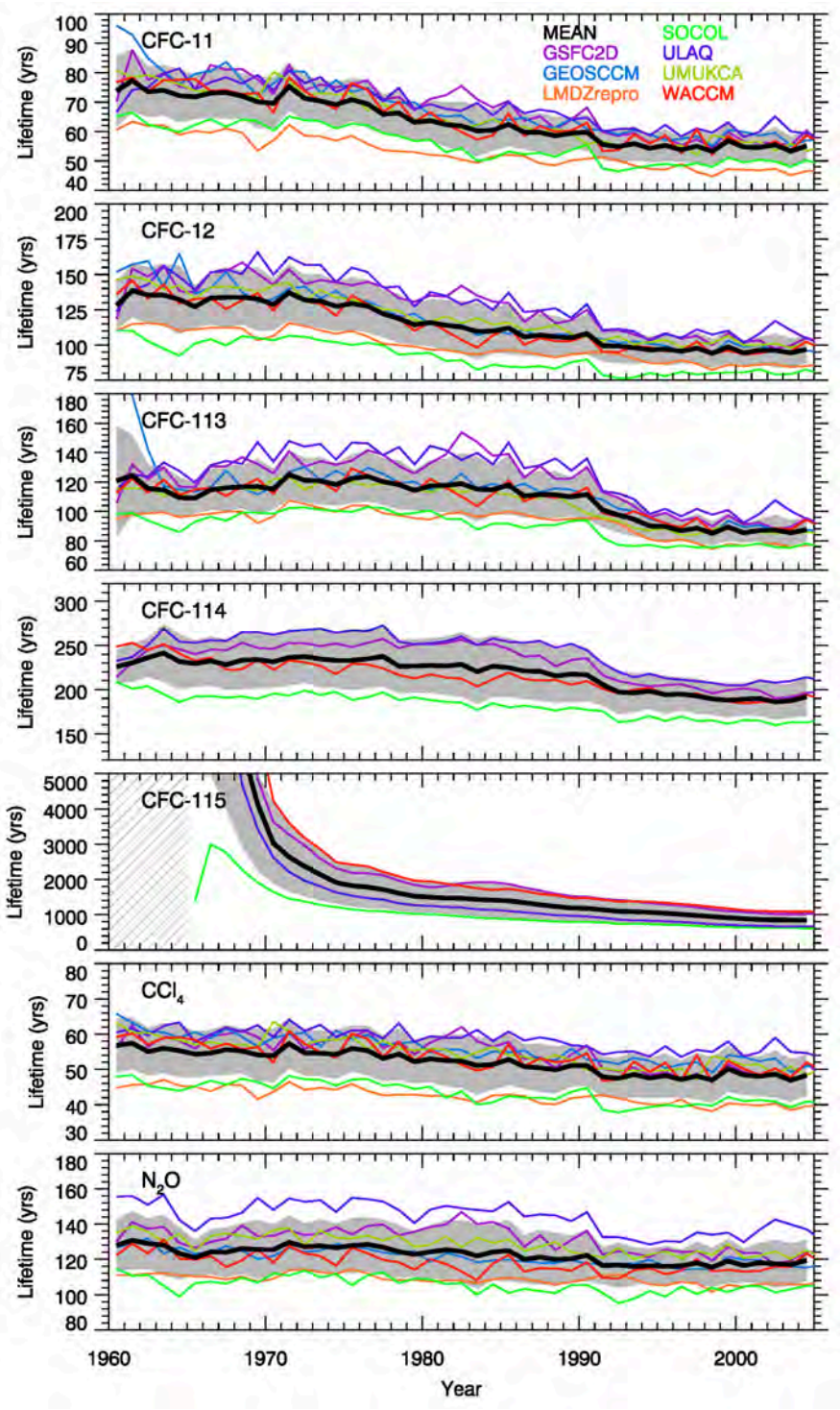

Figure 5.A3. Time evolution of modelled atmospheric partial lifetimes, τ_{atmos}, (yrs) of SR species between 1960 and 2006 from the TRANS simulations. Model mean lifetimes (thick black lines) and 1-σ variance (gray shadings) are also shown. The gray hatching area indicates where atmospheric concentrations of the corresponding ODS are close-to-zero.

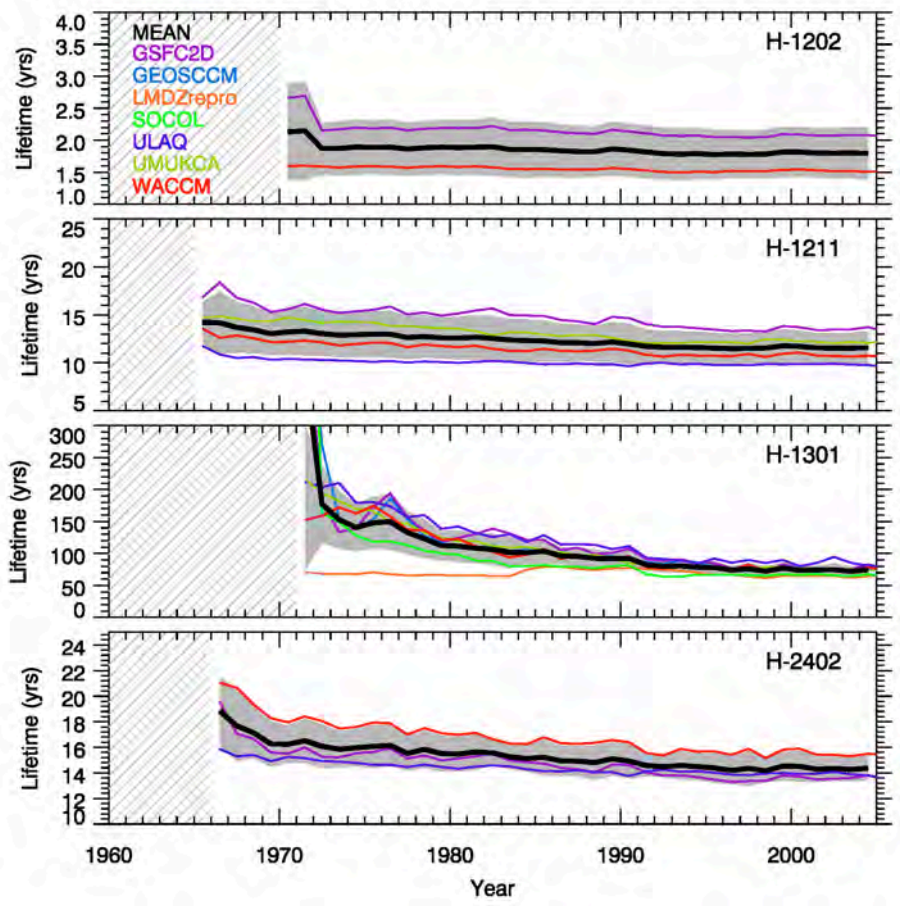

Figure 5.A4. As Figure 5.A3, but for modelled Halon lifetimes.

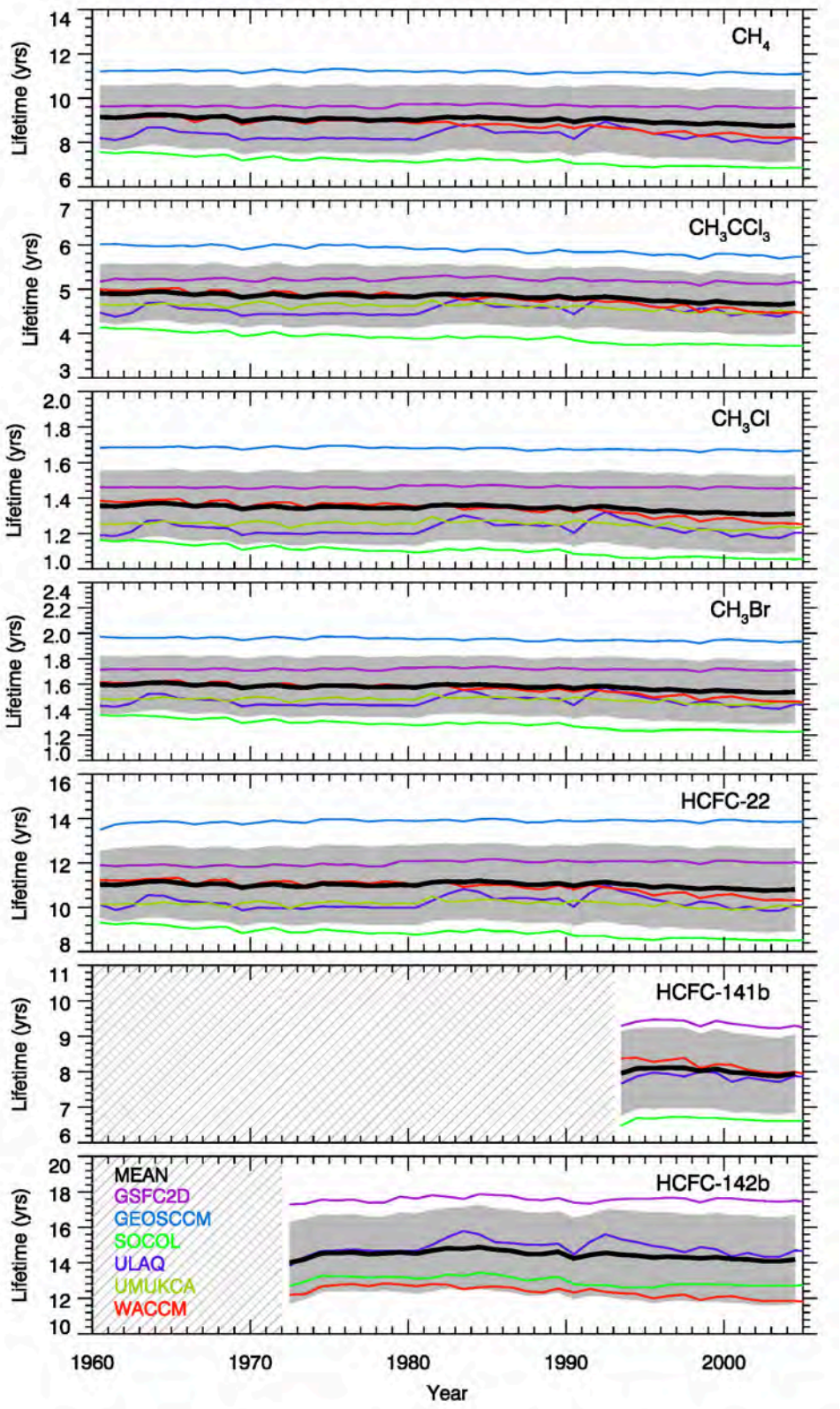

Figure 5.A5. As Figure 5.A3, but for modelled lifetimes of TR species.

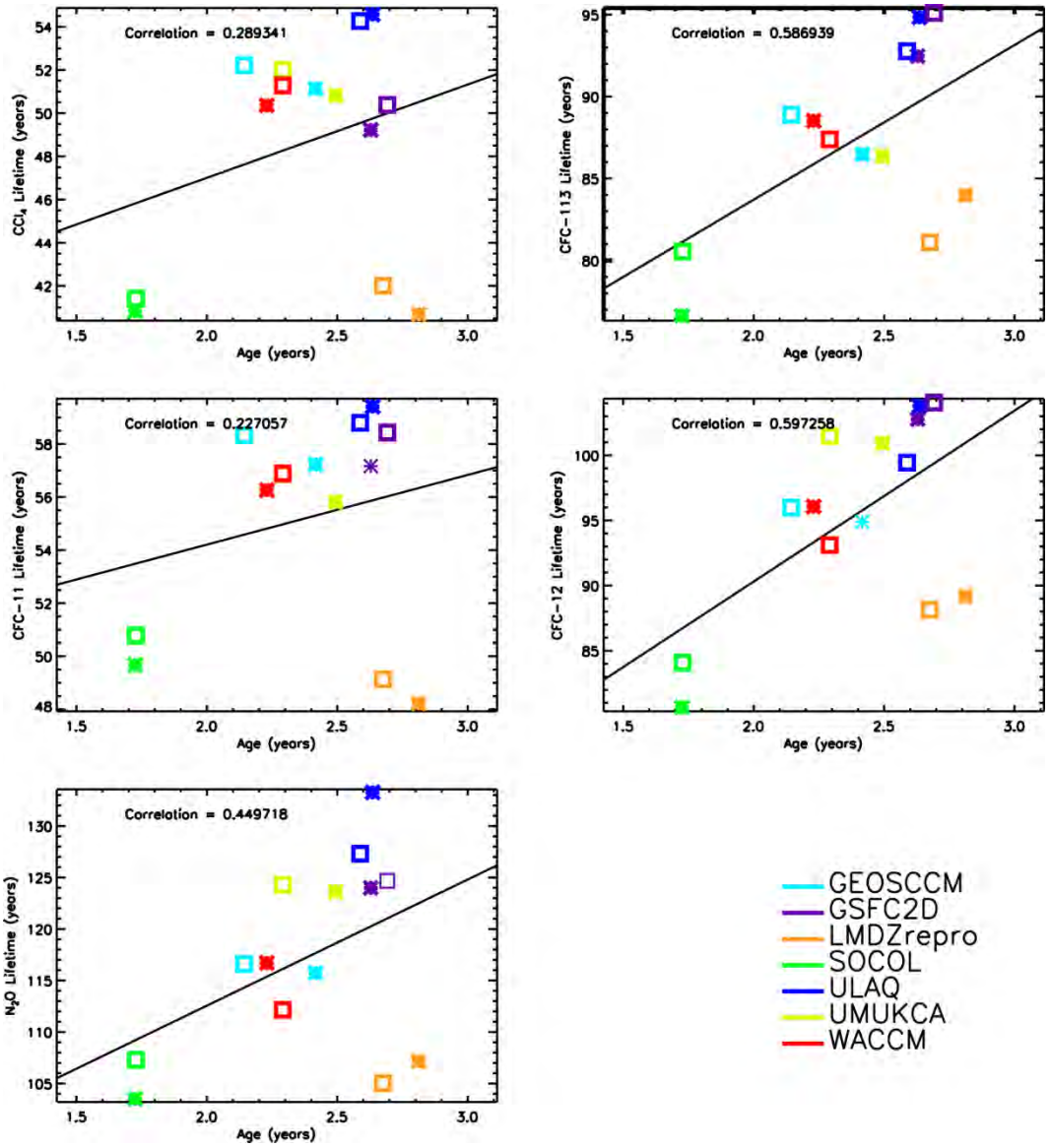

Figure 5.A6. As Figure 5.17, but with results for LMDZrepro.

5.11 References

AFEAS (Alternative Fluorocarbons Environmental Acceptability Study), *Production, Sales and Atmospheric Releases of Fluorocarbons through 2000*, Arlington, VA, USA, 2001.

Allen, M., and J. E. Frederick, Effective photodissociation cross sections for molecular oxygen and nitric oxide in the Schumann-Runge bands, *J. Atmos. Sci.*, *39,* 2066-2075, 1982.

Anderson Jr., D. E., and S. A. Lloyd, Polar twilight UV-visible radiation field: Perturbations due to multiple scattering, ozone depletion, stratospheric clouds, and surface albedo, *J. Geophys. Res*., 95, 7429-7434, 1990.

Bacmeister, J. T., M. R. Schoeberl, M. E. Summers, J. E. Rosenfield, and X. Zhu, Descent of long-lived trace gases in the winter polar vortex, *J. Geophys. Res., 100,* 11669-11684, 1995.

Bony, S., and K. A. Emanuel, A parameterization of the cloudiness associated with cumulus convection; evaluation using TOGA COARE data, *J. Atmos. Sci*., *58*, 3158-3183, 2001.

Bousquet, P., D. A. Hauglustaine, P. Peylin, C. Carouge, and P. Ciais, Two decades of OH variability as inferred by an inversion of atmospheric transport and chemistry of methyl chloroform, *Atmos. Chem. Phys*., *5*, 2635-2656, 2005.

Butchart, N., A. J. Chariton-Perez, I. Cionni, S. C. Hardiman, P. H. Haynes, K. Krüger, P. J. Kushner, P. A. Newman, S. M. Osprey, J. Perlwitz, M. Sigmond, L. Wang, H. Akiyoshi, J. Austin, S. Bekki, A. Baumgaertner, P. Braesicke, C. Brühl, M. Chipperfield, M. Dameris, S. Dhomse, V. Eyring, R. Garcia, H. Garny, P. Jöckel, J.-F. Lamarque, M. Marchand, M. Michou, O. Morgenstern, T. Nakamura, S. Pawson, D. Plummer, J. Pyle, E. Rozanov, J. Scinocca, T. G. Shepherd, K. Shibata, D. Smale, H. Teyssèdre. W. Tian, D. Waugh, and Y. Yamashita, Multimodel climate and variability of the stratosphere, *J. Geophys. Res., 116*, D05102, doi: 10.1029/2010JD014995, 2011.

Chou, M.-D., M. J. Suarez, X.-Z. Liang, and M.-H. Yan, *A thermal infrared radiation parameterization for atmospheric studies,* NASA Tech. Memo, NASA/TM-2001-104606, 9, 56 pp., Greenbelt, MD, USA, 2001.

Considine, D. B., A. R. Douglass, and C. H. Jackman, Effects of a polar stratospheric cloud parameterization on ozone depletion due to stratospheric aircraft in a two-dimensional model, *J. Geophys. Res., 99*, 18879-18894, 1994.

Crutzen, P., and P. H. Zimmermann, The changing photochemistry of the troposphere, *Tellus*, *43* AB, 136-151, 1991.

Dahlback, A., and K. Stamnes, A new spherical model for computing the radiation field available for photolysis and heating at twilight, *Planet. Space Sci.*, *39,* 671-683, 1991.

Douglass, A. R., and S. R. Kawa, Contrast between 1992 and 1997 high-latitude spring Halogen Occultation Experiment observations of lower stratospheric HCl, *J. Geophys. Res., 104* (D15), 18739-18754, doi: 10.1029/1999JD900281, 1999.

Douglass, A. R., C. H. Jackman, and R. S. Stolarski, Comparison of model results transporting the odd nitrogen family with results transporting separate odd nitrogen species, *J. Geophys. Res., 94*, 9862-9872, 1989.

Douglass, A. R., R. S. Stolarski, M. R. Schoeberl, C. H. Jackman, M. L. Gupta, P. A. Newman, J. E. Nielsen, and E. L. Fleming, Relationship of loss, mean age of air and the distribution of CFCs to stratospheric circulation and implications for atmospheric lifetimes*, J. Geophys. Res., 113*, D14309, doi: 10.1029/2007JD009575, 2008.

Dufresne, J.-L., M.-A. Foujols, S. Denvil, A. Caubel, O. Marti, O. Aumont, Y. Balkanski, S. Bekki, H. Bellenger, R. Benshila, S. Bony, L. Bopp, P. Braconnot, P. Brockmann, P. Cadule, F. Cheruy, F. Codron, A. Cozic, D. Cugnet, N. de Noblet, J.-P. Duvel, C. Ethé, L. Fairhead, T. Fichefet, S. Flavoni, P. Friedlingstein, J.-Y. Grandpeix, L. Guez, E. Guilyardi, D. Hauglustaine, F. Hourdin, A. Idelkadi, J. Ghattas, S. Joussaume, M. Kageyama, G. Krinner, S. Labetoulle, A. Lahellec, M.-P. Lefebvre, F. Lefevre, C. Levy, Z. X. Li, J. Lloyd, F. Lott, G. Madec, M. Mancip, M. Marchand, S. Masson, Y. Meurdesoif, J. Mignot, I. Musat, S. Parouty, J. Polcher, C. Rio, M. Schulz, D. Swingedouw, S. Szopa, C. Talandier, P. Terray, N. Viovy, and N. Vuichard, Climate change projections using the IPSL-CM5 Earth System Model: From CMIP3 to CMIP5, *Clim. Dynam., 40,* 2123-2165, doi: 10.1007/s00382-012-1636-1, 2013.

Egorova, T., E. Rozanov, V. Zubov, E. Manzini, W. Schmutz, and T. Peter, Chemistry-climate model SOCOL: A validation of the present-day climatology, *Atmos. Chem. Phys.*, *5*, 1557-1576, doi: 10.5194/acp-5-1557-2005, 2005.

Emmons, L. K., S. Walters, P. G. Hess, J.-F. Lamarque, G. G. Pfister, D. Fillmore, C. Granier, A. Guenther, D. Kinnison, T. Laepple, J. Orlando, X. Tie, G. Tyndall, C. Wiedinmyer, S. L. Baughcum, and S. Kloster, Description and evaluation of the Model for Ozone and Related chemical Tracers, version 4 (MOZART-4), *Geosci. Model Dev.*, *3*, 43-67, 2010.

Eyring, V., N. R. P. Harris, M. Rex, T. G. Shepherd, D. W. Fahey, G. T. Amanatidis, J. Austin, M. P. Chipperfield, M. Dameris, P. M. De F. Forster, A. Gettelman, H. F. Graf, T. Nagashima, P.A. Newman, S. Pawson, M. J. Prather, J. A. Pyle, R. J. Salawitch, B. D. Santer, and D. W. Waugh, A strategy for process-orientated validation of coupled chemistry-climate models, *Bull. Am. Meteorol. Soc.*, *86*, 1117-1133, 2005.

Eyring, V., N. Butchart, D. W. Waugh, H. Akiyoshi, J. Austin, S. Bekki, G. E. Bodeker, B. A. Boville, C. Brühl, M. P. Chipperfield, E. Cordero, M. Dameris, M. Deushi, V. E. Fioletov, S. M. Frith, R. R. Garcia, A. Gettelman, M. A. Giorgetta, V. Grewe, L. Jourdain, D. E. Kinnison, E. Mancini, E. Manzini, M. Marchand, D. R. Marsh, T. Nagashima, P. A. Newman, J. E. Nielsen, S. Pawson, G. Pitari, D. A. Plummer, E. Rozanov, M. Schraner, T. G. Shepherd, K. Shibata, R. S. Stolarski, H. Struthers, W. Tian, and M. Yoshiki, Assessment of temperature, trace species, and ozone in chemistry-climate model simulations of the recent past, *J. Geophys. Res.*, *111*, D22308, doi: 10.1029/2006JD007327, 2006.

Eyring, V., I. Cionni, G. E. Bodeker, A. J. Charlton-Perez, D. E. Kinnison, J. F. Scinocca, D. W. Waugh, H. Akiyoshi, S. Bekki, M. P. Chipperfield, M. Dameris, S. Dhomse, S. M. Frith, H. Garny, A. Gettelman, A. Kubin, U. Langematz, E. Mancini, M. Marchand, T. Nakamura, L. D. Oman, S. Pawson, G. Pitari, D. A. Plummer, E. Rozanov, T. G. Shepherd, K. Shibata, W. Tian, P. Braesicke, S. C. Hardiman, J. F. Lamarque, O. Morgenstern, D. Smale, J. A. Pyle, and Y. Yamashita, Multi-model assessment of stratospheric ozone return dates and ozone recovery in CCMVal-2 models, *Atmos. Chem. Phys.*, *10*, 9451-9472, doi: 10.5194/acp-10-9451-2010, 2010.

Fleming, E. L., C. H. Jackman, D. B. Considine, and R. S. Stolarski, Simulation of stratospheric tracers using an improved empirically based two-dimensional model transport formulation, *J. Geophys. Res., 104*, 23911-23934, 1999.

Fleming, E. L., C. H. Jackman, D. K. Weisenstein, and M. K. W. Ko, The impact of inter-annual variability on multidecadal total ozone simulations, *J. Geophys. Res., 112*, D10310, doi: 10.1029/2006JD007953, 2007.

Fleming, E. L., C. H. Jackman, R. S. Stolarski, and A. R. Douglass, A model study of the impact of source gas changes on the stratosphere for 1850-2100, *Atmos. Chem. Phys.*, *11*, 8515-8541, doi: 10.5194/acp-11-8515-2011, 2011.

Fouquart, Y., and B. Bonnel, Computations of solar heating of the Earth's atmosphere: A new parameterization, *Contrib. Atmos. Phys*., *53*, 35-62, 1980.

Gallery, W. O., F. X. Kneizys, and S. A. Clough, Air Mass Computer Program for Atmospheric Transmittance/Radiance Calculations: FSCATM, AFGL-TR-83-0065, 1983.

Garcia, R. R., D. Marsh, D. E. Kinnison, B. Boville, and F. Sassi, Simulations of secular trends in the middle atmosphere, 1950-2003, *J. Geophys. Res.*, *112*, D09301, doi: 10.1029/2006JD007485, 2007.

Hall, T., D. Waugh, K. Boering, and R. Plumb, Evaluation of transport in stratospheric models, *J. Geophys. Res*., *104*, 18815-18839, 1999.

Hewitt, H. T., D. Copsey, I. D. Culverwell, C. M. Harris, R. S. R. Hill, A. B. Keen, A. J. McLaren, and E. C. Hunke, Design and implementation of the infrastructure of HadGEM3: The next-generation Met Office climate modelling system, *Geosci. Model Dev.*, *4*, 223-253, doi: 10.5194/gmd-4-223-2011, 2011.

Hourdin, F., and A. Armengaud, The use of finite-volume methods for atmospheric advection trace species: 1. Tests of various formulations in a general circulation model, *Mon. Weather Rev*., *127*, 822-837, 1999.

Hourdin, F., I. Musat, S. Bony, P. Braconnot, F. Cordron, J. Dufresne, L. Fairhead, M.-A. Filiberti, P. Friedlingstein, J.-Y. Grandpeix, G. Krinner, and P. Levan, The LMDZ4 general circulation model: Climate performance sensitivity to parameterized physics with emphasis on tropical convection, *Clim. Dynam., 27* (7-8), 787-813, doi: 10.1007/s00382-006-0158-0, 2006.

IPCC, *Climate Change 2007: The Physical Science Basis. Contribution of Working Group I to the Fourth Assessment Report of the Intergovernmental Panel on Climate Change* (S. Solomon, D. Qin, M. Manning, Z. Chen, M. Marquis, K. B. Averyt, M. Tignor, and H. L. Miller (eds.), Cambridge University Press, Cambridge, United Kingdom, and New York, NY, USA, 996 pp., 2007.

Jackman, C. H., A. R. Douglass, R. B. Rood, R. D. McPeters, and P. E. Meade, Effect of solar proton events on the middle atmosphere during the past two solar cycles as computed using a two-dimensional model, *J. Geophys. Res.*, *95*, 7417-7428, 1990.

Jackman, C. H., E. L. Fleming, S. Chandra, D. B. Considine, and J. E. Rosenfield, Past, present, and future modeled ozone trends with comparisons to observed trends, *J. Geophys. Res., 101*, 28753-28767, 1996.

Jourdain, L., S. Bekki, F. Lott, and F. Lefevre, The coupled chemistry-climate model LMDz-REPROBUS: description and evaluation of a transient simulation of the period 1980-1999, *Ann. Geophys., 26*, 1391-1413, 2008.

Kärcher, B., and U. Lohmann, A parameterization of cirrus cloud formation: homogeneous freezing including effects of aerosol size, *J. Geophys. Res.*, *107*, 4698, doi: 10.1029/2001JD001429, 2002.

Krol, M. C., J. Lelieveld, D. E. Oram, G. A. Sturrock, S. A. Penkett, C. A. M. Brenninkmeijer, V. Gros, J. Williams, and H. A. Scheeren, Continuing emissions of methyl chloroform from Europe, *Nature*, 421 (6919), 131-135, doi: 10.1038/nature01311, 2003.

Lamarque, J.-F., T. C. Bond, V. Eyring, C. Granier, A. Heil, Z. Klimont, D. Lee, C. Liousse, A. Mieville, B. Owen, M. G. Schultz, D. Shindell, S. J. Smith, E. Stehfest, J. van Aardenne, O. R. Cooper, M. Kainuma, N. Mahowald, J. R. McConnell, V. Naik, K. Riahi, and D. P. van Vuuren, Historical (1850-2000) gridded anthropogenic and biomass burning emissions of reactive gases and aerosols: methodology and application, *Atmos. Chem. Phys., 10*, doi: 10.5194/acp-10-7017-2010, 7017-7039, 2010.

Lamarque, L., G. P. Kyle, M. Meinshausen, K. Riahi, S. J. Smith, D. P. van Vuuren, A. J. Conley, and F. Vitt, Global and regional evolution of short-lived radiatively-active gases and aerosols in the Representative Concentration Pathways, *De Change*, *109*, 191-212, doi: 10.1007/s10584-011-0155-0, 2011.

Laval, K., R. Sadourny, and Y. Serafini, Land surface processes in a simplified general circulation model, *Geophys. Astrophys. Fluid Dyn., 17*, 129-150, 1981.

Lawrence, M. G., P. Jöckel, and R. von Kuhlmann, What does global mean OH concentration tell us, *Atmos. Chem. Phys.*, *1*, 37-49, doi: 10.5194/acp-1-37-2001, 2001.

Lean, J., G. Rottman, J. Harder, and G. Kopp, Source contributions to new understanding of global change and solar variability, *Solar Phys., 230*, 27-53, 2005.

Liang, Q., R. S. Stolarski, A. R. Douglass, P. A. Newman, and J. E. Nielsen, Evaluation of emissions and transport of CFCs using surface observations and their seasonal cycles and simulation of the GEOS CCM with emissions-based forcing, *J. Geophys. Res., 113*, D14302, doi: 10.1029/2007JD009617, 2008.

Lin, P., and Q. Fu, Changes in various branches of the Brewer-Dobson circulation from an ensemble of chemistry climate models, *J. Geophys. Res.*, *118*, 73-84, doi: 10.1029/2012JD018813, 2013.

Lin, S.-J., A "vertically Lagrangian" finite-volume dynamical core for global models, *Mon. Weather Rev., 132* (10), 2293-2307, 2004.

Lin, S. J., and R. B. Rood, Multidimensional flux-form semi-Lagrangian transport schemes, *Mon. Wea. Rev.*, *124*, 2046-2068, 1996.

Lott, F., Alleviation of stationary biases in a GCM through a mountain drag parameterization and a simple representation of mountain lift forces, *Mon. Weather Rev., 127*, 788-801, 1999.

Lott, F., L. Fairhead, F. Hourdin, and P. Levan, The stratospheric version of LMDz: dynamical climatologies, Arctic oscillation, and impact on the surface climate, *Clim. Dynam., 25*, 851-868, doi: 10.1007/s00382-005-0064-x, 2005.

Louis, J.-F., A parametric model of vertical eddy fluxes in the atmosphere, *Boundary-Layer Meteorol., 17*, 187-202, 1979.

Madronich, S., and S. Flocke, The role of solar radiation in atmospheric chemistry, Handbook of Environmental Chemistry, edited by P. Boule, Springer-Verlag, Heidelberg, pp. 1-26, 1998.

Martinerie, P., E. Nourtier-Mazauric, J.-M. Barnola, W. T. Sturges, D. R. Worton, E. Atlas, L. K. Gohar, K. P. Shine, and G. P. Brasseur, Long-lived halocarbon trends and budgets from atmospheric chemistry modelling constrained with measurements in polar firn, *Atmos. Chem. Phys., 9,* 3911-3934, 2009.

McCulloch, A., P. Ashford, and P. M. Midgley, Historic emissions of fluorotrichloromethane (CFC-11) based on a market survey, *Atmos. Environ.*, *35* (26), 4387-4397, 2001.

McCulloch, A., P. M. Midgley, and P. Ashford, Releases of refrigerant gases (CFC-12, HCFC-22, and HFC-134a) to the atmosphere, *Atmos. Environ.*, *37* (7), 889-902, 2002.

Miller, B. R., M. Rigby, L. J. M. Kuijpers, P. B. Krummel, L. P Steele, M. Leist, P. J. Fraser, A. McCulloch, C. Harth, P. Salameh, J. Mühle, R. F. Weiss, R. G. Prinn, R. H. J. Wang, S. O'Doherty, B. R. Greally, and P. G. Simmonds, HFC-23 (CHF_3) emission trend response to HCFC-22 ($CHClF_2$) production and recent HFC-23 emission abatement measures, *Atmos. Chem. Phys.*, *10*, 7875-7890, doi: 10.5194/acp-10-7875-2010, 2010.

Minschwaner, K., R. Salawitch, and M. McElroy, Absorption of solar radiation by O2: Implications for O_3 and lifetimes of N_2O, $CFCl_3$ and CF_2Cl_2, *J. Geophys. Res., 98,* 10543-10561, 1993.

Montzka, S. A., M. Krol, E. Dlugokencky, B. Hall, P. Jöckel, and J. Lelieveld, Small interannual variability of global atmospheric hydroxyl, *Science, 331* (67), doi: 10.1126/science.1197640, 2011.

Morcrette, J.-J., L. Smith, and Y. Fouquart, Pressure and temperature dependence of the absorption in longwave radiation parameterizations, *Contrib. Atmos. Phys., 59* (4), 455-469, 1986.

Moorthi, S., and M. J. Suarez, Relaxed Arakawa–Schubert, A parameterization of moist convection for general circulation models, *Mon. Wea. Rev., 120*, 978-1002, 1992.

Morgenstern, O., P. Braesicke, F. M. O'Connor, A. C. Bushell, C. E. Johnson, S. M. Osprey, and J. A. Pyle, Evaluation of the new UKCA climate-composition model – Part 1: The stratosphere, *Geosci. Model Dev.*, *2*, 43-57, doi: 10.5194/gmd-2-43-2009, 2009.

Morgenstern, O., M. A. Giorgetta, K. Shibata, V. Eyring, D.W. Waugh, T. G. Shepherd, H. Akiyoshi, J. Austin, A. J. G. Baumgaertner, S. Bekki, P. Braesicke, C. Brühl, M. P. Chipperfield, D. Cugnet, M. Dameris, S. Dhomse, S. M. Frith, H. Garny, A. Gettelman, S. C. Hardiman, M. I. Hegglin, D. E. Kinnison, J.-F. Lamarque, E. Mancini, E. Manzini, M. Marchand, M. Michou, T. Nakamura, J. E. Nielsen, G. Pitari, D. A. Plummer, E. Rozanov, J. F. Scinocca, D. Smale, H. Teyssèdre, M. Toohey, W. Tian, and Y. Yamashita, Review of the formulation of present-generation stratospheric chemistry-climate models and associated external forcings, *J. Geophys. Res.*, *115*, D00M02, doi: 10.1029/2009JD013728, 2010.

Neu, J. L., M. J. Prather, and J. E. Penner, Global atmospheric chemistry: Integrating over fractional cloud cover, *J. Geophys. Res., 112*, D11306, doi: 10.1029/2006JD008007, 2007.

Park, J. H., M. K.W. Ko, C. H. Jackman, R. A. Plumb, J. A. Kaye, and K. H. Sage (Eds.): *Models and Measurements Intercomparison II,* NASA Tech. Memo., TM-1999-209554, Hampton, VA, USA, 1999.

Pawson, S., R. S. Stolarski, A. R. Douglass, P. A. Newman, J. E. Nielsen, S. M. Frith, and M. L. Gupta, Goddard Earth Observing System chemistry-climate model simulations of stratospheric ozone-temperature coupling between 1950 and 2005, *J. Geophys. Res*., *113*, D12103, doi: 10.1029/2007JD009511, 2008.

Pitari, G., E. Mancini, V. Rizi, and D. Shindell, Impact of future climate and emission changes on stratospheric aerosol and ozone, *J. Atmos. Sci*., *59*, 414-440, 2002.

Prather, M. J., and C. M. Spivakovsky, Tropospheric OH and the lifetimes of hydrochlorofluorocarbons, *J. Geophys. Res*., *95*, 18723-18729, 1990.

Poisson, N., M. Kanakidou, and P. J. Crutzen, Impact of nonmethane hydrocarbons on tropospheric chemistry and the oxidizing power of the global troposphere: 3-dimensional modeling results, *J. Atmos. Chem*., *36*, 157-230, 2000.

Prinn, R. G., R. F. Weiss, B. R. Miller, J. Huang, F. N. Alyea, D. M. Cunnold, P. J. Fraser, D. E. Hartley, and P. G. Simmonds, Atmospheric trends and lifetime of CH_3CCl_3 and global OH concentrations, *Science*, *269*, 187-192, 1995.

Prinn, R. G., J. Huang, R. F. Weiss, D. M. Cunnold, P. J. Fraser, P. G. Simmonds, A. McCulloch, C. Harth, P. Salameh, S. O'Doherty, R. J. J. Wang, L. Porter, and B. R. Miller, Evidence for substantial variations of atmospheric hydroxyl radicals in the past two decades, *Science*, *292*, 1882-1888, 2001.

Prinn, R. G., J. Huang, R. F. Weiss, D. M. Cunnold, P. J. Fraser, P. G. Simmonds, A McCulloch, C. Harth, S. Reimann, P. Salameh, S. O'Doherty, R. H. J. Wang, . W. Porter, B. R. Miller, and P. B. Krummel, Evidence for variability of atmospheric hydroxyl radicals over the past quarter century, *Geophys. Res. Lett., 32*, L07809, doi: 10.1029/2004GL022228, 2005.

Rayner, N. A., D. E. Parker, E. B. Horton, C. K. Folland, L. V. Alexander, D. P. Rowell, E. C. Kent, and A. Kaplan, Global analyses of SST, sea ice and night marine air temperature since the late nineteenth century. *J. Geophys. Res., 108*, 4407, doi: 10.1029/2002JD002670, 2003.

Rigby, M., R. G. Prinn, S. O'Doherty, S. A. Montzka, A. McCulloch, C. M. Harth, J. Mühle, P. Salameh, R. F. Weiss, D. Young, P. G. Simmonds, B. D. Hall, G. S. Dutton, D. Nance, D. J. Mondeel, J. W. Elkins, P. B. Krummel, L. P. Steele, and P. J. Fraser, Re-evaluation of the lifetimes of the major CFCs and CH_3CCl_3 using atmospheric trends, *Atmos. Chem. Phys., 13*, 2691-2702, doi: 10.5194/acp-13-2691-2013, 2013.

Rosenfield, J. E., D. B. Considine, P. E. Meade, J. T. Bacmeister, C. H. Jackman, and M. R. Schoeberl, Stratospheric effects of Mount Pinatubo aerosol studied with a coupled two-dimensional model, *J. Geophys. Res., 102,* 3649-3670, 1997.

Sander, S. P., J. Abbatt, J. R. Barker, J. B. Burkholder, R. R. Friedl, D. M. Golden, R. E. Huie, C. E. Kolb, M. J. Kurylo, G. K. Moortgat, V. L. Orkin, and P. H. Wine, *Chemical Kinetics and Photochemical Data for Use in Atmospheric Studies, Evaluation No. 17*, JPL Publication 10-6, Jet Propulsion Laboratory, Pasadena, 2011 http://jpldataeval.jpl.nasa.gov, 2011.

Savage, N. H., K. S. Law, J. A. Pyle, A. Richter, H. Nüß, and J. P. Burrows, Using GOME NO_2 satellite data to examine regional differences in TOMCAT model performance, *Atmos. Chem. Phys., 4*, 1895-1912, 2004.

Schraner, M., Rozanov, E., Schnadt Poberaj, C., Kenzelmann, P., Fischer, A. M., Zubov, V., Luo, B. P., Hoyle, C. R., Egorova, T., Fueglistaler, S., Brönnimann, S., Schmutz, W., and T. Peter, Technical Note: Chemistry-climate model SOCOL: Version 2.0 with improved transport and chemistry/microphysics schemes, *Atmos. Chem. Phys.*, *8*, 5957-5974, doi: 10.5194/acp-8-5957-2008, 2008.

SPARC CCMVal (Stratospheric Processes And their Role in Climate), *Report on the Evaluation of Chemistry-Climate Models,* edited by V. Eyring, T. G. Shepherd, and D. W. Waugh, SPARC Report No. 5, WCRP-132, WMO/TD-No. 1526, available: http://www.atmosp.physics.utoronto.ca/SPARC/ccmval_final/index.php, 2010.

Spivakovsky, C. M., R. Yevich, J. A. Logan, S. C. Wofsy, M. B. McElroy, and M. J Prather, Tropospheric OH in a three-dimensional chemical tracer model: An assessment based on observations of CH_3CCl_3, *J. Geophys. Res.*, 95, 18441-18471, 1990.

Spivakovsky, C. M., J. A. Logan, S. A. Montzka, Y. J. Balkanski, M. Foreman-Fowler, D. B. J. Jones, L. W. Horowitz, A. C. Fusco, C. A. M. Brenninkmeijer, M. J. Prather, S. C. Wofsy, and M. B. McElroy, Three-dimensional climatological distribution of tropospheric OH: Update and evaluation, *J. Geophys. Res.*, *105* (D7), 8931-8980, doi: 10.1029/1999JD901006, 2000.

Szopa, S., Y. Balkanski, M. Schulz, S. Bekki, D. Cugnet, A. Fortems-Cheiney, S. Turquety, A. Cozic, C. Déandreis, D. Hauglustaine, A. Idelkadi, J. Lathière, F. Lefevre, M. Marchand, R. Vuolo, N. Yan, and J.-L. Dufresne, Aerosol and ozone changes as forcing for climate evolution between 1850 and 2100, *Clim. Dynam.,* doi: 10.1007/s00382-012-1408-y, 2012.

Telford, P. J., N. L. Abraham, A. T. Archibald, P. Braesicke, M. Dalvi, O. Morgenstern, F. M. O'Connor, N. A. D. Richards, and J. A. Pyle, Implementation of the Fast-JX photolysis scheme (v6.4) into the UKCA component of the MetUM chemistry climate model (v7.3), *Geosci. Model Dev.*, *6*, 161-177, doi: 10.5194/gmd-6-161-2013, 2013.

Toon, O., C. McKay, T. Ackerman, and K. Santhanam, Rapid calculation of radiative heating rates and photodissociation rates in inhomogeneous multiple scattering atmospheres, *J. Geophys. Res., 94,* 16287-16301, 1989.

Velders, G. J. M., D. W. Fahey, J. S. Daniel, M. McFarland, and S. O. Andersen, The large contribution of projected HFC emissions to future climate forcing, *Pro. Nat. Acad. Sci.*, doi: 10.1073/pnas.0902817106, 2009.

Wang, Y., J. A. Logan, and D. J. Jacob, Global simulation of tropospheric O**3**-NO**x**-hydrocarbon chemistry, 2. model evaluation and global ozone budget, *J. Geophys. Res.*, *103*, 10727-10755, 1998.

Wang, J. S., M. B. McElroy, J. A. Logan, P. I. Palmer, W. L. Chameides, Y. Wang, and I. A. Megretskaia, A quantitative assessment of uncertainties affecting estimates of global mean OH derived from methyl chloroform observations, *J. Geophys. Res.*, *113*, D12302, doi: 10.1029/2007JD008496, 2008.

Waugh, D., and V. Eyring, Quantitative performance metrics for stratospheric-resolving chemistry-climate models, *Atmos. Chem. Phys.*, *8*, 5699-5713, 2008.

WMO, *Scientific Assessment of Ozone Depletion: 2010, Global Ozone Research and Monitoring Project-Report No. 52*, 516 pp., Geneva, Switzerland, 2011.

Zubov, V., E. Rozanov, and M. E. Schlesinger, Hybrid scheme for three-dimensional advective transport, *Mon. Weather Rev.*, *127*(6), 1335-1346, 1999.

CHAPTER 6

Recommended Values for Steady-State Atmospheric Lifetimes and their Uncertainties

Lead-Authors:
Malcolm K. W. Ko
Paul A. Newman
Stefan Reimann
Susan E. Strahan

Co-Authors:
Elliot L. Atlas
James B. Burkholder
Martyn Chipperfield
Andreas Engel
Qing Liang
Wahid Mellouki
R. Alan Plumb
Richard S. Stolarski
C. Michael Volk

CHAPTER 6

Recommended Values for Steady-State Atmospheric Lifetimes and Their Uncertainties

Contents

This report assesses the current understanding of processes that control the lifetimes of trace gases in the atmosphere, the ability of models to simulate these processes, and how observations and models are used to provide lifetime estimates. This chapter draws from the results of Chapters 2 to 5 to derive recommended values for the steady-state atmospheric lifetimes of the species listed in Table 1.1. We emphasize that this chapter discusses only findings that have direct implications for the determination of steady-state lifetimes. Readers are urged to look at the summary of each chapter for other findings. We present results and the methodology used to obtain values for the steady-state lifetimes by addressing the following questions:

- **What is new in this reevaluation specific to the issue of steady-state lifetimes?**
- **What methods were used to determine values for steady-state lifetimes?**
- **What are the recommended steady-state lifetimes and uncertainties?**
- **What can be done in future studies to reduce the uncertainties?**

6.1 What Is New in This Reevaluation Specific to the Issue of Steady-State Lifetimes?

In this chapter, we use the term global atmospheric lifetime (GAL) to refer to the lifetime defined as the burden divided by the removal rate from the atmosphere. In the calculation, the burden and the removal rate can be from model simulations or observations. The calculation can be performed for a snap shot in time, or as an average over an annual cycle, or as an average over several years. It is recognized that the GAL takes on different values when the emissions are changing with time. The term steady-state lifetime refers to the GAL calculated when an annually repeated emission pattern is used to sustain the burden, and the removal is balanced by the emission to the extent possible given the inter-annual variability inherent in the atmosphere.

To derive trace gas lifetimes and quantify the associated uncertainties, we must assess the entire theoretical knowledge/understanding, the relevant kinetics and photochemistry, the observations, and the models used to calculate burdens and losses. The most important findings in this report that are relevant to lifetime determination include:

With respect to the definition of lifetimes (see Chapter 2):

- The global atmospheric lifetime is not solely defined by the molecule's photochemistry and kinetics. It also depends on the interaction with the Earth system (atmosphere, land, and ocean), and the emission history.
- Observed concentrations of a species in the atmosphere, along with model calculations, can be used to determine its global atmospheric lifetime for the time period when the observations were taken.
- In theory, the steady-state lifetime of a species depends on the spatial pattern of the surface emissions. However, for the species listed in Table 1.1, the steady-state atmospheric lifetime for all surface emissions can be approximated, to within a few percent, with a single value.
- The steady-state response lifetime is defined as the incremental change in burden in response to an incremental change in emission. It has the unique property in that it provides a measure of the time-integrated change in burden following a pulse emission of the same spatial pattern.
- For the species listed in Table 1.1 (with the exceptions of nitrous oxide (N_2O) and methane (CH_4)), the steady-state response lifetime can be approximated by the steady-

state lifetime because there is no large background concentration in the current atmosphere.

With respect to kinetics and photochemistry (see Chapter 3):

- The dominant loss process for the CFCs, CCl_4, N_2O, CF_3Br (Halon-1301), and NF_3 is photolysis, primarily in the stratosphere in the 190-230 nanometer (nm) wavelength region. For the Halons CF_2Br_2 (Halon-1202), CF_2ClBr (Halon-1211), and CF_2BrCF_2Br (Halon-2402), photolysis from wavelengths >286 nm (which are effective in the troposphere) also contributes to their atmospheric removal.
- For hydrogen containing molecules (CH_3CCl_3, CH_3Cl, CH_3Br, HCFCs, and HFCs), loss due to the OH reaction in the troposphere is dominant (>90%).
- There are a number of new findings since the publication of the JPL-10-6 kinetic data evaluation (Sander *et al.,* 2011):
  - New experimental data are evaluated for CF_3CF_2Cl (CFC-115), NF_3, CF_2Br_2 (Halon-1202), CF_2ClBr (Halon-1211), and CF_2BrCF_2Br (Halon-2402) and used to compute lifetimes in the two-dimensional (2-D) model.
  - Lyman-α absorption cross-section recommendations, which have not been considered in previous evaluations, are provided and uncertainties estimated. Lyman-α photolysis is shown to be a dominant mesospheric loss process, but makes only a minor contribution to the global lifetime.
  - To correct errors in previously reported values, the ultraviolet (UV) absorption cross-section parameterizations for use in model calculations for $CFCl_3$ (CFC-11), CF_2Cl_2 (CFC-12), $CFCl_2CF_2Cl$ (CFC-113), CF_2ClCF_2Cl (CFC-114), $CHClF_2$ (HCFC-22), CH_3CCl_3, CH_3Cl, and CH_3Br are revised. The impacts on the computed lifetime are small, ~ a few percent.
  - The estimated uncertainty in the hydroxyl radical (OH), electronically excited atomic oxygen ($O(^1D)$), and atomic chlorine (Cl) reaction rate coefficients given in this report are, in general, less than those given in the JPL10-6 (Sander *et al.,* 2011) and the IUPAC (Atkinson *et al.*, 2008) data evaluations.
- All the 3-D models used kinetics from *Sanders et al.* (2011) to calculate the lifetimes in this study. In addition, a 2-D model was used to calculate lifetimes and uncertainties using the new kinetic data and evaluate the differences between these kinetic data. The (2-σ) range in calculated atmospheric lifetime due solely to uncertainty in the kinetic and photochemical data of the source gas (at the 2 σ limit) is expressed as a percentage of the value calculated using the recommended values. The lifetime uncertainties range from a low of 6% to as high as 40% (see Table 9 in Chapter 3).
- The contribution of the uncertainties in the molecular oxygen (O_2) absorption cross sections in the Schumann-Runge bands and Herzberg continuum (which were not evaluated in this report) to the model calculated uncertainties in the lifetimes of species primarily removed in the stratosphere (SR) was quantified. The 2σ uncertainties in calculated lifetimes due to uncertainty in O_2 cross sections are estimated to be 15% and 9% for CFC-11 and CFC-12, respectively; the lifetime uncertainty due to uncertainty in the ozone (O_3) cross sections is small (<0.5%) for CFC-11 and CFC-12.

With respect to observation-based methods used to determine lifetimes (see Chapter 4 and Section 6.2 for further descriptions)

- Global atmospheric lifetimes for CFC-11, CFC-12, CFC-113, and CH_3CCl_3 were determined using an inverse modeling method for the period from the late 1990's to the

present. In addition, the model was used in the forward mode to derive steady-state lifetimes using the retrieved parameters. For CFC-11, CFC-12, and CH_3CCl_3 the global lifetimes derived using observations from this time period is within 1% of its respective steady-state lifetime. For CFC-113, the difference is less than 5%.

- Mean regional tropospheric OH abundances were inferred using CH_3CCl_3 observations in a Bayesian inversion using a 12-box model. A modeling exercise confirmed that the 12-box model successfully retrieves the appropriate OH values from three-dimensional (3-D) model simulated time series of surface concentrations for a flux boundary condition tracer simulation. This provides confidence that the OH values inferred from CH_3CCl_3 can be used in the forward model to compute the steady-state lifetimes of the hydrochlorofluorocarbons (HCFCs) and hydrofluorocarbons (HFCs) in Table 1.1.
- Modeled photochemical loss has been combined with observed global distributions of CFC-11, CFC-12 and N_2O in the stratosphere and surface concentrations to calculate the global atmospheric lifetimes (satellite hybrid model). Adjustments were made to estimate the steady-state lifetimes.
- Tracer-tracer correlations have been used to obtain steady-state stratospheric (partial) lifetimes for CFC-12, CFC-113, CCl_4, H-1301, and N_2O relative to CFC-11. This method requires the stratospheric lifetime of CFC-11 as input. The tracer-tracer method was also used to determine the stratospheric lifetimes for CH_3CCl_3, CH_3Cl, H-1211, H-1301, HCFC-22, HCFC-141b, and HCFC-142b. However, those values were not used in deriving the steady state lifetimes for those species in this report.

With respect to model simulated results (see Chapters 3 and 5)

- Lifetimes (global atmospheric and steady-state) were calculated using seven global models (six 3-D CCMs and one 2-D model) using the same standard photochemical data (JPL-10-6).
- Most models perform well on most of the photochemical, kinetic, and transport diagnostics. No overall disqualifying implementation errors were identified in any of the models. However, some specific results from individual models were excluded because of implementation errors.
- Model results from Chapter 5 show that the steady-state lifetime can be approximated by the global atmospheric lifetime during the period when emissions are decreasing.
- Species that are predominantly removed by OH show a large range of lifetimes between models. However, for many models the lifetimes show good straight-line correlations with the simple metrics of global mean tropospheric OH or the lifetime of a reference species such as CH_3CCl_3.
- Species that are destroyed in the stratosphere show a range of model-calculated lifetimes. The lifetimes show a clear correlation with the simulated tropical mean age profile, which depends on the Brewer-Dobson circulation. In particular, the tropical ascent rate through the altitudes of large loss is critical to the calculated lifetimes with faster ascent rates producing shorter lifetimes. The uncertainty (variance) of the 7-model mean lifetime is smaller than the uncertainty due to photochemistry and $\sigma(O_2)$ discussed in Chapter 3.
- It is not clear how the lifetimes of SR (primarily stratospheric removal) species will change by 2100. Some, but not all models, indicate a faster Brewer-Dobson circulation in 2100 and a younger age-of-air. However, for other models the circulation change is not so clear. A thicker (recovered) ozone layer in 2100 leads to reduced photolysis. These two processes lead to cancelling effects on lifetimes in the models. Finally, the change in lifetime will depend on the assumed emission scenarios for the greenhouse gases.

- For a 2100 atmosphere the majority of models indicate a decrease in TR (primarily tropospheric removal) species lifetime due to the combined impact of increasing OH and increasing air temperature.

6.2 What Methods Were Used to Determine Values for Steady-State Lifetimes?

Five methods were used to derive lifetimes (global atmospheric lifetime (GAL) and steady-state lifetime). This section focuses on the four methods which derived steady-state lifetimes using observed concentrations of species in the atmosphere. On the other hand, results from model simulations reported in Chapters 3 and 5 provide values for the modeling method. The modeling method requires photochemical data as input. While no observation is used directly in deriving the model lifetimes, one should not overlook the fact that observations of many species were used to guide the development and provide validation for the models. Chemistry and Transport Models (2-D and 3-D), have improved tremendously since the 1994 lifetimes assessment (Kaye *et al.,* 1994). Some of the models have evolved into comprehensive atmospheric chemistry climate models that provide a self-consistent framework for calculating lifetimes. However, their accuracy depends on their ability to realistically represent important atmospheric processes involving chemistry, transport, and radiation. Errors in loss rates or in the transport time through the altitude range where loss is important will lead to biases in model calculated lifetimes. Model lifetimes in this report are calculated for a particular climate (e.g., present day composition and meteorology) based on the current global budgets, with corrections for being out of steady state. In the modeling studies, the focus has been on lifetime as defined by photochemical reactions occurring in the atmosphere. Effects on removal by deposition (to land or ocean) are added afterward as a partial lifetime.

The steady-state global lifetime is not a directly observable quantity. However, observed concentrations of a species in the atmosphere can be used to determine lifetimes with the help of a model. Lifetimes derived from this combined method have greatly improved with the availability of global, satellite-based retrievals of gas concentrations. Because the measured concentrations are influenced by actual emission histories and the state of the atmosphere at the time of the measurements, they can only provide information on the global atmospheric lifetime at the measurement time. Nevertheless, these values can be adjusted to obtain estimates for the steady-state lifetime. For species with available observations, four methods were used to derive lifetimes:

(1) Inverse modeling (Section 4.3.1) uses a 12-box model to retrieve the global atmospheric lifetime from the time series of observed burden (derived from surface concentrations) and the emissions. This method does not require detailed knowledge of the chemical properties of the molecule, but the information is useful for choosing an a priori value in the inversion process, and in relating burden to surface concentration. The retrieved lifetime values can be used in the same 12-box model in the forward mode to compute steady-state lifetimes. This method was used to derive lifetimes for CFC-11, CFC-12, CFC-113, and CH_3CCl_3.
(2) A satellite hybrid method (Section 4.3.4) uses vertically resolved concentrations of the species in the stratosphere and photolysis model-derived loss rates to derive global lifetimes. This method is most useful for SR species. The calculated values can be adjusted to approximate the steady-state lifetimes. This method is used in this report to derive lifetimes for CFC-11, CFC-12, and N_2O.

(3) The tracer-tracer correlation method (Section 4.4) uses simultaneously observed concentrations of a pair of species in the stratosphere (either in situ or satellite) to determine relative stratospheric lifetimes. Data are available for CFC-11, CFC-12, CFC-113, CCl_4, N_2O, H-1211, H-1301, CH_3CCl_3, CH_3Cl, CH_4, HCFC-22, HCFC-141b, and HCFC-142b. A stratospheric lifetime for CFC-11 is required to estimate the absolute lifetimes.

(4) The proxy tropospheric OH concentration is a by-product of the inverse modeling retrieval when applied to CH_3CCl_3 (Section 4.3.1.4). The partial lifetime due to OH loss in the troposphere for other hydrogen-containing species (e.g., HCFCs and HFCs) is computed using the 12-Box forward model. The method is equivalent to the scaling using the reaction rate constant with OH (Spivakovsky *et al.,* 2000). The partial lifetime is then combined with other information to obtain steady-state lifetimes.

Figure 6.1 explains the flow of information on how the lifetime values from the five methods are combined to provide a single recommended value. The best estimate and the associated uncertainty from each method are provided in the relevant chapter. We treat the value from each method as an estimator of the recommended steady-state lifetime. The best estimate from a method is often the mean of several individual estimates obtained using different data or tools. For example, simulated lifetime values from different models are considered to be individual estimates, and the mean value is identified as the best estimate. For observation-based methods, individual estimates arise when different data sets are used to derive the lifetime. Through analyses of the methodology and by propagating the uncertainties of the input data, we derive an associated uncertainty estimate for each method. The best estimates from each method (the estimators) are then combined using a weighted average to produce the recommended lifetime. We provide two ranges for the recommended lifetime uncertainties (both are 2σ). The first range, defined by Equation (6.11) in the Appendix, is the weighted mean of the variances from each method taking into account the covariance between estimators. This provides the range for the most likely values. The second, defined by Equation (6.6) in the Appendix, corresponds to the joint distribution of the individual variances around the arithmetic (i.e., unweighted) mean of the estimators. This represents the full range of the lifetime value estimates. The interpretation is that values outside of this second range are unlikely to be supported by future evaluations. Details of the uncertainty derivations are provided in the Appendix.

6.3 What Are the Recommended Steady-State Lifetimes and Uncertainties?

The recommended steady-state lifetimes are presented in three tables, grouped essentially by the methods used for determining the steady-state lifetimes. The species in Table 6.1 include most of the stratospheric removal (SR) species. For some species, data are available for several observation-based methods. Species in Table 6.2 are all tropospheric (primarily OH) removal species (TR). As will be discussed below, the lifetimes in this group are determined using the 12-box forward model. Table 6.3 provides results for three Halons and NF_3. These lifetimes are from the 2-D model calculated using new photochemical data from this report. All mean lifetimes and uncertainties are calculated by averaging the inverse of lifetime (i.e., loss rates). The uncertainty range is calculated formally using the methodology described in the Appendix. The column LOSU (Level of Scientific Understanding) is an expert judgment of the reliability of the recommended value, taking into account the number of estimators, and the ability of the estimator(s) to provide good estimates for the steady-state lifetimes.

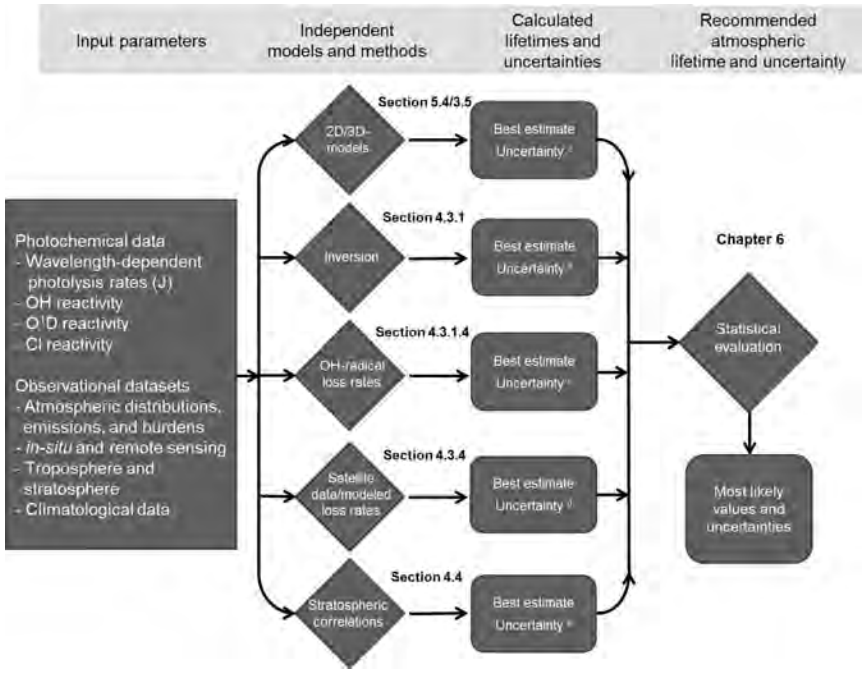

Figure 6.1. Information flow chart for producing recommended steady-state atmospheric lifetime values and uncertainties.

[a] **2-D/3-D models:** Best estimate: Model averages; Uncertainty: model variance + uncertainty from kinetic data.
[b] **Inversion:** Best estimate: Average based on independent retrievals using NOAA and AGAGE time series; Uncertainty: From retrieval model based on knowledge of emission history, length of time series.
[c] **OH-Radical Loss Rates:** Best estimate: from 12-box forward model + 2-D model stratospheric partial lifetime; Uncertainty: from uncertainties in retrieved tropospheric OH concentration and uncertainty in k-OH.
[d] **Satellite data/modeled loss rates:** Best estimate: average from several satellite data sets; Uncertainty: estimated from uncertainties in concentrations and kinetic data.
[e] **Stratospheric correlations (tracer-tracer):** Best estimate: weighted average from different data sets made at different location and time; Uncertainty: standard deviation, and uncertainty in the assumed CFC-11 stratospheric lifetime (as determined from the other methods).
Details of the methods are explained in the respective chapters. All averaging is done using the inverse of lifetime (i.e., loss rates).

Figure 6.2 graphically summarizes the steady-state lifetime estimates determined for the 27 species listed in Table 1.1, including estimates of the uncertainty distribution. Only CFC-11, CFC-12, CFC-113, and N_2O have sufficient observations to allow lifetimes to be determined using three or four methods. We treat the value from each method as an estimator of the steady-state lifetime. The recommended estimates of the lifetime (shown by the black vertical bars in Figure 6.2) correspond to the weighted-mean of the different estimators. Each method has an associated estimate of the variance or uncertainty. For readability, we have combined the observation-based estimated values into one single distribution as explained in the Appendix.

Four species in Table 6.1 (CFC-11, CFC-12, CFC-13, and N_2O) have more than two observation-based estimators for determining the recommended steady-state lifetime. Three of the four are designated as having high LOSU in the recommended value. In general, the

inversion method has the smallest estimated uncertainties. This is a result of the long data record, and the fact that their emissions have been close to zero over the past decade. The satellite methods have larger uncertainties. For CFC-11, the available satellite data simply do not have fine enough resolution to resolve the vertical gradient in the lower stratosphere. In calculating the weighted average for CFC-11, the satellite method was assigned a 0.17 weighting (as opposed to 1/3) as one of the three estimators. Finally, the estimated uncertainties associated with the model derived lifetimes are smaller than those associated with the other estimators. These model weightings are 0.47 for CFC-11, 0.40 for CFC-113, and 0.44 for N_2O (as opposed to 1/3); and 0.33 for CFC-12 (as opposed to ¼).

We included (up to) three covariance terms in computing the most likely values for the six source gases in Table 6.1. These covariances are found between:

- The model and the satellite estimators arising from the uncertainty in the chemical data for the source gas, and from the uncertainty in the O_2 cross-section.
- The tracer-tracer and model estimators arising from the uncertainty in the O_2 cross section and the uncertainty in model transport. Both these uncertainties similarly affect the model-derived lifetimes of the source gas and of CFC-11, the latter of which is needed to determine the lifetime of the source gas from the tracer-tracer method.
- The tracer-tracer and the satellite estimators arising from the uncertainty in the O_2 cross-section.

All of the covariance terms are positive and increase the range of the most likely values. Our results suggest that a reduction in the uncertainty in the O_2 cross-section will reduce the range for the most likely values for the six source gases.

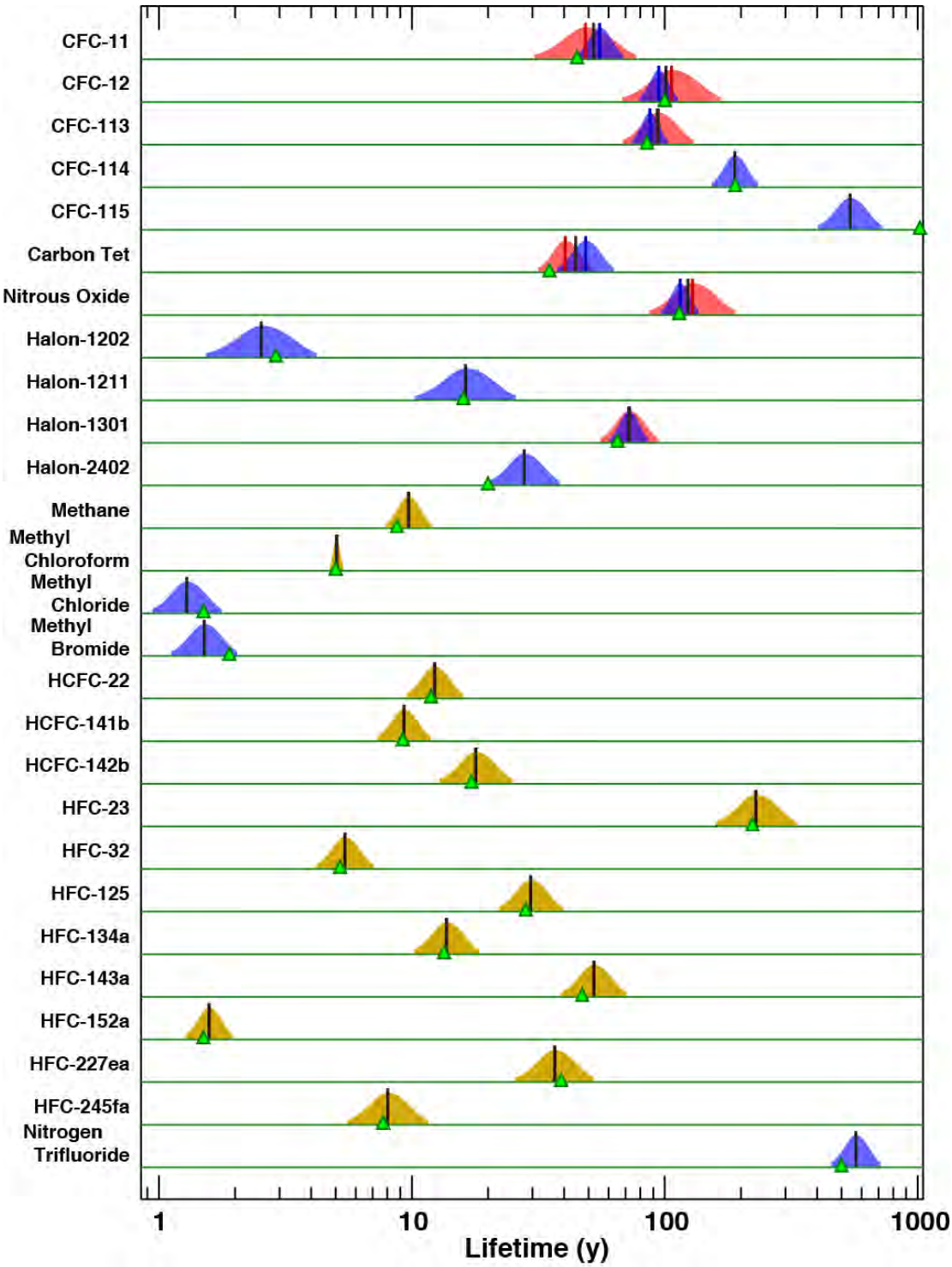

Figure 6.2. Recommended steady-state lifetime estimates (vertical black lines), lifetime estimates from models (blue) and observations (red) for the species in Table 1.1. The estimated uncertainties from models (light blue) and observations (light red) are also shown. The uncertainty estimates for the HCFCs and HFCs (shown in green) are from the uncertainty in the retrieved OH concentration and uncertainties in the reaction rate constants. Lifetime estimates from previous reports (WMO, 2011; IPCC, 2007) are indicated by the green triangles.

Table 6.1. Recommended estimates for steady-state lifetimes of stratospheric removal species. Values are for steady-state lifetime due to photochemical removal in the atmosphere. See text for discussion of the "most likely values", the "possible range". The weighting factors for the estimators, defined to be proportional to the inverse of the standard deviation (σ), are included.

Species	WMO (2011)	Observation-Derived Inverse Lifetime						Model-Derived Inverse Lifetime		Recommended Lifetime					Level of Scientific Understanding (LOSU)
		Inversion		Tracer-Tracer*		Satellite.					Possible range				
	τ (Yr)	Weight 1/τ (Yr $^{-1}$)	σ(%)	Weight 1/τ (Yr $^{-1}$)	σ(%)	Weight 1/τ (Yr $^{-1}$)	σ(%)	Weight 1/τ (Yr $^{-1}$)	σ(%)	τ (Yr)		Most likely range			
CFC-11	45	0.36 (53)$^{-1}$	15%			0.17 (45)$^{-1}$	25%	0.47 (55)$^{-1}$	12%	**52**	35	43	67	89	High
CFC-12	100	0.21 (111)$^{-1}$	17%	0.25 (102)$^{-1}$	13%	0.20 (107)$^{-1}$	18%	0.33 (95)$^{-1}$	9%	**102**	78	88	122	151	High
CFC-113	85	0.38 (109)$^{-1}$	11%	0.22 (83)$^{-1}$	15%			0.40 (87)$^{-1}$	9%	**93**	69	82	109	138	Medium Same method as CFC-11 and CFC-12, but shorter data record
CCl_4 [a]	35			0.47 (40)$^{-1}$	14%			0.53 (49)$^{-1}$	15%	**44**	33	36	58	67	Medium Fewer estimators than CFC-11 and CFC-12
Nitrous Oxide	114			0.33 (144) $^{-1}$	16%	0.23 (116) ^{1}	18%	0.44 (115) $^{-1}$	9%	**123**	91	104	152	192	High
Halon-1301	65			0.38 (72)$^{-1}$	15%			0.62 (72)$^{-1}$	9%	**72**	58	61	89	97	Medium Fewer estimators than CFC-11 and CFC-12
CFC-114	190							1.0 (189)$^{-1}$	12%	**189**	153			247	Low No observation-based numbers
CFC-115 [b]	1020							1.0 (540)$^{-1}$	17%	**540**	404			813	Low No observation-based numbers

[a] The lifetime corresponds to the steady-state lifetime due to photochemical removal in the stratosphere. See text for the discussion of total lifetime including ocean and soil sinks.

[b] The model value is from the 2-D model using the photochemical data from this report.

Table 6.2. Recommended estimates for steady-state lifetimes for tropospheric removal species. The quoted possible range corresponds to 2σ uncertainty.

Species	WMO (2011)	Observation-Derived Inverse Lifetime				Model-Derived Inverse Lifetime		Recommended Lifetime			Level of Scientific Understanding (LOSU)
		Inversion		Forward 12-Box Model + Modeled Stratospheric Lifetime							
	τ (Yr)	1/τ (Yr $^{-1}$)	σ(%)	1/τ (Yr $^{-1}$)[1]	σ(%)[a]	1/τ (Yr $^{-1}$)	σ(%)	τ (Yr))	Possible range		
Methyl Chloroform [b]	5.0	$(5.0)^{-1}$	3%	$(5.4)^{-1}$	12%			**5.0**	4.7	5.4	High Based on inversion of CH_3CCl_3, but has to parameterize ocean sink.
HCFC-22	12			$(12)^{-1}$	16%			**12**	9.3	18	Medium Observation constraint based on CH_3CCl_3
HCFC-141b	9.2			$(9.4)^{-1}$	15%			**9.4**	7.2	13.5	
HCFC-142b	17.2			$(18)^{-1}$	14%			**18**	14	25	
HFC-23	222			$(228)^{-1}$	21%			**228**	160	394	
HFC-32	5.2			$(5.4)^{-1}$	17%			**5.4**	4.0	8.2	
HFC-125	28.2			$(31)^{-1}$	18%			**31**	22	48	
HFC-134a	13.4			$(14)^{-1}$	18%			**14**	10	21	
HFC-143a	47.1			$(51)^{-1}$	19%			**51**	38	81	
HFC-152a	1.5			$(1.6)^{-1}$	15%			**1.6**	1.2	2.2	
HFC-227ea	38.9			$(36)^{-1}$	21%			**36**	25	61	
HFC-245fa	7.7			$(7.9)^{-1}$	22%			**7.9**	5.5	14	
Methane [c]	8.7/12			$(9.8)^{-1}$	15%			**9.8**	7.6	14	
Methyl Chloride [d]	1.5					$(1.3)^{-1}$	18%	**1.3**	0.9	2.0	Medium See footnote d
Methyl Bromide [d]	1.9					$(1.5)^{-1}$	17%	**1.5**	1.1	2.3	

[a] The quoted standard deviation accounts for the uncertainties in the retrieved OH, and OH reaction rate constant as derived in Chapter 3.

[b] The number in the WMO column is the total lifetime (including the ocean sink). The value from the inversion method for CH_3CCl_3 also corresponds to the total global atmospheric lifetime. The recommended value is the steady-state lifetime based on the inversion. The steady-state partial lifetime due to photochemical removal in the atmosphere is also provided in the "forward 12-box model" column. When combined with the 94 year lifetime from the ocean sink, this will provide a total lifetime of 5.1 years. This is well within the uncertainty associated with the inversion value.

[c] The 12-year value in the WMO column is the response lifetime. All other values correspond to the steady-state lifetime for CH_4.

[d] The values (including the WMO column) correspond to lifetime due to removal by OH. The values in the table are from model simulations. We could have (but did not) use the forward model in this calculation.

The CFC-11 lifetime is a weighted average of the model estimates, the satellite-hybrid observation method, and the inverse model of observations. The CFC-12 lifetime uses the same techniques but also includes the tracer-tracer observations method. CFC-11 and CFC-12 have recommended lifetimes of 52 and 102 years, respectively. These are not significantly different from the values provided in previous assessments (see Figure 6.3). What is more notable is that while previous assessments provided uncertainty estimates for each estimator, we combine the uncertainties into two ranges. As explained in Section 6.2, these are given as a "most likely" range and a "possible" range. For CFC-11 the possible range is 37 - 92 years (thin red line on RHS of Figure 6.3) while the likely range is 43 - 67 years (thick red line on RHS of Figure 6.3). Similarly, for CFC-12 the possible range is 78 – 149 (thin blue line on RHS of Figure 6.3) while the likely range is 88 - 122 years (thick blue line on RHS of Figure 6.3). As noted above, these possible ranges span the uncertainties of all of the estimated 2σ values. The most likely ranges reflect a reduction in the uncertainty resulting from the overlap of the distributions, and therefore a tighter estimate of the recommended uncertainty. It is clear from Figure 6.3 that these combined ranges are, in most cases, smaller than the individual ranges cited in previous assessments.

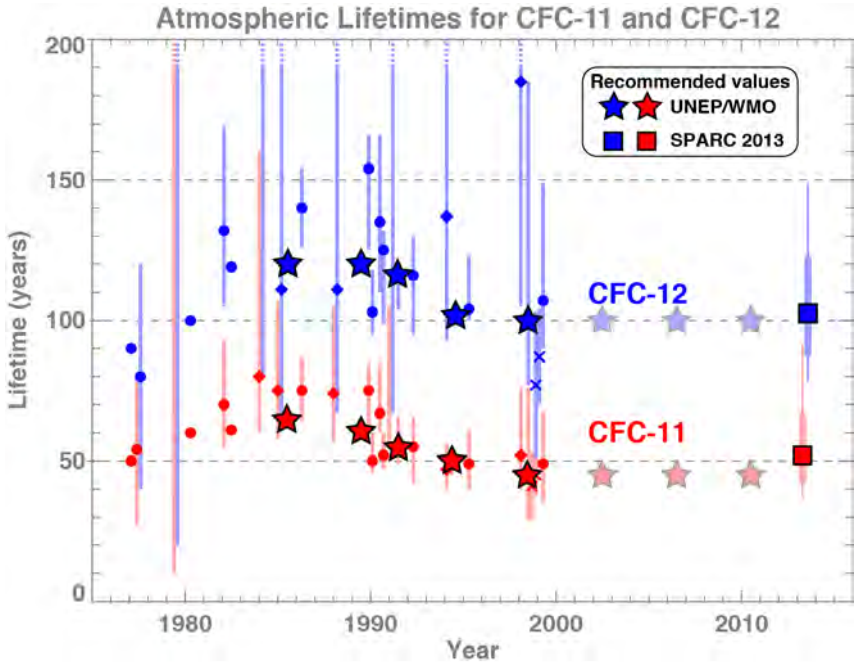

Figure 6.3. Recommended steady-state lifetimes and uncertainty ranges for CFC-11 and CFC-12. Results from previous assessment reports are shown with respect to the year they were published. The recommended values of CFC-11 and CFC-12 from this report are 52 and 102 years, respectively (right hand side). The possible ranges are 37-92 years (thin red) for CFC-11 and 78-149 years (thin blue) for CFC-12. The most likely ranges are 43-67 years (thick red) for CFC-11 and 88-122 years (thick blue) for CFC-12.

For CCl_4 the recommended steady-state lifetime of 44 years is calculated only from the removal by photochemical reactions in the stratosphere (excluding the ocean uptake and soil removal). This is larger than the 35 years from recent WMO reports. Previously, the 35 year lifetime was combined with an oceanic removal lifetime of 94 years to obtain a total lifetime of 26 years. That lifetime was found to be too short to reconcile the observed tropospheric trends with estimated emissions. The current estimate for the oceanic lifetime is 81 years,

with a soil removal lifetime of 195 years (see Chapter 4). The combined lifetime is 25 years. Thus, the issue for the CCl_4 budget, as discussed in Montzka and Reimann (2011), remains.

Values in Table 6.2 were generated using the 12-box model described in Section 4.3.1. An inversion exercise was first performed using the time series of the observed surface concentration for CH_3CCl_3. The 12-box model retrieval gives a total global atmospheric lifetime of 5.0 years for CH_3CCl_3. The uncertainty is 3%, giving a 2-σ range of 4.7 – 5.3 years. In the inversion, an ocean sink corresponding to a partial lifetime of 83 years was assumed along with in situ photochemical removal in each of the 12-boxes. The retrieved removal rate in the troposphere can be converted to an average OH concentration in each box. It is estimated that the uncertainty for the average OH concentration is 12%. This includes the uncertainty associated with assigning the ocean partial lifetime for CH_3CCl_3, and the uncertainty in the reaction rate constant of CH_3CCl_3 with OH.

The averaged OH values were then used in the forward model to compute the partial steady-state lifetime due to reaction with OH in the troposphere for the rest of the species listed in Table 6.2. The tropospheric partial lifetime was combined with the partial stratospheric lifetime (appropriately defined to coincide with the stratosphere in the 12-box model) from the 2-D model to provide a total lifetime. The uncertainty range is based on the uncertainty in the average OH concentration, the uncertainty in the reaction constant with OH, and the uncertainty in the partial stratospheric lifetime.

The 3-D models use JPL-10-6 photochemical data in their simulations. There were significant revisions in the data for the 4 species listed in Table 6.3 based on the work in Chapter 3. As a result, we base the lifetime recommendation on the 2-D model results which used this new kinetic data.

Table 6.3. Model-calculated values for steady-state lifetimes. The values are from the 2-D model using the kinetic data from this report. The quoted possible range corresponds to 2σ uncertainty.

Species	WMO (2011)	Model derived Inverse Lifetime		Recommended Lifetime			Level of Scientific Understanding (LOSU)
	τ (Yr)	1/τ (Yr^{-1})	σ(%)	τ (Yr)	Possible range		
Halon-1202	2.9	$(2.5)^{-1}$	33%	**2.5**	1.5	7.3	Low
Halon-1211	16	$(16)^{-1}$	29%	**16**	10	39	Low
Halon-2402	20	$(28)^{-1}$	19%	**28**	20	45	Low
NF_3	500	$(569)^{-1}$	13%	**569**	454	764	Low

6.4 What Can Be Done in Future Studies to Reduce the Uncertainties?

This report documents the use of advances in photochemical data and chemistry climate modeling, along with an abundance of high quality observations, to improve estimates of lifetimes and their uncertainties for many ODSs and related species. For some species, uncertainties remain large due to limited observations or uncertainties related to loss processes. Further improvements to lifetime estimates may be obtained with gains in knowledge in two areas: first, the scientific understanding of the processes influencing lifetimes and applying the new understanding to analyses of existing data; and second, more (different locations and times) accurate measurements to constrain budgets.

The photolysis rate of a species depends on the absorption cross-section of the species and the availability of photons. In a photolysis calculation, the latter depends on the parameterization of the O_2 cross sections in the Schumann-Runge Bands. While no attempt was made in this report to examine atmospheric opacity, it is noted as an important uncertainty (up to 15% (2-σ uncertainty) for CFC-11). Measurements of short-wave actinic fluxes in the tropical stratosphere could help to better constrain CFC loss rates. Finally, the temperature dependence of the absorption spectra of CFC-11 and CFC-12 has been identified in this report as major sources of uncertainty.

Important questions have emerged on the limitation of the theoretical understanding of the impact of inter-annual variability and the long-term trends of stratospheric circulation on quantities relevant for lifetime estimates. This suggests that some of the differences between lifetime estimates based on observations in different years could be real, rather than reflecting inaccuracies in different estimates. Another source of uncertainty is the variability of lifetime estimates due to the interannual variability in stratospheric transport caused by the quasi-biennial oscillation (QBO) (e.g., Tian *et al.,* 2006; Punge *et al.,* 2009).

There is scientific debate regarding the theoretical basis for using tracer-age correlations to estimate absolute lifetimes. The lifetimes of stratospheric removal (SR) species depend critically on atmospheric transport in the lower-mid stratosphere, in particular ascent rates in the tropics and recirculation mixing rates from mid-latitudes into the tropics. Numerous diagnostics exist for testing model transport in this region (SPARC, 2010; Strahan *et al.,* 2011), but their usefulness depends on the quality and coverage of observations. Improved observational constraints on tropical transport processes could be provided with wider coverage of tracers that diagnose age-of-air or age spectrum (e.g., CO_2 and N_2O) and the tropical 'tape recorder' (e.g., H_2O and CO). The interpretation of the observations, however, may depend strongly on an improved understanding of how the QBO and interannual variability affect stratospheric transport, and consequently lifetimes.

Surface flux boundary conditions (FBCs) for tracers allow chemistry and transport to evolve in a self-consistent manner within a model. Their use in CCM simulations would remove the artificial constraint imposed by specifying mixing ratio boundary conditions (MBCs) from a pre-computed scenario. However, the database for emission and surface sink estimates is not sufficient to allow all tracers discussed in this report to be treated in this way. Where sufficient data exist models should use FBCs, especially for species that have a large trend in atmospheric burden. For species with poorly constrained atmospheric emissions and/or surface sinks, or a fairly constant atmospheric burden, MBCs are still preferable.

Chapter 4 concludes that accurate and highly vertically resolved CFC profiles are essential for the techniques deducing CFC lifetimes from observations. For the satellite hybrid method (Minschwaner *et al.,* 2013), accurate, high vertical resolution profiles in the tropics are most important. For the tracer/tracer correlation methods, accurate information is needed on tracer slopes in the lower extratropical stratosphere, close to the tropopause. Here, improved retrievals of previously analysed data sets (e.g., MIPAS) and the extension of the analysis to additional data sets (e.g., HIRDLS) may lead to more accurate vertical profiles. However, the vertical resolution of the satellite data results is a fundamental limitation on the possible degree of the uncertainty reduction. *In situ* observations in the lower stratosphere will help to constrain this fundamental limitation of the satellite data when used for the satellite hybrid method and the tracer/tracer method.

It is essential to continue and extend ground-based measurement networks. Further, solidly vetted emission data sets for all the compounds evaluated herein and a better characterization of non-atmospheric (e.g., oceanic) sinks of these compounds is important for both inverse and forward model studies for some of the compounds.

The lifetimes of tropospheric removal (TR) species depend overwhelmingly on the abundance of tropospheric OH. Using direct observations to constrain the highly variable local OH concentration is problematic, although an observation-inferred global mean OH abundance has been derived in this report. Additional observational constraints on OH are needed, especially the mean abundance in the tropical lower troposphere where a large fraction of TR species' destruction occurs. Modelled tropospheric mean OH values vary considerably. Model-model intercomparisons are needed to understand the cause of these differences. While there are a number of surface stations measuring TR species, there are few measurements of their vertical and latitudinal distributions. Observations of a range of species with primarily OH loss would constrain both model estimate of losses and transport pathways.

The 44-year steady-state atmospheric lifetime of CCl_4 determined in this report is substantially longer than the 35 years from WMO (2011). However, the estimate of the partial lifetime for the oceanic sink has decreased from 93 years to 81 years (Section 4.3.3.2). Assuming a 195-year partial lifetime for the soil sink (Montzka and Reimann *et al.,* 2011), this yields a total global lifetime of 25 years, comparable to the 26 years from WMO (2011). This confirms the imbalance between sinks and sources as elaborated therein. However, the value for the soil sink is only based on a few campaigns in specific ecosystems and the value for the oceanic sink comes from a single study (Yvon-Lewis and Butler, 2002). Therefore, the new total lifetime of 25 years should only be used in a qualitative way for assessing the global sources until soil and oceanic sink terms are better constrained.

6.5 References

Atkinson, R., D. L. Baulch, R. A. Cox, J. N. Crowley, R. F. Hampson, R. G. Hynes, M. E. Jenkin, M. J. Rossi, J. Troe, and T. J. Wallington, Evaluated kinetic and photochemical data for atmospheric chemistry: Volume IV - gas phase reactions of organic halogen species, *Atmos. Chem. Phys.*, *8*, 4141-4496, 2008.

IPCC, Climate Change 2007: The Physical Science Basis. Contribution of Working Group I to the Fourth Assessment Report of the Intergovernmental Panel on Climate Change (S. Solomon, D. Qin, M. Manning, Z. Chen, M. Marquis, K. B. Averyt, M. Tignor, and H. L. Miller (eds.), Cambridge University Press, Cambridge, United Kingdom, and New York, NY, USA, 996 pp., 2007.

Kaye, J. A., S. A. Penkett, and F. M. Ormond (eds.), *Report on Concentrations, Lifetimes, and Trends of CFCs, Halons, and Related Species*, NASA Reference Publication 1339, Washington, D.C., 1994.

Minschwaner, K., L. Hoffmann, A. Brown, M. Riese, R. Müller, and P. B. Bernath, Stratospheric loss and atmospheric lifetimes of CFC-11 and CFC-12 derived from satellite observations, *Atmos. Chem. Phys., 13,* 4253-4263, 2013.

Montzka, S. A., and S. Reimann (Coordinating Lead Authors), A. Engel, K. Krüger, S. O'Doherty, and W. T. Sturges (Lead Authors), Ozone-Depleting Substances (ODSs) and Related Chemicals, Chapter 1 in *Scientific Assessment of Ozone Depletion: 2010, Global Ozone Research and Monitoring Project–Report No. 52*, 516 pp., World Meteorological Organization, Geneva, Switzerland, 2011.

Punge, H. J., P. Konopka, M. A. Giorgetta, and R. Müller, Effects of the quasi-biennial oscillation on low-latitude transport in the stratosphere derived from trajectory calculations, *J. Geophys. Res.*, *114*, D03102, doi: 10.1029/2008JD010518, 2009.

Sander, S. P., J. Abbatt, J. R. Barker, J. B. Burkholder, R. R. Friedl, D. M. Golden, R. E. Huie, C. E. Kolb, M. J. Kurylo, G. K. Moortgat, V. L. Orkin, and P. H. Wine, *Chemical Kinetics and Photochemical Data for Use in Atmospheric Studies, Evaluation Number 17,* JPL Publication 10-6, Jet Propulsion Laboratory, California Institute of Technology 2011.

SPARC CCMVal (Stratospheric Processes And their Role in Climate), *SPARC CCMVal Report on the Evaluation of Chemistry-Climate Models*, edited by V. Eyring, T. G. Shepherd, and D. W. Waugh, SPARC Report No. 5, WCRP-132, WMO/TD-No. 1526, http://www.atmosp.physics.utoronto.ca/SPARC/ccmval_final/index.php, 2010.

Spivakovsky, C. M., J. A. Logan, S. A. Montzka, Y. J. Balkanski, M. Foreman-Fowler, D. B. J. Jones, L. W. Horowitz, A. C. Fusco, C. A. M. Brenninkmeijer, M. J. Prather, S. C. Wofsy, and M. B. McElroy, Three-dimensional climatological distribution of tropospheric OH: Update and evaluation, *J. Geophys. Res.*, *105* (D7), 8931-8980, doi: 10.1029/1999JD901006, 2000.

Strahan, S. E., A. R. Douglass, R. S. Stolarski, H. Akiyoshi, S. Bekki, P. Braesicke, N. Butchart, M. P. Chipperfield, D. Cugnet, S. Dhomse, S. M. Frith, A. Gettelman, S. C. Hardiman, D. E. Kinnison, J.-F. Lamarque, E. Mancini, M. Marchand, M. Michou, O. Morgenstern, T. Nakamura, D. Olivié, S. Pawson, G. Pitari, D. A. Plummer, J. A. Pyle, J. F. Scinocca, T. G. Shepherd, K. Shibata, D. Smale, H. Teyssèdre, W. Tian, and Y. Yamashita, Using transport diagnostics to understand chemistry climate model ozone simulations, *J. Geophys. Res., 116,* D17302, doi: 10.1029/2010JD015360, 2011.

Tian, W., M. P. Chipperfield, L. J. Gray, and J. M. Zawodny, Quasi-biennial oscillation and tracer distributions in a coupled chemistry-climate model, *J. Geophys. Res.*, *111*, D20301, doi: 10.1029/2005JD006871, 2006.

WMO (World Meteorological Organization), *Scientific Assessment of Ozone Depletion: 2010, Global Ozone Research and Monitoring Project–Report No. 52*, Geneva, Switzerland, 2011.

Yvon-Lewis, S. A., and J. H. Butler, Effect of oceanic uptake on atmospheric lifetimes of selected trace gases. *J. Geophys. Res.*, *107* (D20), 4414, doi: 10.1029/2001JD001267, 2002.

Appendix: Estimating Uncertainties of Joint and Sampling Distributions

Each lifetime measurement (or estimate or observation) is described by a true value and an uncertainty (following standard statistical methods, e.g., Wilks, 1995). We express this mathematically as:

$$x_{ai} = A_a + \varepsilon_{ai} \tag{6.1}$$

The x denotes the measurement, the a subscript denotes the a^{th} "technique" (e.g., a satellite observation, model observation, inversion, etc.), the i subscript denotes that this is the i^{th} observation (assuming we can repeat the observation multiple times), A denotes the true value that we are trying to measure, and ε_{ai} is the error of the observation that is random and normally distributed. The mean ($\bar{x}_a$) and variance (S_a)are conventionally estimated as:

$$\bar{x}_a = \frac{\sum_{i=1}^{n} x_{ai}}{n}, S_a^2 = \frac{\sum_{i=1}^{n} (x_{ai} - \bar{x}_a)^2}{n-1} \tag{6.2}$$

The Joint Distribution

We first consider combining values from three techniques into a joint distribution (hereafter abbreviated as the J-distribution):

$$\begin{aligned} x &= [x_{a1}, x_{a2}, x_{a3}, ..., x_{b1}, x_{b2}, x_{b3}, ..., x_{c1}, x_{c2}, x_{c3}, ...] \\ &= [A_a + \varepsilon_{a1}, A_a + \varepsilon_{a2}, A_a + \varepsilon_{a3}, ... \\ &\quad A_b + \varepsilon_{b1}, A_b + \varepsilon_{b2}, A_b + \varepsilon_{b3}, ... \\ &\quad A_c + \varepsilon_{c1}, A_c + \varepsilon_{c2}, A_c + \varepsilon_{c3}, ...] \end{aligned} \tag{6.3}$$

Here the a subscript denotes the first technique for estimating a lifetime, while the b and c subscripts denotes the second and third techniques. There are n_a, n_b , and n_c observations in the three observation distributions respectively. The mean ($\bar{x}_J$) and variance (S_J^2) of this J-distribution (denoted by the J subscript) are written:

$$\bar{x}_J = \frac{n_a \bar{x}_a + n_b \bar{x}_b + n_c \bar{x}_c}{n_a + n_b + n_c} \tag{6.4}$$

$$S_J^2 = \frac{(n_a - 1)S_a^2 + (n_b - 1)S_b^2 + (n_c - 1)S_c^2 + n_a(\bar{x}_a^2 - \bar{x}_J^2) + n_b(\bar{x}_b^2 - \bar{x}_J^2) + n_c(\bar{x}_c^2 - \bar{x}_J^2)}{(n_a + n_b + n_c - 1)} \tag{6.5}$$

The J-distribution's S_J quantifies the full range of our lifetime value estimates. In this formulation, there are a total of n_a+n_b +n_c observations in the J-distribution. If we assume that $n_a = n_b = n_c = n$, and that $n >> 1$, then we can simplify Equations (6.4) and (6.5) to:

$$\bar{x}_J = \frac{\bar{x}_a + \bar{x}_b + \bar{x}_c}{3}, S_J^2 = \frac{S_a^2 + S_b^2 + S_c^2 + \bar{x}_a^2 + \bar{x}_b^2 + \bar{x}_c^2 - 3\bar{x}_J^2}{3} \tag{6.6}$$

This expression shows that S_J^2 is a function of both the individual variances of the separate distributions, and of the differences of the means from $\bar{x}_J$.

As a simple example of the J-distribution (Figure 6.A1), we will assume three normally distributed functions with means and one standard deviations of: (a) 55.3±6.5 (red), (b) 53.0±7.8 (blue), and (c) 44.7±11.4 (green). In this example, we use the lifetime values directly, but note that the actual calculations in Chapter 6 are performed using loss frequencies (i.e., the inverse of the lifetime, e.g., 1/55.3, 1/53.0, and 1/44.7). Using a normal distribution random number generator, we generate a large number of values to represent each distribution and then "estimate" the individual means and variances ($\bar{x}_a, \bar{x}_b, \bar{x}_c, S_a^2, S_b^2$, and S_c^2.) according to Equation (6.2). As expected, these values correspond to the mean values and standard deviations that were assigned. Similarly, we combine all of these values according to (6.3) and estimate the mean and standard deviations, again using Equation (6.2) to obtain $\bar{x}_J$ and S_J^2. The J-distribution is shown in Figure 6.A1 as the black curve.

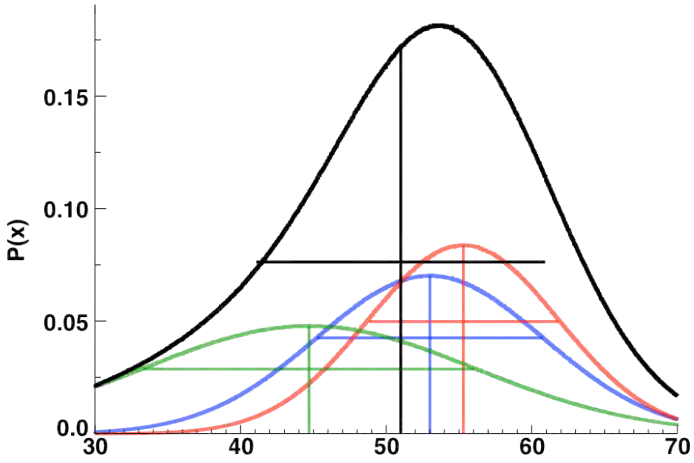

Figure 6.A1. Three normal distributions representing the results from measurements made using three difference methods are combined to form the Joint-distribution (J-distribution). The probability distribution functions of the three populations (red, blue, and green) with different means (vertical lines) and standard deviations (horizontal lines) as shown. The J-distribution is shown in black. The magnitudes of the red, blue, and green distributions have been decreased by 1/3 to show how they sum to the black curve.

The direct estimate of the mean from this J-distribution is 51 with a standard deviation of 9.9, determined from (6.2). These direct estimates are in near exact agreement with the values derived from the individual distribution estimates using (6.6). The mean value in Figure 6.A1 is shown by the vertical black line, while the horizontal black bar shows the ±1σ values (square root of the variance estimate S_J^2) about the mean. As is clear from the figure, this variance describes the range of all of the values. Note that this distribution is not normally distributed.

The Sampling Distribution

An alternative to the J-distribution is to sample from each technique and then perform a weighted average of those samples together. We will refer to this as the sampling distribution of the weighted mean (hereafter, the SWM-distribution). We can describe this technique mathematically assuming three observational techniques according to:

$$\begin{aligned} x &= [w_a x_{a1} + w_b x_{b1} + w_c x_{c1},\ \ w_a x_{a2} + w_b x_{b2} + w_c x_{c2},\ w_a x_{a3} + w_b x_{b3} + w_c x_{c3},\ ...] \\ &= [w_a A_a + w_b A_b + w_c A_c + w_a \varepsilon_{a1} + w_b \varepsilon_{b1} + w_c \varepsilon_{c1},\ ...] \end{aligned} \tag{6.7}$$

Here, the *w* values represent the weightings for the three techniques. Using this formulation, we find that the weighted-mean is:

$$\begin{aligned} \overline{x}_{SWM} &= w_a A_a + w_b A_b + w_c A_c + \frac{1}{n}\sum_{i=1}^{n}(w_a \varepsilon_{ai} + w_b \varepsilon_{bi} + w_c \varepsilon_{ci}) \\ &= w_a \overline{x}_a + w_b \overline{x}_b + w_c \overline{x}_c \end{aligned} \tag{6.8}$$

Using Equation (6.2) we can derive the variance of this SWM-distribution:

$$S^2_{SWM} = \frac{\sum_{i=1}^{n}(w_a^2 \varepsilon_{ai}^2 + w_b^2 \varepsilon_{bi}^2 + w_c^2 \varepsilon_{ci}^2 + 2w_a \varepsilon_{ai} w_b \varepsilon_{bi} + 2w_a \varepsilon_{ai} w_c \varepsilon_{ci} + 2w_b \varepsilon_{bi} w_c \varepsilon_{ci})}{n-1} \tag{6.9}$$

Assuming the errors of the distributions are random and uncorrelated, (6.9) reduces to:

$$S^2_{SWM} = \frac{\sum_{i=1}^{n}(w_a^2 \varepsilon_{ai}^2 + w_b^2 \varepsilon_{bi}^2 + w_c^2 \varepsilon_{ci}^2)}{n-1} = w_a^2 S_a^2 + w_b^2 S_b^2 + w_c^2 S_c^2 \tag{6.10}$$

From this equation, we see that the SWM-distribution has a normal distribution, and that the differences between the individual means are not a factor in the variance estimate.

If errors are correlated, (6.9) reduces to:

$$\begin{aligned} S^2_{SWM} &= w_a^2 S_a^2 + w_b^2 S_b^2 + w_c^2 S_c^2 \\ &\quad + 2w_a w_b Cov(x_a, x_b) + 2w_a w_c Cov(x_a, x_c) + 2w_b w_c Cov(x_b, x_c) \end{aligned} \tag{6.11}$$

In this expression, the covariance (*Cov*) is calculated according to:

$$Cov(x_a, x_b) = \frac{\sum_{i=0}^{n}(x_{ai} - \overline{x}_a)(x_{bi} - \overline{x}_b)}{n-1} \tag{6.12}$$

It is also useful to express (6.11) in terms of correlation coefficients ($r_{a,b}$). In this form, (6.11) is written

$$S_{SWM}^2 = w_a^2 S_a^2 + w_b^2 S_b^2 + w_c^2 S_c^2 + 2w_a S_a w_b S_b r_{a,b} + 2w_a S_a w_c S_c r_{a,c} + 2w_b S_b w_c S_c r_{b,c} \quad (6.13)$$

When combining estimates, it is important to examine how errors could be correlated. An example of this correlation is found when calculating CFC-11 loss rates. In this case, errors associated with photolysis would be correlated between the satellite estimate and the model estimate. Also note that the total variance of the J-distribution depends on the correlation sign - an anti-correlation reduces the variance since errors between two estimates would tend to cancel each other.

Using the example shown in Figure 6.A1 we can test the concept as follows. The weighting factor is defined to be proportional to the inverse of the standard deviation, i.e., $w_a \; \alpha \; 1/S_a$, $w_b \; \alpha \; 1/S_b$, and $w_c \; \alpha \; 1/S_c$ (normalized to sum to a value of 1). Taking the obviously "non-normal" J-distribution in Figure 6.A1, we randomly select "measurements" from each of the three distributions and average those three measurements multiple times using the adopted weighting. Figure 6.A2 shows the distribution of these multiple 3-point averages. The distribution shown in Figure 6.A2 (as predicted) is normally distributed (with the 3rd and 4th moments ~ 0). Since we did not make any assumption about the covariance among the three methods, the estimated variance of this distribution is exactly as predicted from (6.10).

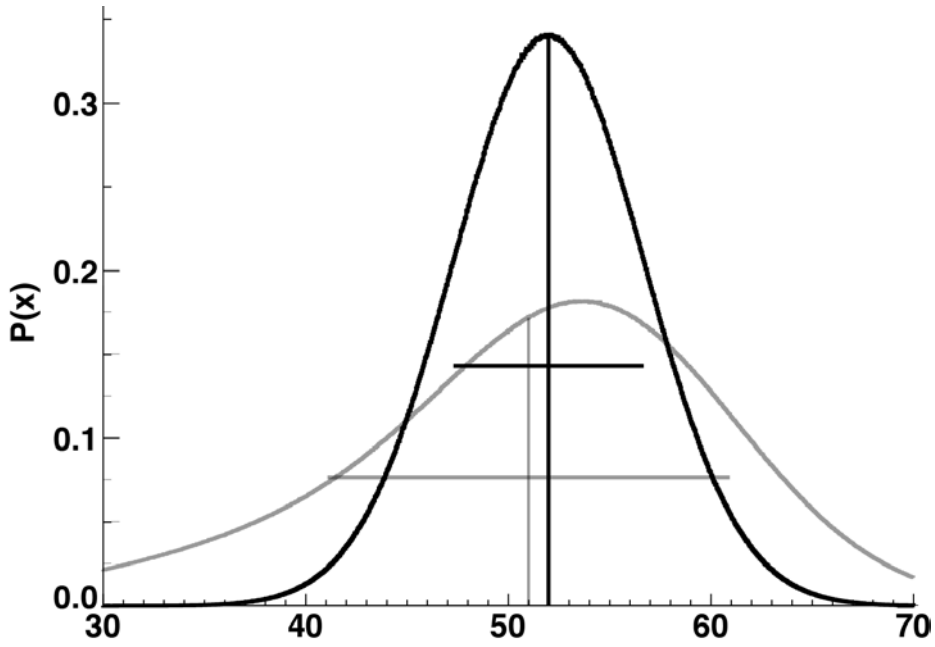

Figure 6.A2. The normal distribution of the variances from the SWM-distribution of the weighted mean. The J-distribution graph from Figure 6A-1 is included in grey for comparison. The mean of this weighted distribution is 52 (vertical line), and the standard deviation is 4.7 (horizontal line).

Conclusions

The J-distribution and the SWM-distributions provide techniques for deriving the mean and uncertainties of our observational estimates. Equation (6.6) provides a liberal or "possible" estimate of the uncertainty of the lifetimes, while Equation (6.11) provides a tight estimate yielding a "most likely" estimate. This derivation is based upon the assumptions that: 1) the errors are reasonable representations of the distributions for large numbers of sample estimates, and 2) the errors are relatively normally distributed..

For the J-distribution we use Equation (6.6) and refer to this $\pm 2\sigma$ as the "possible range" around the arithmetic mean. For the SWM-distribution we use Equation (6.11) and refer to this $\pm 2\sigma$ as the "most likely" range around the weighted mean. These equations are used to calculate of the uncertainties given in Table 6.1.

Reference

Wilks, D. S., *Statistical Methods in the Atmospheric Sciences: An Introductio*n, Academic Press, San Diego, CA, pp. 467, 1995.

APPENDIX A

Acronyms and Chemical Nomenclature

ACRONYMS

ACE	Atmospheric Chemistry Experiment
AFEAS	Alternative Fluorocarbons Environmental Acceptability Study
AGAGE	Advanced Global Atmospheric Gases Experiment
ALE	Atmospheric Lifetime Experiment
ASHOE	Airborne Southern Hemisphere Ozone Experiment
ASTRO-SPAS	Astronomical Shuttle Pallet Satellite
ATMOS	Atmospheric Trace Molecule Spectroscopy Experiment
BDC	Brewer-Dobson circulation
CAM4	Community Atmosphere Model Version 4 (NCAR)
CCM	chemistry climate model
CCMI	Chemistry-Climate Modelling Initiative
CCMVAL	Chemistry-Climate Model VALidation activity for SPARC
CESM	Community Earth System Model
CFC	chlorofluorocarbon
CIRRUS	Cryogenic Infrared Radiance Instrumentation for Shuttle
CLAES	Cryogenic Limb Array Etalon Spectrometer
CMIP	Coupled Model Intercomparison Project
CNRS	Centre National de la Recherche Scientifique (France)
CONST	constant boundary conditions
CRISTA	Cryogenic Infrared Spectrometers and Telescopes for the Atmosphere
CTM	chemical transport model
ESRL	Earth System Research Laboratory (NOAA)
FBC	flux boundary conditions
FTS	Fourier transform spectrometer
GAGE	Global Atmospheric Gases Experiment
GAL	global atmospheric lifetime
GHG	greenhouse gas
GEOS	Goddard Earth Observing System
GSFC	Goddard Space Flight Center
GWP	global warming potential
HAGAR	High Altitude Gas Analyser
HALOE	Halogen Occultation Experiment
Halon	halomethane or fluorochlorobromocarbon
HCFC	hydrochlorofluorocarbon
HFC	hydrofluorocarbon
HIRDLS	High Resolution Dynamics Limb Sounder
IPCC	Intergovernmental Panel on Climate Change
IR	infrared
IUPAC	International Union of Pure and Applied Chemistry
JPL	Jet Propulsion Laboratory
km	kilometer
MAESA	Measurements for Assessing the Effects of Stratospheric Aircraft
MBC	mixing ratio boundary condition
MIPAS	Michelson Interferometer for Passive Atmospheric Sounding
MLS	Microwave Limb Sounder

MPI	Max-Planck-Institut (Germany)
NASA	National Aeronautics and Space Administration
NCAR	National Center for Atmospheric Research
NDRL/NIST	Notre Dame Radiation Laboratory/National Institute of Standards and Technology
NIWA	National Institute of Water and Atmospheric Research (New Zealand)
nm	nanometer
NMHC	non-methane hydrocarbons
NOAA	National Oceanic and Atmospheric Administration
ODS	ozone depleting substance
ODP	ozone depletion potential
ppb, ppm, ppt	parts per parts per billion, million, trillion
PSS	photochemical steady state
QBO	quasi-biennial oscillation
QPS	quarantine and pre-shipment
RAS	relaxed Arakawa Schubert
RCP	Representative Concentration Pathway
SAD	surface area densities
SAMS	Stratospheric And Mesospheric Sounder
SICs	sea ice concentrations
SOGE	System for Observation of halogenated Greenhouse gases in Europe
SORCE	Solar Radiation and Climate Experiment
SPARC	Stratospheric Processes and Their Role in Climate
SR	stratospheric removal
SST	sea surface temperature
TR	tropospheric removal
TUV	Tropospheric and Ultraviolet Visible
UARS	Upper Atmosphere Research Satellite
UC Irvine	University of California, Irvine
UEA	University of East Anglia
UM	unified model
UNEP	United Nations Environment Programme
UV	ultraviolet
VMR	volume mixing ratio
VOC	volatile organic compound
VSLS	very short-lived species
VUV	vacuum ultraviolet
WACCM4	Whole-Atmosphere Community Climate Model Version 4
WCRP	World Climate Research Programme
WMO	World Meteorological Organization
1-D	one-dimensional
2-D	two-dimensional
3-D	three-dimensional

CHEMICAL NOMENCLATURE

Br	atomic bromine
BrO	bromine monoxide
C_2H	ethynyl radical
CCl_4	carbon tetrachloride
CF_2Cl_2	dichlorodifluoromethane
$CFCl_3$	trichlorofluoromethane
$CHBr_3$	bromoform
CH_2Br_2	dibromomethane
CH_3Br	methyl bromide, bromomethane
CH_3CCl_3	methyl chloroform
CH_4	methane
Cl	atomic chlorine
ClO	chlorine monoxide
Cl_x	inorganic chlorine oxides
CO	carbon monoxide
CO_2	carbon dioxide
H	atomic hydrogen
H_2O	water
HO_x	odd hydrogen (H, OH, HO_2, H_2O_2)
N_2O	nitrous oxide
NF_3	nitrogen trifluoride
NO	nitric oxide
NO_3	nitrogen trioxide
NO_x	nitrogen oxides (NO + NO_2)
NO_y	total reactive nitrogen
$O(^3P)$	atomic oxygen (ground state)
$O(^1D)$	atomic oxygen (first excited state)
O_2	molecular oxygen
O_3	ozone
OH	hydroxyl radical
CCl_3F	CFC-11
CCl_2F_2	CFC-12
CCl_2FCClF_2	CFC-113
$CClF_2CClF_2$	CFC-114
CCl_2FCF_3	CFC-114a
$CClF_2CF_3$	CFC-115
CBr_2F_2	Halon-1202
$CBrClF_2$	Halon-1211
$CBrF_3$	Halon 1301
$CBrF_2CBrF_2$	Halon-2402
CH_3Cl	HCC-40
$CHClF_2$	HCFC-22
CH_3CCl_2F	HCFC-141b
CH_3CClF_2	HCFC-142b
CHF_3	HFC-23

CH_2F_2	HFC-32
CHF_2CF_3	HFC-125
CH_2FCF_3	HFC-134a
CH_3CF_3	HFC-143a
CH_3CHF_2	HFC-152a
CF_3CHFCF_3	HFC-227ea
$CHF_2CH_2CF_3$	HFC-245fa